



VRIJE UNIVERSITEIT BRUSSEL

FACULTEIT TOEGEPASTE WETENSCHAPPEN
VAKGROEP WERKTUIGKUNDE

TRAJECTORY GENERATION FOR PLANAR
HOPPING AND WALKING ROBOTS:
AN OBJECTIVE PARAMETER AND ANGULAR
MOMENTUM APPROACH

Jimmy Vermeulen

Proefschrift voorgelegd tot het behalen van de academische graad
van Doctor in de Toegepaste Wetenschappen

May 2004

Promotor: Prof. dr. ir. Dirk Lefeber



VRIJE UNIVERSITEIT BRUSSEL

FACULTEIT TOEGEPASTE WETENSCHAPPEN
VAKGROEP WERKTUIGKUNDE

TRAJECTORY GENERATION FOR PLANAR
HOPPING AND WALKING ROBOTS:
AN OBJECTIVE PARAMETER AND ANGULAR
MOMENTUM APPROACH

Jimmy Vermeulen

May 2004

Jury:

Prof. dr. ir. D. Lefebber (VUB), promotor
Prof. dr. ir. A. Cardon (VUB), chairman
Prof. dr. ir. J. Vereecken (VUB), vice-chairman
Prof. dr. ir. P. Kool (VUB), secretary of the chairman
Prof. dr. ir. Y. Baudoin (KMS)
Prof. dr. ir. R. Van Dooren (VUB)
Prof. dr. ir. G. Virk (University of Leeds)

Contact information:

Vrije Universiteit Brussel
Faculty of Applied Sciences
Department of Mechanical Engineering
1050 Brussels
Belgium
http://werk.vub.ac.be/multibody_mechanics.htm
Jimmy.Vermeulen@vub.ac.be
Dirk.Lefeber@vub.ac.be

to Mama

to Hans

"Whether continuing study of nature's solution to locomotion problems has contributed very much to man's development of machines for the purpose of assisting movement is doubtful, except after the fact, since the movement of any animal is very complex, requiring special equipment to determine what is happening and patience and ability on the part of the investigator to understand why and how it happened. Watching the flight of birds, both powered and soaring, created a desire in man to fly, but a detailed understanding of how a bird flies contributed little to the development of the airplane. Lift and drag as a function of shape and orientation were determined by intuition, experiment and analysis. However, an understanding of basic principles contributed to explaining some of nature's solution to flight, which in turn led to improvements in airplane design."

Physical principles of locomotion

[Eberhart, 1976]

Acknowledgements

I would like to use this opportunity to express many thanks to all those who supported me during this research period.

I am particularly grateful to Dirk Lefebber, for his constant support and his many helpful ideas and suggestions. The realization of this thesis would not have been possible without his guidance. Thanks, Dirk, for giving me the opportunity and the confidence.

Thanks to Bram Vanderborght for proofreading my manuscript, to Ronald Van Ham for helping me with the animations, and to Joris Naudet and Michael Vandamme for the useful discussions and their excellent programming skills. Also many thanks to Patrick Kool for his criticism, and for always being ready to discuss robotics-related issues.

There are not enough words for me to express my gratitude towards Björn Verrelst. Not many people have the luck to have their best friend as a colleague. Thanks Björn, for helping me through the difficult moments, for your deep thinking and your contributions to the realization of this thesis, and especially for the many animated discussions on the subject.

A special thanks goes to Hans De Man, who brought me in contact with the subject, and who passed me his knowledge. I was fortunate to work with Hans for a few years, which was not only inspiring for me, but also resulted in a firm friendship.

I am extremely grateful to my parents for their constant support throughout the years. The same feelings go towards Kassie, the love of my life.

Also thanks to Svend, my office mate, for all the fun and for helping me out when I needed it.

And finally I wish to thank my friends for being who they are. Thank you Bart, Indra, Wout, Sas, Peppie, Katrien, Dirk DS, and the whole Brussels bunch.

Brussels
May 2004

Jimmy Vermeulen

Abstract

A real-time joint trajectory generation strategy for dynamically balanced legged robots is proposed. This trajectory planner generates motion patterns based on two specific concepts, being the use of objective locomotion parameters, and exploiting the natural upper body dynamics by manipulating the angular momentum equation.

Using objective locomotion parameters is an elegant way of characterizing steps or hops of a motion pattern. When values for these parameters are specified, such as step length, forward speed, etc., then the trajectory planner translates these goals into feasible joint trajectories, or in other words, into actuator commands.

The trajectory planner uses the angular momentum equation to ensure that the generated polynomial joint trajectories inherently guarantee a high level of dynamical postural stability for the robot. In this work, postural stability is quantified by the distance of the Zero Moment Point to the boundaries of a stability region. The upper body of the robot, with its larger mass and inertia in comparison with the leg links, manifestly affects the position of the Zero Moment Point since generally large ankle torques are required to keep it upright. In this work, the planning method defines the trajectories of the leg links in such a way that the upper body motion is naturally steered, meaning that in theory no ankle torque would be required. To overcome possible external disturbances, a polynomial reference trajectory is established for the upper body motion, which mimics a natural trajectory. Consequently the required ankle torque is low, meaning that it does not cause the Zero Moment Point to move out of the predefined stability region.

Specific trajectory generation strategies are developed for two different types of robots, being a hopping monopod and a walking biped. The main difference between these strategies is that for the hopping monopod a flight phase is present, while for the walking biped a double support phase has to be taken into consideration. Both robot models are assumed to be planar systems, moving in the sagittal plane. The effectiveness of the developed planning strategies is verified by a variety of computer simulations. One of the most interesting aspects of these methods is that they are based on fast converging iteration loops, requiring a limited number of elementary calculations only. The computation time needed for generating feasible trajectories is low, which makes the strategies useful for real-time application.

Contents

Acknowledgements	i
Abstract	iii
List of Figures	xi
List of Tables	xvii
Nomenclature	xix
1 Introduction	1
1.1 Why legged locomotion ?	1
1.2 Dynamic balance	2
1.3 Known difficulties	4
1.4 Scope of the thesis	6
1.4.1 Objectives	6
1.4.2 Evolution	7
1.5 Historical overview	8
1.5.1 Hopping and running robots: history	8
1.5.2 Walking bipeds: state-of-the-art	14
1.6 Outline	17
2 A hopping robot with decoupled motion of upper body and leg	19
2.1 Introduction	19
2.2 Philosophy	21

2.3	General description of the studied model	23
2.4	Kinematics	25
2.4.1	Motion of the COG	25
2.4.2	Rotation around the COG	26
2.4.3	Rotation around the foot	27
2.5	Dynamics	28
2.5.1	Flight phase	28
2.5.2	Impact phase	34
2.5.3	Stance phase	36
2.6	Trajectory generation strategy	38
2.6.1	Flight phase trajectories	39
2.6.2	Stance phase trajectories	43
2.7	Simulations	49
2.8	Summary	55
3	A hopping robot with a foot	59
3.1	Introduction	59
3.2	The model	60
3.3	Kinematics	61
3.3.1	Motion of the COG	61
3.3.2	Rotation around the COG	62
3.4	Dynamics	63
3.4.1	Flight phase	63
3.4.2	Impact phase	64
3.4.3	Stance phase	65
3.5	Trajectory generation strategy	65
3.5.1	Flight phase trajectories	65
3.5.2	Stance phase trajectories	73
3.6	Simulations	77
3.6.1	Steady hopping pattern	77
3.6.2	Non-steady hopping pattern	84
3.7	Summary	89
4	A hopping robot with reduced ankle torque	93
4.1	Introduction	93

4.2	Estimating a desired value for the angular momentum during the flight phase	94
4.3	Angular momentum equation during the stance phase	95
4.3.1	Kinematic expression of the angular momentum with respect to the foot	95
4.3.2	Formal expression of the angular momentum equation	96
4.3.3	Obtaining a desired upper body rotation during the stance phase by tuning the stance time	97
4.3.4	Obtaining the desired angular momentum at take-off	99
4.4	Trajectory generation strategy: steady hopping	100
4.5	Trajectory generation strategy: irregular terrain (non-steady hopping)	104
4.6	Simulations	111
4.6.1	Steady hopping pattern	111
4.6.2	Non-steady hopping pattern: irregular terrain	115
4.7	Summary	117
5	A walking biped with instantaneous double support phase	121
5.1	Introduction	121
5.2	The biped model	125
5.3	Kinematics	127
5.3.1	Motion of the COG	127
5.3.2	Rotation around the supporting foot	128
5.4	Dynamics	129
5.4.1	Angular momentum equation	129
5.4.2	Complete dynamic model	130
5.5	Problem statement	131
5.6	Obtaining the desired upper body motion	133
5.6.1	Upper body angle	134
5.6.2	Upper body angular velocity	137
5.6.3	Upper body angular acceleration	138
5.7	Developing a trajectory generation strategy	139
5.7.1	Objective locomotion parameters	140
5.7.2	Boundary conditions - configuration level	140
5.7.3	Boundary conditions - velocity level	142
5.7.4	Boundary conditions - acceleration level	143
5.7.5	Intermediate condition	145

5.7.6	Establishing polynomial trajectories - iterative procedure . . .	146
5.8	Simulations	150
5.8.1	Hip and swing foot motion	152
5.8.2	Upper body motion	155
5.8.3	Zero moment point and vertical ground reaction force	157
5.8.4	Torques applied by the different actuators	158
5.9	Summary	162
6	A walking biped with impact and double support phase	163
6.1	Introduction	163
6.2	Kinematical aspects during the double support phase	165
6.2.1	The values of the dependent coordinates	167
6.2.2	The first derivatives of the dependent coordinates	167
6.2.3	The second derivatives of the dependent coordinates	168
6.3	Impact of the swing leg on the ground	169
6.4	Upper body behaviour during the double support phase	170
6.4.1	Approximating the natural upper body motion	171
6.4.2	Defining a reference trajectory for the upper body	175
6.5	Upper body behaviour during the single support phase	177
6.5.1	Problem statement	177
6.5.2	Attaining the desired upper body angle at the end of the single support phase	179
6.5.3	Attaining the desired upper body angular velocity at the end of the single support phase	180
6.5.4	Attaining the desired upper body angular acceleration at the end of the single support phase	181
6.6	Position of the ZMP during the double support phase	183
6.6.1	Motion on a horizontal ground	183
6.6.2	Motion on a non-horizontal ground	186
6.7	Trajectory generation strategy	187
6.7.1	General considerations	187
6.7.2	Single support phase	188
6.7.3	Double support phase	194
6.8	Simulation results	195
6.8.1	Hip and foot motion	197
6.8.2	Upper body motion	202

6.8.3	Frequency components of the tracking trajectories	205
6.8.4	Zero moment point and ground reaction forces	208
6.8.5	Applied torques and mechanical energy consumption	209
6.8.6	Influence of certain parameter values on mechanical energy consumption	213
6.9	Summary	215
7	General conclusions and proposed future work	217
	Appendices	225
A	Dynamic model of the hopping robot with foot	225
A.1	Flight phase	225
A.2	Stance phase	228
B	Kinetic energy loss during an impulsive impact	229
C	Applying the mean value theorem for integration	233
D	Dynamic model of the walking biped	235
E	Angular momentum during a single support phase	239
	Bibliography	241

List of Figures

1.1	Future predictions for feasibility of biped walking	5
1.2	Walking biped Lucy	8
1.3	Raibert's 3D hopping biped	9
1.4	The ARL Monopod II	11
1.5	The 3D bow leg hopping robot	13
1.6	The hopping robot Kenken	14
1.7	Sony's humanoid QRIO	14
1.8	Honda humanoid robots P2 and P3	16
1.9	Honda's robot Asimo	16
1.10	Kawada Industries's HRP-2P	17
1.11	Humanoid Johnnie	18
2.1	Two link planar robot as an example	21
2.2	Robot at take-off (to) and at touch-down (td)	24
2.3	Actuators at knee and hip	30
2.4	Percussion on upper body during shock	36
2.5	Free body diagram upper body before and after shock	36
2.6	Flow chart describing different steps in strategy	48
2.7	Stick diagram	51
2.8	Lower leg angle trajectory	51
2.9	Upper leg angle trajectory	52
2.10	Horizontal velocity of the COG	52
2.11	Horizontal position of the foot point F	53

2.12	Vertical position of the foot point F	53
2.13	Angular momentum with respect to the COG	54
2.14	Upper body angle behaviour	54
2.15	Vertical position of the COG	55
2.16	Torque exerted by hip actuator	56
2.17	Torque exerted by knee actuator	56
2.18	Torques exerted by torsional spring and knee actuator during a stance phase	57
3.1	Model geometry of the hopping robot with foot	60
3.2	Actuator torques at ankle, knee and hip	65
3.3	Foot and COG reach a maximum height at the same time	70
3.4	Flow chart describing different steps in strategy	75
3.5	Maximum value for positive ankle torque	76
3.6	Maximum value for negative ankle torque	76
3.7	Stick diagram for one hop of the steady hopping pattern	78
3.8	Horizontal velocity COG	79
3.9	Horizontal position foot	80
3.10	Vertical position foot	80
3.11	Angular momentum with respect to the COG	81
3.12	Absolute angle upper body with respect to horizontal axis	81
3.13	Kinetic energy loss during impact versus k_2	82
3.14	Vertical ground reaction force after impact versus k_3	83
3.15	Horizontal velocity variation during impact versus k_1	83
3.16	Coulomb's kinematic friction coefficient needed during stance phase	84
3.17	Ankle torque during one stance phase	85
3.18	Stick diagram non-steady hopping	86
3.19	Horizontal velocity COG	87
3.20	Vertical position foot	87
3.21	Horizontal position foot	88
3.22	Absolute angle upper body with respect to horizontal axis	88
3.23	Ankle torque during transition stance phase	89
4.1	Vertical position trajectory of the COG during a flight phase	99
4.2	COG at take-off and touch-down for first iteration	102
4.3	Flow chart describing different steps in strategy	105

4.4	Intersection between desired and real angular momentum curves . . .	108
4.5	Flow-chart describing overall strategy non-steady hopping	110
4.6	Upper body angle during one full hop	112
4.7	Upper body angular velocity during one full hop	113
4.8	Horizontal velocity COG during a stance phase	113
4.9	Horizontal position foot during one flight phase	114
4.10	Vertical position foot during one flight phase	114
4.11	Vertical position versus horizontal position foot during 1 flight phase	115
4.12	Upper body angle during non-steady hopping	116
4.13	Angular momentum with respect to COG	117
4.14	Ankle torque during stance phases	118
4.15	Horizontal position foot	118
4.16	Vertical position foot	119
4.17	Horizontal velocity of COG	119
5.1	Model of the walking robot	126
5.2	Actuators acting on biped	131
5.3	Walking pattern	132
5.4	Flow chart describing different steps in strategy	149
5.5	Stick diagram small steps	151
5.6	Horizontal hip position	152
5.7	Vertical hip position	153
5.8	Horizontal air foot position	155
5.9	Vertical air foot position	156
5.10	Upper body angle: polynomial and natural trajectory	156
5.11	Upper body angular velocity: polynomial and natural trajectory . .	157
5.12	Upper body angular acceleration: polynomial and natural trajectory	158
5.13	Zero moment point position	158
5.14	Vertical reaction force on supporting foot	159
5.15	Ankle torque on supporting foot	159
5.16	Knee and hip torques on supporting leg	160
5.17	Knee and hip torques on swing leg	160
5.18	Stick diagram larger steps	161
6.1	Biped during double support phase	166
6.2	Free body diagram of the upper body	171

6.3	Simplified upper body angle behaviour during step	178
6.4	ZMP position during double support phase	183
6.5	Possible behaviour of angular momentum derivative with respect to rear ankle joint during double support phase	185
6.6	ZMP position non-horizontal ground	186
6.7	Biped during single support phase	189
6.8	Flow chart describing different steps in strategy	196
6.9	Stick Diagram	198
6.10	Horizontal hip position	199
6.11	Vertical hip position	199
6.12	Horizontal velocity hip point	200
6.13	Vertical velocity hip point	200
6.14	Horizontal and vertical acceleration hip point	201
6.15	Possible boundary values for horizontal and vertical acceleration of hip point	202
6.16	Horizontal swing foot position	202
6.17	Vertical swing foot position	203
6.18	Upper body angle	203
6.19	Upper body angular velocity	204
6.20	Upper body angular acceleration single support phase	205
6.21	Upper body angular acceleration double support phase	205
6.22	Lower leg trajectory during one period	206
6.23	Spectrum of lower leg angle trajectory	206
6.24	Upper leg trajectory during one period	207
6.25	Spectrum of upper leg angle trajectory	207
6.26	Spectrum of upper body angle trajectory	208
6.27	Zero moment point position	209
6.28	Vertical ground reaction forces	209
6.29	Ankle torque during single support phase	210
6.30	Hip torque front leg during double support phase	210
6.31	Knee and hip torque supporting leg during single support phase	211
6.32	Knee and hip torque air leg during single support phase	212
6.33	Knee torques during double support phase	212
6.34	Mechanical energy consumption during single support phase versus foot lift	214

6.35	Mechanical energy consumption for a full step versus initial horizontal hip velocity	214
6.36	Mechanical energy consumption for a full step when varying mean velocity and step length	215
B.1	Percussion on series of rigid bodies	230

List of Tables

2.1	Inertial parameters of the monopod	24
5.1	Inertial parameters of the biped	126
5.2	Iteration on initial horizontal hip position	153
5.3	Iteration on initial vertical hip acceleration	155

Nomenclature

Acronyms

<i>COG</i>	Center Of Gravity
<i>DOF</i>	Degrees Of Freedom
<i>DS</i>	Double support Phase
<i>FRI</i>	Foot Rotation Indicator
<i>PD</i>	Proportional-Derivative
<i>PPAM</i>	Pleated Pneumatic Artificial Muscle
<i>SS</i>	Single Support Phase
<i>ZMP</i>	Zero Moment Point

Abbreviations

<i>det</i>	determinant
<i>fig</i>	figure
<i>lhs</i>	left hand side
<i>max</i>	maximum
<i>min</i>	minimum
<i>rhs</i>	right hand side
<i>to</i>	take-off
<i>td</i>	touch-down

Greek

δ	step height	m
Δ	variation	
ϵ	intermediate hip elevation	m
ζ	hopping height	m
η_i	mass of link i relative to total robot mass	
θ_i	absolute angle related to link i	rad
θ_{ij}	relative angle related to links i and j	rad
λ	step length	m
Λ	vector of Lagrange's multipliers	
μ	angular momentum	kgm ² /s
ν	horizontal velocity of COG of hopper during flight	m/s
ν	mean horizontal hip velocity of walking biped	m/s
Π	vector of percussions	Ns
σ	foot lift/clearance	m
τ	actuator torque	Nm
ω	angular velocity	rad/s

Roman

\bar{a}	acceleration vector	m ² /s
$C[q, \dot{q}]$	centrifugal matrix	
$D[q]$	inertia matrix	
E	energy consumption	J
f	frequency	Hz
f_k	Coulomb's kinematic friction coefficient	
\bar{F}	force	N
g	acceleration of gravity	m/s ²
$G[q]$	gravitational torque/force vector	
I	moment of inertia	kgm ²
\mathcal{J}	Jacobian matrix	
K	kinetic energy	J
l_i	length of link i	m
m_i	mass of link i	kg
M	total robot mass	kg
P	power consumption	W
\bar{P}	percussion/repercussion	Ns
q_i	generalized coordinate	
Q_i	generalized torque/force associated to q_i	
\bar{R}	reaction force	N
t	time	s
T	external torque/force vector	

T	total step duration	s
T^{fl}	flight time	s
T^{st}	stance time	s
T_D	double support phase duration	s
T_S	single support phase duration	s
U	potential energy	J
\bar{v}	velocity vector	m/s
$\bar{1}_z$	unit vector corresponding to z-axis	

Subscript

A	air (related to swing leg)
b	upper body
F	front
R	rear
F	of ankle point/foot
G	of COG
H	of hip point
K	of knee point
l	leg
S	stance (related to supporting leg)
S	spring
1	of lower leg
2	of upper leg
3	of upper body
$ _z$	z component of cross product

Superscript

des	desired function/value
e	external
nat	natural function
$real$	real calculated/measured value
$shock$	caused by impact phase
D	during double support phase
S	during single support phase
fl	during flight phase
st	during stance phase
to	function evaluated at take-off
td	function evaluated at touch-down
\cdot	derivative with respect to time
$'$	derivative with respect to time
\sim	mean value
$-$	vector

*	prescribed/desired function
+	function evaluated immediately after impact
−	function evaluated at instance of impact
T	transpose
\cdot^n	value after at n-th iteration
\cdot^0	starting value for iteration loop

Chapter 1

Introduction

1.1 Why legged locomotion ?

Research on legged vehicles has been going on for at least a hundred years now. According to Mark Raibert [1986] there are two main reasons for this interest in legged locomotion, being its potential for high mobility, and the fact that building legged machines can help us to understand how animals and humans move.

It is especially the high mobility aspect that makes legged machines attractive from the commercial point of view. To ratify the statement that legged robots indeed show high mobility, often the comparison is made with wheeled and tracked vehicles. Raibert [1986] elegantly demonstrated the superiority of legged robots in comparison with the latter systems on a theoretical basis, by stating that legs can use isolated footholds for support, whereas wheels or tracks require a continuous path of support. From this he concluded that the mobility of a legged robot is generally limited by the best footholds in the reachable terrain, whereas a wheeled vehicle is limited to the worst terrain. In general, when trying to develop a machine in order to interact with humans or to perform tasks normally executed by humans, it should at least be able to move in any environment accessible for human beings, again confirming why in theory legged systems are superior.

Due to the fact that nature provides us with a variety of examples of legged creatures, designers of legged robots are often inspired by biology. One popular way to classify legged robots is based on the number of legs they use. The most common machines can be summarized as follows [Hardarson, 1997]:

- octapods: eight-legged systems, like arachnida (e.g. spiders) and crustacea (e.g. crabs)
- hexapods: six-legged robots based on a large number of insects
- quadrupeds: systems with four legs, like most mammals

- bipeds: robots having two legs similar, like humans, kangaroos and birds. In the particular case where a biped has the similar leg structure as a human, moves in the same manner and tries to mimic its behaviour, such robots are often referred to as humanoids
- monopods: systems having only one leg. Biological systems with one leg only appear in the case of disabled humans or animals. These robots have mostly been studied for theoretical purposes. An advantage of these systems is that they allow to concentrate on a variety of conceptual features of legged locomotion, without having to consider the interactions between multiple legs

An extensive list of possible applications for legged robots can be found at the CLAWAR Network Overview¹. The most obvious commercial applications for legged robots are those where certain inspection and maintenance tasks have to be performed in environments that are hazardous for humans. Nuclear industry and chemical industry where inspection and repair tasks in contaminated zones are not unusual, are good examples. Other examples like humanitarian demining, underwater applications such as the inspection of bridges, forestry work and planetary exploration for space industry have been addressed as possible applications for legged robots. In reality, today the entertainment robots, such as toy robots, pet robots and companion robots, seem to be the only really feasible application, or at least the application gaining most of the attention. This is probably due to the fact that the technical requirements for such robots are a lot lower, especially when compared to robots having to operate in hazardous environments.

For legged machines to be able to carry out the specific task requirements of different types of industries, they will have to be able to walk in a stable manner, to climb vertical surfaces and to negotiate obstacles. Moreover a certain degree of intelligence will be needed in order to perform work that is non-periodical and sometimes unpredictable. Clearly designing and building a legged robot is an extremely multidisciplinary task. A fundamental issue for achieving legged locomotion is the generation of stable motion patterns for a robot. This so-called motion *planning* will be the main topic throughout this work.

1.2 Dynamic balance

Another common way to classify legged robots is based on the way they are balanced. A fundamental distinction exists between *statically* balanced and *dynamically* balanced machines [Raibert, 1986].

A statically balanced system moves slowly such that dynamical effects can be neglected. It avoids tipping motions of the robot and the resulting horizontal accelerations, by keeping the projection of the Center of Gravity (COG) of the

¹<http://www.clawar.com/other/overview.html/>

system within the polygon formed by the supporting feet at all times. Such systems move with gait patterns that maintain this condition throughout the locomotion process, meaning that they work in or near a static equilibrium throughout their gait. For robots having single-point feet, purely static balance during motion is only possible if they consist of at least 4 legs. However, when using feet that are large enough, bipeds can also maintain static stability during single support phases by keeping the COG on top of the supporting leg, with the COG projection lying in the foot surface.

Legged systems maintaining stable locomotion without satisfying the static stability constraint, are referred to as dynamically or actively balanced systems. These systems move with tipping motions that compensate each other. They are allowed to position their feet further away from the COG, which improves their mobility since they can attain higher forward velocities and can make steps with a greater length and a greater height. The consequence is that dynamic balanced systems need very fast control action combined with short reaction time of the actuators. Note that purely dynamically balanced systems demand continuous active actuation to maintain balance. Common examples are riding a bicycle, and balancing an inverted pendulum.

Systems moving with alternating static and dynamic stable phases during the gait cycle are called *quasi-static* or *quasi-dynamic* balanced systems. This kind of motion, where statically balanced moments are generally only interrupted for brief moments, are more stable than purely dynamic balanced systems but are unfortunately also slower [Regele et al., 2003].

Generally a *gait* of a legged machine is the coordinated movement of the legs to produce locomotion [Hardarson, 1997]. When referring to the classification of legged robots based on the number of legs, one can state that the more legs, the more various gaits are possible. Octapods, hexapods and quadrupeds can have a great variety of gaits due to the number of legs. These systems will not be considered in this work. Humans generally move by a walking motion, which consists of alternating single and double support phases. This walking motion can be either statically or dynamically stable, depending on the walking speed. Human running is a dynamically stable gait with alternating flight phases and single support stance phases. Since this type of dynamic walking consists of periods where all feet leave the ground, the COG does not only leave the support polygon like in most dynamic balanced systems, but during these flight phases there is no support polygon at all. Without any ground contact, no fall-back solution is available, and the system relies on the next step to regain balance. Although with this kind of locomotion biped walking can reach very high velocities, technology today is too poor to fulfill the high demands of the required control system [Regele et al., 2003]. Until now fast running has only been achieved with fixed locomotion parameters, from which the best known examples are the robots built by Mark Raibert [1986]. Note that for a monopod there is only one possible way of moving due to its nature, being hopping, which is in fact running on one leg.

1.3 Known difficulties

The motivation for investing in research on legged robots is clearly their potential for high mobility. Despite the rising number of possible applications and the increase in industrial interest for legged robots, their development is however still in an early stage. A lot of research and money has been put into legged robots, which has resulted in several successful machines, but most of them have never been outside a laboratory. Extensive research will have to be done before intelligent light-weight machines with high power-to-weight-ratio and an acceptable degree of autonomy become reality. This is mainly due to the fact that the control of a legged machine is intrinsically a very complex issue. Some major difficulties for the control system are the following [Ridderström, 1999; Pratt, 2000]:

- The robot kinematics and dynamics are non-linear and difficult to accurately model. Robot parameters such as centers of mass, moments of inertia, payload, etc are not known exactly
- The dynamics of the robot depend on which legs are on the ground. In other words, the dynamics change whenever the robot makes a transition between a single support phase and a double support phase or a flight phase, and vice-versa. Moreover, exchange of leg support is accompanied by an impact disturbing the robot's motion
- A legged robot is submitted to intermittent holonomic and nonholonomic constraints
- The environment is unknown and dynamic. The surface might be elastic, sticky, soft or stiff
- Vertical contact forces on the surface are unilateral, meaning that they can not pull the robot against the surface
- The goal of keeping balance is difficult to decompose into actuator commands
- A legged system generally has a lot of degrees of freedom

This work will focus on the hopping motion of monopods and the dynamic walking motion of bipeds. A monopod is difficult to control because of the presence of flight phases and the heavy impact due to the collision of the robot with the ground at the end of each flight phase. Biped walkers, and particularly the human-like walking robots, have the significant disadvantage of a high global center of gravity in combination with a small contact surface with the ground. This results in a small support polygon, meaning that there is a high risk for postural instability.

Even if the control system of a legged robot is able to cope with all these difficulties, then it is still the question if the leg systems are fast enough to perform the

motion commands. Recently an interesting study funded by the European Commission, called ProRobot², which concentrated particularly on the state-of-the-art of humanoid robot technology, has published its results. A short overview of the study can be found in [Regele et al., 2003]. The real bottleneck for dynamic walking seems to be the fact that the reaction speed of the leg system is slowed down by the low speed of the actuators. The actuators used are mostly high precision electrical actuators, which suffer from a low reaction speed and low torques, which limits the operating speeds of the joints they act on. This logically limits the maximum walking speed. Another limiting factor are the sensors used by legged robots for sensing the surrounding environment. Dynamic balanced systems need those sensors in order to detect the good spots for positioning their feet. These sensors mostly work with optical cameras and image processing, which makes them slower than the internal sensors used for feedback information. As a result, bipeds today only achieve a quasi-dynamic walking style. Real robust dynamical walking and running machines until now simply do not exist. Based on thorough analysis performed during the ProRobot Study, it is found that it will take up to ten years before real dynamic bipedal walking will be achieved. A real running motion is only expected to be feasible in up to twenty years. In fig 1.1 taken from [Regele et al., 2003], a prediction for the future development of biped locomotion is given. Note that the legged machines without any kind of intelligence, and which do not interact with their environment, are not considered in this figure. For example, Raibert's running robots (see section 1.5.1) ran with constant objective locomotion parameters without sensing the environment, and can today not be used for any application.

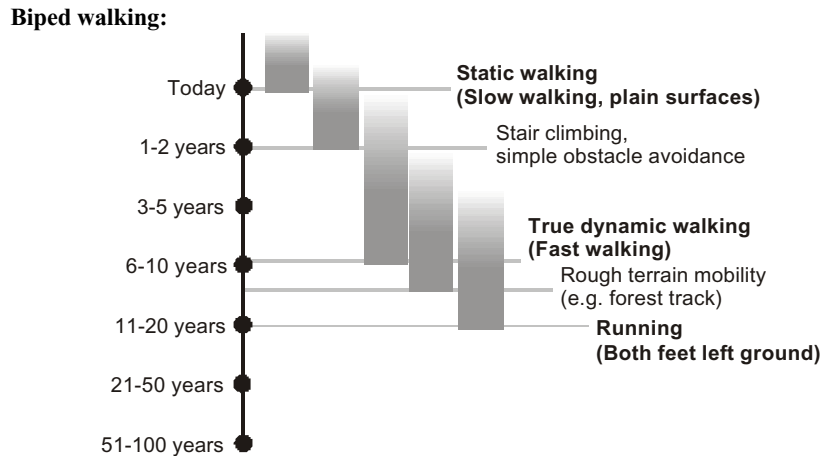


Figure 1.1: Future predictions for feasibility of biped walking

²<http://www.aboutrobotics.net/>

So the conclusion is that despite the fact that bipeds have potential advantages when compared to wheeled vehicles, none of the machines existing today can exploit these advantages. Therefore, when looking at speed, stability and performance, wheeled vehicles are still superior [Regele et al., 2003].

1.4 Scope of the thesis

1.4.1 Objectives

This thesis aims to contribute to the study of dynamically balanced legged robots, by proposing a strategy for generating reference trajectories for the different joints of a robot. The strategy deals with the generation of feasible motion patterns based on a limited number of calculations, in order to avoid long computation times that are generally associated with other methods, e.g. based on numerical optimization techniques, or strategies which incorporate the numerical solution of dynamical equations. Due to the limited computation times needed to generate reference trajectories, the developed method can possibly become the basis for a real-time control algorithm.

The underlying idea of the planning method is to steer the dynamics of a robot in a kinematical way. Basically two different tasks for the algorithm are distinguished. The first task is to define trajectories for all the robot links such that a number of objective locomotion parameters, such as horizontal velocity, step length, etc reach specific desired values. These objective parameters can be altered during the locomotion process, in order to make motion on irregular terrain possible. The second task is to establish the trajectories for the different leg links by taking the upper body motion into account. A legged robot generally consists of legs and an upper body. The upper body usually contains the on-board hard-ware of the control system, as well as the batteries in case of electric actuation, or a pressurized vessel or a compressor in case of pneumatic actuation. In most cases it is therefore the robot link with the largest mass and inertia. The developed planning strategy uses the angular momentum equation to estimate the *natural* dynamics of the upper body, or in other words, the motion of the upper body when it is unactuated. The trajectories for the leg links are then established such that the natural behaviour of the upper body approximates a given desired behaviour. When this desired behaviour, which will be prescribed by a polynomial function, is used as a reference trajectory for the upper body actuator, then the work of this actuator is limited to overcoming the minor differences between the natural and the desired trajectory. The advantage of this strategy is that the resulting motion of the Zero Moment Point [Vukobratovic et al., 1990] during the support phases stays well within the boundaries of the predefined stability region.

The thesis consists in fact of two main parts. The first part focusses on one-legged hopping robots, whereas the second part deals with a walking biped. For

both mechanisms, each performing another type of motion, a specific trajectory generation strategy will be established. Although these strategies are based on the same fundamental principles, they differ particularly because of the presence of flight phases for a hopping robot, and the presence of double support phases for a walking robot.

1.4.2 Evolution

Inspired by the realizations of Mark Raibert, who is a pioneer in the field of hopping and running robots (see section 1.5.1), the Multibody Mechanics Research group of the Vrije Universiteit Brussel started focusing on hopping monopods in the nineties. Being challenged by the fact that no control strategies for the latter machines existed that allow locomotion on irregular terrain, the research of our group specifically addressed that subject. First a strategy has been developed for a hopping monopod with an articulated leg and an upper body being attached to the leg in its center of gravity. This model has no foot and is therefore an underactuated mechanism in both the stance phases and the flight phases. The second model being studied contains a foot and has an upper body placed vertically on the leg, with its center of gravity located above the hip joint, meaning that destabilizing moments on the upper body are generated by gravity. The developed strategy was successfully expanded for application on the new model. The development of this technique forms the first topic of this work.

A parallel research activity of the Multibody Mechanics Research Group, was the development of a novel pneumatic actuator called the PPAM [Daerden, 1999]. Due to its potential for being a suitable actuator for legged vehicles, a prototype of a planar walking robot called Lucy, actuated by these pleated pneumatic artificial muscles, has been built [Verrelst et al., 2002]. Figure 1.2 shows a picture of the robot Lucy. This experimental setup is the ideal opportunity for combining both research fields in one application. Since Lucy is designed to become a planar dynamic walking biped, a control algorithm is needed in order to generate dynamically stable motion patterns. It is the development of a trajectory generation strategy for a walking biped such as Lucy that forms the second part of this thesis. Due to certain similarities between the dynamic principles for dynamic walking and running, some of the basics of the former technique for monopods could be used. However, due to the absence of flight phases and the presence of double support phases in a walking motion, significant differences appear. The technique is developed initially for a model walking with instantaneous double support phases, in order to study all the conceptual features of the single support phase. In a second stage, the double support phase is added, such that a more realistic motion pattern is generated.

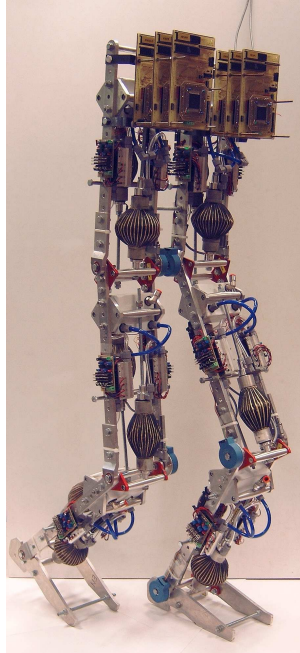


Figure 1.2: Walking biped Lucy

1.5 Historical overview

1.5.1 Hopping and running robots: history

As was mentioned before, running is a specific type of legged locomotion, consisting of intermittent ballistic periods with all feet off the ground. The first robot ever built, achieving such a motion, was built in Japan by Matsuoka [1979, 1980]. His robot was a planar one-legged hopper moving in an artificial low gravity environment. It was sliding on an inclined plane and was thrust by an electric solenoid. The resulting motion was an extreme form of running where nearly the whole hop cycle was spent in flight.

The robots developed in the United States by Mark Raibert are until now the most impressive running robots. The basic control algorithm used in all his robots consists of three decoupled parts: energy stored in a pneumatic spring in the legs is modulated to manipulate hopping height, forward speed is controlled by positioning the legs during the flight phase and body attitude is regulated during the stance phase. Based on this principle a one-legged robot hopping in 2D was constructed [Raibert and Brown Jr., 1984], a one-legged robot hopping in 3D [Raibert et al., 1984], a running robot on four legs [Raibert et al., 1986; Raibert, 1990], a bipedal robot running and being able to execute a forward flip in 2D [Hodgins et al., 1986;

Hodgins and Raibert, 1990], as well as a bipedal robot running and executing a somersault in 3D [Playter and Raibert, 1992]. The geometry of Raibert's 3D hopping biped is shown in figure 1.3, taken from [Playter and Raibert, 1992].

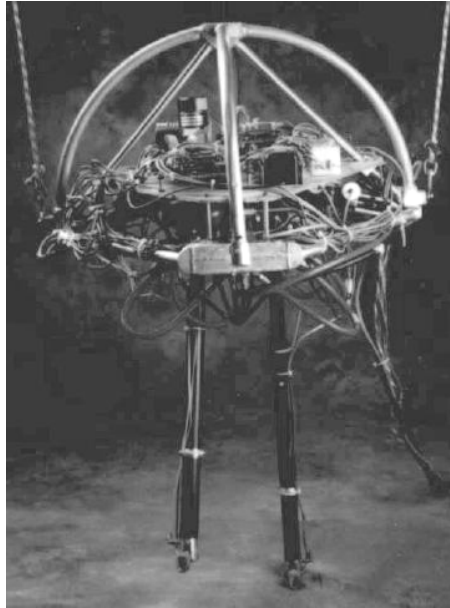


Figure 1.3: Raibert's 3D hopping biped

In Russia, hopping and running robots have also been studied, although mostly on a theoretical basis. Larin [1979, 1980] has considered the stabilization problem of a running bipedal robot. Lapshin [1983] initially studied four-legged and six-legged running robots, and later also the one-legged hopping robot developed by Raibert [Lapshin, 1991a,b, 1992], focusing on the proper orientation of the legs before touch-down.

Inspired by the success of Raibert's work, numerous authors used his one-legged model for further controller development and stability analysis. In order to improve Raibert's control algorithm, Sznajder and Damborg [1989] used an adaptive control algorithm for both horizontal and vertical motion of a 2D hopping robot, deriving a rather simple analytical solution for vertical motion control. Helferty et al. [1989] studied the feasibility of using neural networks to control vertical hopping, resulting in a stable limit cycle in the state space of the robot. Li and He [1990] also studied the robot's limit cycle, using the so called energy-balance method and compared this method to discrete dynamical system theory [Li and He, 1990]. They also showed that by using the angular momentum constraint it is possible to control the orientation of a one-legged hopping robot during its flight phase, which is an

observation that will be used throughout this work too [Li and Montgomery, 1990]. Further studies on the limit cycle of a hopping robot have been made by Koditschek and Bühler [1991]. They showed that the theory of uni-modal return maps can be applied to the dynamics of a one-legged robot. They modelled the robot as a point mass supported by a massless leg acting as a pneumatic spring and studied vertical hopping only. M'Closkey and Burdick [1991]; Vakakis et al. [1991]; M'Closkey and Burdick [1993] showed that the same model exhibits period doubling and chaotic behaviour, both in 1-dimensional and 2-dimensional hopping. A more generally valid feedback control algorithm for a hopping robot, based on return maps, was developed by Ostrowski and Burdick [1993].

Papantoniou [1991a,b] built a complex planar hopping robot actuated by two electrical motors and used a modified version of Raibert's algorithm. Papantoniou tested Raibert's design and control algorithm on his electrically actuated robot in order to increase the power efficiency of a legged system. Except for the first one-legged planar hopper, which was pneumatically actuated, Raibert's designs were actuated by powerful hydraulic actuators and relied on pneumatics for the leg spring only. This permitted him to focus on robot design and control without having to consider actuator power limits. In order to cope with the power limitations of electrical actuation, Papantoniou's one-legged robot had to move with a significantly increased stance phase duration. Rad et al. [1993] presented a leg design with electrical actuation using a ball screw. They employed an open loop continuous torque strategy during the stance phase to control the hopping height. Experiments with their monopod showed that electrical actuation really is feasible for dynamically balanced legged robots, despite severe power limitations. They managed to build a fast running robot ($1.2m/s$), being more energy efficient than previously built hopping robots [Gregorio et al., 1994, 1997].

Meanwhile in the nineties, literature concerning the vertical hopping height control for the Raibert planar hopper kept on growing, although now based on models using electrical actuation. An approach involving a near-inverse of the system dynamics, based on off-line synthesis and inverse dynamics, was suggested by Prosser and Kam [1992a,b]. Their method was later enhanced by applying on-line estimation of controller parameters by Lebaudy et al. [1993]. In Canada, Mehrandezh et al. [1995] again considered the vertical jumping height control for a one-legged hopper. They derived an easy to implement open loop control law using top-to-top tracking of the robot, and reduced the number of hops required to reach a steady hopping height, also for an electrically actuated model. In contrast to the former authors, Schwind and Koditschek [1995] focussed on the control of forward velocity. They used a model where control was solely applied in the forward placement of the foot at touch-down. They derived a closed-form return map, in order to study analytically the stability of the forward velocity equilibrium behaviours.

Another robot worth mentioning is the one developed by Gokan et al. [1994] in Japan. They constructed a rope-hopping robot and assured its balance by controlling the position of the global center of gravity of the system.

Important contributions to energy efficient control for hopping robots have been made by a research group at the McGill University in Canada. Specific gaits associated with no dissipation of energy are called natural or passive regimes, of which the existence depends on mechanical design, and more specifically on the use of springs. Ahmadi and Buehler [1995, 1997] proposed an analysis and a method for the determination of trajectories which approximate the ones associated with the natural regimes. They adapted Raibert's controller in order to monitor in continuous time the tracking of the predetermined trajectories. The idea is to use control just for stabilizing the passive regimes. They performed simulations and observed a substantial reduction of the energy consumption. Later, by using their control strategy, they built an electrically actuated hopping robot, that could run at $1.2m/s$ with a power expenditure of only $48W$ [Ahmadi and Buehler, 1999]. Their ARL Monopod³ is depicted in figure 1.4.

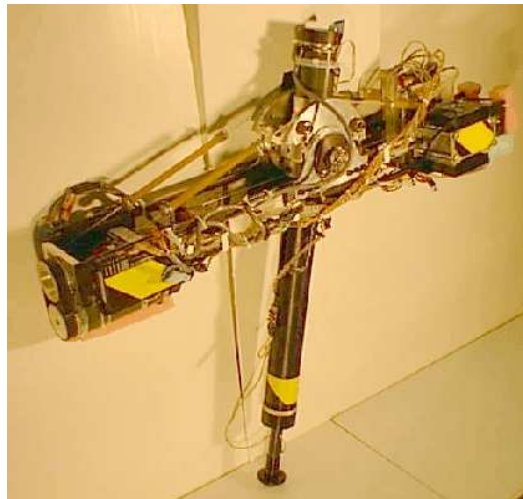


Figure 1.4: The ARL Monopod II

In France, another group also addressed the problem of energy-efficient running legged mechanisms. They viewed the natural regimes as periodic orbits of the system which can be mapped and stabilized on a return map [François and Samson, 1997, 1998]. The control inputs were no longer calculated as continuous inputs as was done by Ahmadi and Buehler, but consisted of piecewise-constant forces calculated at the beginning of each step and were applied at suitable distributed time instants.

Since the late-nineties, the Multibody Mechanics Research group at the Vrije Universiteit Brussel started developing control strategies for hopping robots. As

³<http://www.cim.mcgill.ca/~arlweb/monopod2/monopod2.htm>

an alternative for Raibert's algorithm, which is basically suitable for steady hopping patterns, De Man et al. [1996] developed a powerful trajectory generation strategy based on a number of objective locomotion parameters, being horizontal velocity, step length and step height. The technique was demonstrated on a model similar to the one used by Raibert, being a model with a telescopic leg and a horizontally placed upper body with its COG located at the hip joint. The model was able to change the values of the objective parameters from one hop to another, making the strategy useful for locomotion on irregular terrain. Unfortunately a control strategy for the upper body attitude was not added. Later, this strategy was implemented on a model with an articulated leg, thus introducing a higher degree of non-linearity [De Man et al., 1997, 1998a,b,c]. The trajectory generation strategy was adapted by using the angular momentum equation during the stance phase, in order to control also the upper body motion. Vermeulen et al. [2000] significantly improved the applied strategy by showing the use of non-zero angular momentum during the flight phase of the studied model. Later, the same strategy was implemented on a more complex model of the hopping robot, having a vertically placed upper body with the COG not coinciding with the hip joint, and a foot actuated during the stance phase [Vermeulen et al., 2003]. These strategies form the basis of this work and will thus be extensively described in the following chapters.

Ben Brown, a former coworker of Mark Raibert, came up with an original design for a novel planar hopping robot, consisting of a highly resilient leg resembling an archer's bow [Brown and Zeglin, 1998; Zeglin and Brown, 1998]. The robot features a passive stance phase and a natural pitch stability. It is controlled with actuators that configure the leg angle and stored leg energy during the flight phase. During the stance phase, the actuators are decoupled from the leg and the stored energy is released. Later their idea was implemented on a 3D Bow Leg, with a gimbal used for the hip instead of a pin joint [Zeglin and Brown Jr, 2002]. A picture of the 3D Bow Leg robot⁴ is shown in figure 1.5.

In France, Chevallereau and Aoustin [1999] have been studying running robots as well, although on a theoretical basis. They simulated the motion of a planar running biped without ankle actuators and developed an off-line trajectory generation strategy. The coefficients of polynomial reference trajectories for the different robot joints were used as optimization variables in order to numerically minimize the input energy to produce a required gait. The resulting reference trajectories guarantee that all objectives concerning the gait parameters are fulfilled and that the motion is cyclic. Chevallereau [2002] proposed a control strategy to follow the designed reference trajectories, to make the simulated runner converge to the desired cyclic motion. An on-line adaptation of the reference trajectories was proposed, in order to become a convenient final state of the robot during the flight phase.

Kajita, Nagasaki, Yokoi, Kaneko and Tanie [2002] proposed a method to generate

⁴source: <http://zuff.info/BowLegHopper/Images.html>

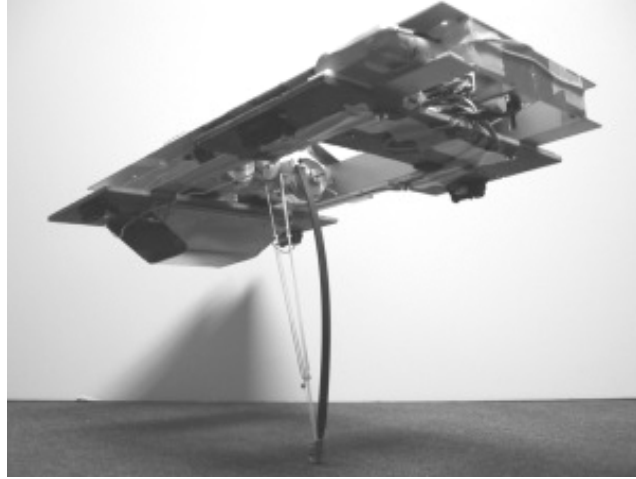


Figure 1.5: The 3D bow leg hopping robot

running patterns for the existing humanoid robot HRP1 developed in Japan, using the dynamics of an inverted pendulum during the stance phase. During the flight phase, running speed was controlled by using Raibert's algorithm based on foot positioning [Raibert, 1986]. They simulated high speed running for their model in order to evaluate the required performance of the actuators. Their robot seems to consume a power which is ten times the power consumed by humans performing the same motion, which indicates that the running pattern has to be improved.

Also in Japan, recently a new one-legged hopping robot was simulated and constructed by Hyon et al. [2003]. Their robot Kenken has a structure based on the hind-limb model of a dog, consisting of three links. The robot Kenken⁵ is depicted in figure 1.6. It uses two hydraulic actuators as muscles and linear springs as a tendon. The controller is empirically derived based on characteristic dynamics. Earlier experiments with an articulated hopper with a structure based on an animal leg were performed at the MIT by Lee and Raibert [1991] and Zeglin [1991]. The latter built the planar robot Uniuroo having a leg similar to a kangaroo.

Recently an astonishing new humanoid robot was revealed by Sony Corporation⁶, which is depicted in figure 1.7. They developed an integrated walking, running and jumping motion control technology that enables the humanoid robot QRIO to smoothly combine conventional walking movement with new running and jumping motions. For the running motion, QRIO takes steps that, over a period of about 10 seconds, get progressively faster until maximum speed is achieved. That speed is about 14 meters per minute, which corresponds more to a slow jog than running. The main reason for the low running speed is the fact that the robot only leaves

⁵http://www.mechatronics.mech.tohoku.ac.jp/research/Kenken/kenken_en.htm#kenken

⁶<http://www.sony.net/SonyInfo/QRIO/>

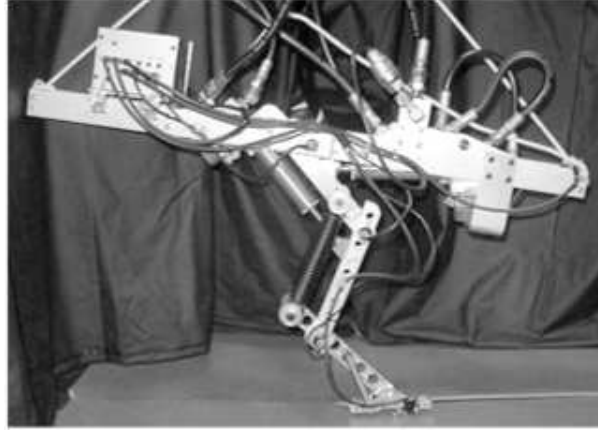


Figure 1.6: The hopping robot Kenken

the ground with both feet for about twenty milliseconds. Since QRIO runs by accelerating from zero to its maximum velocity, and afterwards decelerates back to zero velocity, it is nevertheless a fantastic accomplishment, which certainly opens the door for new revelations by Sony and its competitors.



Figure 1.7: Sony's humanoid QRIO

1.5.2 Walking bipeds: state-of-the-art

Ever since the early activities of Prof. Kato at Waseda University in Japan, an enormous number of powered bipedal walking robots have been built by various groups all over the world. Due to the large number of existing publications on the

subject, a detailed historical overview of walking bipeds has been presented many times. Todd [1985] gives an overview of early walking history and describes the basic principles of walking robots. Raibert [1986] extensively describes the general principles of dynamically balanced machines and gives a historical overview of the legged machines using this principle. Especially in Japan, several research groups have been working on biped robots. Furusho and Sano [1990] elegantly summarized the Japanese activities between the early seventies and 1990 in a well-ordered table of related work. Pratt [2000] gives an excellent overview of powered bipedal robots from the early beginning until the year 2000. As mentioned higher, the ProRobot study⁷, reported extensively on the state-of-the-art of humanoid robot technology. Their results give an overview of the humanoids developed all over the world, between the eighties and the year 2003. So instead of giving a complete chronological overview of walking bipeds, only a few of the recently developed walking bipeds are mentioned in this work. Note that at this point an overview is given on general accomplishments in the field of walking bipeds. An extensive overview, specifically focusing on the subject of trajectory generation strategies, will be given in chapter 5.

Honda is without any doubt the leading company in the development of humanoid robot technology. In 1996, they revealed the development of the robot P2 [Hirai et al., 1998], a humanoid with 6 actuated degrees of freedom in each leg. A somewhat more advanced version, called P3, was revealed in 1997. Both robots were mainly controlled by playing pre-recorded joint trajectories, acquired from measurements on humans. Three additional controllers were added to modify these trajectories, being a ground reaction force controller, a Zero Moment Point (ZMP) controller and a foot landing position controller. With this control scheme, the robot was able to walk up and down stairs and to turn in place. The ground reaction force controller in combination with a compliant ankle allowed the robot to walk on an uneven surface. Figure 1.8 shows both robots⁸ P2 and P3, where it can be seen that P3 was made significantly smaller. A even more evolved version of P3 was released by Honda under the name Asimo. The latest version of Asimo walks more smoothly, more flexibly than its predecessors. It is able to move freely in unstructured environments, including climbing and descending stairways and slopes. Asimo can walk with speeds up to 1.6 km/h, and can continuously change directions. Moreover, it is able to understand human gestures and movements as well as sounds, such that it can interact with humans. Figure 1.9 shows the robot Asimo⁹ while descending stairs. It is about 120 cm tall and weighs approximately 43 kg.

The robot HRP-2P, is a humanoid robot developed at Kawada Industries in Japan, within the framework of the Humanoid Robotics Project. The robot was designed at the National Institute of Advanced Industrial Science and Technology, and is

⁷<http://www.aboutrobotics.net/>

⁸source: <http://www.plyojump.com/pseries.html>

⁹source: <http://www.plyojump.com/asimo.html>

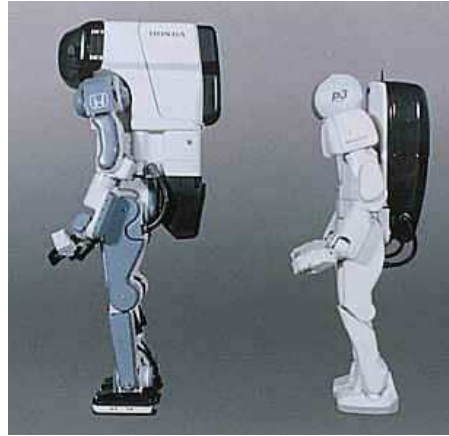


Figure 1.8: Honda humanoid robots P2 and P3



Figure 1.9: Honda's robot Asimo

approximately 154 cm tall and weighs about 58 kg including batteries. It is comparable to the Honda robots in fluidity of motion and advanced navigation. It is nearly unique in having a flexible hip, which allows the robot to walk in narrow paths. Due to a high density electronics installation, HRP-2P does not need a backpack, containing batteries etc. HRP-2P is even able to lie down and stand up again on its own. It is depicted in figure 1.10, on a photograph¹⁰ taken at Robodex 2002.

Sony Corporation's robot QRIO was already discussed in section 1.5.1. It was

¹⁰source: <http://www.plyojump.com/hrp.html>



Figure 1.10: Kawada Industries’s HRP-2P

depicted in figure 1.7. By using a real-time gait pattern generation control, QRIO achieves a stable and smooth gait for walking. It is even able to run, although with extremely short flight phase duration, which limits the running speed.

Worth mentioning as the most advanced walking biped in Europe, is the robot Johnnie [Pfeiffer et al., 2003]. Johnnie was built at the Institute for Applied Mechanics at the Technical University of Munich. It can walk on uneven ground and can climb stairs. Moreover, by using a 3D vision system, it is able to negotiate obstacles, by stepping over them or planning a path around them. Johnnie¹¹, being depicted in figure 1.11, is 180 cm tall and weighs 45 kg.

1.6 Outline

Chapters 2, 3 and 4 of the thesis deal with the generation of stable motion patterns for planar one-legged hopping robots. In chapter 2, a simple model is studied, which consists of an articulated leg and an upper body horizontally placed upon the leg. The center of gravity of the upper body coincides with the hip, which causes a decoupled motion of the upper body and the leg. The concept of objective locomotion parameters is introduced, while the use of a non-zero angular momentum during the flight phase is proven by tuning its value such that the upper body motion is stabilized. In chapter 3 a foot is introduced in the model, in order to make it fully actuated during the stance phases. Moreover, the upper body is placed vertically upon the leg, now with its center of gravity not coinciding with the hip joint. In chapter 4, the developed trajectory generation strategy during the stance phase is adapted, such that the position of the Zero Moment point stays in the vicinity of the ankle joint. This is done by exploiting the concept of the natural upper body

¹¹source: <http://www.amm.mw.tu-muenchen.de/index.e.html>



Figure 1.11: Humanoid Johnnie

motion as was described in section 1.4.1.

Chapters 5 and 6 treat the generation of a stable motion for a planar walking biped with actuated feet. In chapter 5, the walking motion considered consists of successive single support phases, separated by instantaneous double support phases, while the impact phase is avoided. The motion is defined based on the concept of objective locomotion parameters, and the upper body is controlled while avoiding postural instability, again by using the concept of natural dynamics. In chapter 6, the double support phase is introduced, and the developed strategy is adapted. Finally, overall conclusions are drawn in chapter 7, where also an enumeration of possible future work is given.

Chapter 2

A hopping robot with decoupled motion of upper body and leg

2.1 Introduction

When speaking about hopping robots, one inevitably has to mention Mark Raibert. The robots developed at the MIT by Raibert [1986] and his team are probably the best-known hopping and running robots all over the world. By using a very simple control algorithm, they built a one-legged hopping robot, a bipedal runner and also a quadrupedal runner, all with telescopic legs. However, the algorithm used by Raibert was basically a steady-state algorithm and had little control on the placement on possible footholds, making its usefulness for locomotion on irregular terrain quite limited [Hodgins, 1989]. It was the challenge to develop an algorithm suitable for irregular terrain that brought the Multibody Mechanics Research Group of the Vrije Universiteit Brussel to focus on one-legged hopping robots. In the late-nineties De Man et al. [1996] developed a powerful trajectory generation strategy based on a number of objective locomotion parameters, being horizontal velocity, step length and step height. The technique was demonstrated on a model similar to the one used by Raibert, being a model with telescopic leg and a horizontally placed upper body with its center of gravity (COG) located at the hip joint. The model was able to change the values of the objective parameters from one hop to another, making the strategy useful for locomotion on irregular terrain. Unfortunately a control strategy for the upper body attitude was not added. Because of the lack of a control methodology for body attitude, a drift on the upper body motion was present. The proposed solution by De Man et al. was to use Raibert's algorithm and switch to the other strategy whenever obstacles had to be cleared, or generally when other values for the objective locomotion parameters were desired. However, still driven by the challenge, De Man et al. [1997, 1998a,b,c] developed an extension to the existing technique, in order to avoid the drift on the upper body motion. This time the method was implemented on a model with an articulated

leg, thus introducing a higher degree of non-linearity. The method to control the upper body motion was based on the design of correction functions, which were added to the nominal trajectories for the leg links. These correction functions did not change the values of the objective locomotion parameters and contained the necessary information to compensate during the stance phase the body rotation introduced during the flight phase. An experimental prototype OLIE (One Leg Is Enough) was built [De Man et al., 1998a,b,c] to test this strategy. Unfortunately, in some cases the correction functions generated by the technique became unrealistic with high frequency components and amplitude and therefore untrackable by the controllers of the leg links, resulting in unstable behaviour. As suggested in [Vermeulen et al., 2000] the reason for this failure was the fact that the imposed behaviour of the upper body by the correction functions differed too much from its natural behaviour. The expression *natural behaviour* is used here to describe the behaviour without the correction functions, or in other words, how the dynamics *wants* the upper body to move when no actuator is used to steer it. According to Vermeulen et al. [2000] the weakness of the former technique seemed to be the improper use of the angular momentum. During the flight phase the angular momentum is conserved. Whenever this momentum is not zero, a drift term is introduced in the control system [De Luca and Oriolo, 1995], [Godhavn et al., 1997]. This drift term is usually seen as a burden and therefore it is mostly set to zero in the case of planar hoppers [Raibert, 1986; De Man et al., 1997, 1998a,b,c]. In several applications, the use of a non-zero angular momentum has however clearly been indicated, as shown by Hodgins and Raibert [1990] and Playter and Raibert [1992] where a biped performs a somersault, by Lefeber et al. [1996] who simulated a monopod performing a somersault, and also by Crawford and Sastry [1995] where a planar diver is performing a 1,5 and 2.5 somersault dive. Moreover, Ramey [1973] showed the significance of the initial angular momentum for a human performing a long jump. Choosing improper values for the momentum clearly resulted in poorer performance. During the flight phase of a hopping robot, the robot rotates its leg forwards, such that a non-zero angular momentum seems logical when rotations of the upper body are desired to be small. It is the scope of this chapter to show that a proper choice of the value of the angular momentum during flight can result in a stable upper body motion for the studied model. Instead of setting its value equal to zero, an expression is established which allows one to calculate the necessary angular momentum during flight, such that a rotation of the upper body originating from the flight phase, is automatically compensated during the next stance phase, meaning that the method exploits the natural motion of the upper body during the stance phase. To test the methodology, a steady hopping pattern of consecutive hops is performed. A proper value for the stance time is chosen, leading to an equal value of the angular momentum with respect to the COG during the consecutive flight phases. The effectiveness of the technique is verified by the simulation results.

In section 2.2, the underlying idea of the developed strategy for tuning the an-

gular momentum of a hopping robot is illustrated by a simple example. The full description of the studied robot model is given in section 2.3. The robot's kinematic aspects are brought up in section 2.4, followed by the dynamics being handled in section 2.5. A detailed mathematical description of the trajectory generation strategy is given in section 2.6. Eventually the technique is tested by the simulation of a steady hopping pattern. The results of this simulation are reported in section 2.7, followed by some conclusions in section 2.8.

2.2 Philosophy

To clearly understand the basic idea of tuning the angular momentum during the flight phase of a hopping robot, a simple example is used. Consider a planar two-link robot as shown in figure 2.1 consisting of a leg and an upper body, connected by the hip joint H.

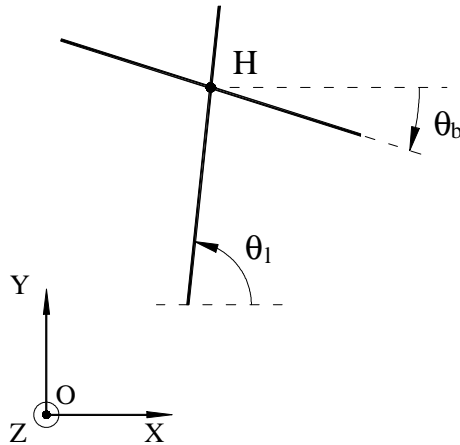


Figure 2.1: Two link planar robot as an example

Suppose that body and leg respectively have moment of inertia I_b and I_l with respect to their own COG. It is well known that for a hopping robot during a ballistic flight phase the angular momentum with respect to the system's COG is conserved, meaning that it is a constant, equal to the initial value when leaving the ground. The angular momentum equation states:

$$\mu_G = \mu_G^0 \quad (2.1)$$

In approximation, the kinematic expression for the angular momentum with respect to the global COG can be written as (it is assumed that the COG's of both rigid bodies are located close to the hip joint):

$$\mu_G \approx I_l \dot{\theta}_l + I_b \dot{\theta}_b \quad (2.2)$$

After integration over the flight phase duration T the angular momentum equation then becomes:

$$\mu_G^0 T \approx I_l \Delta\theta_l + I_b \Delta\theta_b \quad (2.3)$$

where $\Delta\theta_l$ and $\Delta\theta_b$ represent the variation of the corresponding absolute angles measured between the initial and final instance of the flight phase. In literature [Raibert, 1986; De Man et al., 1997] the angular momentum is often chosen zero such that the rotation of the upper body due to the leg swing becomes:

$$\mu_G^0 = 0 \quad \Rightarrow \quad \Delta\theta_b \approx -\frac{I_l}{I_b} \Delta\theta_l \quad (2.4)$$

The conclusion being drawn by the authors is that in order to keep the upper body rotation small, its moment of inertia has to be large in comparison with the one of the leg:

$$I_b \gg I_l \quad \Rightarrow \quad \Delta\theta_b \ll \Delta\theta_l \quad (2.5)$$

The resulting small rotation of the upper body has to be compensated during the next stance phase [Raibert, 1986], where often large actuator power consumption is the consequence of having artificially increased the body moment of inertia.

The alternative approach used in this work, is to determine a value for the angular momentum at the beginning of the flight phase, which causes the upper body rotation to be equal to a given desired value. Moreover, I_b does not necessarily have to be significantly larger than I_l . Suppose e.g. that a zero rotation of the upper body during the flight phase is required, then from equation (2.3) it is found that the following value for the angular momentum would be suitable:

$$\Delta\theta_b^{des} = 0 \quad \Rightarrow \quad \mu_G^{0,des} \approx \frac{I_l}{T} \Delta\theta_l \quad (2.6)$$

In general, when no actuator is explicitly steering the upper body angle during the stance phase, the upper body will rotate due to the dynamics of the system. This means that trying to realize a zero rotation during the stance phase will consume energy, even if the upper body rotation during the flight phase was zero. The strategy applied in this work calculates the rotation of the upper body during the stance phase, and uses this value to calculate an appropriate value for the angular momentum with respect to G during the flight phase. Suppose that during the stance phase a rotation $\Delta\theta_b^*$ occurs, then:

$$\Delta\theta_b^{des} = -\Delta\theta_b^* \quad \Rightarrow \quad \mu_G^{0,des} \approx \frac{1}{T} (I_l \Delta\theta_l - I_b \Delta\theta_b^*) \quad (2.7)$$

and this value for the angular momentum will cause the upper body rotation during the flight phase and stance phase respectively to have equal and opposite values, meaning that no extra actuator action would be required to become zero rotation over one full hop.

The strategy for upper body motion control being developed in this chapter is based on the principle used in this example. The studied model is however more complex, since it consists of an articulated leg. The exact kinematic expressions and dynamic equations for the model considered will be derived, rather than using simplified expressions as was done here.

2.3 General description of the studied model

The gait of a hopping robot can be seen as a sequence of steps, each composed of a stance phase where the robot prepares to bounce up, and a flight phase during which the robot has no contact with the ground [François and Samson, 1998]. These phases are separated by instantaneous transitions called *take-off* and *touch-down* respectively. Throughout this work, the indexes *to* and *td* will be used to characterize all variables at the time step of these transitions. At the instance of touch-down, a collision of the leg with the ground occurs. This collision is assumed to be an inelastic impulsive impact, introducing discontinuities on the generalized velocities. Therefore a distinction is made between the instance before the occurrence of the shock (being touch-down) and the instance immediately after the shock. An index *+* will be used to characterize the variables at the latter instance.

The robot model considered in this chapter is depicted in figure 2.2, where it is shown at the instance of take-off and touch-down. The model geometry as well as all the lengths, mass and inertial parameters are based on the experimental prototype OLIE once built at the Department of Mechanical Engineering at the Vrije Universiteit Brussel.

To be able to study the conceptual features of a running machine, such as its underactuated and nonholonomic nature, without unnecessarily increasing the complexity, only one leg is considered. For simplicity reasons the motion is restricted to the sagittal plane.

The simplified model of the robot is a planar multibody system, consisting of three segments: a lower leg (segment 1), an upper leg (segment 2) and an upper body (segment 3). The different links are connected to each other through rotational uniaxial joints, generally called pin joints.

The length of the *i*-th link is l_i , its mass is m_i and the moment of inertia around its center of mass G_i is I_i . The absolute angle between the horizontal axis and the *i*-th segment is θ_i . The knee angle is defined as the relative angle between lower and upper leg $\theta_{12} = \theta_2 - \theta_1$, and the hip angle as the relative angle between upper leg and body $\theta_{23} = \theta_3 - \theta_2$.

The joint axis position of the connection between the upper body and the upper leg will be referred to as the hip and is represented by point H. Analogously, the joint axis position of the connection between upper and lower leg will be referred

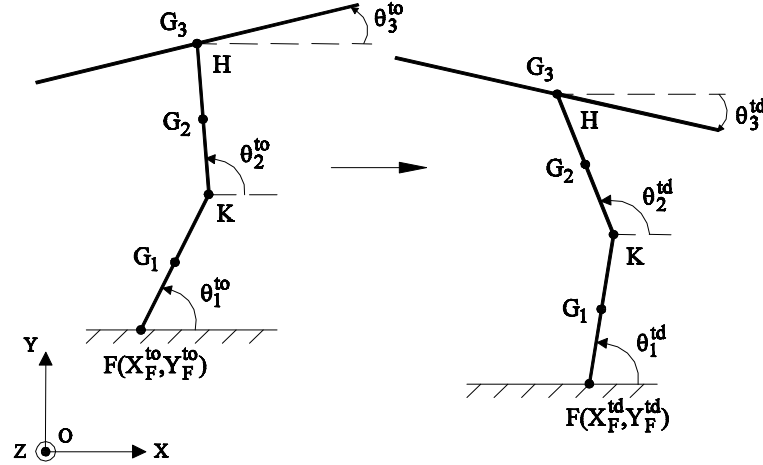


Figure 2.2: Robot at take-off (to) and at touch-down (td)

to as the knee and is represented by point K. Since the robot has no foot link, contact of the robot with the ground will be made by the lowest point of the lower leg. This point will be virtually considered as the foot and is called F. The location of the center of mass G_1 of the lower leg and the location of the center of mass G_2 of the upper leg are given by $FG_1 = \alpha l_1$ and $KG_2 = \beta l_2$, where $0 < \alpha, \beta < 1$. In this model the center of mass G_3 of the body coincides with the hip. In chapter 3 a more general model will be studied.

The inertial parameters of the robot are given in table 2.1. The total mass of the

i	Length l_i (m)	Mass m_i (kg)	Moment of Inertia I_i (kgm^2)
1	0.342	1.781	0.0138
2	0.308	1.373	0.0218
3	0.666	8.507	0.7979

Table 2.1: Inertial parameters of the monopod

model is 11.66 kg. The positions of the centers of mass of lower and upper leg are determined by the values of α and β respectively, as mentioned higher. For OLIE those values are the following:

$$\alpha = 0.868$$

$$\beta = 0.557$$

As is shown in figure 2.3 there are two actuators present, being placed at the hip and knee joint respectively. These actuators will be used to steer the angles θ_1 and

θ_2 . During the flight phase, the robot has five DOF and during the stance phase three DOF, such that the robot is underactuated during both phases of the motion.

2.4 Kinematics

The fact that the COG G_3 of the upper body coincides with the hip, leads to a decoupling between leg motion and body rotation. The angle θ_3 which describes the orientation of the upper body does not appear in the expression of the position of the global COG G . It has therefore no influence on the values of the different objective parameters. During the flight phase the robot has no contact with the ground. The system's motion can then be described by a translation of the COG and a rotation around the COG. The internal configuration can be changed by steering the angles θ_1 and θ_2 . During the stance phase the whole system rotates around the foot point F , which is then considered as a virtual pin joint. The configuration can again be changed by steering θ_1 and θ_2 , thereby changing the position of the COG. The kinematical variables of importance are thus the position of the COG and its first and second derivatives, as well as the angular momentum with respect to the COG during flight, and the angular momentum with respect to the foot point F during stance.

2.4.1 Motion of the COG

From figure 2.2, the vectors defining the position of the local COG's for the three links are derived:

$$\overline{OG}_1 = (X_F, Y_F)^T + \alpha l_1 (\cos \theta_1, \sin \theta_1)^T \quad (2.8)$$

$$\overline{OG}_2 = (X_F, Y_F)^T + l_1 (\cos \theta_1, \sin \theta_1)^T + \beta l_2 (\cos \theta_2, \sin \theta_2)^T \quad (2.9)$$

$$\overline{OG}_3 = (X_F, Y_F)^T + l_1 (\cos \theta_1, \sin \theta_1)^T + l_2 (\cos \theta_2, \sin \theta_2)^T \quad (2.10)$$

The position of the global center of gravity G of the robot at a certain time step t is then given by:

$$\overline{OG} = (X_G, Y_G)^T \quad (2.11)$$

with:

$$X_G = X_F + a \cos \theta_1 + b \cos \theta_2 \quad (2.12)$$

$$Y_G = Y_F + a \sin \theta_1 + b \sin \theta_2 \quad (2.13)$$

and:

$$a = (\alpha \eta_1 + \eta_2 + \eta_3) l_1 \quad (2.14)$$

$$b = (\beta\eta_2 + \eta_3)l_2 \quad (2.15)$$

and:

$$\eta_i = \frac{m_i}{\sum_{i=1}^3 m_i} = \frac{m_i}{M} \quad (2.16)$$

where M is the total mass of the robot. Differentiation with respect to time yields the following expressions for the velocity of G:

$$\dot{X}_G = \dot{X}_F - a \sin \theta_1 \dot{\theta}_1 - b \sin \theta_2 \dot{\theta}_2 \quad (2.17)$$

$$\dot{Y}_G = \dot{Y}_F + a \cos \theta_1 \dot{\theta}_1 + b \cos \theta_2 \dot{\theta}_2 \quad (2.18)$$

and for the acceleration of G:

$$\ddot{X}_G = \ddot{X}_F - a(\sin \theta_1 \ddot{\theta}_1 + \cos \theta_1 \dot{\theta}_1^2) - b(\sin \theta_2 \ddot{\theta}_2 + \cos \theta_2 \dot{\theta}_2^2) \quad (2.19)$$

$$\ddot{Y}_G = \ddot{Y}_F + a(\cos \theta_1 \ddot{\theta}_1 - \sin \theta_1 \dot{\theta}_1^2) + b(\cos \theta_2 \ddot{\theta}_2 - \sin \theta_2 \dot{\theta}_2^2) \quad (2.20)$$

2.4.2 Rotation around the COG

The amount of rotation of the robot around its COG can be described by the angular momentum with respect to G. For the 3-link chain considered, this momentum can be calculated with the following general formula [Janssens and Lefeber, 1984]:

$$\bar{\mu}_G = \sum_{i=1}^3 \left(\overline{GG}_i \times m_i \dot{\overline{GG}}_i + I_i \dot{\theta}_i \bar{1}_z \right) \quad (2.21)$$

When writing

$$\overline{GG}_i = \overline{OG}_i - \overline{OG} \quad (i = 1, \dots, 3)$$

the kinematical expressions from section 2.4.1 can be used. The following expression is found for $\bar{\mu}_G$, which is perpendicular to the XY-plane:

$$\bar{\mu}_G = \mu_G \bar{1}_z \quad (2.22)$$

with:

$$\mu_G = c\dot{\theta}_1 + d\dot{\theta}_2 + e(\dot{\theta}_1 + \dot{\theta}_2) \cos(\theta_1 - \theta_2) + f\dot{\theta}_3 \quad (2.23)$$

and the following constants depending on the lengths and the inertial parameters of the links:

$$c = I_1 + \frac{l_1^2}{M} m_1 (m_2 + m_3) (1 - \alpha)^2 \quad (2.24)$$

$$d = I_2 + \frac{l_2^2}{M} \left(m_2 m_3 (1 - \beta)^2 + m_1 m_2 \beta^2 + m_1 m_3 \right) \quad (2.25)$$

$$e = \frac{l_1 l_2}{M} m_1 (\beta m_2 + m_3) (1 - \alpha) \quad (2.26)$$

$$f = I_3 \quad (2.27)$$

Further (2.23) can be rewritten as follows:

$$\mu_G = h + I_3 \dot{\theta}_3 \quad (2.28)$$

with

$$h = c\dot{\theta}_1 + d\dot{\theta}_2 + e(\dot{\theta}_1 + \dot{\theta}_2) \cos(\theta_1 - \theta_2) \quad (2.29)$$

being independent of θ_3 .

2.4.3 Rotation around the foot

During the stance phase, the robot rotates around the foot point F. The amount of rotation of the system can be described by the angular momentum with respect to the foot. This can be calculated with the general formula [Janssens and Lefeber, 1984]:

$$\bar{\mu}_F = \sum_{i=1}^3 \left(\overline{FG}_i \times m_i \dot{\overline{FG}}_i + I_i \dot{\theta}_i \bar{1}_z \right) \quad (2.30)$$

Again the kinematical expressions from section 2.4.1 can be used. The following expression is found for $\bar{\mu}_F$, which is also perpendicular to the XY-plane:

$$\bar{\mu}_F = \mu_F \bar{1}_z \quad (2.31)$$

with:

$$\mu_F = p\dot{\theta}_1 + q\dot{\theta}_2 + r(\dot{\theta}_1 + \dot{\theta}_2) \cos(\theta_1 - \theta_2) + s\dot{\theta}_3 \quad (2.32)$$

and the following constants depending on the lengths and the inertial parameters of the links:

$$p = (\alpha^2 m_1 + m_2 + m_3) l_1^2 + I_1 \quad (2.33)$$

$$q = (\beta^2 m_2 + m_3) l_2^2 + I_2 \quad (2.34)$$

$$r = (\beta m_2 + m_3) l_1 l_2 \quad (2.35)$$

$$s = I_3 \quad (2.36)$$

Further (2.32) can be rewritten as follows:

$$\mu_F = k + I_3 \dot{\theta}_3 \quad (2.37)$$

with

$$k = p\dot{\theta}_1 + q\dot{\theta}_2 + r(\dot{\theta}_1 + \dot{\theta}_2) \cos(\theta_1 - \theta_2) \quad (2.38)$$

being independent of θ_3 .

2.5 Dynamics

2.5.1 Flight phase

During flight the robot has five DOF, so that five generalized coordinates will be needed to fully describe the robot's motion. The robot only has two actuators steering the knee and hip joint angles, so the system is underactuated with three degrees of underactuation. Due to the ballistic motion, three constraints acting on the generalized coordinates can however be found. These constraints can be derived by applying the linear and angular momentum theorem to the entire robot. In this section, the three constraints are established. Further the complete dynamic model of the robot will be derived, such that the equations of motion for the flight phase of the robot are obtained in a standard matrix form. Eventually simple expressions for the torques corresponding to the actuators in knee and hip will be found.

Linear momentum theorem

When neglecting air drag and other possible friction forces due to any physical system used to restrict the robot's motion to the sagittal plane, during the ballistic flight phase the COG of the robot tracks a parabolic trajectory. It can be considered as an object in free fall. The linear momentum theorem is given by [Janssens and Lefeber, 1984]:

$$M\bar{a}_G = \sum_k \bar{F}_k^e \quad (2.39)$$

with M being the total mass and \bar{F}_k^e being the external forces acting on the robot. Since the only external force here is due to gravity, applying this theorem to the robot as a whole yields:

$$\ddot{X}_G = 0 \quad (2.40)$$

$$\ddot{Y}_G = -g \quad (2.41)$$

These expressions can be integrated to determine the velocity of G at a certain time step t :

$$\dot{X}_G = \dot{X}_G^{t^o} \quad (2.42)$$

$$\dot{Y}_G = -g(t - t^{t^o}) + \dot{Y}_G^{t^o} \quad (2.43)$$

where $\dot{X}_G^{t^o}$ and $\dot{Y}_G^{t^o}$ are the initial values of the components of the velocity of G . It can be seen that the horizontal velocity is invariant during the flight phase. A second integration yields the position of G at a certain time step:

$$X_G = \dot{X}_G^{t^o}(t - t^{t^o}) + X_G^{t^o} \quad (2.44)$$

$$Y_G = -g \frac{(t - t^{to})^2}{2} + \dot{Y}_G^{to}(t - t^{to}) + Y_G^{to} \quad (2.45)$$

So the touch-down conditions of the robot's COG are completely determined by the take-off conditions.

Angular momentum theorem

The angular momentum theorem with respect to a point P of the robot is given by [Janssens and Lefeber, 1984]:

$$\dot{\bar{\mu}}_P = \sum_k \bar{M}_k^e + M(\bar{v}_G \times \bar{v}_P) \quad (2.46)$$

with \bar{M}_k^e being the momentum with respect to P, caused by the external forces acting on the robot. When applying the angular momentum theorem with respect to the robot's COG, the right hand side is equal to zero since gravity applies at G:

$$\dot{\bar{\mu}}_G = 0 \quad \Leftrightarrow \quad \mu_G = \mu_G^{to} \quad (2.47)$$

meaning that the angular momentum with respect to G is conserved during the flight phase. Introducing the kinematic expression for μ_G results in the following constraint on the generalized velocities:

$$\mu_G^{to} = c\dot{\theta}_1 + d\dot{\theta}_2 + e(\dot{\theta}_1 + \dot{\theta}_2) \cos(\theta_1 - \theta_2) + f\dot{\theta}_3 \quad (2.48)$$

Expression (2.48) represents a system with a cyclic coordinate [Goldstein et al., 2000], being θ_3 . The system Lagrangian is independent of this coordinate, although it does contain the generalized velocity corresponding to this coordinate. Such a constraint leads to a reduced state-space model with the right hand side independent of θ_3 . Mechanical systems with this structure are referred to as non-holonomic Caplygin systems [De Luca and Oriolo, 1995]. When $\dot{\theta}_1$ and $\dot{\theta}_2$ are considered as the inputs of the system, one obtains the following control system with 2 inputs and three states:

$$\begin{aligned} \dot{\theta}_1 &= u_1 \\ \dot{\theta}_2 &= u_2 \\ \dot{\theta}_3 &= \frac{\mu_G^{to}}{I_3} - \frac{e \cos(\theta_1 - \theta_2) + c}{I_3} u_1 - \frac{e \cos(\theta_1 - \theta_2) + d}{I_3} u_2 \end{aligned}$$

When the angular momentum μ_G^{to} is non-zero this is called a nonholonomic system with drift term [De Luca and Oriolo, 1995], [Godhavn et al., 1997]. This is clearly seen when setting the inputs equal to zero. Because of the drift term $\frac{\mu_G^{to}}{I_3}$ no equilibrium is reached. For certain systems, like e.g. a planar diver [Crawford

and Sastry, 1995], the drift term can be very useful in the design of the control law. In other systems, such as free-floating space robots, this may not be the case [Dubowsky and Papadopoulos, 1993], [De Luca and Oriolo, 1995].

Note that a Caplygin system allows one to write the constraint equation (2.48) in an integral form, in order to determine the behaviour of the cyclic coordinate θ_3 :

$$\theta_3 = \theta_3^{t^o} + \frac{\mu_G^{t^o}}{I_3} (t - t^o) - \frac{1}{I_3} \int_{t^o}^t h dt \quad (2.49)$$

The function h was defined in (2.29), and represents the part of the angular momentum resulting from the leg links. Expression (2.49) can be calculated if θ_1 and θ_2 are known functions of t .

Complete dynamic model

During the flight phase the robot has five DOF since it is a planar mechanism consisting of three rigid bodies connected by two pin joints. Two actuators are present at knee and hip respectively, as shown in figure 2.3.

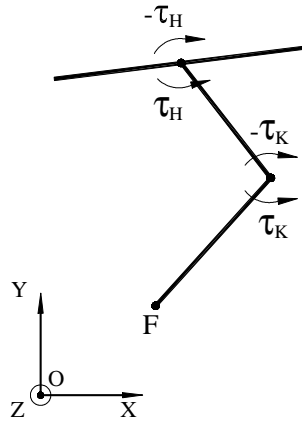


Figure 2.3: Actuators at knee and hip

The dynamic model can be derived by applying the Lagrange equations:

$$\frac{d}{dt} \left\{ \frac{\partial K}{\partial \dot{q}_i} \right\} - \frac{\partial K}{\partial q_i} + \frac{\partial U}{\partial q_i} = Q_i \quad (i = 1 \dots 5) \quad (2.50)$$

where K and U are respectively the total kinetic and potential energy of the robot, and Q_i represent the generalized forces. The generalized coordinates q_i are (see

figure 2.2):

$$q = (\theta_1, \theta_2, \theta_3, X_F, Y_F)^T$$

The positions of the centers of mass of the three links were determined in section 2.4.1. The total potential energy of the robot in flight becomes:

$$U = \sum_{i=1}^3 m_i g Y_{G_i} \quad (2.51)$$

or:

$$\begin{aligned} U = m_1 g (Y_F + \alpha l_1 \sin \theta_1) + m_2 g (Y_F + l_1 \sin \theta_1 + \beta l_2 \sin \theta_2) \\ + m_3 g (Y_F + l_1 \sin \theta_1 + l_2 \sin \theta_2) \end{aligned} \quad (2.52)$$

The total kinetic energy of the robot is given by:

$$K = \sum_{i=1}^3 \left(\frac{1}{2} m_i v_{G_i}^2 + \frac{1}{2} I_i \dot{\theta}_i^2 \right) \quad (2.53)$$

where $\bar{v}_{G_i} = (\dot{X}_{G_i}, \dot{Y}_{G_i})^T$ is the velocity of the center of mass of link i . The kinetic energy of the different links is given by:

$$\begin{aligned} K_1 = \frac{1}{2} (I_1 + m_1 \alpha^2 l_1^2) \dot{\theta}_1^2 \\ + \frac{1}{2} m_1 (\dot{X}_F^2 + \dot{Y}_F^2) \\ + \alpha l_1 m_1 \dot{\theta}_1 (\cos \theta_1 \dot{Y}_F - \sin \theta_1 \dot{X}_F) \end{aligned} \quad (2.54)$$

$$\begin{aligned} K_2 = \frac{1}{2} m_2 l_1^2 \dot{\theta}_1^2 \\ + \frac{1}{2} m_2 (\dot{X}_F^2 + \dot{Y}_F^2) \\ + \frac{1}{2} (I_2 + m_2 \beta^2 l_2^2) \dot{\theta}_2^2 \\ + m_2 \beta l_1 l_2 \cos(\theta_1 - \theta_2) \dot{\theta}_1 \dot{\theta}_2 \\ + l_1 m_2 \dot{\theta}_1 (\cos \theta_1 \dot{Y}_F - \sin \theta_1 \dot{X}_F) \\ + \beta l_2 m_2 \dot{\theta}_2 (\cos \theta_2 \dot{Y}_F - \sin \theta_2 \dot{X}_F) \end{aligned} \quad (2.55)$$

$$\begin{aligned}
K_3 &= \frac{1}{2}I_3\dot{\theta}_3^2 \\
&+ \frac{1}{2}m_3l_1^2\dot{\theta}_1^2 \\
&+ \frac{1}{2}m_3l_2^2\dot{\theta}_2^2 \\
&+ \frac{1}{2}m_3\left(\dot{X}_F^2 + \dot{Y}_F^2\right) \\
&+ m_3l_1l_2\cos(\theta_1 - \theta_2)\dot{\theta}_1\dot{\theta}_2 \\
&+ l_1m_3\dot{\theta}_1\left(\cos\theta_1\dot{Y}_F - \sin\theta_1\dot{X}_F\right) \\
&+ l_2m_3\dot{\theta}_2\left(\cos\theta_2\dot{Y}_F - \sin\theta_2\dot{X}_F\right)
\end{aligned} \tag{2.56}$$

then the total kinetic energy K is found as:

$$K = K_1 + K_2 + K_3 \tag{2.57}$$

The calculation of the derivatives on the lhs of (2.50) is straightforward.

To determine the right hand side of the equations (2.50), an infinitesimal variation on the five DOF is imposed. The variation of the work of the external forces δW can be calculated as:

$$\begin{aligned}
\delta W &= -\tau_K^{fl}(\delta\theta_2 - \delta\theta_1) - \tau_H^{fl}(\delta\theta_3 - \delta\theta_2) \\
&= \tau_K^{fl}\delta\theta_1 + \left(\tau_H^{fl} - \tau_K^{fl}\right)\delta\theta_2 - \tau_H^{fl}\delta\theta_3
\end{aligned} \tag{2.58}$$

Note that there are no forces acting on the foot point F, and only two torques can be exerted, namely the ones at the knee and the hip joint. One has:

$$Q_1 = \tau_K^{fl} \tag{2.59}$$

$$Q_2 = \tau_H^{fl} - \tau_K^{fl} \tag{2.60}$$

$$Q_3 = -\tau_H^{fl} \tag{2.61}$$

$$Q_4 = 0 \tag{2.62}$$

$$Q_5 = 0 \tag{2.63}$$

Since all different terms of (2.50) are known, the five equations of motion can be established. They will be written in the following matrix form [Spong and Vidyasagar, 1989]:

$$D^{fl}[q]\ddot{q} + C^{fl}[q, \dot{q}]\dot{q} + G^{fl}[q] = T^{fl} \tag{2.64}$$

where $D^{fl}[q]$ is the inertia matrix, which is symmetric and positive definite, $C^{fl}[q, \dot{q}]$ is the centrifugal matrix which contains the centrifugal torques (involving \dot{q}_i^2) and the coriolis torques (involving $\dot{q}_i \dot{q}_j$ for $i \neq j$), $G^{fl}[q]$ is the gravitational torque vector, T^{fl} is the external torque vector and $q = (\theta_1, \theta_2, \theta_3, X_F, Y_F)^T$.

The gravitational torque vector becomes:

$$G^{fl}[q] = \begin{bmatrix} \frac{\partial U}{\partial \theta_1} \\ \frac{\partial U}{\partial \theta_2} \\ \frac{\partial U}{\partial \theta_3} \\ \frac{\partial U}{\partial X_F} \\ \frac{\partial U}{\partial Y_F} \end{bmatrix} = \begin{bmatrix} (\alpha m_1 + m_2 + m_3) g l_1 \cos \theta_1 \\ (\beta m_2 + m_3) g l_2 \cos \theta_2 \\ 0 \\ 0 \\ Mg \end{bmatrix} \quad (2.65)$$

The external torque vector is given by:

$$T^{fl} = \begin{bmatrix} Q_1 \\ Q_2 \\ Q_3 \\ Q_4 \\ Q_5 \end{bmatrix} = \begin{bmatrix} \tau_K^{fl} \\ \tau_H^{fl} - \tau_K^{fl} \\ -\tau_H^{fl} \\ 0 \\ 0 \end{bmatrix} \quad (2.66)$$

The elements of the inertia matrix are given by:

$$\begin{aligned} d_{11} &= I_1 + l_1^2 (m_1 \alpha^2 + m_2 + m_3) \\ d_{12} &= d_{21} = l_1 l_2 (\beta m_2 + m_3) \cos (\theta_1 - \theta_2) \\ d_{14} &= d_{41} = -l_1 (\alpha m_1 + m_2 + m_3) \sin \theta_1 \\ d_{15} &= d_{51} = l_1 (\alpha m_1 + m_2 + m_3) \cos \theta_1 \\ d_{22} &= I_2 + l_2^2 (\beta^2 m_2 + m_3) \\ d_{33} &= I_3 \\ d_{24} &= d_{42} = -l_2 (\beta m_2 + m_3) \sin \theta_2 \\ d_{25} &= d_{52} = l_2 (\beta m_2 + m_3) \cos \theta_2 \\ d_{44} &= M \\ d_{55} &= M \end{aligned}$$

and all other elements are zero.

The elements of the centrifugal matrix can be found using the Christoffel symbols c_{ijk} [Spong and Vidyasagar, 1989]. The k,j -th element of the matrix $C^{fl}[q, \dot{q}]$ is

defined as:

$$\begin{aligned} c_{kj} &= \sum_{i=1}^5 c_{ijk} \dot{q}_i \\ &= \sum_{i=1}^5 \frac{1}{2} \left\{ \frac{\partial d_{kj}}{\partial q_i} + \frac{\partial d_{ki}}{\partial q_j} - \frac{\partial d_{ij}}{\partial q_k} \right\} \dot{q}_i \end{aligned} \quad (2.67)$$

with the elements d_{ij} coming from the matrix $D^{fl}[q]$. The elements of the centrifugal matrix become:

$$\begin{aligned} c_{12} &= l_1 l_2 (\beta m_2 + m_3) \sin(\theta_1 - \theta_2) \dot{\theta}_2 \\ c_{21} &= -l_1 l_2 (\beta m_2 + m_3) \sin(\theta_1 - \theta_2) \dot{\theta}_1 \\ c_{41} &= -l_1 (\alpha m_1 + m_2 + m_3) \cos \theta_1 \dot{\theta}_1 \\ c_{42} &= -l_2 (\beta m_2 + m_3) \cos \theta_2 \dot{\theta}_2 \\ c_{51} &= -l_1 (\alpha m_1 + m_2 + m_3) \sin \theta_1 \dot{\theta}_1 \\ c_{52} &= -l_2 (\beta m_2 + m_3) \sin \theta_2 \dot{\theta}_2 \end{aligned}$$

all other elements are zero. Note that there are no coriolis terms, as expected, since the equations of motion are expressed in terms of absolute angles only.

The equations (2.64) contain linear combinations of the three equations resulting from the linear momentum theorem and the angular momentum theorem. After simplification the following expressions are determined for the torques at knee and hip respectively:

$$\tau_K^{fl} = e \sin(\theta_1 - \theta_2) \dot{\theta}_2^2 + c \ddot{\theta}_1 + e \cos(\theta_1 - \theta_2) \ddot{\theta}_2 \quad (2.68)$$

$$\tau_H^{fl} = e \cos(\theta_1 - \theta_2) (\ddot{\theta}_1 + \ddot{\theta}_2) + c \ddot{\theta}_1 + d \ddot{\theta}_2 + e \sin(\theta_1 - \theta_2) (\dot{\theta}_2^2 - \dot{\theta}_1^2) \quad (2.69)$$

with the constants c , d and e respectively defined by (2.24), (2.25) and (2.26).

2.5.2 Impact phase

According to Zheng and Hemami [1985] the discrete variation of the generalized velocities due to the inelastic impulsive impact with the ground can be calculated as follows:

$$\Delta \dot{q} = D^{-1}[q] J^T (J D^{-1}[q] J^T)^{-1} \Delta \dot{O}F \quad (2.70)$$

with

$$\Delta \dot{q} = (\Delta \dot{\theta}_1, \Delta \dot{\theta}_2, \Delta \dot{\theta}_3, \Delta \dot{X}_F, \Delta \dot{Y}_F)^T \quad (2.71)$$

$$\Delta \dot{O}F = (\Delta \dot{X}_F, \Delta \dot{Y}_F)^T \quad (2.72)$$

$$\Delta \dot{q}_i = \dot{q}_i^+ - \dot{q}_i^- = \dot{q}_i^+ - \dot{q}_i^{td} \quad (2.73)$$

$D[q]$ is the generalized inertia matrix as calculated in section 2.5.1 and J being the following Jacobian matrix:

$$J = \left[\frac{\partial S}{\partial \theta} \right] = \begin{bmatrix} \frac{\partial S_1}{\partial \theta_1} & \frac{\partial S_1}{\partial \theta_2} & \frac{\partial S_1}{\partial \theta_3} & \frac{\partial S_1}{\partial X_F} & \frac{\partial S_1}{\partial Y_F} \\ \frac{\partial S_2}{\partial \theta_1} & \frac{\partial S_2}{\partial \theta_2} & \frac{\partial S_2}{\partial \theta_3} & \frac{\partial S_2}{\partial X_F} & \frac{\partial S_2}{\partial Y_F} \end{bmatrix} = \begin{bmatrix} 0 & 0 & 0 & 1 & 0 \\ 0 & 0 & 0 & 0 & 1 \end{bmatrix} \quad (2.74)$$

where S_1 and S_2 are two constraints which express the fact that the robot does not slip and does not bounce back respectively. Note that X_E and Y_E represent the coordinates of the landing position of the foot.

$$S_1 = X_F - X_E = 0 \quad (2.75)$$

$$S_2 = Y_F - Y_E = 0 \quad (2.76)$$

With expression (2.70) the values of $\dot{\theta}_1^+$, $\dot{\theta}_2^+$ and $\dot{\theta}_3^+$ can be calculated (\dot{X}_F^+ and \dot{Y}_F^+ are obviously zero). Note that the inertia matrix is symmetric and positive definite and therefore non-singular, meaning that it is invertible. The matrix $D^{-1}[q]$ is also a symmetric positive definite matrix. Since the Jacobian J has rank 2, the matrix $J D^{-1}[q] J^T$ is also symmetric and positive definite, thus it is invertible [Nakamura, 1991].

To calculate the angular accelerations $\ddot{\theta}_1^+$ and $\ddot{\theta}_2^+$ after the impact, the equations of motion for the stance phase can be used. The motor torques are considered to remain unchanged during the infinitesimal short time interval of the impact. Their values are those measured at the instance of touch-down:

$$\tau_K^+ = \tau_K^{td} \quad (2.77)$$

$$\tau_H^+ = \tau_H^{td} \quad (2.78)$$

Introducing these torques and the values of $\dot{\theta}_1^+$ and $\dot{\theta}_2^+$ in (2.94) and (2.95) leads to a set which can be solved for the accelerations.

Remark: Upper body during impact

Due to the fact that the COG of the upper body G_3 coincides with the hip joint, the angular velocity of the upper body remains unchanged during the shock. Indeed since the percussion on the upper body acts on the hip joint, it can not generate a torque around G_3 , as can be seen in figure 2.4 representing the free body diagram during the shock. Indeed applying the angular momentum theorem during the shock leads to

$$I_3 \left(\dot{\theta}_3^+ - \dot{\theta}_3^{td} \right) = 0 \quad \Rightarrow \quad \dot{\theta}_3^+ = \dot{\theta}_3^{td} \quad (2.79)$$

The same is true for the angular acceleration of the upper body, as can easily be seen in fig. 2.5. Note that \bar{R}_3 is an internal reaction force. Applying the angular

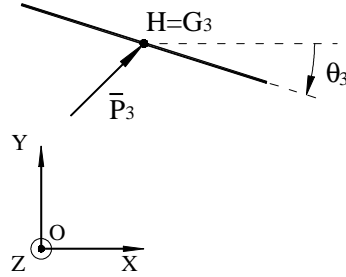


Figure 2.4: Percussion on upper body during shock

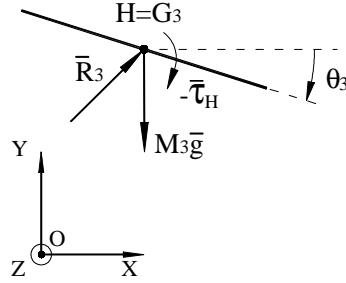


Figure 2.5: Free body diagram upper body before and after shock

momentum theorem before and after the shock gives:

$$I_3 \ddot{\theta}_3^{td} = -\tau_H^{td} \quad (2.80)$$

$$I_3 \ddot{\theta}_3^+ = -\tau_H^+ \quad (2.81)$$

and taking (2.78) into account leads to:

$$\ddot{\theta}_3^+ = \ddot{\theta}_3^{td} \quad (2.82)$$

2.5.3 Stance phase

During the stance phase, when assuming a non-slippery rigid ground, the robot has three DOF. Due to the fact that no foot torque is applied, the robot is still an underactuated mechanism, with one degree of underactuation. When applying the angular momentum theorem to the entire robot with respect to the foot, a constraint on the generalized coordinates can be found.

Angular momentum theorem

When writing the angular momentum theorem with respect to the foot point F, the external ground reaction forces vanish and the only external force present is

the gravity force. Applying (2.46) in F yields (note that F is considered as a fixed point such that $\bar{v}_F = 0$):

$$\dot{\mu}_F = \overline{FG} \times M\bar{g} \quad (2.83)$$

Or when integrating over time and considering only the non-zero z-component which is perpendicular to the plane of motion:

$$\mu_F = \mu_F^+ - Mg \int_{t^+}^t (X_G - X_F) dt \quad (2.84)$$

with μ_F^+ representing the angular momentum with respect to the foot after impact:

$$\mu_F^+ = \mu_F^{td} + \Delta\mu_F^{shock} \quad (2.85)$$

Since the impulsive impact occurs at the foot point F, the percussions can not generate a torque around F. Therefore the angular momentum with respect to F can theoretically not change during the impact:

$$\Delta\mu_F^{shock} = 0 \quad \Leftrightarrow \quad \mu_F^+ = \mu_F^{td} \quad (2.86)$$

For a real robot, the variation of the angular momentum with respect to the foot should be calculated by measuring the joint velocities before and after the shock. Since this is difficult to realize in practice, the values of the angular velocities are often predicted with the impulsive impact model.

Introducing (2.37) and assuming that the coordinate system is located at the supporting foot ($X_F = 0$) gives

$$k + I_3\dot{\theta}_3 = \mu_F^+ - Mg \int_{t^+}^t X_G dt \quad (2.87)$$

or:

$$\dot{\theta}_3 = \frac{1}{I_3} \left[\mu_F^+ - k - Mg \int_{t^+}^t X_G dt \right] \quad (2.88)$$

Note that, due to the fact that the COG of the upper body G_3 is located at the hip joint, again the right hand side is independent of θ_3 . This makes it possible to write the constraint in an integral form to determine the value of θ_3 at all times during the stance phase.

Complete dynamic model

The equations of motion for the stance phase are found analogously as in section 2.5.1. The Lagrange equations are now expressed in terms of the following generalized coordinates q_i : $q = (\theta_1, \theta_2, \theta_3)^T$:

$$D^{st}[q]\ddot{q} + C^{st}[q, \dot{q}]\dot{q} + G^{st}[q] = T^{st} \quad (2.89)$$

with the following generalized inertia matrix:

$$D^{st}[q] = \begin{bmatrix} I_1 + l_1^2 (m_1 \alpha^2 + m_2 + m_3) & l_1 l_2 (\beta m_2 + m_3) \cos(\theta_1 - \theta_2) & 0 \\ l_1 l_2 (\beta m_2 + m_3) \cos(\theta_1 - \theta_2) & I_2 + l_2^2 (\beta^2 m_2 + m_3) & 0 \\ 0 & 0 & I_3 \end{bmatrix} \quad (2.90)$$

the centrifugal matrix:

$$C^{st}[q] = \begin{bmatrix} 0 & l_1 l_2 (\beta m_2 + m_3) \sin(\theta_1 - \theta_2) \dot{\theta}_2 & 0 \\ -l_1 l_2 (\beta m_2 + m_3) \sin(\theta_1 - \theta_2) \dot{\theta}_1 & 0 & 0 \\ 0 & 0 & 0 \end{bmatrix} \quad (2.91)$$

the gravitational torque vector:

$$G^{st}[q] = \begin{bmatrix} (\alpha m_1 + m_2 + m_3) g l_1 \cos \theta_1 \\ (\beta m_2 + m_3) g l_2 \cos \theta_2 \\ 0 \end{bmatrix} \quad (2.92)$$

and the external torque vector:

$$T^{st} = \begin{bmatrix} \tau_K^{st} \\ \tau_H^{st} - \tau_K^{st} \\ -\tau_H^{st} \end{bmatrix} \quad (2.93)$$

Making linear combinations of the resulting equations leads to the following expressions for the torques at knee and hip respectively:

$$\tau_K^{st} = r \sin(\theta_1 - \theta_2) \dot{\theta}_2^2 + p \ddot{\theta}_1 + r \cos(\theta_1 - \theta_2) \ddot{\theta}_2 + g M a \cos \theta_1 \quad (2.94)$$

$$\begin{aligned} \tau_H^{st} &= r \cos(\theta_1 - \theta_2) (\ddot{\theta}_1 + \ddot{\theta}_2) + p \ddot{\theta}_1 + q \ddot{\theta}_2 + r \sin(\theta_1 - \theta_2) (\dot{\theta}_2^2 - \dot{\theta}_1^2) \\ &\quad + g M (a \cos \theta_1 + b \cos \theta_2) \end{aligned} \quad (2.95)$$

with the constants p , q and r respectively defined by (2.33), (2.34) and (2.35), and the constants a and b respectively given by (2.14) and (2.15).

2.6 Trajectory generation strategy

The control algorithm for the robot has to fulfill two independent requirements:

- The motion of the leg links has to ensure that all the objective locomotion parameters reach their desired values
- The motion of the robot links has to be established in such a way that the upper body motion is free of drift

2.6.1 Flight phase trajectories

General assumptions

- at take-off the foot is positioned in the origin of the coordinate system:

$$X_F^{to} = 0 \quad (2.96)$$

$$Y_F^{to} = 0 \quad (2.97)$$

- at take-off the foot does not slip:

$$\dot{X}_F^{to} = 0 \quad (2.98)$$

$$\dot{Y}_F^{to} = 0 \quad (2.99)$$

$$\ddot{X}_F^{to} = 0 \quad (2.100)$$

$$\ddot{Y}_F^{to} = 0 \quad (2.101)$$

- take-off time is zero and the flight time T^{fl} is defined as the elapsed time between take-off and touch-down:

$$T^{fl} = t^{td} - t^{to} = t^{td} \quad (2.102)$$

Objective parameters

The following parameters are introduced:

- Horizontal velocity of G during flight: $\nu = \dot{X}_G^{to}$
- Step length: $\lambda = X_F^{td} - X_F^{to} = X_F^{td}$
- Step height: $\delta = Y_F^{td} - Y_F^{to} = Y_F^{td}$

These parameters will be frequently used in this and the following chapters.

Boundary conditions

Two polynomial functions $\theta_1^{fl}(t)$ and $\theta_2^{fl}(t)$ will be established, to be tracked by the actuators exerting the torques at knee and hip respectively. These trajectories will guarantee the desired behaviour of the robot during the flight phase. This behaviour is described by the imposed values of the objective parameters.

Suppose that the configuration of the leg at take-off and touch-down is chosen, such that $\theta_1^{to}, \theta_2^{to}$ and $\theta_1^{td}, \theta_2^{td}$ are determined. This means that also the values of $X_G^{to}, Y_G^{to}, X_G^{td}$ and Y_G^{td} are fixed, assuming that the step length and step height are chosen.

By evaluating (2.44) at touch-down, the following expression for the flight time can be found:

$$T^{fl} = \frac{X_G^{td} - X_G^{to}}{\dot{X}_G^{to}} \quad (2.103)$$

After substitution of (2.12) evaluated at take-off and touch-down respectively, and by taking into account the objective parameters, the flight time T^{fl} becomes:

$$T^{fl} = \frac{1}{\nu} \left[\lambda + a (\cos \theta_1^{td} - \cos \theta_1^{to}) + b (\cos \theta_2^{td} - \cos \theta_2^{to}) \right] \quad (2.104)$$

Note that this expression can not be used for hopping in place, since then $\nu = 0$. In case of hopping in place, the flight time can be found from (2.45) evaluated at touch-down. In that case T^{fl} is the positive solution from a quadratic equation:

$$\frac{g}{2} T^{fl2} - \dot{Y}_G^{to} T^{fl} + Y_G^{td} - Y_G^{to} = 0 \quad (2.105)$$

Hopping in place is however a type of motion for which easier strategies can be found, like e.g. Raibert's algorithm [Raibert, 1986], and will thus not be considered in this work.

The necessary vertical velocity of G at take-off \dot{Y}_G^{to} can be derived when evaluating (2.45) at touch-down:

$$\dot{Y}_G^{to} = \frac{Y_G^{td} - Y_G^{to}}{T^{fl}} + \frac{gT^{fl}}{2} \quad (2.106)$$

Introducing (2.13) evaluated at take-off and touch-down respectively in (2.106), and taking into account the objective parameters, yields:

$$\dot{Y}_G^{to} = \frac{1}{T^{fl}} \left[\delta + a (\sin \theta_1^{td} - \sin \theta_1^{to}) + b (\sin \theta_2^{td} - \sin \theta_2^{to}) \right] + \frac{gT^{fl}}{2} \quad (2.107)$$

A parameter often encountered in the literature is the hopping height. It is defined as the difference between the maximum height of G during flight and its height at take-off:

$$\zeta = \frac{(\dot{Y}_G^{to})^2}{2g} \quad (2.108)$$

One could consider to choose the hopping height as an extra objective locomotion parameter in order to distinguish high, short jumps from low, long jumps. The calculations are somewhat different, since one chosen angle at touch-down has to be dropped. This has been published in [De Man et al., 1996, 1998c] and will not be repeated here.

The values of ν and \dot{Y}_G^{to} can be introduced in (2.17) and (2.18) respectively, both evaluated at the instance of take-off. These two equations form a linear set that can be solved for $\dot{\theta}_1^{to}$ and $\dot{\theta}_2^{to}$:

$$\dot{\theta}_1^{to} = -\frac{\nu \cos \theta_2^{to} + \dot{Y}_G^{to} \sin \theta_2^{to}}{a \sin (\theta_1^{to} - \theta_2^{to})} \quad (2.109)$$

$$\dot{\theta}_2^{to} = \frac{\nu \cos \theta_1^{to} + \dot{Y}_G^{to} \sin \theta_1^{to}}{b \sin (\theta_1^{to} - \theta_2^{to})} \quad (2.110)$$

When substituting (2.40) in (2.19) and (2.41) in (2.20) respectively, and evaluating the resultant expressions at take-off, another linear set is obtained which can be solved for $\ddot{\theta}_1^{to}$ and $\ddot{\theta}_2^{to}$:

$$\ddot{\theta}_1^{to} = \frac{g \sin \theta_2^{to} - a \left(\dot{\theta}_1^{to} \right)^2 \cos (\theta_1^{to} - \theta_2^{to}) - b \left(\dot{\theta}_2^{to} \right)^2}{a \sin (\theta_1^{to} - \theta_2^{to})} \quad (2.111)$$

$$\ddot{\theta}_2^{to} = -\frac{g \sin \theta_1^{to} - b \left(\dot{\theta}_2^{to} \right)^2 \cos (\theta_1^{to} - \theta_2^{to}) - a \left(\dot{\theta}_1^{to} \right)^2}{b \sin (\theta_1^{to} - \theta_2^{to})} \quad (2.112)$$

The values of $\dot{\theta}_1^{td}$ and $\dot{\theta}_2^{td}$ and $\ddot{\theta}_1^{td}$ and $\ddot{\theta}_2^{td}$ can be found analogously. However, as an example in this chapter the touch-down conditions will be chosen such that the orientation of the leg is fixed. This solution corresponds to a foot velocity and acceleration equal to that of the global COG. Formally this means:

$$\dot{\theta}_1^{td} = 0 \quad (2.113)$$

$$\dot{\theta}_2^{td} = 0 \quad (2.114)$$

$$\ddot{\theta}_1^{td} = 0 \quad (2.115)$$

$$\ddot{\theta}_2^{td} = 0 \quad (2.116)$$

Since now boundary conditions at take-off as well as at touch-down are known for both the angles θ_1 and θ_2 and their first and second derivatives, two 5th order polynomial tracking functions can be established. For example, the tracking function for θ_1 during the flight phase would be:

$$\theta_1^{fl}(t) = a_0 + a_1 t + a_2 t^2 + a_3 t^3 + a_4 t^4 + a_5 t^5$$

with

$$a_0 = \theta_1^{to}$$

$$a_1 = \dot{\theta}_1^{to}$$

$$\begin{aligned}
a_2 &= \frac{1}{2} \ddot{\theta}_1^{to} \\
a_3 &= \frac{10}{T^{fl3}} (\theta_1^{td} - \theta_1^{to}) - \frac{6}{T^{fl2}} \dot{\theta}_1^{to} - \frac{3}{2T^{fl}} \ddot{\theta}_1^{to} \\
a_4 &= \frac{-15}{T^{fl4}} (\theta_1^{td} - \theta_1^{to}) + \frac{8}{T^{fl3}} \dot{\theta}_1^{to} + \frac{3}{2T^{fl2}} \ddot{\theta}_1^{to} \\
a_5 &= \frac{6}{T^{fl5}} (\theta_1^{td} - \theta_1^{to}) - \frac{3}{T^{fl4}} \dot{\theta}_1^{to} - \frac{1}{2T^{fl3}} \ddot{\theta}_1^{to}
\end{aligned}$$

The polynomial function for θ_2 can be found in the same manner.

Calculating body rotation

Now that flight time as well as the tracking functions for the angles of the leg links are known, the expression for the body rotation during the flight phase can be rewritten from (2.49) as:

$$\Delta\theta_3^{fl} = \frac{\mu_G^{to}}{I_3} T^{fl} - \frac{1}{I_3} \int_0^{T^{fl}} \left[c\dot{\theta}_1^{fl} + d\dot{\theta}_2^{fl} + e(\dot{\theta}_1^{fl} + \dot{\theta}_2^{fl}) \cos(\theta_1^{fl} - \theta_2^{fl}) \right] dt \quad (2.117)$$

where $\Delta\theta_3^{fl} = \theta_3^{td} - \theta_3^{to}$. At this point the value of μ_G^{to} is unknown. It is determined by the initial value of $\dot{\theta}_3^{to}$. It will be shown in section 2.6.2 that there is an ideal value for this parameter. The integral on the right hand side partially has to be integrated numerically. One can rewrite (2.117):

$$\Delta\theta_3^{fl} = \frac{1}{I_3} (\mu_G^{to} T^{fl} - c\Delta\theta_1^{fl} - d\Delta\theta_2^{fl} - e \int_0^{T^{fl}} (\dot{\theta}_1^{fl} + \dot{\theta}_2^{fl}) \cos(\theta_1^{fl} - \theta_2^{fl}) dt) \quad (2.118)$$

or

$$\Delta\theta_3^{fl} = \frac{\mu_G^{to} T^{fl} + A^{fl}}{I_3} \quad (2.119)$$

with

$$A^{fl} = -c\Delta\theta_1^{fl} - d\Delta\theta_2^{fl} - e \int_0^{T^{fl}} (\dot{\theta}_1^{fl} + \dot{\theta}_2^{fl}) \cos(\theta_1^{fl} - \theta_2^{fl}) dt \quad (2.120)$$

$$\Delta\theta_1^{fl} = \theta_1^{td} - \theta_1^{to} \quad (2.121)$$

$$\Delta\theta_2^{fl} = \theta_2^{td} - \theta_2^{to} \quad (2.122)$$

In order to avoid drift on the upper body motion, the rotation $\Delta\theta_3^{fl}$ resulting from the leg swing during the flight phase has to be compensated during the next stance phase. Since there are only two actuators steering the absolute angles of the leg links, this rotation will be controlled indirectly by using the angular momentum equation during the stance phase.

2.6.2 Stance phase trajectories

General assumptions

- The stance phase starts after the impact phase. Start time is noted as t^+ and the duration is given by the stance time T^{st}
- The ground surface is inelastic
- During the stance phase the foot does not slip, meaning that the horizontal reaction force R_x is assumed to be large enough to ensure that

$$\dot{X}_F(t) = 0 \quad (2.123)$$

$$\ddot{X}_F(t) = 0 \quad (2.124)$$

- The connection with the rigid ground is unilateral. The vertical reaction force R_y can only exert a push action and no pull action. It will be assumed that

$$\dot{Y}_F(t) = 0 \quad (2.125)$$

$$\ddot{Y}_F(t) = 0 \quad (2.126)$$

However, when designing reference trajectories for the leg links, the resulting trajectory of the vertical acceleration of the COG has to be taken into account. It may never reach gravity acceleration, since in that case the unilateral contact with the ground would be lost. In other words it has to be verified if $\dot{Y}_G \geq -g$. Moreover, when assuming a Coulomb friction model between the foot F and the ground, to avoid slipping of the foot it should be guaranteed that $|R_x| < f_s |R_y|$ with f_s the static friction coefficient.

Boundary conditions

For the robot to perform the desired motion during the flight phase of a hop, some control is needed during the preceding stance phase, yielding the necessary take-off conditions. The stance phase following a hop also has to be controlled such that at the end of that stance phase the necessary initial conditions for the flight phase of the next hop are reached. Since at this point steady hopping is

considered, the desired trajectories for $\theta_1(t)^{st}$ and $\theta_2(t)^{st}$ can be constructed in an analogous way as during the flight phase. The value for θ_1 and θ_2 , and their first and second derivatives at the end of the stance phase are those of the beginning of the next flight phase, being θ_1^{to} , $\dot{\theta}_1^{to}$, $\ddot{\theta}_1^{to}$ and θ_2^{to} , $\dot{\theta}_2^{to}$, $\ddot{\theta}_2^{to}$ respectively. The values for θ_1 and θ_2 and their first and second derivatives at the beginning of the stance phase are those measured after impact, being noted as θ_1^+ , $\dot{\theta}_1^+$, $\ddot{\theta}_1^+$ and θ_2^+ , $\dot{\theta}_2^+$, $\ddot{\theta}_2^+$ respectively. Again six boundary conditions have to be satisfied for each angle, such that 5th order polynomials can be established for the stance phase. There is however another parameter that has to be specified, being the stance time T^{st} . Contrary to the flight phase, where the flight time is determined by the dynamics, the stance time can be chosen. This is also due to the fact that no passive elements are added to the model. In the next paragraph the stance time will be determined in a specific way, such that a set of polynomial functions can be computed. These polynomial functions will be the desired trajectories which have to be tracked by the actuators at hip and knee during the stance phase. The robot is then able to perform consecutive hops, with a steady behaviour of the leg.

Stance phase duration

In case of steady hopping, the translational as well as the rotational motion of the robot have to be identical during each hop. For the rotational motion this can be formulated as:

$$\mu_G^{to} = \mu_G^{td} \quad (2.127)$$

with μ_G^{to} being the angular momentum with respect to G of the next flight phase, and μ_G^{td} the momentum of the preceding flight phase. Integrating the angular momentum equation (2.83) with respect to F from 0 to T^{st} gives (note that for simplicity reasons $t^+ = 0$ has been assumed):

$$\Delta\mu_F^{st} = \mu_F^{to} - \mu_F^+ = -Mg \int_0^{T^{st}} X_G dt \quad (2.128)$$

Taking into account that for an inelastic impulsive impact in F:

$$\Delta\mu_F^{shock} = 0 \quad \Leftrightarrow \quad \mu_F^+ = \mu_F^{td} \quad (2.129)$$

Expression (2.128) then becomes:

$$\Delta\mu_F^{st} = \mu_F^{to} - \mu_F^{td} = -Mg \int_0^{T^{st}} X_G dt \quad (2.130)$$

The transport equation for the angular momentum between G and the foot point F yields following expressions at take-off and touch-down:

$$\mu_F^{to} = \mu_G^{to} + (\overline{FG}^{to} \times M\bar{v}_G^{to})|_z \quad (2.131)$$

$$\mu_F^{td} = \mu_G^{td} + (\overline{FG}^{td} \times M\overline{v}_G^{td})|_z \quad (2.132)$$

These two expressions can now be substituted in the lhs of (2.130):

$$\Delta\mu_F^{st} = \mu_G^{to} + (\overline{FG}^{to} \times M\overline{v}_G^{to})|_z - \mu_G^{td} - (\overline{FG}^{td} \times M\overline{v}_G^{td})|_z \quad (2.133)$$

The latter expression is rather interesting, since it allows one to determine a desired value for $\Delta\mu_F^{st*}$ by introducing (2.127):

$$\Delta\mu_F^{st*} = (\overline{FG}^{to} \times M\overline{v}_G^{to})|_z - (\overline{FG}^{td} \times M\overline{v}_G^{td})|_z \quad (2.134)$$

The value of (2.134) can be calculated since it only depends on the leg motion. Substituting this desired value (2.134) into the dynamic equation (2.130) leads to a condition on the stance time T^{st} :

$$-Mg \int_0^{T^{st}} X_G dt = \Delta\mu_F^{st*} \quad (2.135)$$

or when using the kinematic expression for X_G :

$$-Mg \int_0^{T^{st}} (a \cos \theta_1 + b \cos \theta_2) dt = \Delta\mu_F^{st*} \quad (2.136)$$

There are two different ways to ensure that condition (2.136) and thus (2.127) is satisfied:

- Solve (2.136) numerically for T^{st} . The disadvantage of this technique is that the mean horizontal velocity can not be chosen, and that possibly the COG will excessively decelerate and re-accelerate during stance.
- Determine the stance time by choosing the mean horizontal velocity. When setting this velocity e.g. equal to the horizontal velocity during flight ν , the stance time can be calculated as $T^{st} = \frac{\Delta X_G^{st}}{\nu}$. This has however the implication that the take-off and touch-down configurations for the leg have to be adapted in order to satisfy (2.136).

In practice, a combination of both approaches will be used in order to become a feasible stance phase for the robot.

Determining body rotation and angular momentum μ_G^{to}

Once the stance time is fixed, the tracking functions θ_1^{st} and θ_2^{st} for the leg links during the stance phase are known. The body angular velocity during stance is

given by (2.88):

$$\dot{\theta}_3 = \frac{1}{I_3} \left[\mu_F^+ - k - Mg \int_0^t X_G dt \right] \quad (2.137)$$

Integrating this equation from 0 to T^{st} yields an expression for the upper body rotation during the stance phase:

$$\Delta\theta_3^{st} = \frac{1}{I_3} \left[\mu_F^+ T^{st} - \int_0^{T^{st}} k dt - Mg \int_0^{T^{st}} (T^{st} - t) X_G dt \right] \quad (2.138)$$

with:

$$\Delta\theta_3^{st} = \theta_3^{to} - \theta_3^+ = \theta_3^{to} - \theta_3^{td} \quad (2.139)$$

since the configuration parameters of a robot do not change during an impulsive impact.

When introducing (2.38) and the kinematic expression for X_G (2.12), expression (2.138) becomes:

$$\begin{aligned} \Delta\theta_3^{st} = \frac{1}{I_3} \left[-p\Delta\theta_1^{st} - q\Delta\theta_2^{st} - r \int_0^{T^{st}} (\dot{\theta}_1 + \dot{\theta}_2) \cos(\theta_1 - \theta_2) dt \right. \\ \left. + \mu_F^+ T^{st} - Mg \int_0^{T^{st}} (T^{st} - t)(a \cos \theta_1 + b \cos \theta_2) dt \right] \end{aligned} \quad (2.140)$$

with

$$\Delta\theta_1^{st} = \theta_1^{to} - \theta_1^+ = \theta_1^{to} - \theta_1^{td} \quad (2.141)$$

$$\Delta\theta_2^{st} = \theta_2^{to} - \theta_2^+ = \theta_2^{to} - \theta_2^{td} \quad (2.142)$$

and

$$\mu_F^+ = \mu_F^{td} = \mu_G^{td} + (\overline{FG}^{td} \times M\overline{v}_G^{td})|_z \quad (2.143)$$

Such that the rotation of the upper body during the stance phase becomes:

$$\Delta\theta_3^{st} = \frac{(\mu_G^{to} + B^{st})T^{st} - A^{st}}{I_3} \quad (2.144)$$

with:

$$\begin{aligned} A^{st} = p\Delta\theta_1^{st} + q\Delta\theta_2^{st} + r \int_0^{T^{st}} (\dot{\theta}_1 + \dot{\theta}_2) \cos(\theta_1 - \theta_2) dt \\ + Mg \int_0^{T^{st}} (T^{st} - t)(a \cos \theta_1 + b \cos \theta_2) dt \end{aligned} \quad (2.145)$$

and:

$$B^{st} = (\overline{FG}^{td} \times M\overline{v}_G^{td})|_z \quad (2.146)$$

In section 2.6.1 a similar relation was found between the rotation during flight $\Delta\theta_3^{fl}$ and the angular momentum μ_G^{to} , being (2.119). At this point the steady state condition concerning body rotation can be imposed. The rotation during flight needs to be compensated by the rotation during stance, or in other words:

$$\Delta\theta_3^{fl} + \Delta\theta_3^{st} = 0 \quad (2.147)$$

Introducing (2.119) and (2.144) results in an expression that can be solved for μ_G^{to} :

$$\mu_G^{to*} = \frac{A^{fl} + A^{st} - B^{st}T^{st}}{T^{fl} + T^{st}} \quad (2.148)$$

With expression (2.23) a desired value for $\dot{\theta}_3^{to}$ can then be found:

$$\dot{\theta}_3^{to*} = \frac{1}{I_3} \left[\mu_G^{to*} - c\dot{\theta}_1^{to} - d\dot{\theta}_2^{to} - e(\dot{\theta}_1^{to} + \dot{\theta}_2^{to}) \cos(\theta_1^{to} - \theta_2^{to}) \right] \quad (2.149)$$

So when the robot starts its first flight phase with angular velocity of the body equal to $\dot{\theta}_3^{to*}$, and when the actuators track the desired polynomials during flight and stance respectively, the robot reaches steady state motion. This steady state behaviour guarantees the same values for the objective locomotion parameters during the consecutive hops, as well as a stabilized, bounded motion of the upper body.

In order to clearly summarize the different steps of the strategy generating the trajectories, a flow chart is given in figure 2.6.

Remark: Upper body angular acceleration

The angular momentum equation with respect to F during the stance phase (2.83) can be written as:

$$\dot{\mu}_F = -MgX_G \quad (2.150)$$

The time derivative of the kinematic expression (2.37) gives:

$$\dot{\mu}_F = \dot{k} + I_3\ddot{\theta}_3^{st} \quad (2.151)$$

Substituting (2.151) in (2.150) leads to the following dynamic expression for $\ddot{\theta}_3$:

$$\ddot{\theta}_3^{st} = -\frac{MgX_G + \dot{k}}{I_3} \quad (2.152)$$

Evaluating this expression at take-off shows that if the applied strategy is applied as described above, the take-off upper body angle will be the same for every hop, such that the same will be true for the acceleration $\ddot{\theta}_3^{to}$.

During the flight phase the angular momentum with respect to G is conserved:

$$\dot{\mu}_G = 0 \quad (2.153)$$

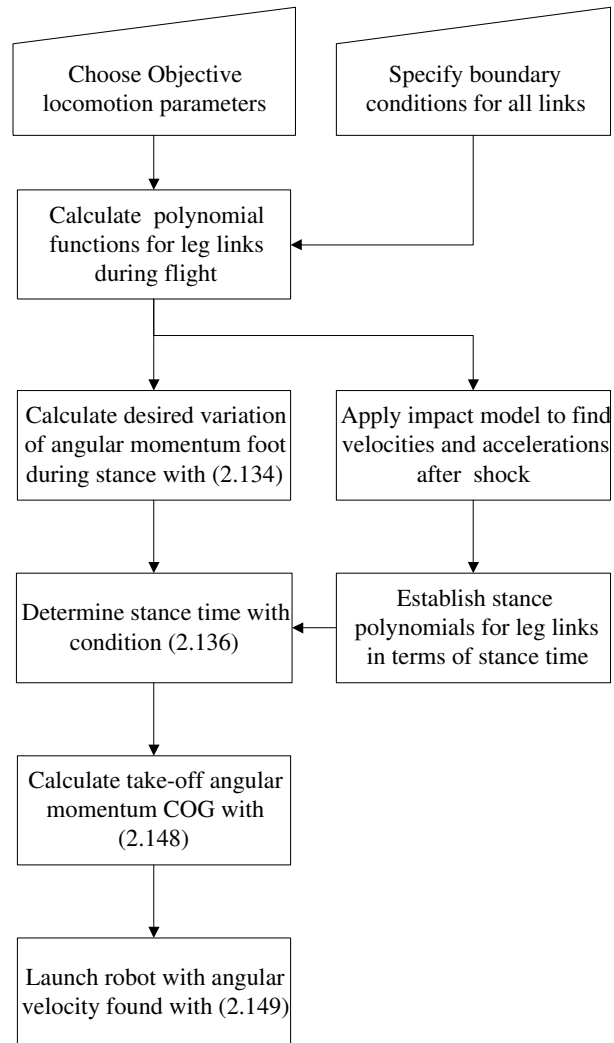


Figure 2.6: Flow chart describing different steps in strategy

Introducing the derivative with respect to time of the kinematic expression (2.28) leads to:

$$\ddot{\theta}_3^{fl} = -\frac{\dot{h}}{I_3} \quad (2.154)$$

Evaluating this expression at touch-down shows that a steady behaviour of the legs during the consecutive hops guarantees an identical value of $\ddot{\theta}_3^{td}$ for each hop.

The conclusion is that, when using this trajectory generation strategy, a steady behaviour of the upper body angular acceleration is automatically achieved.

2.7 Simulations

In this section, the results of a simulation of a hopping motion are presented. The simulation is performed using the multibody code *Mechanica Motion*. An important remark has to be made concerning the ground model. As mentioned earlier, the control algorithm uses an inelastic impulsive impact phase to estimate the angular velocities after the shock. This model is used because in reality it is difficult to measure these velocities. Not only will the sensors on the robot be disturbed because of the shock, but it is also difficult to measure the exact duration of the impact phase. On a real robot, there will always be an error on the first point of the polynomial functions for the stance phase, due to the predictions made by the impact model. In order to simulate the difference between the ground model used by the control algorithm and the ground on which the real robot would have to move, the simulations with *Mechanica Motion* are performed with another ground model. A parallel spring and damper system is used to model the real ground. Moreover, the actuators are simulated by PD-controlled torques, which have to track the polynomial steer functions calculated by the algorithm. In this way, the algorithm is tested in case of non-perfect tracking of the reference trajectories.

To test the specified algorithm a hopping pattern consisting of a number of consecutive hops has been simulated. Since a steady state hopping pattern is considered, the values of the desired objectives, being forward velocity during flight, step length, and step height are the same for all hops. The chosen parameters are the following:

- $\nu = 1$ m/s
- $\lambda = 0.5$ m
- $\delta = 0$

To illustrate the orientation of the leg at take-off and touch-down, the angle between the horizontal axis and a virtual line connecting the foot point and the COG is specified:

- $\theta_G^{to} = 78.5^\circ$

- $\theta_G^{td} = 102^\circ$

This results in:

- $T_{fl} = 0.286$ s
- $\zeta = 0.1$ m (hopping height)
- $\Delta\theta_3^{fl} = 0.1084$ rad
- $T_{st} = 0.34$ s
- $\mu_G^{to} = 0.622$ kgm^2/s
- $\Delta\theta_3^{st} = -0.1084$ rad

The trajectories tracked by the actuators of the leg links during the stance phase, which guarantee that the desired values for the objective locomotion parameters are attained, cause a clockwise natural rotation for the upper body. Therefore a counterclockwise rotation of the upper body during the flight phase is suitable, since then both rotations can compensate each other. Suppose that a zero angular momentum would have been chosen during the flight phase, then the upper body would rotate in the clockwise direction, due to the leg swing in the counterclockwise direction. In that case the global upper body rotation would drift during the consecutive hops unless an actuator acted on it during the stance phase [De Man et al., 1996]. This situation can simply be avoided by choosing a positive value for the angular momentum during the flight phase, as shown in the results here.

Figure 2.7 shows a stick diagram for one hop of the hopping pattern executed by the robot.

The polynomial functions being tracked by the actuators for lower and upper leg are displayed in figures 2.8 and 2.9 respectively.

Figure 2.10 shows the horizontal velocity \dot{X}_G of the global COG versus time. The horizontal parts of the graph represent the velocity during the flight phase, being equal to the desired value of $1m/s$. During the stance phase, the horizontal velocity of the COG is decelerated with approximately 60% and is re-accelerated afterwards. One could remark here that this deceleration is too large, or in other words that the stance time is too long. As explained in section 2.6.2 this can be avoided by changing the take-off and touch-down configuration of the robot. Indeed, shifting the initial and final value for the horizontal position X_G of the COG will influence the value of the integral of X_G during the stance phase. Since it is not the scope of this chapter, this adaptation is not done here.

Figure 2.11 shows the horizontal position X_F of the foot point F versus time. The horizontal parts of the graph give the position of the foot during the successive stance phases. It can be seen that the difference between the position during two successive stance phases is equal to the desired step length of 0.5 m.

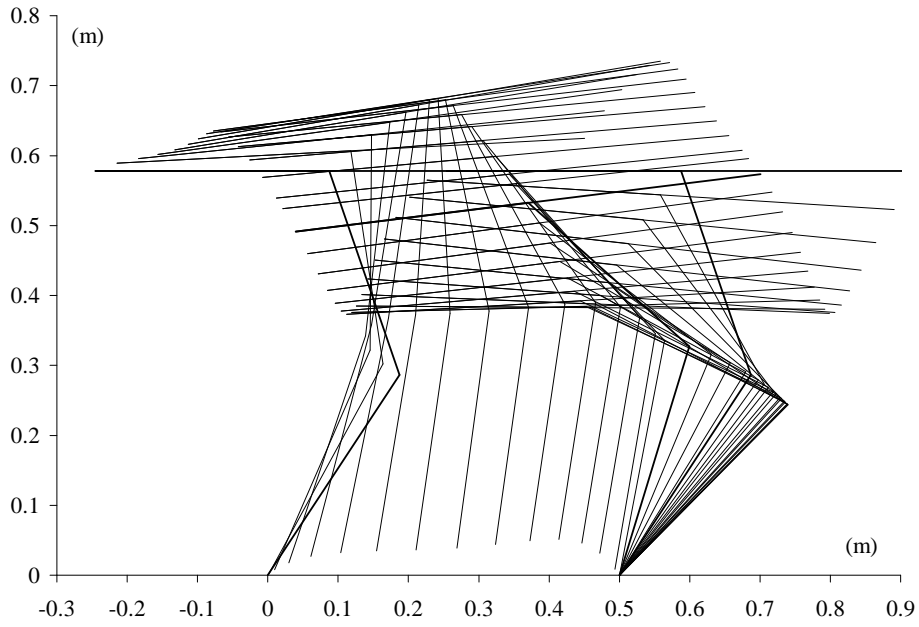


Figure 2.7: Stick diagram

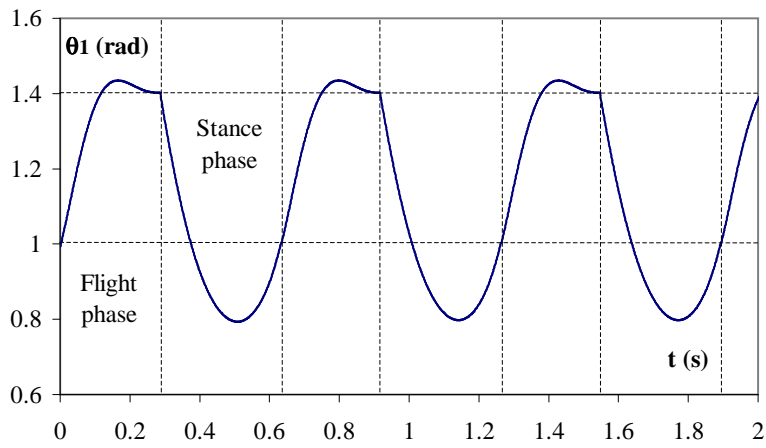


Figure 2.8: Lower leg angle trajectory

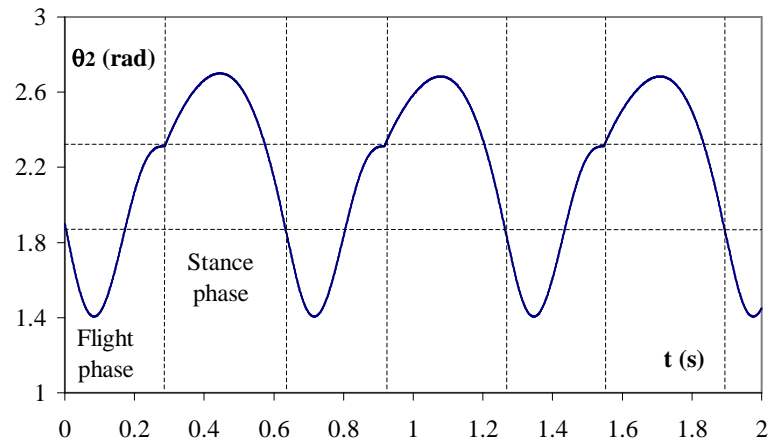


Figure 2.9: Upper leg angle trajectory

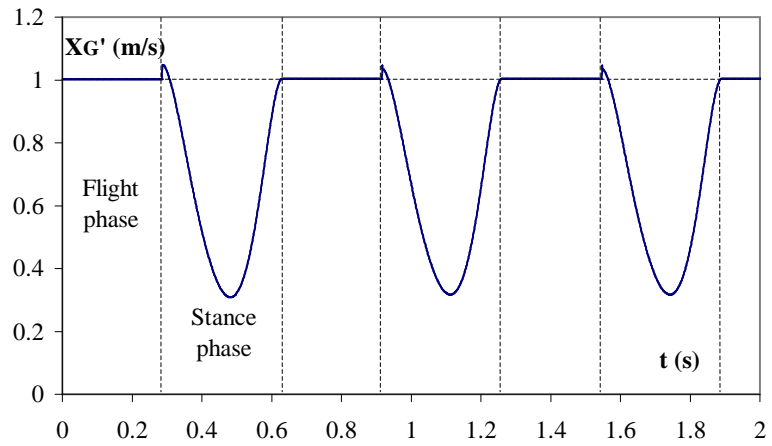


Figure 2.10: Horizontal velocity of the COG

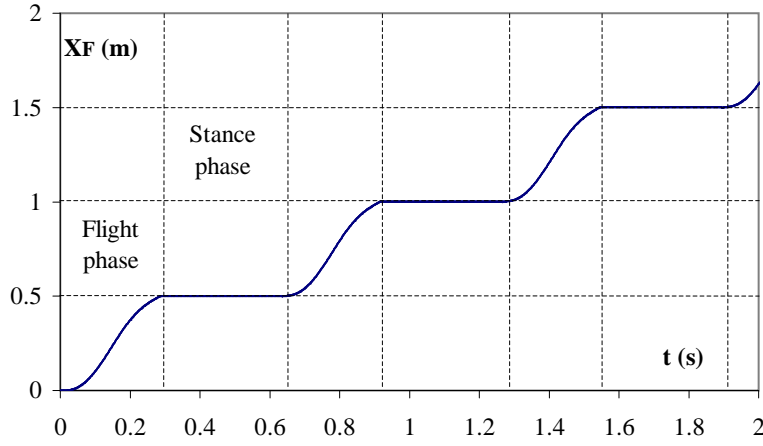


Figure 2.11: Horizontal position of the foot point F

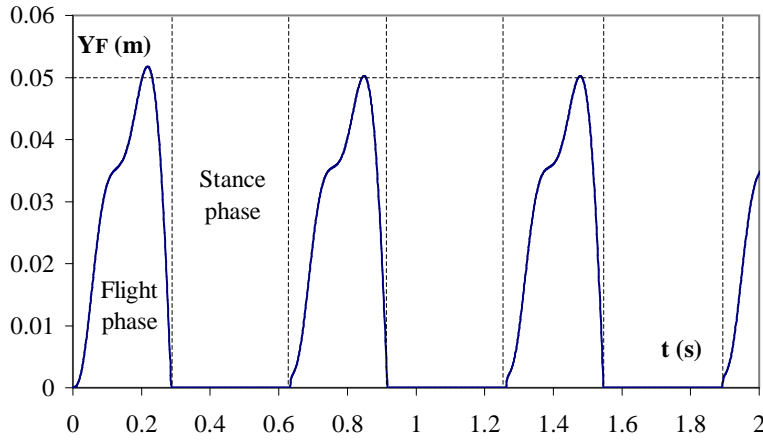


Figure 2.12: Vertical position of the foot point F

Figure 2.12 gives the vertical position Y_F of the foot point F versus time. Since the robot hops on flat terrain, the vertical position during the stance phase is equal to 0.

Figure 2.13 gives the angular momentum μ_G with respect to G versus time. The horizontal parts of the graph represent the momentum during the flight phase, being equal to the ideal value as calculated by the control algorithm.

Figure 2.14 shows the rotation of the upper body θ_3 versus time. It can be seen that the rotation during stance is equal and opposite to the rotation during flight. Thus, after one full hop, the angle equals zero again. After each flight phase, the upper body angle is equal to the desired value of approximately 0.11 rad or 6° , as

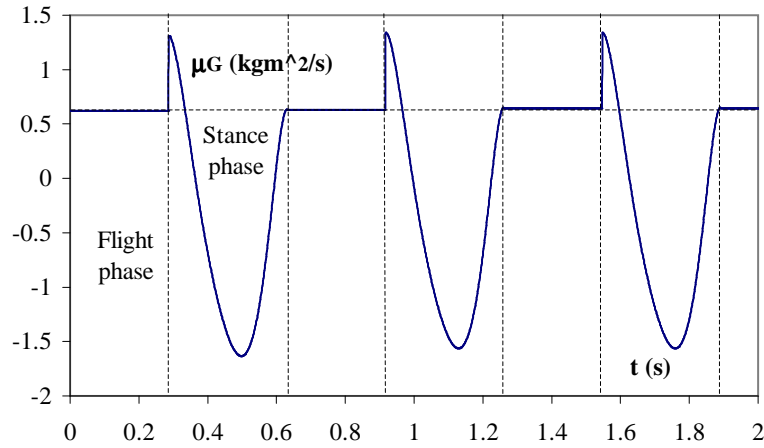


Figure 2.13: Angular momentum with respect to the COG

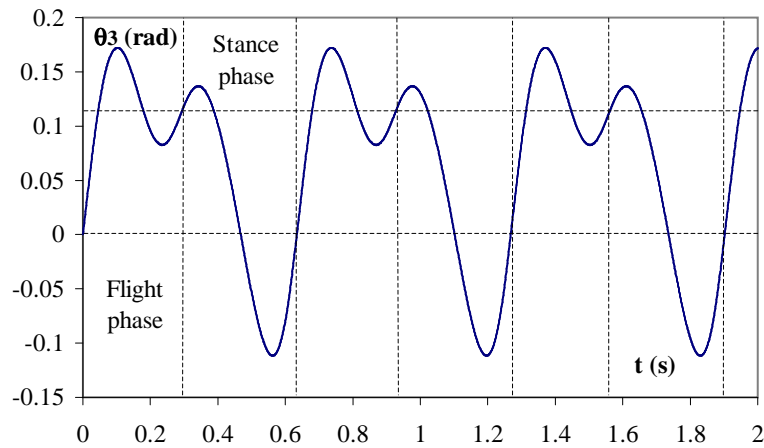


Figure 2.14: Upper body angle behaviour

indicated by the intersection of the highest horizontal dotted line with the vertical lines representing the consecutive instances of touch-down. After each stance phase it is equal to 0, as indicated by the intersection of the lowest horizontal dotted line with the vertical lines representing the instances of take-off. The mean value for the upper body angle is approximately 6.6° during flight and 0.8° during stance.

Graph 2.15 gives the vertical position of the COG as a function of time. The highest horizontal line on the graph represents the maximum value of the vertical position of G during flight. The lowest line represents the height of G at take-off. The difference between these lines is equal to the hopping height. It can be seen that the hopping height is equal to 0.1 m.

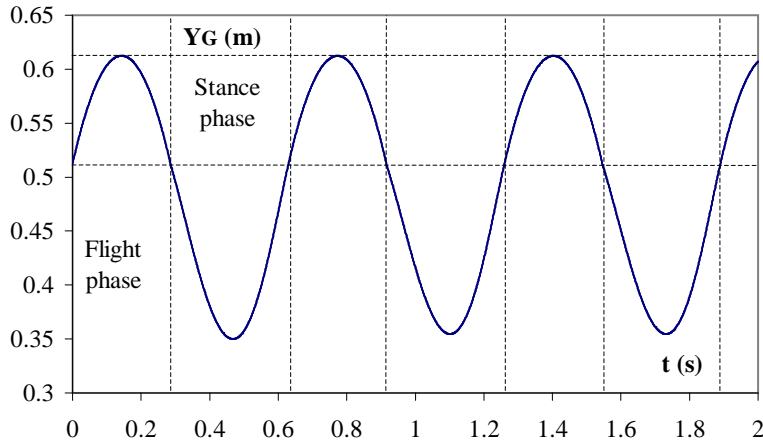


Figure 2.15: Vertical position of the COG

Figures 2.16 and 2.17 give the exerted torques by hip and knee actuator respectively. The peak value of the hip torque is smaller than 40 Nm during one full hop. The peak value of the knee torque is significantly higher, being approximately 70 Nm during the stance phase. The remark can be made here that using a passive element, e.g. a torsional spring, can severely reduce this peak value. This is especially due to the fact that the trajectory of the necessary knee torque does not change its sign during the stance phase, and can be fitted by the trajectory of a mechanical torsional spring. The prototype OLIE contained a torsional spring located at the knee joint, characterized by a spring constant $k = 60 \frac{\text{Nm}}{\text{rad}}$, and a rest angle of $\theta_0 = 0.85 \text{ rad}$, corresponding to approximately 49° . The torque exerted by the spring is then $T_S = k(\theta_{12} - \theta_0)$. The simulation of one hop of the pattern was repeated by adding such a spring to the knee joint, parallel to the PD-actuator. In figure 2.18 it can clearly be seen that the peak torque of the actuator during the stance phase is reduced to approximately 15 Nm , and that indeed most of the action is covered by the spring.

2.8 Summary

In this chapter a trajectory generation strategy for a one-legged hopping robot with an articulated leg is developed. The robot has no foot, and is therefore underactuated in both the stance and the flight phase. Due to the fact that the COG of the upper body is located at the hip joint, the motion of the robot's leg and its body are completely decoupled. The upper body rotation has no influence on the motion of the global COG of the robot. The algorithm is therefore built up by two independent tasks, being the control of a number of objective locomotion parameters, and the control of the upper body motion. The objective locomotion

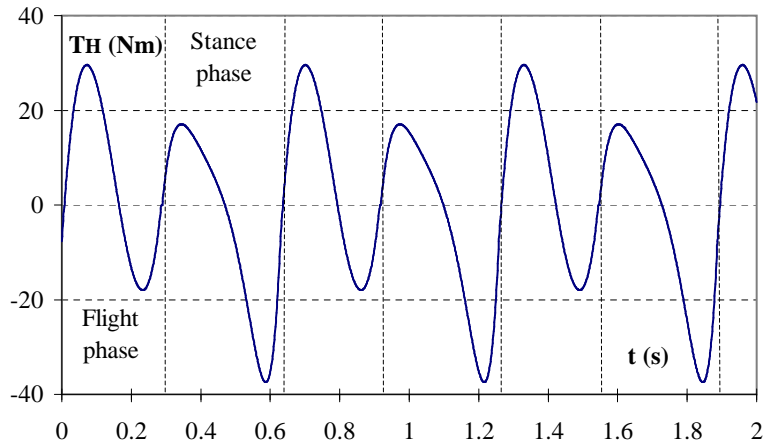


Figure 2.16: Torque exerted by hip actuator

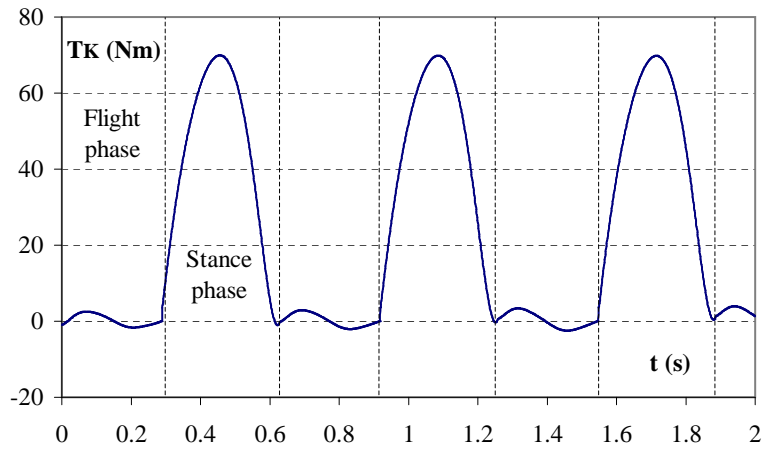


Figure 2.17: Torque exerted by knee actuator

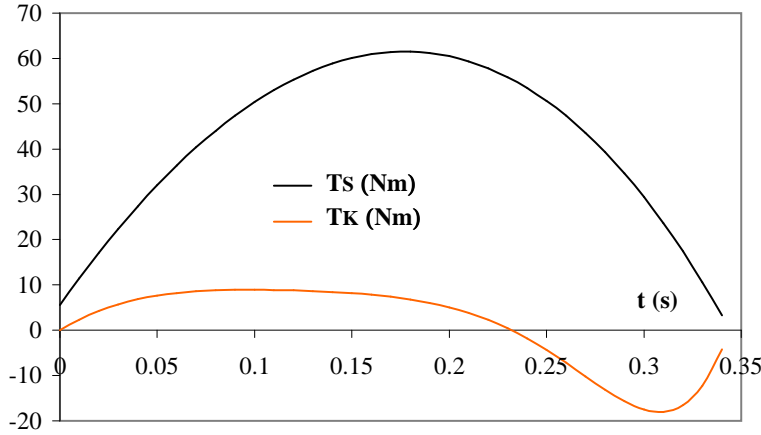


Figure 2.18: Torques exerted by torsional spring and knee actuator during a stance phase

parameters considered are horizontal velocity during flight, step length and step height. The control of the upper body motion is based on an adequate choice of the angular momentum with respect to the COG during flight. As opposed to other strategies used in literature, the angular momentum is not chosen zero, but its value is chosen in such a way that a rotation during flight is automatically compensated during the next stance phase without any extra torque directly acting on the upper body. Using this specific value for the angular momentum and by choosing a well-determined value for the stance time, the robot is able to perform a steady pattern of consecutive hops without any drift on the upper body rotation and thereby reaching all the desired values for the different objective locomotion parameters. However, the following important remarks have to be made:

- The angular momentum with respect to the COG is conserved during the flight phase, meaning that it can only be changed during the stance phase. To be able to initiate the hopping motion with the ideal value of the angular momentum during flight, the robot has to be launched with a specific value for the angular velocity of the upper body. Due to the fact that the system is underactuated, this can not be done with the above strategy. Therefore a foot has to be added, which will be done in the following chapter. For the steady hopping motion considered here, the work of the foot would be limited to the initiation of the motion only.
- The applied strategy is not suitable for non-steady hopping. The objective parameters could be altered from one hop to another without any problem, but the current indirect control of the upper body would not be possible. During the stance phase the algorithm can compensate the rotation of the upper body of the preceding flight phase, but it can not at the same time

guarantee the desired value of the angular momentum with respect to the COG for a flight phase of a hop which differs from the preceding one. This is also due to the fact that the robot is underactuated during the stance phase.

- The simulation does not introduce external disturbances to the motion. Such disturbances would also cause a drift on the upper body motion because of the lack of a controller acting directly on this link. The overall conclusion is that a foot has to be introduced, in order to make the robot fully actuated during the stance phase.

Chapter 3

A hopping robot with a foot

3.1 Introduction

As was concluded in the preceding chapter, the planning strategy that was developed for the model of the robot OLIE, can in its present state not be implemented on a real robot. It should be seen as a purely theoretical study to prove the use of a non-zero angular momentum during the flight phase of a planar hopper, and to introduce the idea of trajectory generation based on objective locomotion parameters. In this chapter the model of the hopping robot will be adapted in order to develop a strategy which is more generally applicable. A first adaptation will be the introduction of a foot, to overcome all the reported problems in the conclusions of chapter 2. For simplicity purposes this foot will be assumed to have an ignorable inertia. Furthermore, the COG of the upper body will not be located at the hip joint, and the upper body will be placed upright upon the leg. This means that now the motion of the leg and the upper body will no longer be decoupled. The scope of this chapter is to develop a control strategy which is based on a limited number of elementary calculations to reduce the computation time, such that it can be real-time applicable to the model [Vermeulen et al., 2003]. The strategy allows the robot to move on irregular terrain, by changing its objective locomotion parameters from one hop to another. More specifically, the robot is able to transfer from a chosen initial configuration to a chosen end configuration, while simultaneously controlling its forward velocity, its step length and its step height. The foot is being placed exactly on chosen footholds compatible with the environment, while simultaneously the upper body motion is controlled.

In section 3.2 of this chapter a description of the robot model is given. Section 3.3 introduces the kinematical aspects of the model, whereas in section 3.4 the dynamical equations are derived. Special attention will be given to the loss of kinetic energy during impact, since it will be shown that this loss can be limited by making an appropriate choice of the touch-down conditions of the foot. The overall

trajectory generation strategy is described in section 3.5. During the flight phase an adequate choice of the angular momentum with respect to the COG is made, based on the desired upper body rotation during that phase. During the stance phase the model will be considered as fully actuated, since a foot actuator is placed at the ankle joint. This strategy will, at this stage, not take any Zero Moment Point (ZMP) considerations [Vukobratovic et al., 1990], [Goswami, 1999] into account. Simulation results are presented in section 3.6, followed by conclusions in section 3.7.

3.2 The model

In figure 3.1 the new model geometry is depicted. Point F now represents the connection between the lower leg and the foot, and it coincides therefore with the ankle joint. Note that in figure 3.1, the foot is placed on a horizontal ground, such that its orientation is parallel with the horizontal X-axis of the reference frame XYZ. In case of an inclined ground surface, the foot orientation will be determined by the environment. The upper body is placed in an upright position, such that its

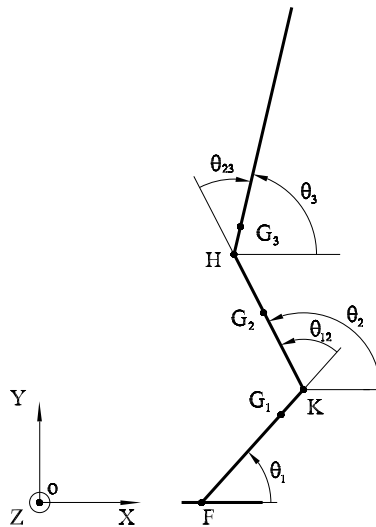


Figure 3.1: Model geometry of the hopping robot with foot

COG G_3 does no longer coincide with the hip joint H. Its position is now determined by $HG_3 = \gamma l_3$ where $0 < \gamma < 1$. For the simulations performed here, a distance of 10cm between H and G_3 was chosen, corresponding to $\gamma = 0.15$. Note that all the lengths, mass and inertial parameters for the model can be found in table 2.1 of chapter 2.

The robot now has three actuators, since one actuator is added at the ankle joint. This actuator is only used during the stance phase, in order to be able to exert a limited external torque between the ground and the lower leg. During the flight phase, this actuator is however of no use, since the foot is assumed to have zero inertia. It can be concluded that during the flight phase the robot is still underactuated, since it has five DOF and only two useful actuators, while it now becomes fully actuated during the stance phase, due to the three actuators and the three DOF when a non-slippery rigid ground is assumed. Note that the foot is not considered here as a toe link, or in other words rotation of the foot during the stance phase will be avoided, such that the number of DOF is not altered.

3.3 Kinematics

The fact that the COG of the upper body does no longer coincide with the hip, has some major consequences. The orientation of the upper body now has an influence on the position of the global COG. This means that there is no decoupling between the motion of the COG and the motion of the upper body, which is the main difference between this model and the model of OLIE studied in chapter 2. The orientation of the upper body will influence the values of the objective locomotion parameters, such that a deviation from the desired upper body motion will cause the robot to land at the wrong time instance and at the wrong place.

The kinematic variables of importance in this chapter are the position of the COG and its derivatives, and the angular momentum with respect to the global COG. The following set of generalized coordinates q_i will be used:

$$q = \{\theta_{12}, \theta_{23}, \theta_3, X_F, Y_F\}^T$$

Instead of expressing the kinematics and dynamics in terms of the absolute angles θ_1 and θ_2 as was done in chapter 2, now two relative angles $\theta_{12} = \theta_2 - \theta_1$ and $\theta_{23} = \theta_3 - \theta_2$ are used. The subtle advantage of this will become clear when writing the angular momentum with respect to G during the flight phase.

3.3.1 Motion of the COG

From figure 3.1, the vectors defining the positions of the local COG's for the three links can be derived in terms of the chosen generalized coordinates:

$$\overline{OG}_1 = (X_F, Y_F)^T + \alpha l_1 \{ \cos(\theta_3 - \theta_{23} - \theta_{12}), \sin(\theta_3 - \theta_{23} - \theta_{12}) \}^T \quad (3.1)$$

$$\begin{aligned} \overline{OG}_2 &= (X_F, Y_F)^T + l_1 \{ \cos(\theta_3 - \theta_{23} - \theta_{12}), \sin(\theta_3 - \theta_{23} - \theta_{12}) \}^T \\ &\quad + \beta l_2 \{ \cos(\theta_3 - \theta_{23}), \sin(\theta_3 - \theta_{23}) \}^T \end{aligned} \quad (3.2)$$

$$\begin{aligned} \overline{OG}_3 &= (X_F, Y_F)^T + l_1 \{ \cos(\theta_3 - \theta_{23} - \theta_{12}), \sin(\theta_3 - \theta_{23} - \theta_{12}) \}^T \quad (3.3) \\ &\quad + l_2 \{ \cos(\theta_3 - \theta_{23}), \sin(\theta_3 - \theta_{23}) \}^T \\ &\quad + \gamma l_3 (\cos \theta_3, \sin \theta_3)^T \end{aligned}$$

The position of the global center of gravity G of the robot at a certain time step t is then given by:

$$\overline{OG} = (X_G, Y_G)^T$$

with:

$$X_G = X_F + a \cos(\theta_3 - \theta_{12} - \theta_{23}) + b \cos(\theta_3 - \theta_{23}) + c \cos \theta_3 \quad (3.4)$$

$$Y_G = Y_F + a \sin(\theta_3 - \theta_{12} - \theta_{23}) + b \sin(\theta_3 - \theta_{23}) + c \sin \theta_3 \quad (3.5)$$

and

$$a = (\alpha \eta_1 + \eta_2 + \eta_3) l_1 \quad (3.6)$$

$$b = (\beta \eta_2 + \eta_3) l_2 \quad (3.7)$$

$$c = \gamma \eta_3 l_3 \quad (3.8)$$

Note that the η_i were defined in (2.16). Calculation of the derivatives of (3.4) and (3.5) is straightforward.

3.3.2 Rotation around the COG

The angular momentum with respect to G can be calculated with the general formula (2.21). It can formally be written as:

$$\mu_G = A_3 \dot{\theta}_3 + A_{23} \dot{\theta}_{23} + A_{12} \dot{\theta}_{12} \quad (3.9)$$

with:

$$A_3 = d_1 + d_2 + d_3 + 2e_{12} \cos \theta_{12} + 2e_{23} \cos \theta_{23} + 2e_{13} \cos(\theta_{12} + \theta_{23}) \quad (3.10)$$

$$A_{23} = -[d_1 + d_2 + 2e_{12} \cos \theta_{12} + e_{23} \cos \theta_{23} + e_{13} \cos(\theta_{12} + \theta_{23})] \quad (3.11)$$

$$A_{12} = -[d_1 + e_{12} \cos \theta_{12} + e_{13} \cos(\theta_{12} + \theta_{23})] \quad (3.12)$$

and:

$$d_1 = I_1 + \frac{l_1^2}{M} m_1 (m_2 + m_3) (1 - \alpha)^2 \quad (3.13)$$

$$d_2 = I_2 + \frac{l_2^2}{M} \left\{ \beta^2 m_1 m_2 + [m_1 + (1 - \beta)^2 m_2] m_3 \right\} \quad (3.14)$$

$$d_3 = I_3 + \frac{l_3^2}{M} \gamma^2 m_3 (m_1 + m_2) \quad (3.15)$$

$$e_{12} = \frac{l_1 l_2}{M} m_1 (1 - \alpha) (\beta m_2 + m_3) \quad (3.16)$$

$$e_{13} = \frac{l_1 l_3}{M} \gamma m_1 m_3 (1 - \alpha) \quad (3.17)$$

$$e_{23} = \frac{l_2 l_3}{M} \gamma m_3 [m_1 + (1 - \beta) m_2] \quad (3.18)$$

It was shown in chapter 2 that the angular momentum of a hopping robot is conserved during the flight phase. This means that during the flight phase the following constraint is found:

$$\mu_G^{to} = A_3 \dot{\theta}_3 + A_{23} \dot{\theta}_{23} + A_{12} \dot{\theta}_{12} \quad (3.19)$$

with μ_G^{to} being the value of the momentum at the instance of take-off. Since the right hand side is independent of θ_3 , this is again a nonholonomic Caplygin system (see 2.5.1). Indeed, (3.19) can be rewritten such that $\dot{\theta}_3$ is isolated on the lhs and the rhs is independent of θ_3 :

$$\dot{\theta}_3 = \frac{1}{A_3} \left(\mu_G^{to} - A_{23} \dot{\theta}_{23} - A_{12} \dot{\theta}_{12} \right) \quad (3.20)$$

Note that with the current lengths, mass and inertial parameters of the model, even in the impossible case where all the cosines in the formal expression (3.10) for A_3 are set to -1 , one obtains $A_3 = 0.887$. Since this is the lowest value for A_3 , (3.20) always has a finite solution.

If the angular momentum with respect to G had been expressed in absolute angles only, the angular momentum equation would be as follows:

$$\begin{aligned} \mu_G^{to} = & [d_1 + e_{12} \cos(\theta_1 - \theta_2) + e_{13} \cos(\theta_1 - \theta_3)] \dot{\theta}_1 \\ & + [d_2 + e_{12} \cos(\theta_1 - \theta_2) + e_{23} \cos(\theta_2 - \theta_3)] \dot{\theta}_2 \\ & + [d_3 + e_{13} \cos(\theta_1 - \theta_3) + e_{23} \cos(\theta_2 - \theta_3)] \dot{\theta}_3 \end{aligned} \quad (3.21)$$

which is not a Caplygin form. It can not be written in an integral form to solve for θ_3 , which clearly proves the usefulness of expressing μ_G in terms of two relative angles and one absolute angle.

3.4 Dynamics

3.4.1 Flight phase

The dynamical aspects that were discussed in section 2.5.1 of chapter 2 are still valid for this model, being

- Conservation of angular momentum during flight
- Parabolic trajectory of the COG when air drag is neglected

Analogously as in section 2.5.1, the equations of motion are established in the following form:

$$D^{fl}[q]\ddot{q} + C^{fl}[q, \dot{q}]\dot{q} + G^{fl}[q] = T^{fl} \quad (3.22)$$

where $D^{fl}[q]$ is the inertia matrix, $C^{fl}[q, \dot{q}]$ is the centrifugal matrix, $G^{fl}[q]$ is the gravitational torque vector, and T^{fl} is the external torque vector. All details can be found in section A.1 of appendix A.

3.4.2 Impact phase

Calculation of angular velocities and accelerations after impact

The inelastic impulsive impact model was described in section 2.5.2 of chapter 2. The calculation of the velocity discontinuities is done analogously here.

Loss of kinetic energy during impact

It can be shown (see appendix B), that the variation of the kinetic energy during an impulsive impact in a given point F of an interconnected series of rigid bodies can be written as:

$$\Delta K = K^+ - K^- = \frac{1}{2} \bar{P}_1 \cdot (\bar{v}_F^+ + \bar{v}_F^-) \quad (3.23)$$

where \bar{P}_1 is the external percussion in the point F , corresponding to the impact. The velocity of the point F before the impact is denoted by \bar{v}_F^- whereas its velocity after the shock is represented by \bar{v}_F^+ . In case of the hopping robot, the point F represents the ankle point of the foot.

In the particular case of an inelastic impulsive impact without slip, the velocity of the foot point F is zero after the shock, meaning:

$$\bar{v}_F^+ = 0 \quad \Rightarrow \quad \Delta K = \frac{1}{2} \bar{P}_1 \cdot \bar{v}_F^- \quad (3.24)$$

As can be clearly seen in (3.24), the amount of energy loss is proportional to the velocity of the foot before impact. Moreover, since the foot has a velocity different from zero before the shock, and it has a zero velocity after the shock, the percussion and the velocity should always point in the opposite direction. This implies that the variation of the kinetic energy during the impact is always negative, or in other words, an inelastic impact implies a loss of kinetic energy [Janssens, 1983].

When designing the flight phase trajectories for the hopping robot, an adequate choice of the touch-down velocity of the foot will be chosen in order to reduce the amount of energy loss. Theoretically, even hopping without impact would be possible, simply by choosing the velocity of the foot at touch-down equal to zero [Daberkow et al., 1990].

3.4.3 Stance phase

The dynamical model is analogously derived as in section 2.5.1. The equations of motion are:

$$D^{st}[q]\ddot{q} + C^{st}[q, \dot{q}]\dot{q} + G^{st}[q] = T^{st} \quad (3.25)$$

All details can be found in section A.2 of appendix A. Note that the external torque vector now also contains an ankle torque τ_F , as can be seen in figure 3.2.

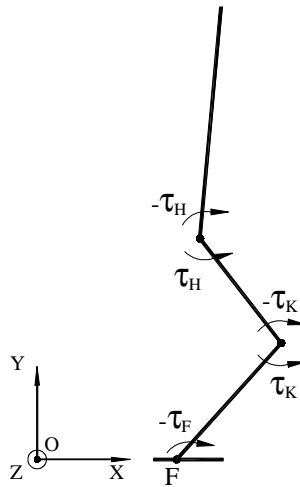


Figure 3.2: Actuator torques at ankle, knee and hip

3.5 Trajectory generation strategy

3.5.1 Flight phase trajectories

General assumptions

Suppose that the configuration of the robot at take-off and touch-down is chosen. This determines the values of:

- take-off: $\theta_{12}^{to}, \theta_{23}^{to}, \theta_3^{to}$
- touch-down: $\theta_{12}^{td}, \theta_{23}^{td}, \theta_3^{td}$

Three objective locomotion parameters are introduced, being:

- horizontal velocity of the COG during flight: ν

- step length: λ
- stepping height: δ

Assuming that the foot is positioned in the origin of the coordinate system at the moment of take-off, yields:

- $X_F^{to} = 0$
- $Y_F^{to} = 0$
- $X_F^{td} = \lambda$
- $Y_F^{td} = \delta$

It is assumed that the foot does not slip at take-off:

- $\dot{X}_F^{to} = 0$
- $\dot{Y}_F^{to} = 0$
- $\ddot{X}_F^{to} = 0$
- $\ddot{Y}_F^{to} = 0$

The velocity of the foot at touch-down determines the amount of kinetic energy loss during impact as was shown in section 3.4.2 and also in [Janssens, 1983], [Daberkow et al., 1990], and [François and Samson, 1998]. Performing touch-down with an improper choice for the foot velocity at touch-down can cause high energy losses during impact. The velocity of the foot at touch-down will be defined here proportional to the velocity of the COG:

- $\dot{X}_F^{td} = k_1 \dot{X}_G^{td}$
- $\dot{Y}_F^{td} = k_2 \dot{Y}_G^{td}$

where $k_1, k_2 \in \mathfrak{R}$ are parameters. Choosing k_1 and k_2 both equal to zero would cause the percussion velocities to be zero, meaning that there would be no shock and no energy loss. This is a rather unrealistic behaviour which is difficult to realize in practice. For the simulations considered, the vertical velocity of the foot is chosen by setting $0 < k_2 < 1$, causing a softer vertical impact. The horizontal velocity \dot{X}_F^{td} can be chosen in the opposite direction as the horizontal velocity of the COG with a value of k_1 in the interval $-1 < k_1 < 0$. This causes a horizontal percussion in the same direction as the velocity of the COG, since the percussion is directed in the opposite direction of the foot velocity \dot{X}_F^{td} . The percussion will cause the COG to accelerate after the shock. This can easily be seen when writing the linear

momentum theorem for the robot over the infinitesimal short time interval of the impact in the horizontal direction:

$$M(\dot{X}_G^+ - \dot{X}_G^-) = P_x$$

which leads to $\dot{X}_G^+ > \dot{X}_G^-$ since $P_x > 0$ here. Generally the COG lies behind the foot point F during the first half of the stance phase, meaning that it is decelerated by gravity. This action can be somewhat counteracted by the accelerating effect of the impact.

Note that nevertheless a loss of kinetic energy is found when referring to (3.24):

$$\Delta K = \frac{1}{2} \left(P_x \dot{X}_F^- + P_y \dot{Y}_F^- \right) < 0$$

The acceleration of the foot at touch-down has an influence on the amplitude of the ground reaction force immediately after impact. Since no distinct advantage resulted from different chosen values for the horizontal acceleration of the foot, it is chosen zero here. The vertical acceleration of the foot is defined proportional to the acceleration of the COG:

- $\ddot{X}_F^{td} = 0 = \ddot{X}_G^{td}$
- $\ddot{Y}_F^{td} = k_3 \ddot{Y}_G^{td}$

where $k_3 \in \mathfrak{R}$ is a parameter. The choice of k_3 will have an influence on the vertical component of the ground reaction force. It is important that this vertical reaction force R_y after impact is large enough, or in other words, that the vertical acceleration of the COG has a value far from $-g$ such that a firm contact with the ground is ensured. The higher R_y when compared to R_x , the lower the risk for slipping. Choosing $k_3 > 1$ results in a higher downward vertical acceleration of the foot than caused by gravity. This introduces a pushing effect of the foot on the ground, resulting in a larger amplitude of R_y .

Constructing the polynomial functions

Since the position of the foot and the configuration of the robot are known at take-off as well as at touch-down, equations (3.4) and (3.5) determine the values of X_G^{to} , Y_G^{to} and X_G^{td} , Y_G^{td} , allowing one to calculate the flight time with (2.103):

$$T^{fl} = \frac{X_G^{td} - X_G^{to}}{\nu} \quad (3.26)$$

The necessary vertical velocity of G at take-off \dot{Y}_G^{to} can be found with (2.106):

$$\dot{Y}_G^{to} = \frac{Y_G^{td} - Y_G^{to}}{T^{fl}} + \frac{gT^{fl}}{2} \quad (3.27)$$

During the flight phase the leg will swing forward, in order to position the foot on a chosen foothold compatible with the environment. Due to the fact that the angular momentum is conserved during the flight phase, the leg swing will cause the upper body to rotate as well, leading to a certain touch-down angle $\theta_{3,real}^{td}$ of the upper body. If a certain desired value for the upper body angle at touch-down θ_3^{td} is chosen, then the value of the angular momentum with respect to the COG at take-off μ_G^{to} will determine whether this desired rotation is attained or not. Since it is difficult to predict which value for this angular momentum is suitable, its value will be determined by an iterative procedure.

This iterative procedure will be started with an approximation of the angular velocity $\dot{\theta}_3^{td}$ of the upper body at the instance of touch-down. It is assumed initially that the body rotates with a constant angular velocity from θ_3^{to} to θ_3^{td} such that:

$$\dot{\theta}_3^{td} \approx \frac{\Delta\theta_3^{fl}}{\Delta t^{fl}} = \frac{\theta_3^{td} - \theta_3^{to}}{T^{fl}} \quad (3.28)$$

Evaluating the first derivatives of (3.4) and (3.5) at touch-down and identifying them with the dynamic expressions (2.42) and (2.43), a linear set of 2 equations is found which can be solved for $\dot{\theta}_{12}^{td}$ and $\dot{\theta}_{23}^{td}$. These values can be introduced in the angular momentum equation (3.19) evaluated at touch-down, allowing one to calculate a first approximation of $\mu_G^{to} = \mu_G^{td}$.

Then, when evaluating the same three expressions at take-off, the values of $\dot{\theta}_{12}^{to}$, $\dot{\theta}_{23}^{to}$ and $\dot{\theta}_3^{to}$ are found.

Next, evaluating the second derivatives of (3.4) and (3.5) at take-off and identifying them with the dynamic expressions (2.40) and (2.41), yields 2 equations in the three unknowns $\ddot{\theta}_{12}^{to}$, $\ddot{\theta}_{23}^{to}$ and $\ddot{\theta}_3^{to}$. A third equation is found when evaluating the first derivative of the angular momentum equation (3.19) at take-off, allowing one to calculate the three angular accelerations.

Finally when evaluating the same three equations at touch-down, the values of $\ddot{\theta}_{12}^{td}$, $\ddot{\theta}_{23}^{td}$ and $\ddot{\theta}_3^{td}$ are also found.

As a result of the preceding computations the values for θ_{12} and θ_{23} at take-off and touch-down as well as their first and second derivatives are found, and are used to establish two fifth order polynomial functions for $\theta_{12}^{fl}(t)$ and $\theta_{23}^{fl}(t)$. These polynomial functions are the trajectories to be tracked during the flight phase by the actuators at knee and hip respectively.

The real touch-down angle of the upper body $\theta_{3,real}^{td}$ results from numerically integrating (3.20) over time during the flight phase:

$$\theta_{3,real}^{td} = \theta_3^{to} + \int_0^{T^{fl}} \left(\frac{\mu_G^{to} - A_{23}\dot{\theta}_{23}^{fl} - A_{12}\dot{\theta}_{12}^{fl}}{A_3} \right) dt \quad (3.29)$$

This angle will differ from the desired value of θ_3^{td} , since an approximated expression

for $\dot{\theta}_3^{td}$ was used. The value of $\dot{\theta}_3^{td}$ will now be adjusted by iteration with:

$$\dot{\theta}_3^{td,n+1} = \dot{\theta}_3^{td,n} + \frac{1}{T_{fl}} (\theta_3^{td} - \theta_{3,real}^{td}) \quad (3.30)$$

where θ_3^{td} is the desired value of the absolute angle of the upper body at touch-down, and the above calculations are repeated. A variety of simulations showed that in all cases the error made by the approximation of $\dot{\theta}_3^{td}$ seemed to be rather small, such that this procedure converges in a few (less than 5) iterations.

Pulling up the foot

The behaviour of the polynomial functions $\theta_{12}^{fl}(t)$ and $\theta_{23}^{fl}(t)$ is completely determined by the boundary points only. The hopping height, as defined by (2.108), is in this case not an objective parameter, but its value is determined by the values of the different objective parameters. Particularly during hops with a smaller value for the hopping height, the foot can hit the ground during the swing. Therefore a correction on the polynomial functions is introduced. An intermediate point is added to the polynomial functions to make sure that the foot reaches a certain desired height at $t = t^*$, where t^* is the time step where G reaches its maximum height:

$$\dot{Y}_G(t^*) = 0 \quad (3.31)$$

Note that in case an obstacle has to be cleared by the robot, the reference trajectories will be designed such that the COG reaches its highest position while jumping over the obstacle. The correction functions are introduced such that the foot reaches its maximum height at the same time, as shown in figure 3.3. This strategy is chosen here, since it results in an analytical solution for the correction functions.

From the dynamic equation (2.43) it can be found that:

$$t^* = \frac{\dot{Y}_G^{to}}{g} \quad (3.32)$$

Suppose that the following is demanded for the foot at $t = t^*$:

$$Y_F^{des}(t^*) = \sigma \quad (3.33)$$

$$\dot{Y}_F^{des}(t^*) = 0 \quad (3.34)$$

where the value of σ can be chosen and will be referred to as the foot clearance. Choosing the derivative of the vertical foot position equal to zero aims at a maximum foot height at $t = t^*$ (see figure 3.3)

Two correction functions $C_{12}(t)$ and $C_{23}(t)$ will be added, which do not change the boundary conditions of the polynomial functions:

$$\zeta_{12}(t) = \theta_{12}^{fl}(t) + C_{12}(t) = \theta_{12}^{fl}(t) + K_{12}f(t) \quad (3.35)$$

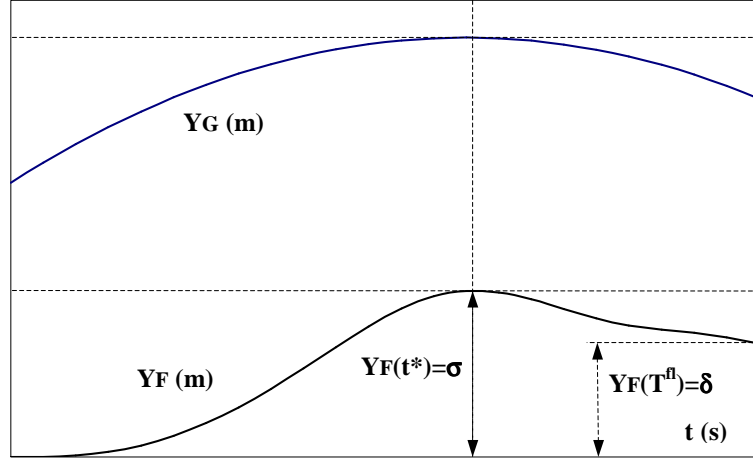


Figure 3.3: Foot and COG reach a maximum height at the same time

$$\zeta_{23}(t) = \theta_{23}^{fl}(t) + C_{23}(t) = \theta_{23}^{fl}(t) + K_{23}f(t) \quad (3.36)$$

with:

$$f(t) = \left[1 - 3(t - t^*) \left(\frac{1}{t^*} - \frac{1}{T^{fl} - t^*} \right) \right] \frac{t^3 (T^{fl} - t)^3}{t^{*3} (T^{fl} - t^*)^3}$$

and K_{12} and K_{23} are constants which have to be determined depending on the value of σ , which is desired height of the foot at $t = t^*$.

These correction functions have the following characteristics:

$$\begin{aligned} C_{ij}(0) &= 0 \\ \dot{C}_{ij}(0) &= 0 \\ \ddot{C}_{ij}(0) &= 0 \\ C_{ij}(T^{fl}) &= 0 \\ \dot{C}_{ij}(T^{fl}) &= 0 \\ \ddot{C}_{ij}(T^{fl}) &= 0 \\ C_{ij}(t^*) &= K_{ij} \\ \dot{C}_{ij}(t^*) &= 0 \end{aligned}$$

Identifying (3.5) with (2.45) and evaluating this expression at t^* gives:

$$\sigma + a \sin(\zeta_3^* - \zeta_{12}^* - \zeta_{23}^*) + b \sin(\zeta_3^* - \zeta_{23}^*) + c \sin \zeta_3^* = -\frac{g}{2} t^{*2} + \dot{Y}_G^{to} t^* + Y_G^{to} \quad (3.37)$$

with the constants a , b and c respectively defined by (3.6), (3.7) and (3.8). The $*$ indicates the evaluation of the functions ζ_{12} and ζ_{23} at time step t^* , and ζ_3^* represents the new value of the absolute angle of the body with respect to the horizontal axis at that time step.

After introducing (3.35) and (3.36) in (3.37) one obtains:

$$\begin{aligned} \sigma + a \sin(\zeta_3^* - \theta_{12}^* - \theta_{23}^* - K_{12} - K_{23}) + b \sin(\zeta_3^* - \theta_{23}^* - K_{23}) + c \sin \zeta_3^* \\ = -\frac{g}{2}t^{*2} + \dot{Y}_G^{to}t^* + Y_G^{to} \end{aligned} \quad (3.38)$$

Further, identifying the first derivative of (3.5) with (2.43) and evaluating this expression at t^* leads to:

$$\begin{aligned} a \cos(\zeta_3^* - \zeta_{12}^* - \zeta_{23}^*) \left(\dot{\zeta}_3^* - \dot{\zeta}_{12}^* - \dot{\zeta}_{23}^* \right) + b \cos(\zeta_3^* - \zeta_{23}^*) \left(\dot{\zeta}_3^* - \dot{\zeta}_{23}^* \right) \\ + c \cos \zeta_3^* \dot{\zeta}_3^* = -gt^* + \dot{Y}_G^{to} \end{aligned} \quad (3.39)$$

Taking into account (2.43) and (3.31) it is seen that the rhs of (3.39) is zero:

$$-gt^* + \dot{Y}_G^{to} = \dot{Y}_G(t^*) = 0$$

After introducing (3.35) and (3.36), equation (3.39) becomes:

$$\begin{aligned} a \cos(\zeta_3^* - \theta_{12}^* - \theta_{23}^* - K_{12} - K_{23}) \left(\dot{\zeta}_3^* - \dot{\theta}_{12}^* - \dot{\theta}_{23}^* \right) \\ + b \cos(\zeta_3^* - \theta_{23}^* - K_{23}) \left(\dot{\zeta}_3^* - \dot{\theta}_{23}^* \right) + c \cos \zeta_3^* \dot{\zeta}_3^* = 0 \end{aligned} \quad (3.40)$$

Equations (3.38) and (3.40) have to be solved for K_{12} and K_{23} . The problem is that the values of ζ_3^* and $\dot{\zeta}_3^*$ are unknown. They depend on the trajectories of ζ_{12} and ζ_{23} , which at this point are unknown. The approximation is made that their values do not change significantly because of the corrections on θ_{12} and θ_{23} :

$$\begin{aligned} \zeta_3^* &\approx \theta_3^* \\ \dot{\zeta}_3^* &\approx \dot{\theta}_3^* \end{aligned}$$

It is assumed that ζ_3^* fluctuates around $\frac{\pi}{2}$:

$$c \cos \zeta_3^* \dot{\zeta}_3^* \approx 0$$

Now the set of equations (3.38) and (3.40) has become of the following form:

$$A_1 \sin \alpha_1 + A_2 \sin \alpha_2 = C_1 \quad (3.41)$$

$$B_1 \cos \alpha_1 + B_2 \cos \alpha_2 = 0 \quad (3.42)$$

with:

$$A_1 = a$$

$$A_2 = b$$

$$C_1 = -\frac{g}{2}t^{*2} + \dot{Y}_G^{to}t^* + Y_G^{to} - c \sin \theta_3^* - \sigma$$

$$B_1 = a \left(\dot{\theta}_3^* - \dot{\theta}_{12}^* - \dot{\theta}_{23}^* \right)$$

$$B_2 = b \left(\dot{\theta}_3^* - \dot{\theta}_{23}^* \right)$$

$$\alpha_1 = \theta_3^* - \theta_{12}^* - \theta_{23}^* - K_{12} - K_{23}$$

$$\alpha_2 = \theta_3^* - \theta_{23}^* - K_{23}$$

This set of (3.41) and (3.42) can easily be solved by applying the following substitutions:

$$X_1 = \sin \alpha_1$$

$$X_2 = \sin \alpha_2$$

$$Y_1 = \cos \alpha_1$$

$$Y_2 = \cos \alpha_2$$

which leads to the following set:

$$X_1^2 + Y_1^2 = 1$$

$$X_2^2 + Y_2^2 = 1$$

$$A_1 X_1 + A_2 X_2 = C_1$$

$$B_1 Y_1 + B_2 Y_2 = 0$$

This set can e.g. be solved for X_2 by eliminating X_1 , Y_1 and Y_2 :

$$X_2^2(A_1^2 B_2^2 - B_1^2 A_2^2) + 2X_2 A_2 B_1^2 C_1 + B_1^2 A_1^2 - B_1^2 C_1^2 - A_1^2 B_2^2 = 0$$

which is a quadratic equation in X_2 .

Note that the correction functions have to be added before the integral (3.29) is calculated. They do have an influence on the angle θ_3^{td} .

3.5.2 Stance phase trajectories

Constructing the polynomial functions

During the stance phase the robot is fully actuated since an extra actuator is considered, located at the ankle joint. For the robot to be able to perform the control of the flight phase described above, there is a certain control needed during the stance phase of the preceding hop, yielding the desired initial conditions at take-off. Using the results of the impact phase and the results of the algorithm developed for controlling the flight phase, three polynomial functions are constructed which have to be tracked during stance. With respect to the desired objectives, being horizontal velocity during flight, step length, step height and foot clearance, both a hopping pattern consisting of different successive hops as well as a steady hopping pattern, can be realized. Steady hopping requires that the leg links as well as the upper body act in the same way every hop, both in the stance phases and the flight phases.

Two polynomial functions will be constructed to steer the internal angles at hip and knee. The third function will be used to steer the absolute angle of the lower leg with respect to the ground. Since the beginning of the stance phase is the end of the impact phase, the initial conditions for the stance phase are determined by the impact model. In the case of steady hopping, the same values for θ_{12}^{to} , θ_{23}^{to} , and θ_3^{to} and their first and second derivatives, as calculated for the preceding flight phase can be used for the construction of the polynomial functions of the stance phase. In fact the ankle steer function is θ_1 , but the boundary values for this function are calculated as:

$$\begin{aligned}\theta_1^+ &= \theta_3^+ - \theta_{23}^+ - \theta_{12}^+ \\ \theta_1^{to} &= \theta_3^{to} - \theta_{23}^{to} - \theta_{12}^{to}\end{aligned}$$

The first and second derivatives are analogously derived.

When a hopping pattern with different consecutive hops is needed, when hopping on irregular terrain e.g. or when accelerating or decelerating, the polynomial functions can be constructed in the same way, but now the take-off conditions are determined by the objective parameters for the next flight phase.

Compared to the steering functions for the flight phase, there is an additional degree of freedom in the construction of these functions for the stance phase. The end of the flight phase is determined by the flight time, which on its term is determined by expression (3.26), whereas the end of the stance phase, being the moment of take-off, can be chosen. At this point, in case of steady hopping, the stance time T^{st} will be chosen such that the mean horizontal velocity during the stance phase \tilde{v}_x^{st} is equal to the take-off velocity \dot{X}_G^{to} :

$$T^{st} = \frac{\Delta X_G^{st}}{\tilde{v}_x^{st}} = \frac{X_G^{to} - X_G^{td}}{\dot{X}_G^{to}} \quad (3.43)$$

with X_G^{to} being determined by the take-off configuration of the next flight phase and X_G^{td} is known from the preceding flight phase. Suppose for non-steady hopping that during the stance phase the horizontal velocity of the COG has to change from $\dot{X}_G^{td} = \dot{X}_G^{to,old}$ at touch-down to $\dot{X}_G^{to,new}$ at take-off. If the mean horizontal velocity is approximated with

$$\tilde{v}_x^{st} \approx \frac{\dot{X}_G^{to,old} + \dot{X}_G^{to,new}}{2}$$

then the following value for the stance time T^{st} is chosen:

$$T^{st} = 2 \frac{X_G^{to} - X_G^{td}}{\dot{X}_G^{to,old} + \dot{X}_G^{to,new}} \quad (3.44)$$

As T^{st} is known, the polynomial functions $\theta_{12}^{st}(t)$, $\theta_{23}^{st}(t)$, $\theta_3^{st}(t)$ can be established. When the controllers for both the flight phase and the stance phase are able to track the prescribed functions, the robot is able to perform any desired hopping pattern, with every hop satisfying the prescribed objective locomotion parameters.

In order to clearly summarize the different steps of the strategy generating the trajectories for the flight phase and the stance phase of each step, a flow chart is given in figure 3.4.

Torque limitations

In terms of geometrical and actuator constraints the hopping pattern has to be physically realizable.

In that context, special attention has to be given to the actuator at the ankle joint. Because of the limited length of the foot, the torque τ_F that can be exerted at the ankle joint is limited. If this torque exceeds a certain value, the foot will start rotating [Goswami, 1999], or in other words the robot will tip over. Depending on the side of the foot where the rotation occurs, two different situations are distinguished, being *heel-off* and *toe-off*. In order to avoid foot rotation, the ankle torque will be truncated. From figures 3.5 and 3.6 it is seen that the following constraints have to be satisfied during the stance phase:

$$\tau_F^{>0} < M \left(\ddot{Y}_G + g \right) l_{F2} \quad (3.45)$$

$$\tau_F^{<0} > -M \left(\ddot{Y}_G + g \right) l_{F1} \quad (3.46)$$

where

$$M \left(\ddot{Y}_G + g \right) = R_y$$

Condition (3.45) has to be satisfied when $\tau_F > 0$ to avoid toe-off, and condition (3.46) in case of $\tau_F < 0$ to avoid heel-off. The length l_{F1} is the length of the foot in front of the ankle point, length l_{F2} is the length of the foot behind the ankle point.

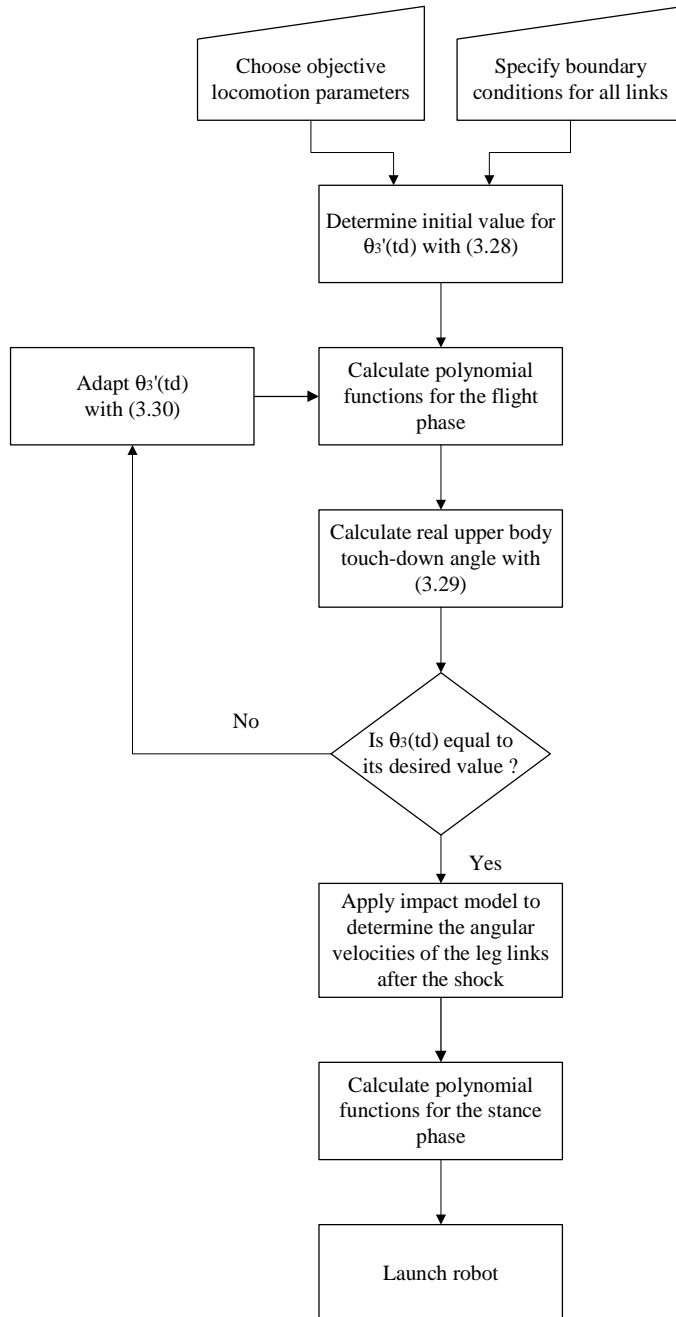


Figure 3.4: Flow chart describing different steps in strategy

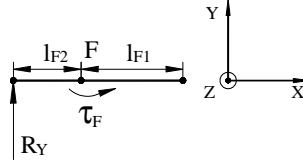


Figure 3.5: Maximum value for positive ankle torque

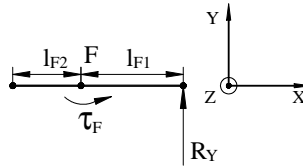


Figure 3.6: Maximum value for negative ankle torque

The constraints (3.45) and (3.46) result from the fact that the ZMP [Vukobratovic et al., 1990], [Goswami, 1999] should remain within the surface of the foot. As can be seen, the magnitude of reaction force R_y has great influence on the torque which can be exerted. The larger R_y , the further the Zero Moment Point stays away from the endpoints of the foot. Therefore the foot generates an extra push at touch-down. This is done by choosing the parameter associated to the vertical acceleration of the foot at touch-down $k_3 > 1$, which alters value of the vertical reaction force immediately after the impact (see section 3.5.1).

Another limitation which is applicable to the exerted torques at hip, knee and ankle joints is due to the limited friction between the foot and the ground. When applying Coulomb's friction law, the following constraint has to be satisfied during the stance phase in order to avoid slipping of the foot:

$$|R_x| < f_k |R_y|$$

with f_k being the kinematic friction coefficient.

A last limitation is due to the performance of the different actuators. Every actuator has a limitation on its maximum power as well as on the maximum torque it can exert.

When the control algorithm generates the reference trajectories, it is possible to take all these constraints into account and calculate the most ideal trajectories depending on the criterion that is used [Chevallereau and Aoustin, 1999]. This method can however not be used in real time because it requires an extensive amount of computation. We suggest to use simulations to determine which take-off and touch-down configurations in combination with which sets of the objective locomotion parameters deliver trajectories which satisfy all the constraints, and store this information in a lookup table. The trajectory planning algorithm of a real robot could then use this information to make sure that the reference trajectories

are calculated such that the maximum torques are not exceeded in some area around the trajectory.

3.6 Simulations

In this section, the results of 2 different simulations are presented. These simulations are again performed using the multibody code *Mechanica Motion*, with a parallel spring and damper system to model the ground. The parallel spring and damper system will introduce other values for the joint discontinuities than the ones predicted by the inelastic impulsive impact model, which is used by the trajectory generation strategy. Immediately after the impact phase, there will thus be a deviation between the real angular velocities and the reference velocities. This allows one to verify if the motion of the robot is significantly disturbed by these initial deviations. Moreover, the actuators are simulated by PD-controlled torques which have to track the polynomial steering functions calculated by the algorithm. Due to the fact that simple PD-controllers are used, the algorithm is tested in case of non-perfect tracking of the reference trajectories. This allows one to verify if the robot's balance is disturbed by these tracking errors.

3.6.1 Steady hopping pattern

To test the strategy, first a hopping pattern consisting of a number of identical consecutive hops has been simulated. Consequently, the desired values of the objective parameters are the same for every hop, as well as the behaviour of the upper body. The chosen parameters are the following:

- $\nu = 1 \text{ m/s}$, $\lambda = 0.4 \text{ m}$, $\delta = 0$
- $\theta_{12}^{to} = 42^\circ$, $\theta_{23}^{to} = -9.5^\circ$, $\theta_3^{to} = 90^\circ$
- $\theta_{12}^{td} = 44^\circ$, $\theta_{23}^{td} = -42.5^\circ$, $\theta_3^{td} = 80^\circ$
- $\dot{X}_F^{td} = -1 \text{ m/s}$ ($k_1 = -1$), $\dot{Y}_F^{td} = -0.47 \text{ m/s}$ ($k_2 = 0.5$)
- $\ddot{X}_F^{td} = 0$, $\ddot{Y}_F^{td} = -19.62 \text{ m/s}^2$ ($k_3 = 2$)
- $\sigma = 0.05 \text{ m}$, $t^* = 0.1 \text{ s}$

This results in the following:

- $T^{fl} = 0.2 \text{ s}$
- $\dot{\theta}_3^{td} = -0.15 \text{ rad/s}$ (3 iterations were needed)
- $\mu_G^{to} = -0.26 \text{ kgm}^2/\text{s}$

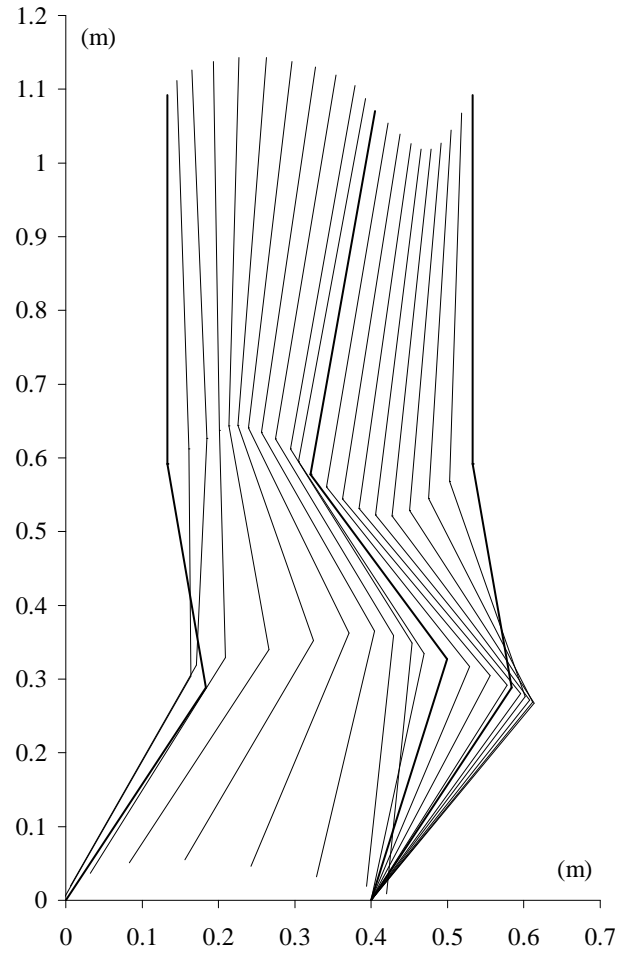


Figure 3.7: Stick diagram for one hop of the steady hopping pattern

- $T^{st} = 0.2 \text{ s}$

Figure 3.7 shows a stick diagram for one hop of the hopping pattern executed by the robot.

Figure 3.8 shows the horizontal velocity \dot{X}_G of the global COG versus time. The horizontal parts of the graph represent the velocity during the flight phases, equaling the desired value of 1 m/s . For the first hop the robot reaches exactly the desired value, because the initial conditions were set manually to start the simulation. The second hop results from a stance phase where the torques are PD-controlled. The deviation due to the non-perfect tracking of the reference trajectories is however very small and does not become larger during the consecutive hops.

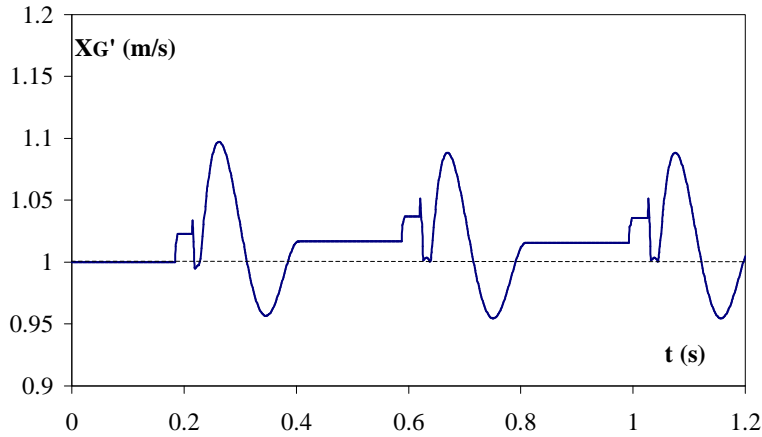


Figure 3.8: Horizontal velocity COG

Figure 3.9 gives the horizontal position X_F of the foot versus time. The horizontal parts of the graph represent the position of the foot during the stance phases. The difference between the position during two successive stance phases equals the desired step length of 0.4 m .

The vertical position of the foot Y_F is shown in graph 3.10. During the stance phases the position is equal to 0 since this is the desired step height. During flight the foot reaches its highest vertical position at $t = 0.1\text{ s}$ as what was chosen. The maximum value differs slightly from the chosen value (about 5 mm) because of the approximations that were made in section 3.5.1. The graph shows also that the robot slightly bounces due to the simulated spring and damper model of the ground. Contrary to what the control algorithm assumes, there is not a perfect inelastic collision. This does however not disturb the motion significantly, since the robot still reaches the prescribed values for its objective locomotion parameters. Note that the bouncing phenomenon is also visible in figure 3.8, where the first touch-down is followed by a short period with a constant horizontal velocity, which indicates that the robot is in flight. After the second touch-down a firm contact with the ground is ensured until the next take-off.

The angular momentum with respect to the global COG μ_G is given in figure 3.11. It shows clearly that a steady state behaviour is reached and that during every flight phase the angular momentum is equal to the value predicted by the control algorithm.

In figure 3.12, the absolute angle θ_3 of the upper body with respect to the horizontal axis is depicted. The rotation which occurs during flight is fully compensated during the next stance phase.

Figure 3.13 shows the loss of kinetic energy during the impact phase as a function of the parameter k_2 , which determines the value of the vertical velocity of the foot

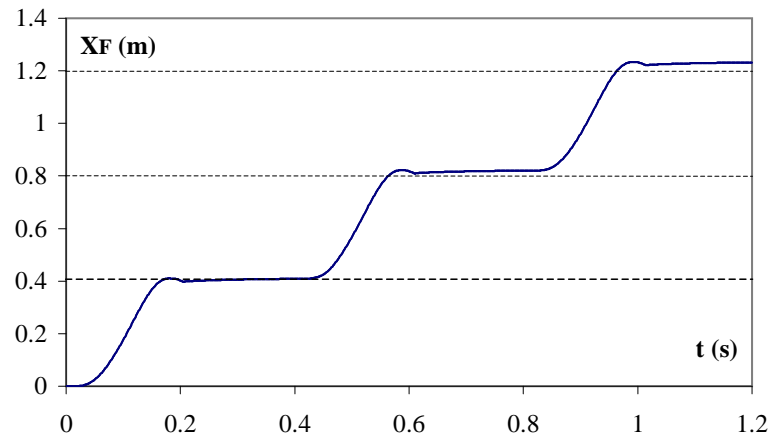


Figure 3.9: Horizontal position foot

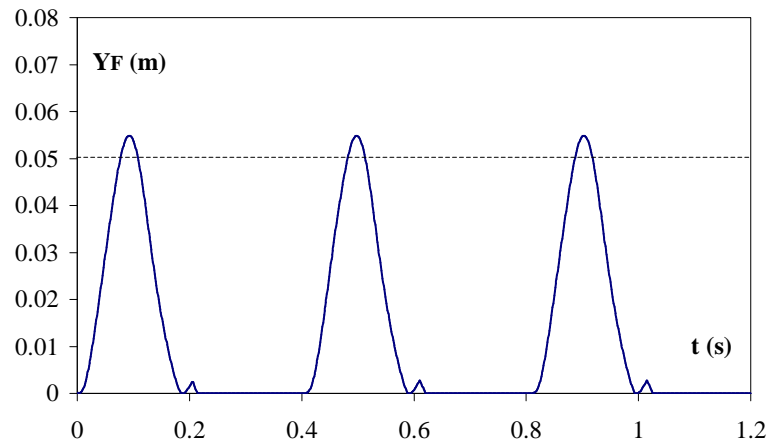


Figure 3.10: Vertical position foot

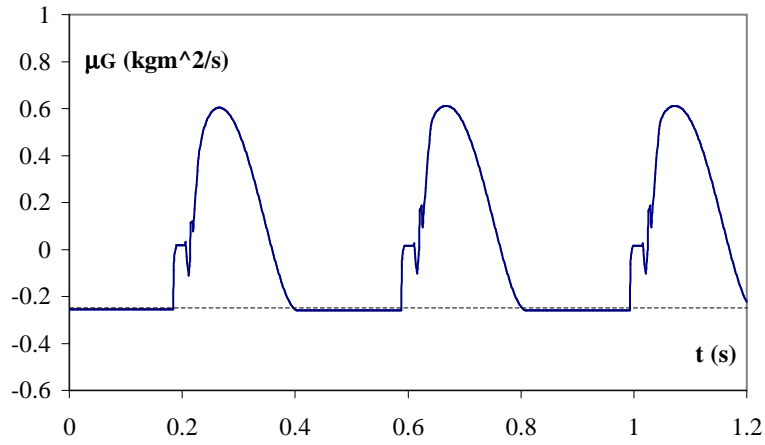


Figure 3.11: Angular momentum with respect to the COG

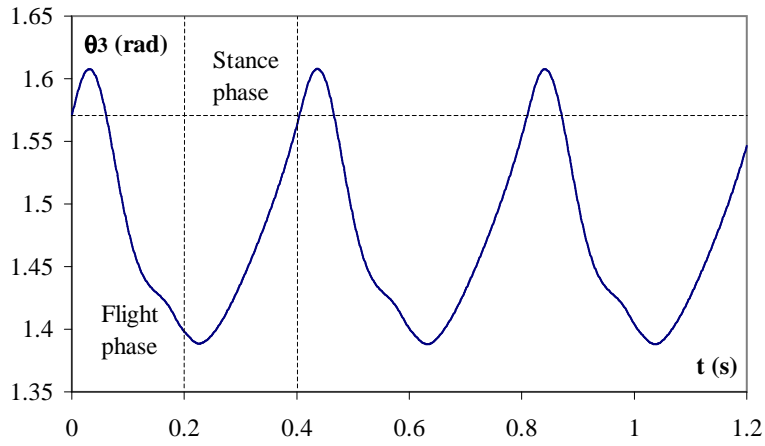


Figure 3.12: Absolute angle upper body with respect to horizontal axis

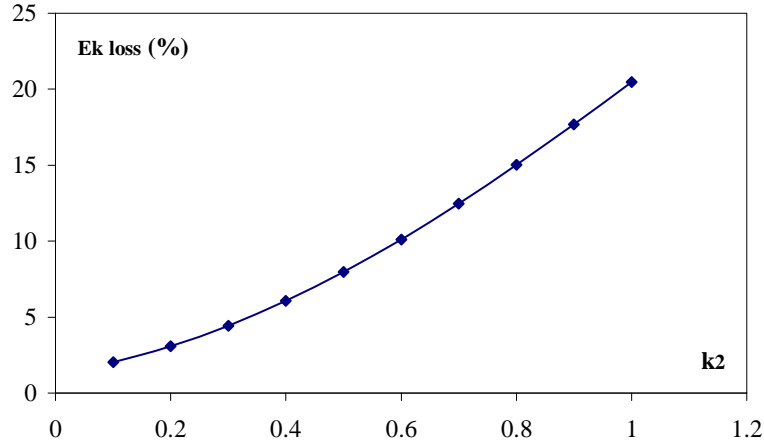


Figure 3.13: Kinetic energy loss during impact versus k_2

(recall that $k_1 = -1$ and $k_3 = 2$ were chosen). The relative energy loss is calculated as:

$$E_{kloss} = \frac{E_k^- - E_k^+}{E_k^-}$$

It is clearly seen that this loss of energy increases with increasing value of k_2 . With the chosen value of $k_2 = 0.5$, the loss of kinetic energy due to the impact is less than 10%.

The pushing effect introduced by choosing k_3 greater than 1 is clearly illustrated in figure 3.14. It shows that the vertical reaction force after impact indeed increases with increasing k_3 . The ground reaction force is nearly doubled when choosing $k_3 = 2$, when compared to the case of $k_3 = 1$.

Further, the effect of choosing a negative value for k_1 is presented in figure 3.15. The variation of the horizontal velocity during the shock, relative to the value during flight, is calculated as:

$$V_{Gxvar} = \frac{\dot{X}_G^+ - \dot{X}_G^-}{\dot{X}_G^-} = \frac{\dot{X}_G^+ - \nu}{\nu}$$

Indeed, when $k_1 = -1$, a horizontal acceleration of 5% of the COG is caused relative to the touch-down velocity, thus reducing the effect of deceleration by gravity.

Figure 3.16 depicts the necessary value for the kinematic friction coefficient f_k during the stance phase, when using the Coulomb's friction model. It can be seen that the maximum value is approximately 0.21, appearing after impact. This value ensures that slip is not to be expected and the assumptions of a fixed foot during stance are indeed valid. According to [Jansson and Grahn, 1995] the kinematic

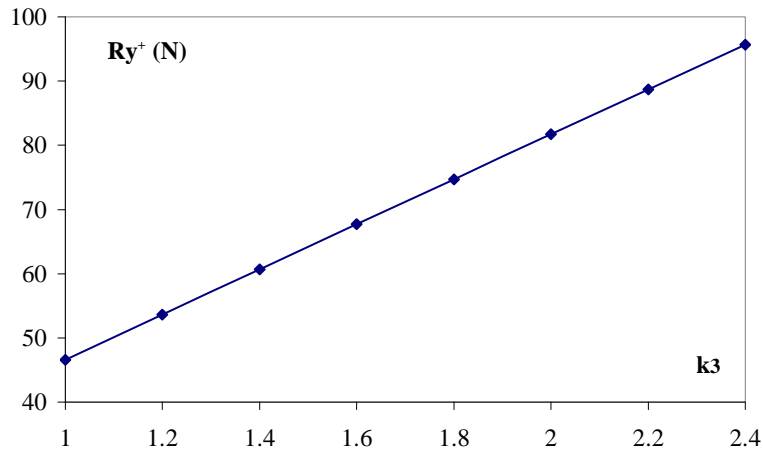


Figure 3.14: Vertical ground reaction force after impact versus k_3

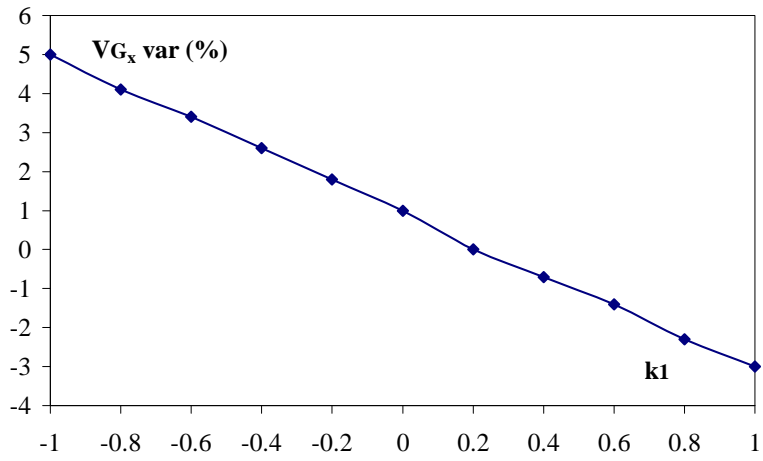


Figure 3.15: Horizontal velocity variation during impact versus k_1

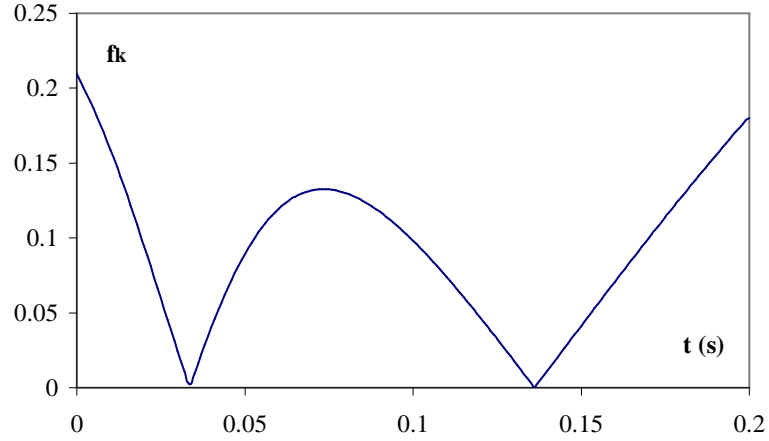


Figure 3.16: Coulomb's kinematic friction coefficient needed during stance phase

friction coefficient for a rubber/asphalt contact would have a value between 0.7-1.0, which is significantly higher than what is found here.

Finally, figure 3.17 gives the value of the ankle torque versus time during the stance phase. The two thin lines on the graph represent the minimum and maximum allowed values of the foot torque calculated with expressions (3.45) and (3.46) respectively. These lines shift when the physical lengths of the foot are varied. In order to make the ankle torque not exceed the limits, the following physical lengths for the foot had to be used:

$$l_{F1} = 8cm \quad (\text{in front of ankle joint})$$

$$l_{F2} = 3cm \quad (\text{behind ankle joint})$$

Reducing the foot lengths would cause the ankle torque to cross the lines representing the minimum and maximum values. These minimal lengths for the foot correspond to the maximum distance of the ZMP to the ankle joint during a stance phase. Unfortunately these distances are not predicted by the algorithm, which can be seen as a drawback of the strategy. In chapter 4 the strategy will be adapted in order to keep the ZMP in the vicinity of the ankle joint.

3.6.2 Non-steady hopping pattern

The following experiment makes the robot change its objective parameters from one hop to another, which simulates the motion on irregular terrain. A first hop is performed with the set of objective parameters given in 3.6.1, and a second hop is performed by increasing both the step length and the forward velocity with 20%. After that, the robot has to reach a steady hopping pattern with the new set

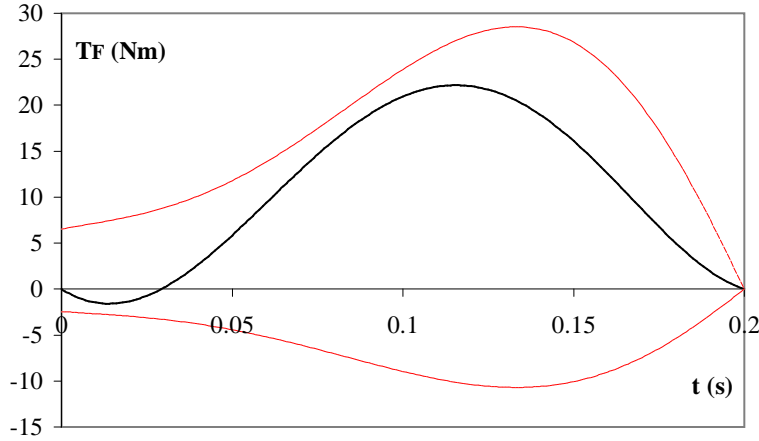


Figure 3.17: Ankle torque during one stance phase

of objective parameters. The transition between the two hopping patterns is made without changing the take-off and touch-down configuration.

The objective parameters of the two hopping patterns and the duration of each phase have the following values:

- Flight phase for pattern 1: $\nu = 1m/s$ $\lambda = 0.4m$ $\delta = 0$ $T^{fl} = 0.2s$
- Transition stance phase: $T^{st} = 0.18s$
- Flight phase for pattern 2: $\nu = 1.2m/s$ $\lambda = 0.5m$ $\delta = 0$ $T^{fl} = 0.25s$
- Stance phase for pattern 2: $T^{st} = 0.17s$

In figure 3.18 the transition between the two hopping patterns is illustrated by a stick diagram

Figures 3.19, 3.20, 3.21 and 3.22 show that, concerning the values of the objective parameters and the orientation of the upper body, the same conclusions can be drawn as in section 3.6.2. Indeed the new steady hopping pattern is attained.

Figure 3.20 shows that during the flight phases of the second hopping pattern the error on the foot height has become larger. This is due to the approximations made in section 3.5.1. Indeed the upper body oscillates back and forth with a greater amplitude during the longer flight phases (see figure 3.22). The approximation of the upper body being vertically oriented during the flight phase, introduces larger errors on the correction functions for the joint trajectories.

Figure 3.23 shows the ankle torque versus time during the transition phase. The thin lines again represent the minimum and maximum values of the torque calculated with expressions (3.45) and (3.46) respectively. In order to make the ankle

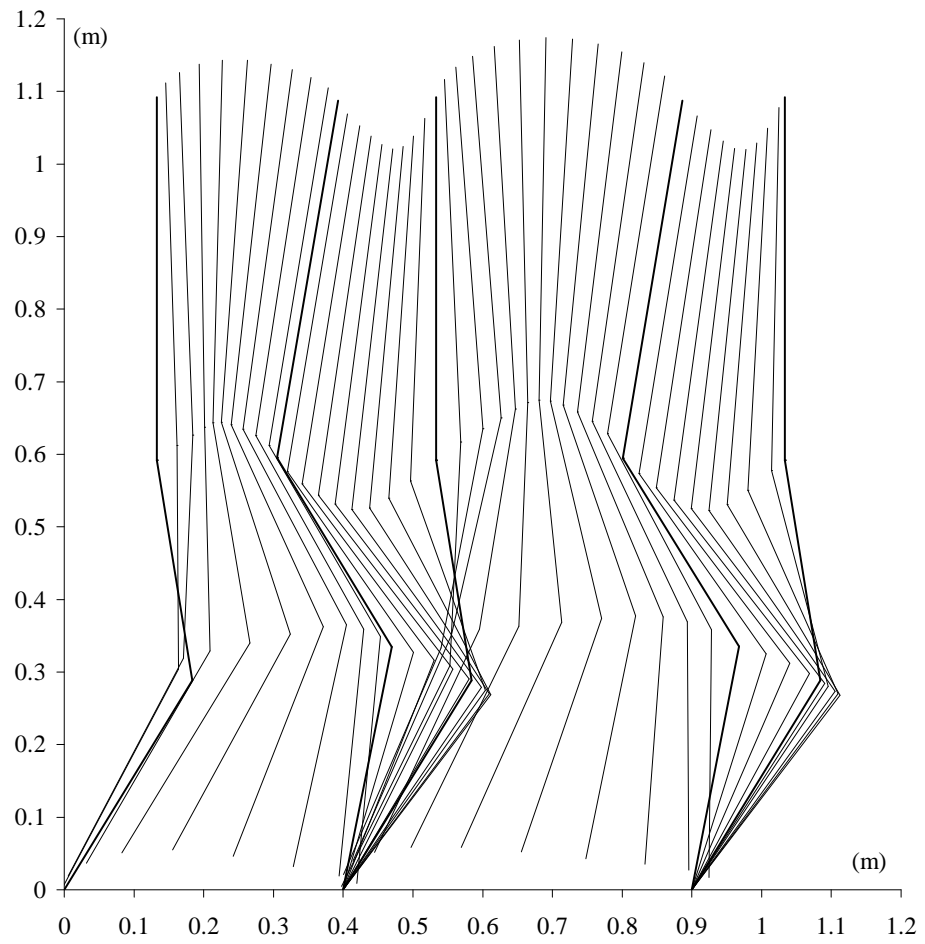


Figure 3.18: Stick diagram non-steady hopping

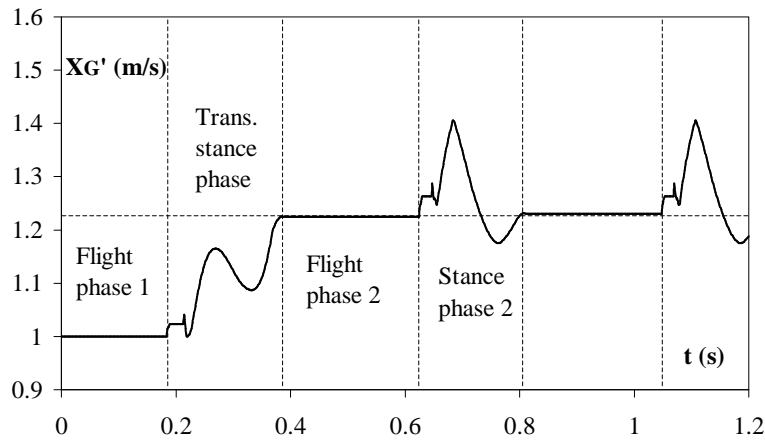


Figure 3.19: Horizontal velocity COG

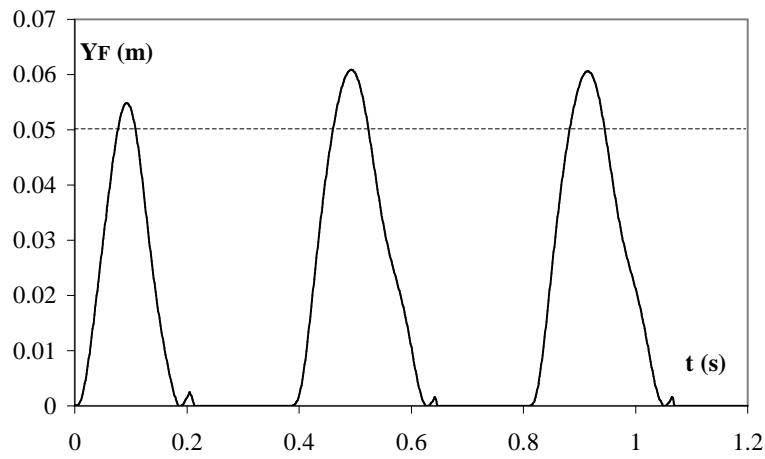


Figure 3.20: Vertical position foot

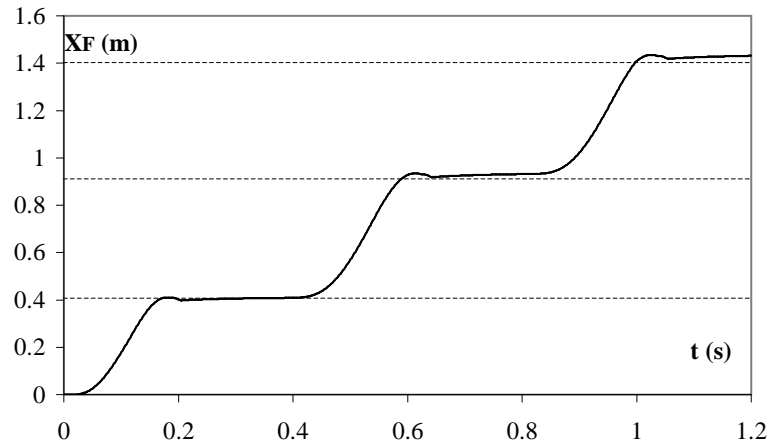


Figure 3.21: Horizontal position foot

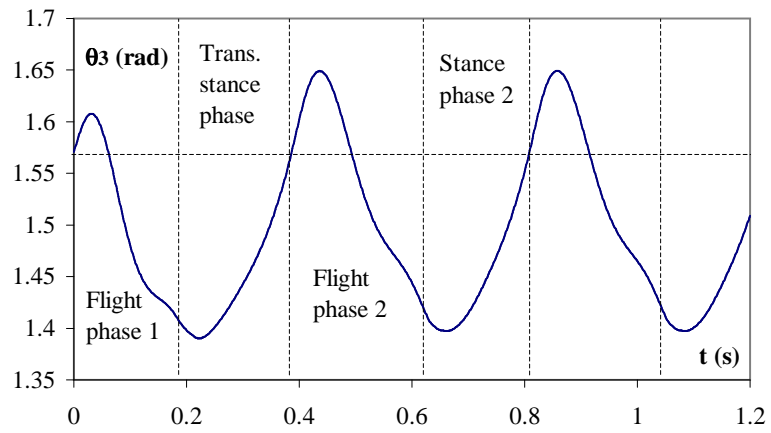


Figure 3.22: Absolute angle upper body with respect to horizontal axis

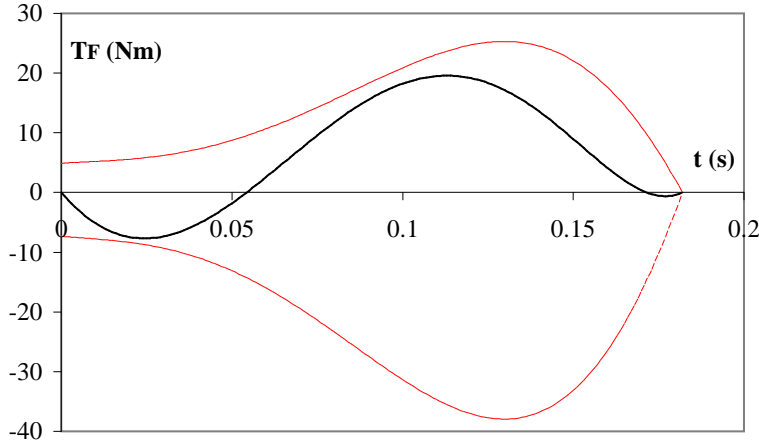


Figure 3.23: Ankle torque during transition stance phase

torque not exceed the limits, the following physical lengths for the foot are needed:

$$l_{F1} = 6\text{cm} \quad (\text{in front of ankle joint})$$

$$l_{F2} = 7\text{cm} \quad (\text{behind ankle joint})$$

The negative part of the foot torque in the beginning of the stance phase leads to a motion of the ZMP in the backwards direction. Due to this backward motion, the foot length behind the ankle joint has to be increased to 7 cm . This motion of the ZMP is of no use, and indicates that a horizontal acceleration on the COG is imposed at the beginning of the stance phase which is too high. Since the horizontal velocity of the COG has to be increased with 20 % during this stance phase, an acceleration is to be expected, but the graph clearly indicates that the imposed acceleration after impact is too high. It is known that gravity tends to decelerate the COG when its print lies behind the ankle joint, such that heavily accelerating the COG at that time can be considered as unnatural. The conclusion that has to be drawn here is that the choice of the stance time by (3.44) is not optimal. Indeed, it is the stance time which determines the mean horizontal velocity of the COG, which on its term determines the amount of horizontal deceleration and acceleration of the COG.

3.7 Summary

A first version of a trajectory generation strategy for a one-legged hopping robot is presented. The robot is able to hop on irregular terrain, since it is possible to change its objective locomotion parameters from one hop to another. For each hop, the velocity as well as the step length and the step height can be altered. Drift

on the upper body motion is avoided, since the rotation resulting from the leg swing during the flight phase is fully compensated during the next stance phase by an ankle actuator which makes the robot fully actuated during the stance phases. During the flight phase the robot is still underactuated. It can however move from a chosen initial configuration to a chosen end configuration. To make this possible, the angular momentum constraint is written in a Caplygin form, and an adequate estimation of the angular momentum with respect to the COG is made. Using an iterative procedure the angular velocity of the upper body at touch-down is adapted until the desired end configuration is reached. Simulations show that few iterations are needed which leads to a real-time applicable strategy based on a small number of simple calculations.

When establishing the proposed strategy, special attention has been given to the touch-down conditions of the foot. It has been shown that tuning the vertical velocity of the foot before impact causes a significant reduction of the kinetic energy loss during the shock. Moreover it was shown that the vertical acceleration of the foot before impact can be used to increase the vertical component of the ground reaction force, thus assuring a more firm foot/ground contact after the shock (pushing effect). Finally, the horizontal velocity of the foot before impact can be used to accelerate the COG in the horizontal direction after the impact, by choosing its direction opposite to the horizontal velocity of the COG.

A more detailed discussion of the simulation results, reveals some strong as well as weaker parts of the strategy. The strategy is built up by two different objectives, namely the part which guarantees that the values of all the objective locomotion parameters are attained, and the part which is responsible for the control of the upper body motion.

From the simulations it can be seen that the first part of the strategy works very well. All desired values for the objective locomotion parameters are reached, even in the case of non-perfect tracking of the reference trajectories by the controllers, and when using an estimated value for the variables after impact. This technique, based on objective locomotion parameters, steers in fact the dynamics of the robot in a kinematic way. Such a strategy has the advantage that errors e.g. introduced by abandoning friction at the joints will not change the shape of the reference trajectories. Indeed, such a friction would only result in underestimated torque values, but as long as the joint controllers are able to track the reference trajectories, the values of the objective parameters would still be reached.

It is the second part of the strategy which shows some drawbacks, as was clearly indicated by the simulation results. Although the control of the upper body works fine for a variety of simulations, the most important drawback is the fact that the motion of the ZMP is not predicted. In case of a real robot having a fixed foot length, the number of possible hopping patterns would be limited by this drawback. It is likely that due to non-optimal choices of the stance time, as well as the take-off and touch-down configurations, foot rotation would occur. To be able to use this method on a real robot, one would indeed be obliged to store all

possible sets of locomotion parameters in combination with take-off and touch-down configurations in a look-up table. All possible transitions between different steady hopping motions would also have to be stored in this table. Although using such a method is possible in theory, it does not seem to be the most optimal way to steer a robot. Besides, the scope of this work is clearly to develop technique which calculates trajectories on-line and in real time.

In the next chapter, adaptations to the applied technique will be made in order to overcome the drawbacks reported here. The following variables are expected to be determined in a more adequate way:

- stance time T^{st}
- position of the COG at take-off X_G^{to} and Y_G^{to}
- position of the COG at touch-down X_G^{td} and Y_G^{td}
- rotation of the upper body during flight $\Delta\theta_3^{fl}$

As was the case in chapter 2, these adaptations will be based on the use of the angular momentum equation during the stance phase.

Chapter 4

A hopping robot with reduced ankle torque

4.1 Introduction

In chapter 3, a trajectory generation strategy was developed for a planar hopping robot with a foot. This robot (see figure 3.1) is an underactuated mechanism during the flight phase, and is fully actuated during the stance phase. Polynomial trajectories were established during the flight phases and stance phases, which guaranteed that the values of a number of objective locomotion parameters were attained, while at the same time the upper body motion was controlled. By using this strategy, the robot was able to perform periodic (or steady) hopping patterns, as well as non-periodic (or non-steady) hopping patterns.

As was concluded in section 3.7 of chapter 3, the trajectories for the stance phase did not take into account the location of the ZMP. Since the foot of a real robot will have a given finite length, the motion of the ZMP has to be limited to the physical dimensions of the foot in order to avoid foot rotation. In this chapter, an adaptation to the developed technique will be introduced such that the ankle torque remains low during the stance phases, or in other words, the ZMP remains in the vicinity of the ankle point. The ankle torque will in fact only be used to correct errors caused by minor approximations of the dynamics. On a real robot, the ankle actuator would also be used to compensate for eventual external disturbances.

The philosophy of the technique is based on a method that was developed in chapter 2, where the upper body of a hopping robot was controlled by manipulating the angular momentum equation during the stance phase. This was achieved without an ankle actuator. The COG of the upper body of the model considered in chapter 2 was located at the hip joint, which caused a decoupling between the leg motion and the upper body motion. Since this simplification is not valid for the current model, a modification of the method is needed.

In section 4.2 an equation is established which allows one to estimate a required value for the angular momentum with respect to the COG at take-off, in order to become a given upper body rotation during that flight phase. During the stance phase, an upper body rotation should be attained that is equal and opposite to the rotation of the flight phase. At the same time, the stance phase trajectories for the leg links should be designed such that the prescribed value for the angular momentum at take-off is reached. These two objectives are achieved by manipulating the angular momentum equation with respect to the ankle point F during the stance phase, which is done in section 4.3. A trajectory generation strategy is developed for steady hopping and for non-steady hopping in sections 4.4 and 4.5 respectively. Simulation results are reported in section 4.6, followed by some concluding remarks in section 4.7.

4.2 Estimating a desired value for the angular momentum during the flight phase

In section 3.5 an iterative strategy was established to compute the angular momentum during the flight phase in order to obtain a specific rotation of the upper body at touch-down. To get a clear view on how the angular momentum at take-off relates to the rotation of the upper body during the flight phase, the angular momentum equation (3.19) is used. This equation is written as:

$$\mu_G^{to} = h_2 + A_3 \dot{\theta}_3 \quad (4.1)$$

with

$$h_2 = A_{23} \dot{\theta}_{23} + A_{12} \dot{\theta}_{12} \quad (4.2)$$

Note that the functions A_3 , A_{12} and A_{23} are defined in section 3.3.2. Integration of (4.1) from 0 to T^{fl} yields:

$$\mu_G^{to} T^{fl} = \int_0^{T^{fl}} h_2 dt + \int_0^{T^{fl}} A_3 \dot{\theta}_3 dt \quad (4.3)$$

It can be shown (see appendix C) that the second integral on the rhs can be written as:

$$\int_0^{T^{fl}} A_3 \dot{\theta}_3 dt = A_3(\kappa) \Delta \theta_3^{fl} + \left(A_3(\eta) - A_3(\kappa) \right) \dot{\theta}_3^{min} \quad (0 < \kappa, \eta < T^{fl}) \quad (4.4)$$

where $\dot{\theta}_3^{min}$ is the minimum value of the upper body angular velocity during the flight phase.

The formal expression for A_3 contains a significant constant part formed by inertial parameters, such that it is not subjected to large variations during the flight phase. The approximation $A_3(t) \approx A_3^{to}$ results in an estimation of the required value for the angular momentum:

$$\mu_G^{to,des} \approx \tilde{h}_2 + \frac{A_3^{to}}{T^{fl}} \Delta\theta_3^{fl*} \quad (4.5)$$

with

$$\Delta\theta_3^{fl*} = \theta_3^{td*} - \theta_3^{to} \quad (4.6)$$

being the desired upper body rotation and

$$\tilde{h}_2 = \frac{1}{T^{fl}} \int_0^{T^{fl}} h_2 dt \quad (4.7)$$

being the mean value of h_2 during the flight phase, which can be calculated when reference trajectories for θ_{12} and θ_{23} are determined.

4.3 Angular momentum equation during the stance phase

In this section, the angular momentum equation with respect to the ankle point F during the stance phase will be established. It will be shown that the rotation of the upper body during the stance phase can be steered to a specific value by choosing a proper value for the stance time T^{st} . Further, it will be shown that a specific value for the angular momentum with respect to the COG at take-off can be attained by tuning the integral of the horizontal position of the COG during the stance phase.

4.3.1 Kinematic expression of the angular momentum with respect to the foot

The amount of global rotation of the robot during the stance phase can be described by the angular momentum with respect to the ankle point F, which can be calculated with the general formula (2.30). When written in terms of the absolute angles of the links with respect to the horizontal axis, the kinematic expression for the angular momentum becomes:

$$\begin{aligned} \mu_F &= C_3 \dot{\theta}_3 + C_2 \dot{\theta}_2 + C_1 \dot{\theta}_1 \\ &= C_3 \dot{\theta}_3 + k \end{aligned} \quad (4.8)$$

with:

$$C_3 = f_3 + g_{13} \cos(\theta_1 - \theta_3) + g_{23} \cos(\theta_2 - \theta_3) \quad (4.9)$$

$$C_2 = f_2 + g_{12} \cos(\theta_1 - \theta_2) + g_{23} \cos(\theta_2 - \theta_3) \quad (4.10)$$

$$C_1 = f_1 + g_{12} \cos(\theta_1 - \theta_2) + g_{13} \cos(\theta_1 - \theta_3) \quad (4.11)$$

and:

$$f_1 = I_1 + (m_1 \alpha^2 + m_2 + m_3) l_1^2 \quad (4.12)$$

$$f_2 = I_2 + (\beta^2 m_2 + m_3) l_2^2 \quad (4.13)$$

$$f_3 = I_3 + \gamma^2 m_3 l_3^2 \quad (4.14)$$

$$g_{12} = (\beta m_2 + m_3) l_1 l_2 \quad (4.15)$$

$$g_{13} = \gamma m_3 l_1 l_3 \quad (4.16)$$

$$g_{23} = \gamma m_3 l_2 l_3 \quad (4.17)$$

4.3.2 Formal expression of the angular momentum equation

When the ankle point F is considered as a fixed point during the stance phase ($\bar{v}_F = 0$), applying the angular momentum theorem (2.46) yields:

$$\dot{\bar{\mu}}_F = \overline{FG} \times M\bar{g} + \bar{T}_F \quad (4.18)$$

It will at this point be assumed that no ankle actuator is used ($\bar{T}_F = 0$), meaning that the robot is an underactuated mechanism during the stance phase, since only the knee and the hip joints are actuated. Equation (4.18) can be rewritten as:

$$\dot{\bar{\mu}}_F = -MgX_G \quad (4.19)$$

and when introducing the kinematic expression (4.8) for the angular momentum in the lhs:

$$C_3 \ddot{\theta}_3 + \dot{C}_3 \dot{\theta}_3 + \dot{k} = -MgX_G \quad (4.20)$$

where C_3 and k also depend on θ_3 . From (3.4) the kinematic expression for X_G in terms of the absolute angles is written as:

$$X_G = X_F + a \cos \theta_1 + b \cos \theta_2 + c \cos \theta_3 \quad (4.21)$$

Equation (4.20) is clearly a second order non-linear differential equation in θ_3 . With known trajectories θ_1 and θ_2 , and with initial conditions $\theta_3(0)$ and $\dot{\theta}_3(0)$, this equation can be numerically solved for the *natural* behaviour $\theta_3(t)$ of the upper body. Since numerically integrating this equation is time consuming, this will not be done here.

It is however easy to understand why problems concerning the ZMP arise in the technique developed in chapter 3. During the stance phase three polynomial functions for θ_1 , θ_2 and θ_3 respectively were established without taking the angular

momentum equation into account. In other words, when introducing the polynomial functions for θ_1 and θ_2 into the dynamic equation (4.20), then the natural solution for θ_3 will differ from the calculated polynomial. This can cause high values for the required ankle torque, which then causes undesired motions of the ZMP.

4.3.3 Obtaining a desired upper body rotation during the stance phase by tuning the stance time

In chapter 3 a value for the duration of the stance phase was calculated by a formula based on the mean horizontal velocity (see (3.43) and (3.44)). As was concluded in section 3.7, the value for the stance time calculated with this formula was far from optimal. In this section a proper value for the stance time will be determined based on the angular momentum equation.

Assume that two polynomials are established for the controlled angles θ_1 and θ_2 based on given boundaries, but that the stance time T^{st} is unknown. Assume also that based on given boundary conditions a desired polynomial trajectory θ_3^* can be calculated, in terms of the unknown stance time.

Integrating the angular momentum equation (4.19) over time from $t^+ = 0$ to t gives:

$$\mu_F = \mu_F^+ - Mg \int_0^t X_G dt \quad (4.22)$$

with μ_F^+ representing the angular momentum with respect to the foot after impact.

Integrating (4.22) a second time, from 0 to T^{st} , after introducing the kinematic expression for μ_F (4.8) yields:

$$\int_0^{T^{st}} C_3 \dot{\theta}_3 dt + \int_0^{T^{st}} k dt - \mu_F^+ T^{st} + Mg \int_0^{T^{st}} (T^{st} - t) X_G dt = 0 \quad (4.23)$$

Recall that the angular momentum with respect to F, after an impulsive impact in F, is equal to its value at touch-down:

$$\mu_F^+ = \mu_F^{td} \quad (4.24)$$

and when applying the transport equation for the angular momentum between F and G at the instance of touch-down:

$$\mu_F^+ = \mu_G^{td} + (\overline{FG}^{td} \times M \overline{v}_G^{td})|_z \quad (4.25)$$

This expression allows one to determine μ_F^+ based on the information from the previous flight phase.

By imposing a desired trajectory θ_3^* , equation (4.23) can be used to determine a necessary value for the stance time. This value of the stance time will ensure that the rotation of the upper body $\Delta\theta_3^{st} = \theta_3^{to} - \theta_3^{td}$ equals a desired rotation $\Delta\theta_3^{st*} = \theta_3^{to*} - \theta_3^{td}$. Note that equation (4.23) is obtained by integrating twice the differential equation (4.20) and evaluating the result at $t = T^{st}$. This corresponds to computing the value of θ_3^{to} that is reached when no ankle torque is applied. Thus, the value of T^{st} is used here to steer θ_3^{to} .

Introducing a desired trajectory θ_3^* in (4.23) yields:

$$\int_0^{T^{st}} C_3^* \dot{\theta}_3^* dt + \int_0^{T^{st}} k^* dt - \mu_F^+ T^{st} + Mg \int_0^{T^{st}} (T^{st} - t) X_G^* dt = 0 \quad (4.26)$$

where all variables appearing with a * contain the desired trajectory θ_3^* .

Now (4.26) can be rewritten in such a way that T^{st} is isolated in the lhs:

$$T^{st} = \frac{Mg \int_0^{T^{st}} t X_G^* dt - \int_0^{T^{st}} k^* dt - \int_0^{T^{st}} C_3^* \dot{\theta}_3^* dt}{Mg \int_0^{T^{st}} X_G^* dt - \mu_F^+} \quad (4.27)$$

Since T^{st} appears also in the integral limits on the rhs of (4.27), T^{st} is obtained in an iterative way as follows:

$$T^{st,n+1} = \frac{Mg \int_0^{T^{st,n}} t X_G^* dt - \int_0^{T^{st,n}} k^* dt - \int_0^{T^{st,n}} C_3^* \dot{\theta}_3^* dt}{Mg \int_0^{T^{st,n}} X_G^* dt - \mu_F^+} \quad \text{for } n \geq 0 \quad (4.28)$$

A starting value $T^{st,0}$ can be calculated with (3.43) or (3.44). Note that (4.28) can only be used when its denominator is different from zero, meaning only for hopping patterns where:

$$Mg \int_0^{T^{st}} X_G^* dt \neq \mu_F^+$$

from (4.22) it is seen that this corresponds to:

$$\mu_F^{to} \neq 0$$

The situation $\mu_F^{to} = 0$ is very unlikely to occur in case of forward hopping, as illustrated in figure 4.1. During a stance phase the robot rotates around the foot point F, about the $-\bar{1}_z$ axis (when hopping from left to right), such that a negative value

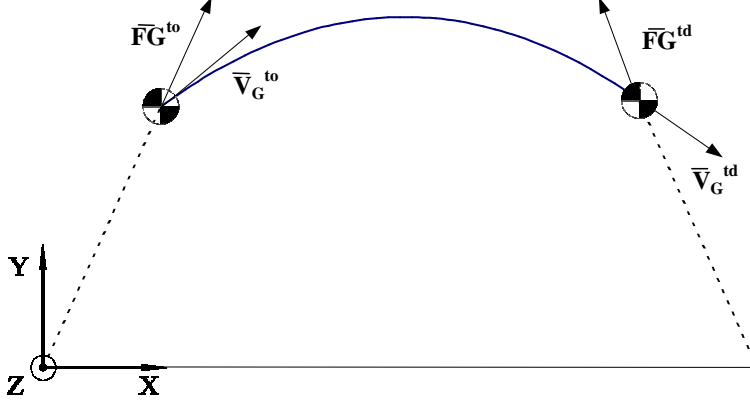


Figure 4.1: Vertical position trajectory of the COG during a flight phase

for μ_F^{to} is expected. Applying the transport equation for the angular momentum between F and the COG at take-off, gives:

$$\mu_F^{to} = \mu_G^{to} + (\overline{FG}^{to} \times M\overline{v}_G^{to})|_z = \mu_G^{to} + M \left(X_G^{to} \dot{Y}_G^{to} - Y_G^{to} \dot{X}_G^{to} \right) \quad (4.29)$$

For the robot considered, with its COG located high above the foot, Y_G^{to} is significantly larger than X_G^{to} , meaning that the second term on the rhs becomes negative (see figure 4.1). Being multiplied by the total mass of the robot, this negative term is dominant over the value of μ_G^{to} , such that indeed μ_F^{to} is negative. This can be verified by the example in section 4.5 and by the results of the performed simulations.

4.3.4 Obtaining the desired angular momentum at take-off

In chapters 2 and 3 a particular value of the angular momentum during flight is used to ensure a certain desired rotation of the upper body during flight. This angular momentum is fixed at the moment of take-off, meaning that it has to be generated during the preceding stance phase. The goal is to define the joint trajectories during the stance phase in such a way that this desired angular momentum is obtained without ankle torque. To achieve this, again the angular momentum constraint with respect to the ankle point F will be used. Recall (4.22), integrated from 0 to T^{st} :

$$\Delta\mu_F^{st} = \mu_F^{to} - \mu_F^+ = -Mg \int_0^{T^{st}} X_G dt \quad (4.30)$$

It was shown in (2.133) that by using the transport equation for the angular momentum from the COG to the foot F, the following expression is found for $\Delta\mu_F^{st}$:

$$\Delta\mu_F^{st} = \mu_G^{to} + (\overline{FG}^{to} \times M\bar{v}_G^{to})|_z - \mu_G^{td} - (\overline{FG}^{td} \times M\bar{v}_G^{td})|_z \quad (4.31)$$

This leads to the following condition when the desired function θ_3^* is introduced:

$$-Mg \int_0^{T^{st}} X_G^* dt = \mu_G^{to,des} + (\overline{FG}^{to} \times M\bar{v}_G^{to})|_z - \mu_G^{td} - (\overline{FG}^{td} \times M\bar{v}_G^{td})|_z \quad (4.32)$$

So if the reference trajectories for the leg angles θ_1 and θ_2 are established in such a way that equation (4.32) holds, then the angular momentum with respect to G of the next flight phase will have the desired value $\mu_G^{to,des}$. Note that μ_G^{td} is the angular momentum during the preceding flight phase, and that the * on X_G^* refers to the fact that it depends on the desired function θ_3^* .

In section 4.4, an iterative procedure is presented in order to satisfy condition (4.32). The value of X_G^{td} , being the horizontal position of the COG at touch-down, will be adapted iteratively to change the value of the integral of X_G^* during the stance phase.

Remark: steady hopping

In case of steady hopping, when $\mu_G^{to} = \mu_G^{td}$, condition (4.32) simplifies to:

$$-Mg \int_0^{T^{st}} X_G^* dt = (\overline{FG}^{to} \times M\bar{v}_G^{to})|_z - (\overline{FG}^{td} \times M\bar{v}_G^{td})|_z \quad (4.33)$$

4.4 Trajectory generation strategy: steady hopping

In section 4.2 it was seen that a predefined upper body rotation can be obtained by choosing a proper value for the angular momentum with respect to G at take-off. In section 4.3.3 it was shown that by adapting the stance time, the upper body rotation during the stance phase can be steered to a specific value. In order to have a zero upper body rotation over one full hop, the following must hold:

$$\Delta\theta_3^{fl} + \Delta\theta_3^{st} = 0 \quad \text{or} \quad \Delta\theta_3^{st} = -\Delta\theta_3^{fl} \quad (4.34)$$

One possibility, which will be used here, is to choose an upright position for the upper body in the boundary points of each phase:

$$\theta_3^{to} = \theta_3^{td} = \frac{\pi}{2} \quad (4.35)$$

This corresponds to the case where $\Delta\theta_3^{fl} = 0 = \Delta\theta_3^{st}$. Note that this is only chosen to limit the number of possible solutions. Since it is desirable to keep the upper body rotation small, this choice seems logical.

During a stance phase not only the rotation has to reach its prescribed value, but also a specific value for the angular momentum with respect to G has to be attained at take-off. It was shown in section 4.3.4 that this can be done by tuning the value of the integral over time of the horizontal position of the COG during the stance phase.

For the sake of clarity, a global strategy will first be established in case of steady hopping, since this will simplify the mathematical expressions. The objective locomotion parameters characterizing a hop were defined in section 3.5.

Establishing flight phase polynomial trajectories

Assuming that the values of the objective locomotion parameters are chosen, then when taking into account that the body has to be upright at take-off and touch-down, the following variables have to be specified at the configuration level for the flight phase:

$$X_G^{to}, Y_G^{to}, X_G^{td}, Y_G^{td} \quad (4.36)$$

Suppose e.g. that X_G^{to} and Y_G^{to} are chosen. Limiting the possible touch-down positions of the COG, one could consider only those hops for which

$$(\overline{FG}^{to} \times M\overline{v}_G^{to})|_z = (\overline{FG}^{td} \times M\overline{v}_G^{td})|_z \quad (4.37)$$

such that these two terms vanish from the rhs of (4.33). By expanding the cross-products, (4.37) can be rewritten as:

$$Y_G^{td} = \frac{g(T^{fl})^2}{2\lambda} (\lambda - X_G^{to} - X_G^{td}) + \frac{\delta}{\lambda} (X_G^{td} - X_G^{to}) + Y_G^{to} \quad (4.38)$$

As was mentioned before, an iterative procedure is used to obtain X_G^{td} . When the origin of the coordinate system is chosen in the ankle point F at the moment of take-off, then a starting value for the first iteration can be (see figure 4.2):

$$X_G^{td,0} = \lambda - X_G^{to} \quad (4.39)$$

For a steady hopping pattern, this starting value imposes a symmetric COG print during a stance phase, since the COG travels an equal horizontal distance behind and in front of the foot point F. Equation (4.38) results in:

$$Y_G^{td,0} = \frac{\delta}{\lambda} (\lambda - 2X_G^{to}) + Y_G^{to} \quad (4.40)$$

From the values of X_G^{to} , Y_G^{to} , $X_G^{td,0}$, and $Y_G^{td,0}$, the angles θ_{12}^{to} , θ_{23}^{to} , θ_{12}^{td} and θ_{23}^{td} are calculated with the kinematic expressions (3.4) and (3.5).

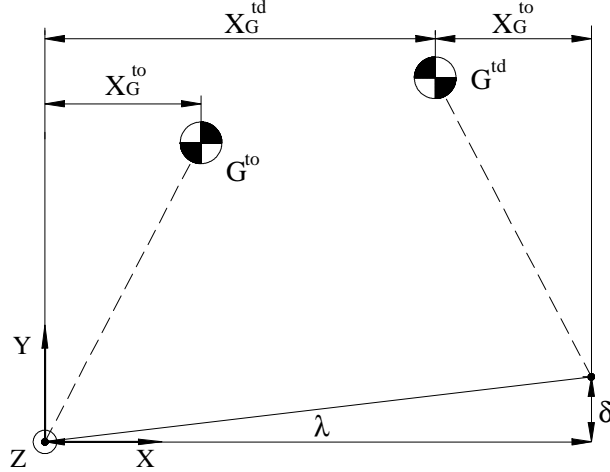


Figure 4.2: COG at take-off and touch-down for first iteration

The flight time T^{fl} and the desired vertical take-off velocity \dot{Y}_G^{to} are determined by (2.103) and (2.106) respectively.

A first estimation of the touch-down angular velocity of the upper body $\dot{\theta}_3^{td}$ can be found with (3.28):

$$\dot{\theta}_3^{td} \approx \frac{\Delta\theta_3^{fl}}{T^{fl}} = 0 \quad (4.41)$$

Now when evaluating the first derivatives of (3.4) and (3.5) at touch-down and identifying them with the dynamic expressions (2.42) and (2.43), a linear set of 2 equations is found which can be solved for $\dot{\theta}_{12}^{td}$ and $\dot{\theta}_{23}^{td}$. These values are introduced in the angular momentum equation (3.19) evaluated at touch-down, allowing one to calculate $\mu_G^{td} = \mu_G^{to}$.

Then, when evaluating the same three expressions at take-off, the values of $\dot{\theta}_{12}^{to}$, $\dot{\theta}_{23}^{to}$ and $\dot{\theta}_3^{to}$ are found.

Next, evaluating the second derivatives of (3.4) and (3.5) at take-off and identifying them with the dynamic expressions (2.40) and (2.41), yields 2 equations in the three unknowns $\ddot{\theta}_{12}^{to}$, $\ddot{\theta}_{23}^{to}$ and $\ddot{\theta}_3^{to}$. A third equation is found by evaluating the first derivative of the angular momentum equation (3.19) at take-off, allowing one to calculate the three angular accelerations.

Finally when evaluating the same three equations at touch-down, the values of $\ddot{\theta}_{12}^{td}$, $\ddot{\theta}_{23}^{td}$ and $\ddot{\theta}_3^{td}$ are also found.

As a result of the preceding computations the values for θ_{12} and θ_{23} at take-off and touch-down as well as their first and second derivatives are found, and are used to establish two fifth order polynomial functions for $\theta_{12}^{fl}(t)$ and $\theta_{23}^{fl}(t)$. These polynomial functions are completed with the corrections defined in section 3.5.1 to

pull up the foot during flight, in order to provide a sufficient ground clearance.

The real touch-down angle of the upper body $\theta_{3,real}^{td}$ after this first iteration is found from (3.29):

$$\theta_{3,real}^{td} = \theta_3^{to} + \int_0^{T^{fl}} \left(\frac{\mu_G^{to} - A_{23}\dot{\theta}_{23}^{fl} - A_{12}\dot{\theta}_{12}^{fl}}{A_3} \right) dt \quad (4.42)$$

This angle will differ from the desired value. Instead of adapting the value of $\dot{\theta}_3^{td}$ with (3.30), now a new value for μ_G^{to} will be calculated using expression (4.5):

$$\mu_G^{to} = \tilde{h}_2 \quad (4.43)$$

Note that with this new value of the angular momentum, the above calculations have to be repeated, meaning that the polynomials $\theta_{12}^{fl}(t)$ and $\theta_{23}^{fl}(t)$ have to be recalculated. This will be repeated until $\theta_{3,real}^{td} = \theta_{3,des}^{td}$.

Establishing stance phase polynomial trajectories

The values of $\dot{\theta}_1^+$, $\dot{\theta}_2^+$ and $\dot{\theta}_3^+$ as well as their first derivatives are determined by an inelastic impulsive impact model.

Since steady hopping is considered, the desired values of θ_1^{to} , θ_2^{to} and θ_3^{to} and their first and second derivatives are the same as for the preceding flight phase.

A first estimation of the stance time will be made by assuming that the COG propagates with a mean horizontal velocity equal to the one during the flight phase:

$$T^{st,0} = \frac{\Delta X_G^{st}}{\nu} \quad (4.44)$$

Normally this value will underestimate the real stance time, since during a stance phase gravity logically first decelerates the COG when it is behind the foot point F, and later re-accelerates it when it is in front of F. The value of T^{st} will however be adapted by iteration as was described in section 4.3.3

With the estimation of $T^{st,0}$ combined with the six boundary conditions at t^+ and t^{to} , two fifth order polynomial trajectories θ_1^{st} and θ_2^{st} are established. In addition, a third polynomial function θ_3^* is analogously established, which is used to approximate a desired behaviour of the upper body during the stance phase.

Now iteration formula (4.28) is used to determine a value for the stance time for which equation (4.26) is satisfied. A variety of simulations showed that this iterative procedure converges extremely fast. In all cases two iterations was sufficient.

Finally, it has to be checked if condition (4.32) is fulfilled, or in other words that

$$\int_0^{T^{st}} X_G^* dt \approx 0 \quad (4.45)$$

This has to be done after fixing the stance time, since changing the stance time also changes the value of this integral. If the integral does not tend to the value on the rhs, the whole strategy for flight phase and stance phase has to be repeated, by adjusting the value of X_G^{td} .

Suppose that the integral can roughly be estimated as (coordinate system located at foot point F, and $\ddot{X}_G = 0$ is assumed):

$$I = \int_0^{T^{st}} X_G^* dt \approx \frac{T^{st}}{2} (X_G^{td} + X_G^{to}) \quad (4.46)$$

If it is assumed that the integral will be varied by changing only X_G^{td} then one can write:

$$\Delta I \approx \frac{T^{st}}{2} \Delta X_G^{td} \quad (4.47)$$

which leads to the following iteration formula:

$$X_G^{td,n+1} = X_G^{td,n} + \frac{2}{T^{st}} (I_{n+1} - I_n) \quad \text{for } n \geq 0 \quad (4.48)$$

with

$$I_{n+1} = 0 \quad (4.49)$$

and I_n is the numerically calculated integral of X_G^* over time for iteration n.

A variety of simulations showed that, due to the good choice of the initial value (4.39) of X_G^{td} , a second iteration is sufficient.

In order to clearly summarize the different steps of the strategy generating the trajectories for the flight phase and the stance phase of each step, a flow chart is given in figure 4.3.

4.5 Trajectory generation strategy: irregular terrain (non-steady hopping)

When attempting to make a robot hop on an irregular terrain, a control strategy has to be implemented that allows the robot to jump over obstacles, and to place its foot on specific footholds such as e.g. the steps of a stair. Moreover, it would be desirable to be able to accelerate and decelerate during the motion. In other words, on an irregular terrain, the objective locomotion parameters would have to be altered from one hop to another. In section 3.5 such a strategy has been developed, using an ankle actuator during the stance phases. However, since the location of the ZMP was not taken into account when designing the reference trajectories for the different controllers, it was not possible to predict in real time if the ZMP remains in the stability region, or in other words if a certain transition

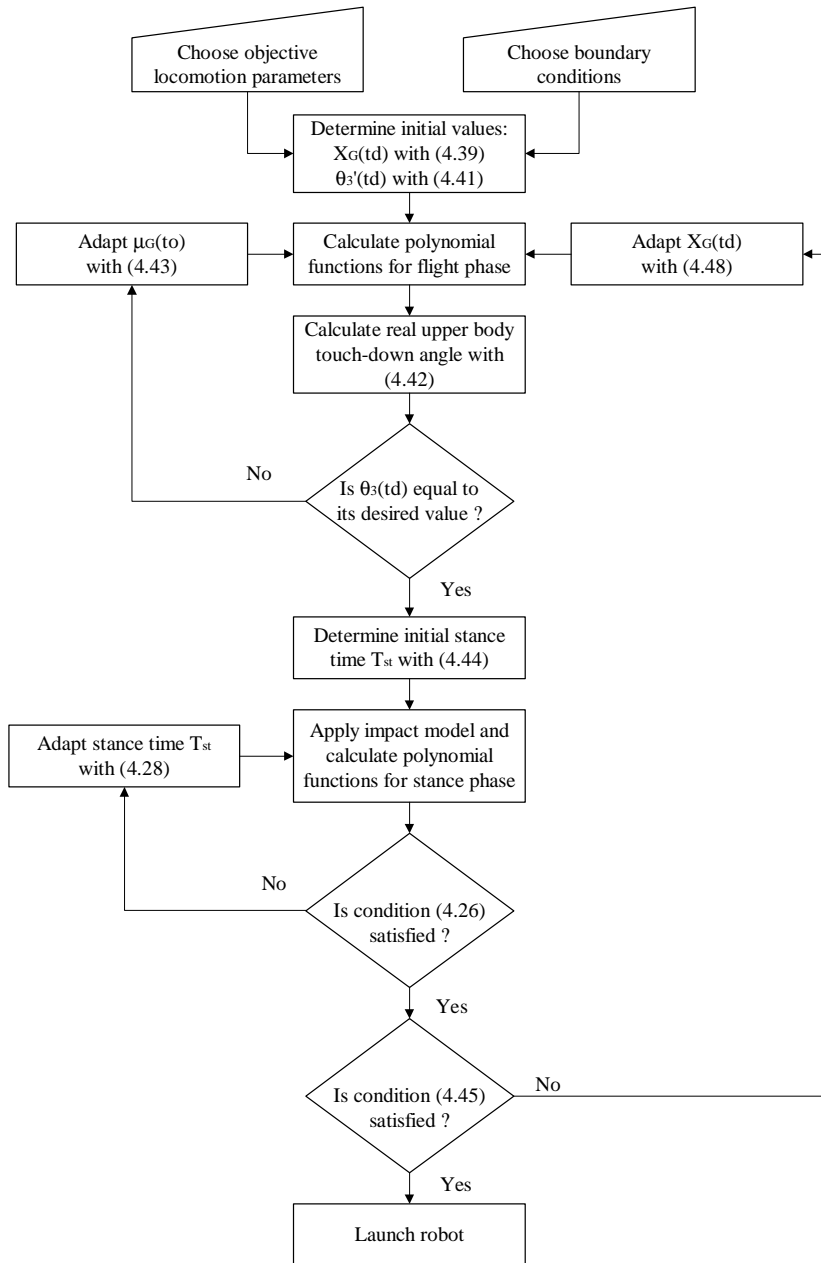


Figure 4.3: Flow chart describing different steps in strategy

between two steady motions is possible. It was suggested to use a look-up table to store a number of precalculated, possible motions. In this section, a strategy will be developed which allows the robot to vary all its objective parameters from one hop to another in such a way that problems concerning ZMP location are avoided. By making a few adaptations to the technique used in section 4.4, the strategy will ensure that the ZMP point is located in the vicinity of the ankle joint during all the successive stance phases, thus significantly limiting the ankle torque and avoiding the use of any look-up table. Even if all the consecutive hops are different, the upper body angle will still be controlled as well as the value of the angular momentum during flight. The strategy will be explained by assuming that the monopod performs a steady hopping pattern with trajectories generated by the strategy in section 4.4, and that it suddenly has to perform a hop with different values for the objective parameters. Flight phase 1 will characterize the first hopping pattern, whereas flight phase 2 will characterize the new hop. Between these flight phases there will be a transition stance phase. Again, the strategy will be developed by assuming that there is no ankle actuator present.

Flight phase 1

Suppose that the robot is performing a hopping pattern with a given set of objective parameters. It moves with a given horizontal velocity ν_1 and places its foot at the desired step length λ_1 and step height δ_1 . The take-off position of the COG, which is determined by X_G^{to1} and Y_G^{to1} , can be chosen. For flight phase 1 it will be assumed that these values are fixed due to the preceding hops. Assuming that the strategy of section 4.4 for steady hopping was applied, the robot will have a certain value for the angular momentum μ_G^{to1} which guarantees a touch-down angle $\theta_3^{td} = \frac{\pi}{2} = \theta_3^{to}$ for the upper body. Since this is a steady hopping pattern, the value of X_G^{td1} and Y_G^{td1} were determined by the strategy of section 4.4 and are considered to be fixed too. Applying the transport equation for angular momentum between the COG and the ankle point F, allows one to calculate the value of the angular momentum with respect to the foot at touch-down:

$$\mu_F^{td1} = \mu_G^{td1} + (\overline{FG}^{td1} \times M\bar{v}_G^{td1})|_z \quad (4.50)$$

Transition stance phase

During the impact phase the angular momentum with respect to the foot remains unchanged:

$$\mu_F^{+1} = \mu_F^{td1} \quad (4.51)$$

which clearly illustrates that the transition stance phase contains the history of the preceding hop. This initial value of the angular momentum will determine whether a certain transition is possible or not. Indeed, when the preceding hop was e.g. a somersault with a high value for the angular momentum $\mu_G^{to1} = \mu_G^{td1}$, this angular

momentum will determine the initial value of the angular momentum with respect to the foot of the stance phase. It is most unlikely that after such a somersault a following different hop with e.g. zero angular momentum during flight will be possible. At least it will not be possible unless a significant torque of the ankle actuator is applied. Writing the angular momentum equation (4.30) with respect to the ankle point F during the transition stance phase in the absence of an ankle actuator, yields:

$$\mu_F^{to2,real} = \mu_F^{+1} - Mg \int_0^{T^{st}} X_G dt \quad (4.52)$$

with $\mu_F^{to2,real}$ the angular momentum with respect to the foot at take-off of the next flight phase. The value of this angular momentum depends on the value of μ_F^{+1} as was remarked higher. Indeed, in the absence of an ankle actuator, the only way to change this momentum is by changing the integral of the horizontal position of the COG. The range of possible values of this integral will determine which are the possible hops that can be performed after this stance phase without ankle actuation.

Flight phase 2

The new hop is characterized by another set of objective locomotion parameters. Suppose that new values for the horizontal velocity ν_2 and the desired step length λ_2 and step height δ_2 have to be reached. In order to reach the desired touch-down angle of the upper body during this flight phase, a certain value for the angular momentum $\mu_G^{to2,des}$ will be needed. Applying the transport equation for the angular momentum between the foot and the COG at take-off yields:

$$\mu_F^{to2,des} = \mu_G^{to2,des} + (\overline{FG}^{to2} \times M\overline{v}_G^{to2})|_z \quad (4.53)$$

which corresponds to a desired value for the angular momentum with respect to the foot at the instance of take-off. It is clear that, without any action, the real value for this angular momentum resulting from the transition stance phase calculated with (4.52), will differ from the desired value.

In order to vary the value of $\mu_F^{to2,real}$ in (4.52), the value of X_G^{to2} will be adapted by iteration. This will however also cause a variation of the value of $\mu_F^{to2,des}$ in (4.53). The variations of the real and the desired angular momentum respectively will vary in the opposite direction, allowing them to converge to a certain value. This can be illustrated by the following example.

Example

Suppose that the robot is hopping with the following set of objective parameters: $\nu_1 = 1 \text{ m/s}$, $\lambda_1 = 0.5 \text{ m}$, $\delta_1 = 0.1 \text{ m}$. It performs the flight phases of these hops with a value of $\mu_G^{to1} = 0.36 \text{ kgm}^2/\text{s}$, and after the impact phase an angular

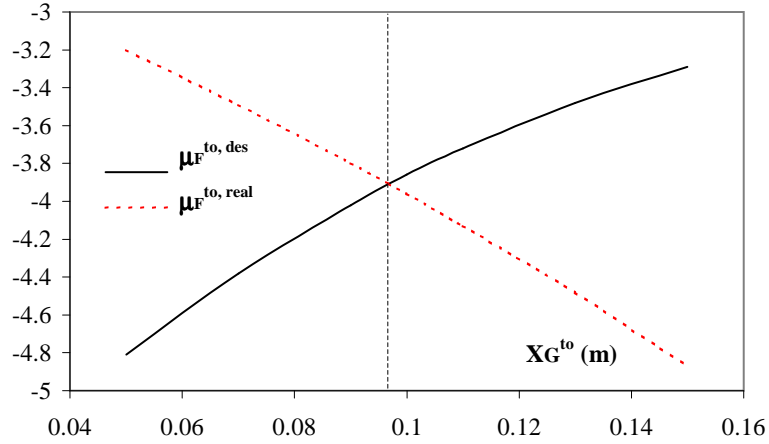


Figure 4.4: Intersection between desired and real angular momentum curves

momentum with respect to the foot $\mu_F^{+1} = -3.87 \text{ kgm}^2/\text{s}$ is found. Suppose then that the robot has to vary its objective locomotion parameters to $\nu_1 = 0.9 \text{ m/s}$, $\lambda_1 = 0.5 \text{ m}$, $\delta_1 = 0.05 \text{ m}$. Figure 4.4 shows the results for $\mu_F^{to2,real}$ and $\mu_F^{to2,des}$ when varying the value of X_G^{to2} from 5 cm to 15 cm in front of the ankle point F during the transition stance phase.

It is seen that the desired angular momentum with respect to F for the next flight phase is a monotonous increasing function, whereas the value of the real angular momentum decreases, for increasing values of X_G^{to2} . This allows one to determine an intersection of the two curves, being at $X_G^{to2} \approx 0.097 \text{ m}$ with $\mu_F^{to2,des} = \mu_F^{to2,real} = -3.91 \text{ kgm}^2/\text{s}$.

The value of $\mu_F^{to2,real}$ decreases with higher values of X_G^{to2} because the integral in the rhs of (4.52) increases. Indeed, altering X_G^{to2} causes a longer trajectory for the COG in front of the foot point, thus altering the value of the integral.

The value of $\mu_F^{to2,des}$ increases (the absolute value decreases) for higher values of X_G^{to2} , which is due to the fact that the robot starts the flight phase with a more oblique orientation with respect to the foot. It was seen in section 4.4 that the touch-down orientation will become more oblique as well ($X_G^{td2} \approx \lambda - X_G^{to2}$). The robot has to perform a larger global rotation during the flight phase, meaning that a larger amplitude for the angular momentum with respect to the COG is needed. This can be understood as follows. The angular momentum during the flight phase of the robot as a whole can roughly be estimated as

$$\mu_G^{to} \approx I \dot{\theta}_G \quad (4.54)$$

where I is the moment of inertia of the robot as a whole, and the angle θ_G corresponds to the angle between a line connecting the foot point F and the COG, and

the horizontal axis. Integration over the flight time gives:

$$\mu_G^{to} T^{fl} \approx I (\theta_G^{td} - \theta_G^{to}) \quad (4.55)$$

When neglecting the variation of I when varying X_G^{to} , the variation of the latter equation leads to:

$$\Delta \mu_G^{to} T^{fl} + \mu_G^{to} \Delta T^{fl} \approx I (\Delta \theta_G^{td} - \Delta \theta_G^{to}) \quad (4.56)$$

and assuming that $\Delta \theta_G^{td} \approx -\Delta \theta_G^{to}$:

$$\Delta \mu_G^{to} \approx -2I \frac{\Delta \theta_G^{to}}{T^{fl}} - \mu_G^{to} \frac{\Delta T^{fl}}{T^{fl}} \quad (4.57)$$

Since e.g. $\Delta X_G^{to} > 0$ corresponds to $\Delta \theta_G^{to} < 0$ and $\Delta T^{fl} < 0$ this clearly causes that $\Delta \mu_G^{to} > 0$. It is seen in (4.53) that the positive contribution on the rhs becomes larger then, meaning that the value of $\mu_F^{to2,des}$ increases.

The iterative procedure for adjusting X_G^{to2} will be based on linear interpolation on the two curves. Therefore two starting points for each curve have to be known. These two points have to be calculated by choosing two different values for X_G^{to} and calculating the corresponding desired and real angular momentum with respect to the foot. After connecting the two points by lines, the intersection will be calculated. To find the intersection of the two resulting lines, the following formula can be used:

$$X_n = \frac{A_{n-1}X_{n-2} - A_{n-2}X_{n-1}}{A_{n-1} - A_{n-2}} \quad \text{for } n \geq 2 \quad (4.58)$$

where X_i represents the value of X_G^{to2} at iteration step i and A_i is defined as:

$$A_i = \mu_F^{to2,des} - \mu_F^{to2,real} \quad (4.59)$$

at iteration step i . By using this interpolation method, the slopes of the two lines are adapted for each iteration. The two first points are arbitrarily chosen. The next iterations can be performed with the two closest points to the desired solution (being the two points having the two smallest values of A_i).

Note that for each iteration step the value of $\mu_F^{to2,real}$ has to be calculated with equation (4.52). Also for each iteration step the value of $\mu_F^{to2,des}$ has to be determined with equation (4.53), which implies that the value of $\mu_G^{to2,des}$ has to be determined with the strategy of section 4.4.

So globally the strategy for steady hopping of section 4.4 is applied for both the hopping patterns. Between the two hopping patterns there is a transition stance phase needed. During this transition stance phase, the stance time is still determined by the iterative formula (4.28), in order to reach $\theta_3^{to} = \frac{\pi}{2}$. After fixing the stance time, it is verified if the real angular momentum with respect to the foot at take-off is equal to its desired value for the new hopping pattern. If this is

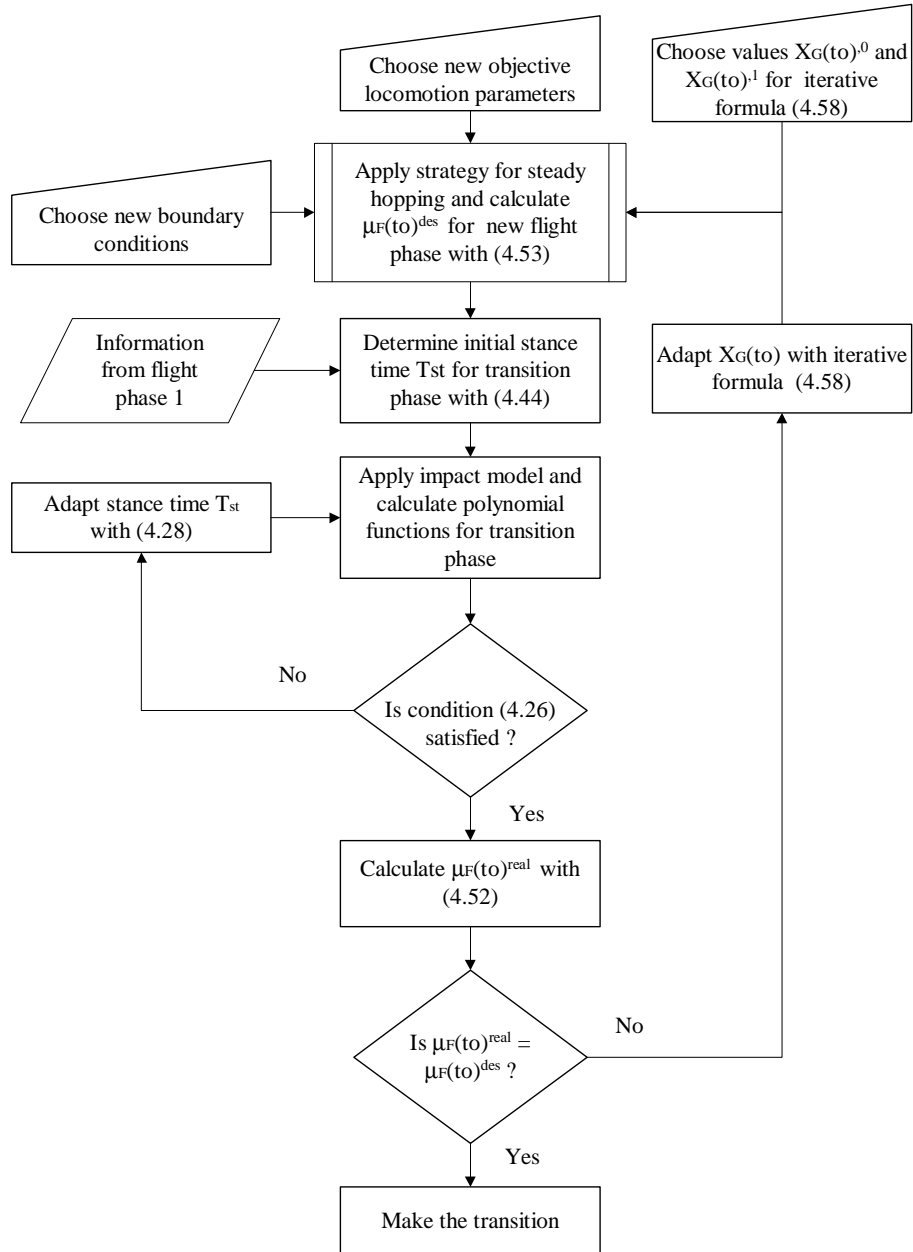


Figure 4.5: Flow-chart describing overall strategy non-steady hopping

not the case, the value of X_G^{to} will be adapted by the iterative formula (4.58). The different steps in the overall strategy are specified by a flow-chart in figure 4.5.

Remark: Upper body polynomial during stance phases

During the stance phases for steady hopping as well as during the transition stance phases, a polynomial function θ_3^* has to be calculated based on the knowledge of the conditions after the impact phase, and of the desired conditions (angular momentum) of the next flight phase. This polynomial function will be used as a tracking trajectory for the ankle actuator. Since this trajectory is constructed by satisfying the angular momentum equation as well as its first and second integral over time in the boundary points of the stance phase, this trajectory tries to mimic the natural upper body trajectory, which is the real solution of the angular momentum equation without ankle actuator. Note that an exact copy of the natural trajectory would cause a zero ankle torque. The simulations being performed showed that trying to mimic the natural trajectory with a fifth order polynomial function does not lead to good results. Indeed, the value of the ankle torque depends mainly on the value of the angular acceleration of the upper body. With a fifth order polynomial function for the angle, the acceleration is only a third order polynomial function having to mimic the solution of the differential angular momentum equation. Due to the fact that the slopes in the end points of the trajectory for the acceleration do not correspond to the slopes of the natural trajectory, significant deviations between the two acceleration trajectories exist. Therefore a seventh order polynomial function will be used, which leads to better results. This seventh order polynomial function can be constructed by differentiating the angular momentum equation (4.20) with respect to time:

$$\ddot{\theta}_3 = -\frac{1}{C_3} \left(Mg\dot{X}_G + \ddot{k} + 2\dot{C}_3\ddot{\theta}_3 + \ddot{C}_3\dot{\theta}_3 \right) \quad (4.60)$$

Evaluating this expression at $t = t^+$ and $t = T^{st}$ allows one to determine the third order derivative in the end points of the trajectory, which are used to design a seventh order polynomial function for the upper body angle.

4.6 Simulations

4.6.1 Steady hopping pattern

To test the new strategy, first a hopping pattern composed of a number of identical consecutive hops has been simulated. Consequently, the desired values of the objective parameters are the same for every hop, as well as the desired behaviour of the upper body. The chosen parameters are the following:

- $\nu = 1 \text{ m/s}$, $\lambda = 0.5 \text{ m}$, $\delta = 0.1 \text{ m}$ (inclined ground surface)
- $\sigma = 0.07 \text{ m}$ (foot lift)

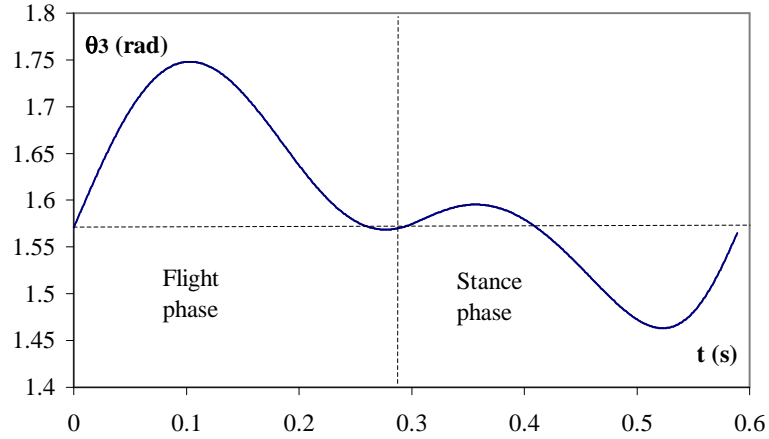


Figure 4.6: Upper body angle during one full hop

- $X_G^{to} = 0.1 \text{ m}$, $Y_G^{to} = 0.54 \text{ m}$
- $\theta_3^{to} = \theta_3^{td} = \frac{\pi}{2}$

This results in the following:

- $T^{fl} = 0.29 \text{ s}$
- $X_G^{td} = 0.39 \text{ m}$, $Y_G^{td} = 0.51 \text{ m}$ (measured from foot at touch-down)
- $\mu_G^{to} = 0.51 \text{ kgm}^2/\text{s}$
- $T^{st} = 0.3 \text{ s}$

For this simulation no ankle torque was applied during the stance phase. The results presented here are the outcome of a classical inverse dynamics approach. The controllers for the actuators are in fact considered to be ideal, in the sense that they are assumed to perfectly track the reference trajectories. Thus, only the results for one flight and stance phase are shown, since all consecutive hops are identical. The results prove the effectiveness of the technique, since all the desired values for the objective locomotion parameters, as well as the desired behaviour of the upper body, are attained.

Figures 4.6 and 4.7 respectively show the upper body angle and angular velocity for one full hop. It is seen that, without use of an ankle actuator, the upper body motion is nearly driftless. The error on the angle at the end of the stance phase was only 0.3° and the error on the angular velocity only 0.03 rad/s .

Graph 4.8 shows the horizontal velocity of the COG with respect to time, during 1 stance phase. During the impact phase the COG is slightly accelerated, as can

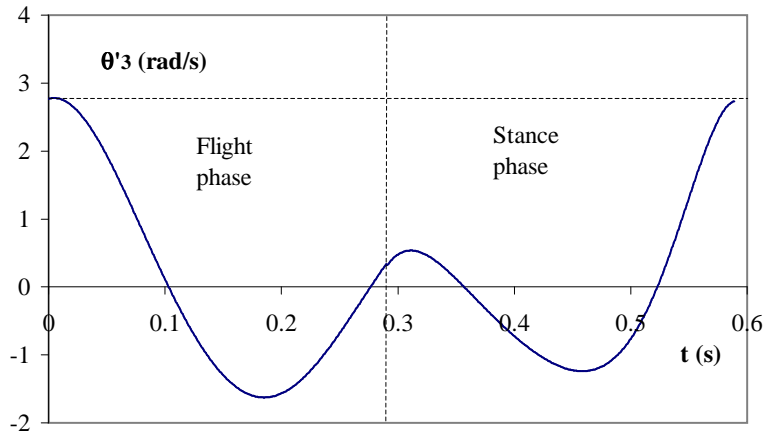


Figure 4.7: Upper body angular velocity during one full hop

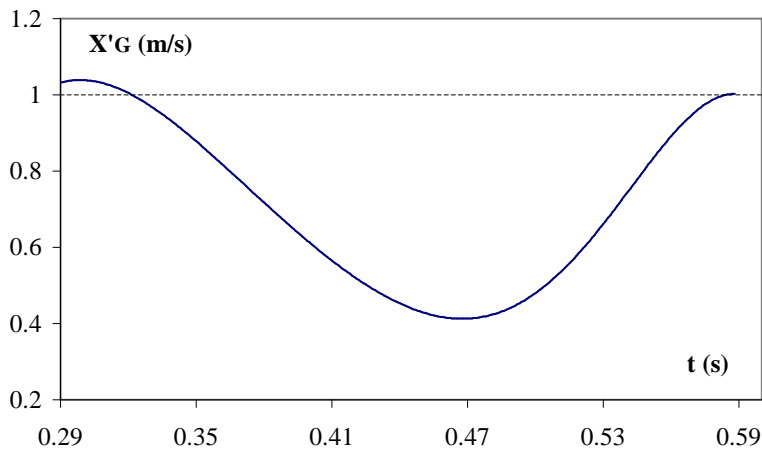


Figure 4.8: Horizontal velocity COG during a stance phase

be seen on the first point of the graph. When comparing this graph to the corresponding graph 3.8 in chapter 3, it can be seen that now a more realistic behaviour for the horizontal velocity is found. The horizontal velocity of the COG decelerates to about 40 % of its initial velocity during the first part of the stance phase. As explained before, this is due to the decelerating effect of gravity when the COG is located behind the ankle joint. This deceleration of the COG is compensated by the acceleration caused by gravity when the COG lies in front of the ankle joint. It is the choice of the take-off conditions and the touch-down conditions in combination with the choice of an adequate value for the stance time that make this strategy work.

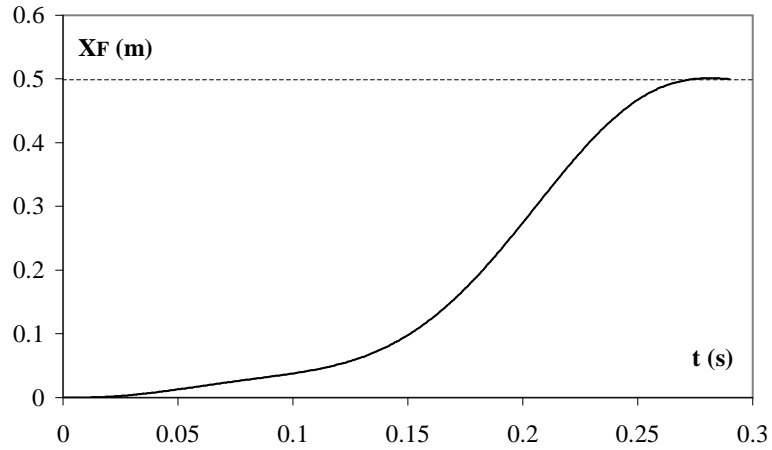


Figure 4.9: Horizontal position foot during one flight phase

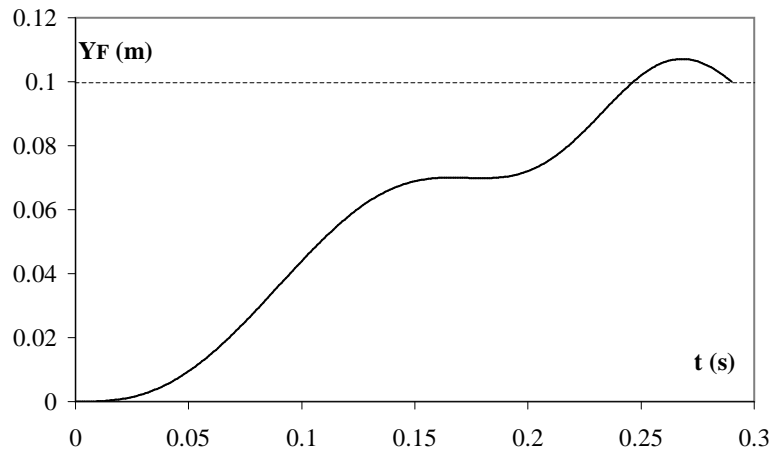


Figure 4.10: Vertical position foot during one flight phase

Graphs 4.9 and 4.10 respectively show the horizontal and the vertical position of the foot during 1 flight phase, indicating that the foot is positioned as desired. Graph 4.11, showing the vertical position of the foot as a function of its horizontal position, indeed confirms that the foot does not collide with the inclined ground surface during the swing. The ground is represented by the dotted inclined line. Recall that a foot clearance of 7 cm was demanded. In case of hopping on a staircase, the foot clearance would have to be altered to a value larger than the step height.

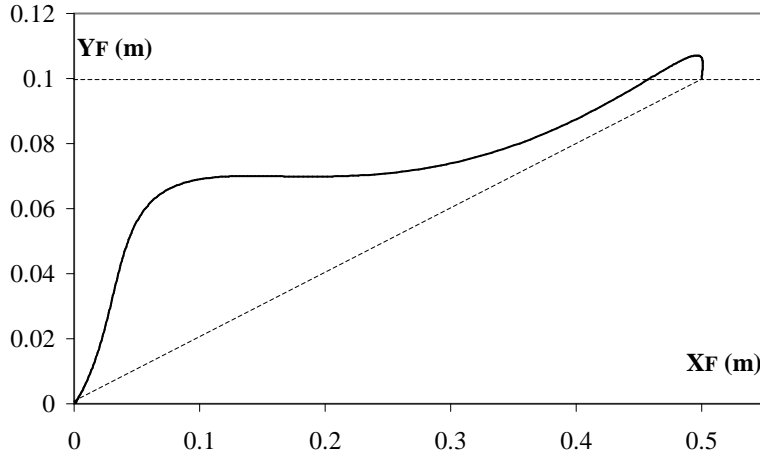


Figure 4.11: Vertical position versus horizontal position foot during 1 flight phase

4.6.2 Non-steady hopping pattern: irregular terrain

To test the developed strategy for motion on irregular terrain, a transition between two steady hopping patterns is considered:

Flight phase 1

- $\nu_1 = 1.2 \text{ m/s}$, $\lambda_1 = 0.5 \text{ m}$, $\delta_1 = 0$ (flat ground)
- $\sigma_1 = 0.05 \text{ m}$ (foot lift)
- $X_G^{to1} = 0.12 \text{ m}$, $Y_G^{to1} = 0.537 \text{ m}$
- $X_G^{td1} = 0.372 \text{ m}$, $Y_G^{td1} = 0.54 \text{ m}$
- $\theta_3^{td1} = \theta_3^{to1} = \frac{\pi}{2}$
- $T^{fl1} = 0.21 \text{ s}$
- $\mu_G^{to1} = 0.59 \text{ kgm}^2/\text{s}$

Transition stance phase and flight phase 2

- $\nu_2 = 1 \text{ m/s}$, $\lambda_2 = 0.4 \text{ m}$, $\delta_2 = 0.1 \text{ m}$ (inclined ground)
- $\sigma_2 = 0.07 \text{ m}$ (foot lift)
- $T^{st} = 0.248 \text{ s}$
- $\theta_3^{td2} = \theta_3^{to2} = \frac{\pi}{2}$
- $\mu_G^{to2} = 0.48 \text{ kgm}^2/\text{s}$

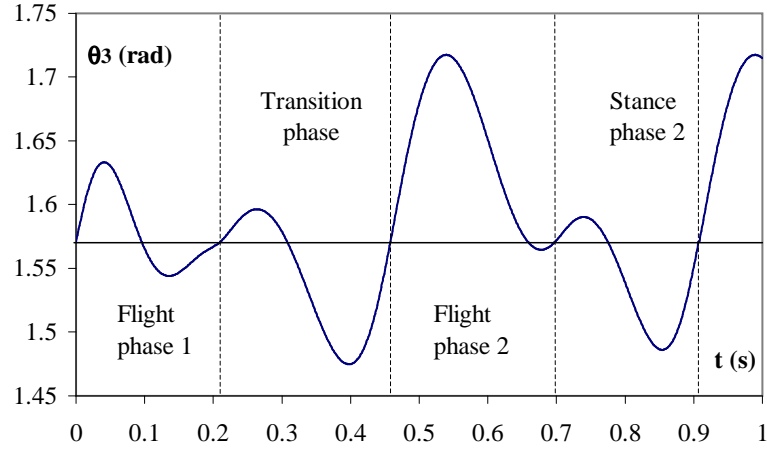


Figure 4.12: Upper body angle during non-steady hopping

- $X_G^{to2} = 0.077 \text{ m}$, $Y_G^{to2} = 0.58 \text{ m}$
- $X_G^{td2} = 0.317 \text{ m}$, $Y_G^{td2} = 0.544 \text{ m}$ (measured from foot at touch-down)
- $T^{fl2} = 0.24 \text{ s}$

The robot's motion transfers from a hopping pattern on flat terrain to a pattern representing a motion on an inclined ground surface. The horizontal velocity as well as the step length are reduced by 20 %. The step height is chosen 10 cm. During the flat terrain hops, the foot is lifted 5 cm to avoid collision with the ground. For the second pattern the foot lift is chosen 7 cm. One can clearly take note of the logical evolution of certain parameters. The flight time of pattern 2 is longer due to the lower horizontal velocity of G. Since the robot has to jump higher and less far, the horizontal take-off position of the COG is lower for the second pattern. The vertical position of the COG at take-off is higher. This explains why the angular momentum during flight phase 2 is lower than the one of the first flight phase. Indeed this is due to the fact that the system has to rotate less around the COG during the second flight phase.

Figure 4.12 shows the upper body angle. It can be seen that the angle equals the imposed value of $\frac{\pi}{2}$ in all the end points of the successive flight and stance phases. The angular momentum with respect to the COG is shown in figure 4.13. After the transition stance phase the desired value of the angular momentum during flight 2 is reached, as can also be verified on figure 4.12 since the upper body angle at the end of flight 2 equals the desired value. After stance phase 2, the same value of the angular momentum is reached, confirming the fact that a new steady hopping motion is generated.

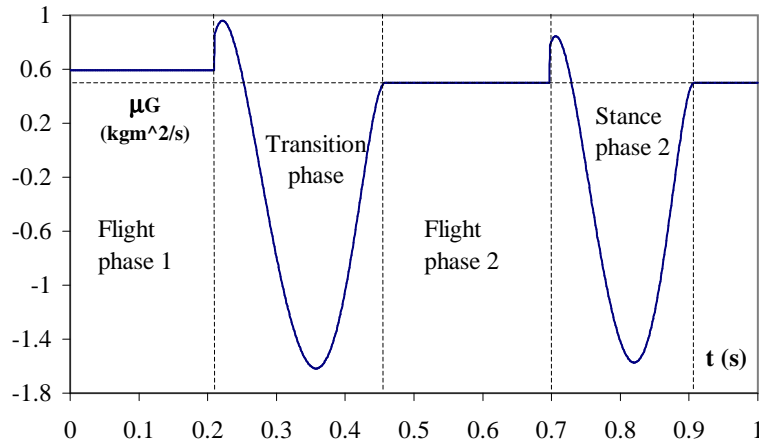


Figure 4.13: Angular momentum with respect to COG

Figure 4.14 gives the ankle torque during the two stance phases. The minimum and maximum values correspond to a length of the foot of 5 cm behind and in front of the ankle joint. It can be clearly verified that the ankle torque is much lower than the maximum and minimum allowed values. The maximum deviation of the ZMP point from the ankle point was approximately 1 cm, assuring a high postural stability of the robot during the stance phases. When compared to the corresponding graphs in section 3.6.2, figure 4.14 illustrates the effectiveness of the applied strategy. Note that the small oscillations on the trajectory of the ankle torque do not correspond to any kind of unstable motion. These oscillations are due to the minor differences between the natural upper body trajectory and the seventh order polynomial function.

The graphs 4.15, 4.16 and 4.17 represent respectively the horizontal foot position, the vertical foot position and the horizontal velocity of the COG. All values of the objective parameters are reached, which again proves the effectiveness of the applied method based on the introduction of objective locomotion parameters.

4.7 Summary

In this chapter, a powerful trajectory generation strategy for a hopping robot has been developed. This strategy consists of two main tasks, namely to control the values of a number of objective locomotion parameters and to control the upper body motion. Since the COG of the upper body is not located at the hip joint, its position influences the position of the global COG of the robot, such that these two tasks can not be considered as independent, but are coupled.

The objective locomotion parameters considered are the horizontal velocity of the

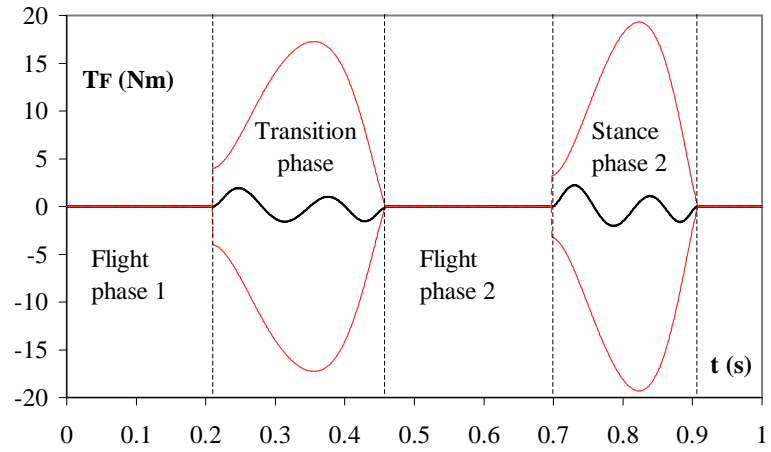


Figure 4.14: Ankle torque during stance phases

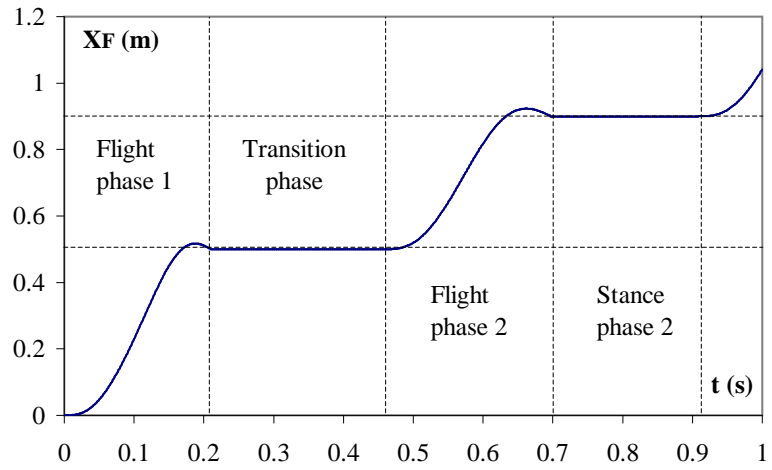


Figure 4.15: Horizontal position foot

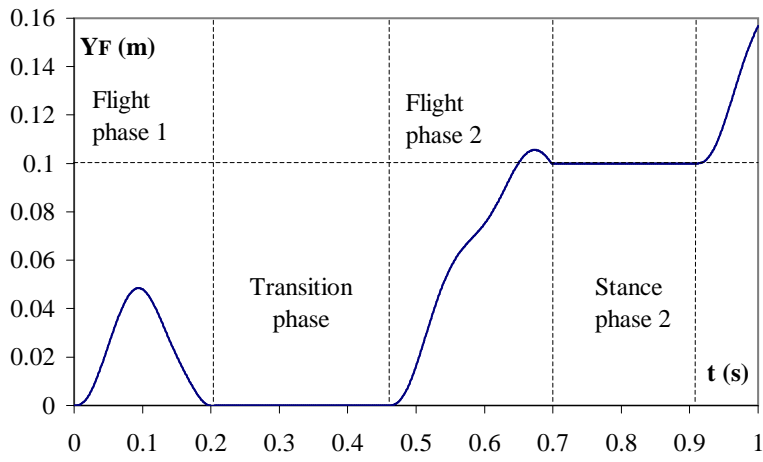


Figure 4.16: Vertical position foot

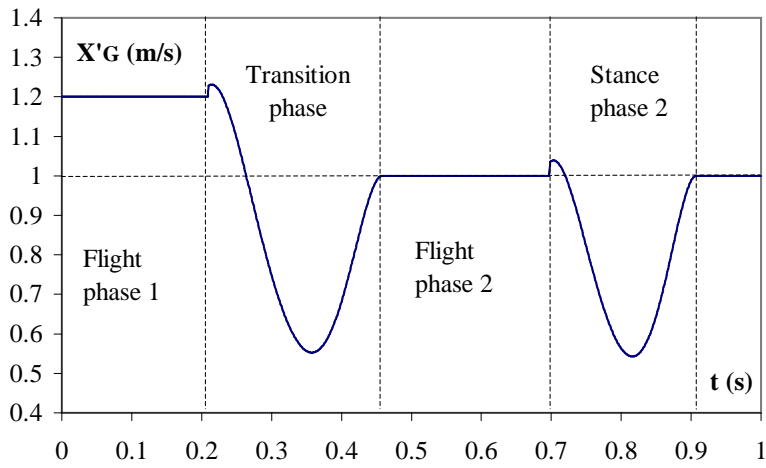


Figure 4.17: Horizontal velocity of COG

COG, the step length and the step height. To avoid an unwanted collision of the foot with the ground during the leg swing, an extra parameter is added which prescribes a specific height of the foot at a given time during the flight phase. This parameter, which is especially interesting when jumping over an obstacle, was called the foot lift or foot clearance. The applied strategy allows the robot to perform steady hopping patterns where all the consecutive hops are identical, as well as locomotion on an irregular terrain, where all the objective locomotion parameters are altered from one hop to another.

Control of the upper body motion is accomplished by using the angular momentum equation. A vertical posture of the upper body in the end points of every flight and stance phase is demanded. By using the angular momentum equation during the flight phase, which expresses conservation of the momentum with respect to G, a certain value for this momentum is determined which guarantees a vertical posture for the upper body at touch-down. During the stance phase, the angular momentum equation with respect to the ankle point F is considered. By manipulating this equation, a given value for the stance time is determined which guarantees a vertical posture of the upper body at take-off. Moreover, a certain value for the horizontal position of the COG at take-off is determined which guarantees that the value of the angular momentum with respect to G at the end of the stance phase equals the desired take-off value. The advantage of this technique is that it influences the natural dynamics of the upper body such that it approximates a desired motion. The upper body naturally satisfies the desired boundary conditions on the position, the velocity and the acceleration level, in the end points of the step. The ankle actuator tracks a seventh order polynomial function, which is built up by the same boundary conditions, such that the polynomial trajectory mimics the natural trajectory. Consequently the required ankle torque is low. Except for the small deviations between the natural trajectory and the polynomial trajectory, the ZMP is located at the ankle joint at all times during the stance phase. This guarantees a high postural stability of the robot during the stance phases.

During the flight phase, two actuators being located at hip and knee respectively track fifth order polynomial functions. During the stance phase, the knee and hip actuator also track fifth order polynomial functions, whereas the ankle actuator tracks a seventh order polynomial function. These trajectories are obtained by introducing the desired values of the objective parameters as well as the desired upper body motion in the kinematic and the dynamic expressions for the robot. By performing elementary calculations, the boundary values for the polynomial trajectories are found. By using these trajectories as steer functions, the dynamics of the robot are in fact steered in a kinematic way.

An interesting aspect of the technique is that it is based on a limited number of elementary calculations, using only minimal approximations of the dynamical equations. As compared to other existing techniques, no numerical optimization technique is used, which reduces the computation time.

Chapter 5

A walking biped with instantaneous double support phase

5.1 Introduction

One of the most crucial aspects of motion control for bipedal robots is the design of reference trajectories for the different joints. It is well known that arbitrarily defining those trajectories can result in all kinds of difficulties, amongst which a high energy consumption of the tracking actuators, and the possible instability of the robot caused by tipping over during the intermittent, unilateral contact phases with the supporting ground, are the most pertinent ones. Most research in this field has been done on humanoid robots, which are bipedal robots having the same locomotive structure as humans. As correctly summarized by Sugihara et al. [2002], the previous works in motion generation for humanoid robots can be classified into 2 main approaches, being *trajectory replaying* and *realtime generation*, or roughly speaking off-line and on-line techniques. Although the latter group is far more promising from the point of view of high-mobility and autonomy of a humanoid, most walking trajectory generation methods successfully applied today belong to the first group. In general, off-line joint trajectories are calculated in advance and are applied to the real robot with no or little on-line modification. The overall motion control is thus divided in two clearly distinct subproblems, being planning and control.

The most trivial way of trajectory replaying was used by Mita et al. [1984], and consists of recording human data and applying a tracking control of the human gait trajectories. Unfortunately, measuring the angle trajectories during human walking for a wide range of step lengths and walking speeds is difficult and time consuming [Capi et al., 2003]. Besides, a humanoid robot does not necessarily have the same kinematical and dynamical properties (e.g. link dimensions, number of DOF, number of actuators, etc.) as a human individual, such that the recorded data from humans has to be manipulated to fit the robot specifications.

Numerous off-line techniques mainly focus on the aspect of optimization of a certain criterion, such as e.g. energy consumption. Since computation time is not an issue there, numerical optimization techniques have been developed in order to obtain energy optimal trajectories. One popular approach is the use of parameterization techniques. Inspired by earlier studies such as [Beletskii et al., 1982], Channon et al. [1992] presented a gait optimization method based on the representation of joint motions by polynomials whose coefficients were adjusted in order to minimize a certain cost function representing the energy consumption of the actuators. A similar technique was applied by Cabodevilla et al. [1995], who used Fourier series to define joint trajectories. In [Roussel et al., 1998] piecewise constant inputs were implemented for the generation of unconstrained optimal trajectories. Later, Chevallereau and Aoustin [2001] made a contribution to this area by designing energy optimized reference trajectories for a biped, with control of the upper body motion and without ankle torque. The walking biped was considered as an underactuated system walking with instantaneous double support phases and keeping its ZMP [Vukobratovic et al., 1990] [Goswami, 1999] constantly located at the supporting ankle joint. Continuity conditions on accelerations at gait phase transitions were not imposed, meaning that actuating torques, together with ground forces are not continuous on the overall gait cycle. Ono and Liu [2002] use an optimal trajectory planning method, in which joint trajectories are modelled by a set of Hermite polynomial functions with unknown variables of the initial and end boundary motion states. Recently, optimal gait cycles in the sagittal plane for a biped were defined by Saidouni and Bessonnet [2003]. They used cubic spline functions connected at uniformly distributed knots along the motion time to become joint trajectories. The performance criterion being minimized was the time integral of the squared actuator torques. The upper body of the studied model had however extremely large mass and moment of inertia when compared to the leg links. This considerably simplifies the control problem since upper body oscillations are practically avoided. Another optimization technique commonly encountered is the application of the Pontryagin Maximum Principle as in [Rostami and Bessonnet, 2001] and [Nikkhah et al., 2003]. The optimization problem is considered here as an optimal control problem. A major interest in using this method lies in its ability to account directly and exactly for limitations and constraints specified on actuating inputs and contact forces. The major drawback of all these optimization methods is that the success mainly depends on the quality of the mathematical model. If e.g. the inertial parameters of the real robot are not accurately estimated, the solutions will not at all be optimal.

To ensure the dynamic stability of a walking robot, several authors focused on walking pattern synthesis based on zero moment point control, prior to energy minimization. Examples are Takanishi et al. [1985], Shih et al. [1990] and Hirai et al. [1998], who basically designed first a desired zero moment point trajectory, and then derived the hip motion or torso motion required to achieve the desired ZMP trajectory. According to Huang et al. [2001] the drawbacks of this method are that not all imposed ZMP trajectories can be attained, and that the hip ac-

celeration in some cases has to be very large. They derived an alternative method where they obtain a smooth hip motion without first designing a specific ZMP trajectory. By iteratively changing hip parameters an eventual trajectory for hip motion is chosen with a large stability margin based on ZMP computation. Their method for planning walking patterns included ground conditions, dynamic stability constraints and actuator specifications. They also used an extremely large mass and moment of inertia for the trunk, such that the orientation of the trunk could be assumed as fixed. Kagami et al. [2002] also presented an off-line technique for generating dynamically equilibrated motions for humanoid robots. Given input motion and the desired ZMP trajectory, their algorithm generates a modified dynamically equilibrated motion for the robot, by using a relationship between the robot's COG and the ZMP. The ZMP trajectory is tracked by varying the horizontal torso position. By introducing the enhanced ZMP to consider three-dimensional contact ranges between robot and environment, they succeeded to make the humanoid robot H5 walk at low speeds and to squat down.

As stated by Sugihara et al. [2002], a real-time generation algorithm has to calculate joint trajectories in accordance with a predefined goal of the motion, while feeding back the present state of the system. Thus, planning and control form one unified task. In order to make real-time generation possible, several authors have developed techniques based on simplification of the dynamics. During the single support phase of a walking biped, the dynamics of the system are similar to the dynamics of an inverted pendulum, whose supporting point is located at the ZMP. Using these simplified dynamics, Sugihara et al. [2002] proposed a real-time trajectory generator based on a dynamical relationship between the ZMP and the COG of the robot. Although all the inertial forces other than the gravitation were not explicitly considered in the control, their approach seemed to be effective as was verified by simulations. An interesting approach developed by Kajita, Kanehiro, Kaneko, Fujiwara, Yokoi and Hirukawa [2002] uses the dynamics of a three-dimensional inverted pendulum whose motion is constrained onto a plane, called the Three-Dimensional Linear Inverted Pendulum Mode. A simple algorithm for walking speed generation was proposed, and tested on a 12 DOF biped robot, which successfully performed a dynamically stable walking motion. Capi et al. [2003] presented a method for real-time walking gait generation based on neural networks. Energy optimal gaits similar with human motion were used to teach the neural network, such that after the learning process the human gait could be quickly generated. The type of network used was a Radial Basis Function Neural Network, which belongs in fact to a curve-fitting problem in a high-dimensional space. Recently an interesting control method based on angular momentum for a walking robot was presented by Mitobe et al. [2004]. The angular momentum of a walking robot was controlled through zero moment point manipulation. The ZMP was considered as an actuating input of the controller, which used the angular momentum of the robot as the feedback signal to update the ZMP target position. Their method can be applied real-time, since it does not require an accurate tracking of joint trajectories. They did however not consider the generation of feasible angular momentum trajectories which

guarantee that the ZMP remains in the stability region. It is that specific task that is considered in this thesis.

Also outside of Japan important contributions to the subject of dynamic stability of biped robots are made. In Korea, Park and Kim [1998] focused on the method of the Linear Inverted Pendulum Mode, once introduced by Kajita and Tani [1991]. They found that, due to the fact that this method initially ignored mass and moment of inertia of the legs, the ZMP point significantly moved away from a presumed position when applied to a model with non-zero mass and moment of inertia. Therefore they proposed a method called the Gravity Compensated Linear Inverted Pendulum Mode [Park and Kim, 1998], which included the dynamics of the free leg motion. Using this technique, they developed an on-line trajectory generation method to increase the stability robustness of locomotion, based on the ZMP equation and the sensed information of the ZMP [Park and Chung, 1999]. This strategy was further refined in [Park and Cho, 2000], where it was also expanded to be used during the double support phase.

In this chapter, a method is presented which calculates reference trajectories for a walking biped without any optimization process and with minimal approximations of the dynamics of the robot. The model of the planar biped is based on the robot Lucy [Verrelst et al., 2002], which recently has been built by the Multibody Mechanics Research Group at the Vrije Universiteit Brussel. This robot will in a later stage be used to test the developed strategy. Compared to humans and a variety of existing humanoid robots, the upper body of Lucy has a significantly smaller mass and moment of inertia (see section 5.2). The COG of the trunk is moreover located rather high above the hip point. This leads to the fact that the motion of the upper body is significant and has to be actively controlled.

The developed trajectory generation strategy manipulates the natural upper body motion such that it approximates a desired upper body motion. Natural motion of the upper body is defined here as the motion generated by an underactuated system, meaning without ankle torque. By using the angular momentum equation in an adequate way, the motion of the leg links can be defined such that the upper body motion is indirectly controlled on the position, the velocity and the acceleration level. Since the upper body performs this motion naturally, the resulting ankle actuator action is limited. It is restricted to covering the minor differences between a polynomial tracking function and the natural trajectory, and the compensation for non-modelled external disturbances. This limited action avoids problems concerning ZMP and foot rotation [Goswami, 1999]. Moreover, the resulting oscillations of the upper body are limited to small back and forth motions.

Another important feature of the technique is that it generates the robot's motion based on objective locomotion parameters, such as introduced by Hurmuzlu [1993] and later reused by several authors [Ma and Wu, 2002], [Vermeulen et al., 2003]. The strategy will at this point generate a walking motion with an instantaneous double support phase. In order to simplify the mathematical principles, a steady walking pattern is considered in which impact is avoided by choosing the touch-

down velocity of the foot of the swing leg equal to zero. This special kinematic requirement was introduced by Beletskii et al. [1982], who described it as the *softness of gait*. According to Blajer and Schiehlen [1992] the impacts due to collision of the legs with the ground create destabilizing effects on the walking cycle, and should therefore be avoided. However, Chevallereau and Aoustin [2001] stated that usually high joint torques are needed in order to achieve this specific requirement, especially when walking at high speeds. This seems logical since one deliberately has to slow down the dynamics in order to avoid the impact. In this chapter, the impact of the swing leg is neglected in order to obtain symmetric steps, with zero velocity and acceleration of the swing foot in both the end-points of the step. This mathematical simplification will allow us to clearly understand some features of such a walking motion, especially on the resulting upper body motion. Impact as well as a double support phase will be considered in chapter 6.

The joint trajectories for the robot are polynomial functions, which ensure continuity at the acceleration level in the transition phases between the steps. The technique is based on two iteration loops which adjust certain hip parameters in order to reach the predefined motion, while the ZMP remains in the vicinity of the ankle joint. Due to the fact that only simple calculations have to be performed and no optimization algorithm is used, the computation time needed is very short, which makes the strategy useful for real-time application.

In section 5.2 a description of the studied model is given. Kinematics and dynamics are respectively covered in sections 5.3 and 5.4. The goals to be reached by the trajectory generation strategy are described in 5.5. The upper body motion of the walking robot is studied on the position, the velocity and the acceleration level in section 5.6. Eventually the mathematical framework of the trajectory generation strategy is given in section 5.7, followed by simulations and concluding remarks respectively in sections 5.8 and 5.9.

5.2 The biped model

The bipedal robot Lucy [Verrelst et al., 2002] can be geometrically described by a simplified planar model in figure 5.1. The index S stands for 'Stance' whereas 'A' stands for 'Air'. The model has two articulated legs, an upper body and two feet. The feet are assumed to have an ignorable inertia. The knees, hips and ankles are uniaxial frictionless joints. The inertial parameters of the biped are given in table 5.1. The length of the i -th link is l_i , its mass is m_i and the moment of inertia around its COG G_i is I_i . The total mass of the robot is 30.5 kg.

The angles between the horizontal axis and the different links of the robot are θ_{1S} and θ_{2S} for the supporting leg, θ_{1A} and θ_{2A} for the leg in the air, and θ_3 for the body. Point F_S represents the connection between the lower leg and the foot of the supporting leg, whereas F_A represents the connection between the lower leg and the foot of the leg in the air. Point H represents the hip, while K_S and K_A

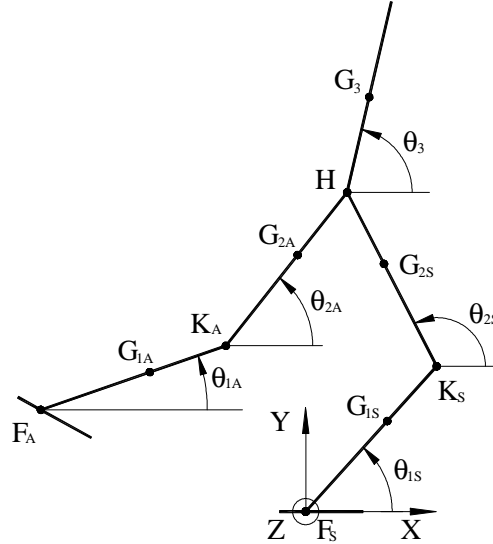


Figure 5.1: Model of the walking robot

i	l_i (m)	m_i (kg)	I_i (kgm^2/s)
1A, 1S	0.5	3.57	0.059
2A, 2S	0.5	3.68	0.061
3	0.5	16	0.6

Table 5.1: Inertial parameters of the biped

represent the two knees. The location of the COG's G_{1S} , G_{1A} of the lower legs, G_{2S} , G_{2A} of the upper legs and G_3 of the body are given by $F_S G_{1S} = F_A G_{1A} = \alpha l_1$, $K_S G_{2S} = K_A G_{2A} = \beta l_2$ and $H G_3 = \gamma l_3$ where $0 < \alpha, \beta, \gamma < 1$:

$$\alpha = 0.618$$

$$\beta = 0.622$$

$$\gamma = 0.5$$

The motion of the robot is limited to the sagittal plane. Since the double support phase is instantaneous, the motion consists of single support phases with instantaneous switching of the supporting foot. Note that this is a limit case between walking and running. This leads to five DOF for the robot at each instant of the motion, except for the switching instant where there are only three DOF due to the instantaneous closed kinematic chain. There are six actuators respectively placed at the hip, knee and ankle joints. Only five of them are used at the same time, since the foot in the air is assumed to be unactuated.

5.3 Kinematics

5.3.1 Motion of the COG

The position vector of the hip point $\overline{OH} = (X_H, Y_H)^T$ will play a crucial role in the generation of the joint trajectories. Therefore the kinematic expression for the global center of gravity will be written relative to the hip position rather than to the supporting foot as was done in the previous chapters. From figure 5.1 it can be seen that

$$X_H = X_{F_S} + l_1 \cos \theta_{1S} + l_2 \cos \theta_{2S} \quad (5.1)$$

$$Y_H = Y_{F_S} + l_1 \sin \theta_{1S} + l_2 \sin \theta_{2S} \quad (5.2)$$

Also from figure 5.1, the vectors defining the position of the local COG's of each of the five links are found as:

$$\overline{OG}_{1S} = (X_{F_S}, Y_{F_S})^T + \alpha l_1 (\cos \theta_{1S}, \sin \theta_{1S})^T \quad (5.3)$$

$$= (X_H, Y_H)^T - (1 - \alpha) l_1 (\cos \theta_{1S}, \sin \theta_{1S})^T - l_2 (\cos \theta_{2S}, \sin \theta_{2S})^T$$

$$\overline{OG}_{2S} = (X_{F_S}, Y_{F_S})^T + l_1 (\cos \theta_{1S}, \sin \theta_{1S})^T + \beta l_2 (\cos \theta_{2S}, \sin \theta_{2S})^T \quad (5.4)$$

$$= (X_H, Y_H)^T - (1 - \beta) l_2 (\cos \theta_{2S}, \sin \theta_{2S})^T$$

$$\overline{OG}_3 = (X_{F_S}, Y_{F_S})^T + l_1 (\cos \theta_{1S}, \sin \theta_{1S})^T + l_2 (\cos \theta_{2S}, \sin \theta_{2S})^T \quad (5.5)$$

$$+ \gamma l_3 (\cos \theta_3, \sin \theta_3)^T$$

$$= (X_H, Y_H)^T + \gamma l_3 (\cos \theta_3, \sin \theta_3)^T$$

$$\overline{OG}_{2A} = (X_{F_S}, Y_{F_S})^T + l_1 (\cos \theta_{1S}, \sin \theta_{1S})^T + l_2 (\cos \theta_{2S}, \sin \theta_{2S})^T \quad (5.6)$$

$$- (1 - \beta) l_2 (\cos \theta_{2A}, \sin \theta_{2A})^T$$

$$= (X_H, Y_H)^T - (1 - \beta) l_2 (\cos \theta_{2A}, \sin \theta_{2A})^T$$

$$\overline{OG}_{1A} = (X_{F_S}, Y_{F_S})^T + l_1 (\cos \theta_{1S}, \sin \theta_{1S})^T + l_2 (\cos \theta_{2S}, \sin \theta_{2S})^T \quad (5.7)$$

$$- l_2 (\cos \theta_{2A}, \sin \theta_{2A})^T - (1 - \alpha) l_1 (\cos \theta_{1A}, \sin \theta_{1A})^T$$

$$= (X_H, Y_H)^T - (1 - \alpha) l_1 (\cos \theta_{1A}, \sin \theta_{1A})^T - l_2 (\cos \theta_{2A}, \sin \theta_{2A})^T$$

The position of the global COG of the robot is:

$$\overline{OG} = (X_G, Y_G)^T \quad (5.8)$$

with:

$$X_G = X_H + a(\cos \theta_{1S} + \cos \theta_{1A}) + b(\cos \theta_{2S} + \cos \theta_{2A}) + c \cos \theta_3 \quad (5.9)$$

$$Y_G = Y_H + a(\sin \theta_{1S} + \sin \theta_{1A}) + b(\sin \theta_{2S} + \sin \theta_{2A}) + c \sin \theta_3 \quad (5.10)$$

and:

$$a = -(1 - \alpha) \eta_1 l_1$$

$$b = -[\eta_1 + (1 - \beta) \eta_2] l_2$$

$$c = \gamma \eta_3 l_3$$

and:

$$\eta_i = \frac{m_i}{2(m_1 + m_2) + m_3}$$

The first and second derivatives of (5.9) and (5.10) are straightforward.

5.3.2 Rotation around the supporting foot

During the stance phase, the robot rotates around the ankle point of the supporting foot F_S . The amount of rotation of the system can be quantified by the angular momentum with respect to that point. Expressing that no slipping occurs and that a continuous contact of the supporting foot with the ground surface is assumed, gives:

$$\bar{v}_{F_S} = 0 \quad (5.11)$$

$$\bar{a}_{F_S} = 0 \quad (5.12)$$

The angular momentum can then be calculated with the general formula [Janssens and Lefeber, 1984]:

$$\bar{\mu}_{F_S} = \sum_{i=1}^5 \left(\overline{F_S G_i} \times m_i \overline{\dot{F_S G_i}} + I_i \dot{\theta}_i \bar{1}_z \right) \quad (5.13)$$

thus making the sum over the 5 links. Since the motion of the robot is restricted to the sagittal plane, $\bar{\mu}_F$ is perpendicular to that plane ($\bar{1}_z$ is the unit vector corresponding to the Z-axis of the local coordinate system in figure 5.1):

$$\bar{\mu}_F = \mu_F \bar{1}_z \quad (5.14)$$

Introducing the kinematical expressions from section 5.3.1 into (5.13) allows the angular momentum to be written as:

$$\mu_{F_S} = A_3 \dot{\theta}_3 + h \quad (5.15)$$

with the function h being independent of the angular velocity of the upper body $\dot{\theta}_3$. More specifically, it is defined as follows:

$$\begin{aligned} h\bar{1}_z = & \overline{F_S G_{1S}} \times m_1 \overline{F_S \dot{G}_{1S}} + I_1 \dot{\theta}_{1S} \bar{1}_z + \overline{F_S G_{2S}} \times m_2 \overline{F_S \dot{G}_{2S}} + I_2 \dot{\theta}_{2S} \bar{1}_z \\ & + \overline{F_S G_{1A}} \times m_1 \overline{F_S \dot{G}_{1A}} + I_1 \dot{\theta}_{1A} \bar{1}_z + \overline{F_S G_{2A}} \times m_2 \overline{F_S \dot{G}_{2A}} + I_2 \dot{\theta}_{2A} \bar{1}_z \\ & + \overline{F_S G_3} \times m_3 \overline{F_S \dot{H}} \end{aligned} \quad (5.16)$$

And the function A_3 is determined by:

$$A_3 \dot{\theta}_3 \bar{1}_z = \overline{F_S G_3} \times m_3 \overline{H \dot{G}_3} + I_3 \dot{\theta}_3 \bar{1}_z \quad (5.17)$$

or:

$$A_3 = I_3 + m_3 \gamma^2 l_3^2 + m_3 \gamma l_3 [(X_H - X_{F_S}) \cos \theta_3 + (Y_H - Y_{F_S}) \sin \theta_3] \quad (5.18)$$

5.4 Dynamics

5.4.1 Angular momentum equation

Taking (5.11) and (5.12) into account, meaning that no slipping of the supporting foot occurs and that a continuous contact with the ground surface is assumed, allows one to write the angular momentum equation with respect to the ankle joint:

$$\dot{\bar{\mu}}_{F_S} = \overline{F_S G} \times M \bar{g} - \bar{T}_{F_S} \quad (5.19)$$

with M being the total mass of the robot and \bar{T}_{F_S} the applied torque at the ankle joint of the supporting foot.

In order to become the natural upper body motion, it is assumed that the ankle actuator is not used. Introducing the kinematic expression (5.15) in the angular momentum equation (5.19) gives:

$$(A_3 \ddot{\theta}_3 + \dot{A}_3 \dot{\theta}_3 + \dot{h}) \bar{1}_z = \overline{F_S G} \times M \bar{g} \quad (5.20)$$

or after expanding the cross product on the rhs:

$$A_3 \ddot{\theta}_3 + \dot{A}_3 \dot{\theta}_3 + \dot{h} = -Mg (X_G - X_{F_S}) \quad (5.21)$$

This dynamic equation will play a key role in the trajectory generation strategy. More specifically it forms the basis for the part of the algorithm steering the upper body motion.

5.4.2 Complete dynamic model

During each single support phase, the robot has 5 DOF, since the supporting foot is assumed to be fixed on the ground. The following vector of angular coordinates is used to describe the different DOF:

$$q = (\theta_{1S}, \theta_{2S}, \theta_3, \theta_{2A}, \theta_{1A})^T = (\theta_1, \theta_2, \theta_3, \theta_4, \theta_5)^T \quad (5.22)$$

The i -th line of the dynamic model can be written as follows by using Lagrange's formalism:

$$\frac{d}{dt} \left\{ \frac{\partial K}{\partial \dot{q}_i} \right\} - \frac{\partial K}{\partial q_i} + \frac{\partial U}{\partial q_i} = Q_i \quad (i = 1 \dots 5) \quad (5.23)$$

where K and U are respectively the total kinetic and gravitational energy of the robot, and Q_i are generalized forces associated with the generalized coordinates q_i .

The kinetic energy K can be written as:

$$K = \frac{1}{2} \dot{q}^T D[q] \dot{q} \quad (5.24)$$

with $D[q]$ being the generalized inertia matrix.

The potential energy due to gravity is simply:

$$U = MgY_G \quad (5.25)$$

where the kinematic expression for Y_G as a function of the angular coordinates q_i is found by introducing (5.2) in (5.10). When neglecting friction in the joints, air drag, and possible friction forces due to any physical system used to restrict the robot's motion to the sagittal plane, the generalized forces consist of the torques applied in both the knee and hip joints and the ankle joint of the supporting foot (see figure 5.2):

$$Q = \begin{bmatrix} \tau_{K_S} - \tau_{F_S} \\ \tau_{H_S} - \tau_{K_S} \\ -\tau_{H_S} - \tau_{H_A} \\ \tau_{H_A} - \tau_{K_A} \\ \tau_{K_A} \end{bmatrix} \quad (5.26)$$

The 5 equations of motion (5.23) can be written in the following matrix form [Spong and Vidyasagar, 1989]:

$$D[q]\ddot{q} + C[q, \dot{q}]\dot{q} + G[q] = T \quad (5.27)$$

This set can be solved for the required external torque vector T after introducing the joint trajectories.

See appendix D for the formal expressions of the matrices D , C and G . Note that the dynamic equation (5.19) is obtained by making the sum of the five Lagrange's equations (5.27).

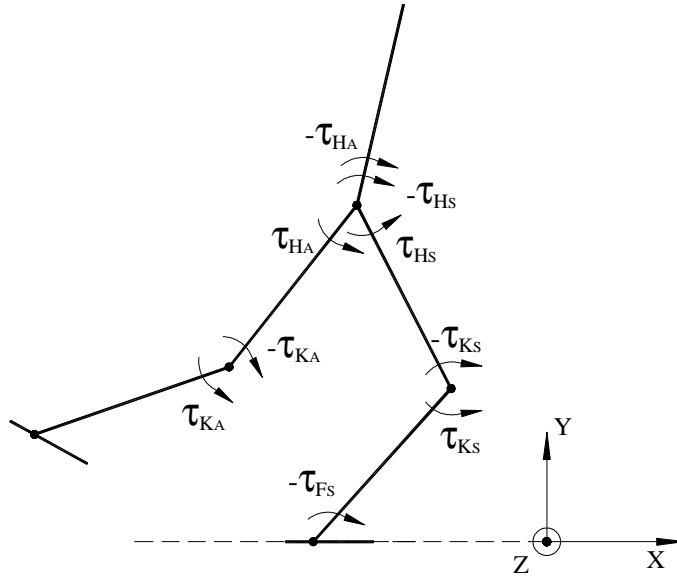


Figure 5.2: Actuators acting on biped

5.5 Problem statement

The goal is to set up a steady walking pattern for the robot with given values for the objective locomotion parameters (see section 5.7.1). This means that the mean horizontal hip velocity, the step length, the step height and the foot lift are imposed, and that these values have to be identical during all the consecutive steps.

Figure 5.2 shows the biped during a single support phase of a step, while figure 5.3 depicts its configuration in the boundary points of such a step. Imposing initially that the ankle of the supporting foot is unactuated, causes the robot to be an underactuated mechanism with one degree of underactuation. When the actuators for the leg links track given reference trajectories, then the resulting upper body motion can be obtained by solving the angular momentum equation with respect to the ankle point of the supporting foot (5.21). Numerically solving this momentum equation, which will not be explicitly done here, leads to a time-varying trajectory for the upper body angle, here referred to as the *natural* upper body motion. Theoretically, if this natural trajectory would be used as a reference trajectory, then the corresponding ankle torque would be zero at all times. Similar to the strategy used for the hopping robot in chapter 4, the natural trajectory will be approximated by a polynomial function. This polynomial function will then be used as a reference trajectory. Doing so, the ankle actuator will produce a torque to compensate for the differences between the natural trajectory and the polynomial trajectory for the upper body angle. When this polynomial function is good approximation of

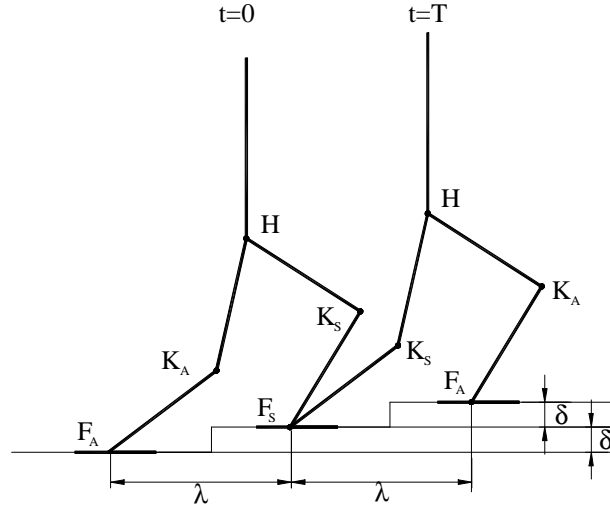


Figure 5.3: Walking pattern

the natural trajectory, which will be realized by manipulating the angular momentum equation, then the resulting ankle torque is small. Recall that large ankle torques can cause the ZMP to move out of the foot surface, which leads to postural instability.

One way to express that a steady walking pattern has to be realized, is to demand that all links behave in exactly the same manner during all consecutive walking cycles. It is assumed here that identical behaviour corresponds to an identical trajectory for the angle, the angular velocity and the angular acceleration associated with each link of the robot. A walking cycle consists of two steps, since after each step the function of support is transferred from the one foot to the other. Two consecutive steps are assumed to be identical, except for the support exchange. To simplify the mathematics at a first stage, the impact phase accompanying the support exchange is avoided by choosing a zero touch-down velocity of the swing foot with respect to the ground. According to our definition for cyclic or steady walking, when using polynomial functions as the tracking trajectories for the 4 actuators of the leg links, these polynomial functions have to satisfy the following periodicity of the boundary conditions (T represents the duration of one step):

- $\theta_{1S}(T) = \theta_{1A}(0)$, $\theta_{2S}(T) = \theta_{2A}(0)$, $\theta_{1A}(T) = \theta_{1S}(0)$, $\theta_{2A}(T) = \theta_{2S}(0)$
- $\dot{\theta}_{1S}(T) = \dot{\theta}_{1A}(0)$, $\dot{\theta}_{2S}(T) = \dot{\theta}_{2A}(0)$, $\dot{\theta}_{1A}(T) = \dot{\theta}_{1S}(0)$, $\dot{\theta}_{2A}(T) = \dot{\theta}_{2S}(0)$
- $\ddot{\theta}_{1S}(T) = \ddot{\theta}_{1A}(0)$, $\ddot{\theta}_{2S}(T) = \ddot{\theta}_{2A}(0)$, $\ddot{\theta}_{1A}(T) = \ddot{\theta}_{1S}(0)$, $\ddot{\theta}_{2A}(T) = \ddot{\theta}_{2S}(0)$

In order to fulfill the demand for steady walking, the following is required for the upper body motion:

- $\theta_3(T) = \theta_3(0)$, $\dot{\theta}_3(T) = \dot{\theta}_3(0)$, $\ddot{\theta}_3(T) = \ddot{\theta}_3(0)$

Since initially the robot is underactuated, these boundary conditions have to be satisfied indirectly by defining the motion of the leg links in a proper way. In other words, the question is how to define the leg link trajectories such that the natural upper body motion automatically satisfies these boundary conditions, without explicitly having to know the natural trajectory.

Globally the trajectory generation strategy will have two different tasks which inevitably depend on each other:

- define a motion for the leg links such that the upper body moves as desired
- define a motion for all the links such that all the values for the objective parameters are attained

Since both tasks influence each other, an iterative procedure will be inevitable. The first task will be handled in section 5.6, whereas the second task will be covered in section 5.7.

5.6 Obtaining the desired upper body motion

When assuming that the supporting foot of the robot is located at the origin of the coordinate system, equation (5.21) representing the angular momentum equation with respect to the ankle point of the supporting foot, in absence of an ankle actuator, is written as ($X_{F_S} = 0$):

$$A_3\ddot{\theta}_3 + \dot{A}_3\dot{\theta}_3 + \dot{h} = -MgX_G \quad (5.28)$$

with h and A_3 as well as X_G being functions of θ_3 . When the 4 actuators track given reference trajectories, equation (5.28) is a second order non-linear differential equation which can be solved for $\theta_3(t)$. Indeed, when the trajectories for θ_{1S} , θ_{2S} , θ_{1A} and θ_{2A} are known, and when initial conditions for $\theta_3(0)$ and $\dot{\theta}_3(0)$ are imposed, (5.28) can be numerically integrated twice to produce a solution $\theta_3(t)$. This solution is defined as the natural trajectory for the upper body angle.

When developing a real-time trajectory generation strategy for the different controllers of the walking robot, this strategy should not be based on solving differential equations. Numerically solving (5.28) is time consuming, and besides, with arbitrarily defined trajectories for θ_{1S} , θ_{2S} , θ_{1A} and θ_{2A} , the solution $\theta_3(t)$ will in general not satisfy the specified boundary conditions.

The strategy used in this chapter, is to manipulate the boundary conditions for the leg link trajectories such that the resulting natural trajectory of the upper body satisfies as good as possible the boundary conditions given in section 5.5. This will be realized by deriving three extra conditions resulting from the angular momentum

equation. Satisfying these conditions will cause the upper body to reach the same orientation, angular velocity and angular acceleration at the beginning and at the end of a step. At the same time a polynomial reference trajectory for the upper body satisfying the same boundary conditions will be established, in order to mimic that specific natural trajectory.

Suppose that a certain desired trajectory (a polynomial function) for the upper body angle $\theta_3^*(t)$ is defined, satisfying the following boundary conditions:

$$\theta_3^*(T) = \theta_3^*(0) \quad (5.29)$$

$$\dot{\theta}_3^*(T) = \dot{\theta}_3^*(0) \quad (5.30)$$

$$\ddot{\theta}_3^*(T) = \ddot{\theta}_3^*(0) \quad (5.31)$$

Then the question is how the trajectories for θ_{1S} , θ_{2S} , θ_{1A} and θ_{2A} , as well as the initial conditions for $\theta_3(0)$ and $\dot{\theta}_3(0)$ have to be chosen, in order to obtain a natural trajectory $\theta_3(t)$ that approximates the desired trajectory $\theta_3^*(t)$. In the following paragraphs, three conditions will be established in order to reach this goal. One condition will act on the initial condition for the angular velocity of the upper body. Two other conditions will act on the motion of the leg links.

5.6.1 Upper body angle

Condition on upper body angular velocity

Integrating (5.19) from $u = 0$ to $u = t$, in case of zero ankle torque, gives:

$$\bar{\mu}_{F_S}(t) - \bar{\mu}_{F_S}(0) = \int_0^t [\overline{F_S G} \times M\bar{g}] du \quad (5.32)$$

or when considering the only non-zero Z-component of this equation:

$$\mu_{F_S}(t) - \mu_{F_S}(0) = -Mg \int_0^t X_G du \quad (5.33)$$

A second integration from $t = 0$ to $t = T$ yields:

$$\int_0^T \mu_{F_S}(t) dt - \mu_{F_S}(0)T = -Mg \int_0^T (T-t) X_G dt \quad (5.34)$$

Now introducing (5.15) into the lhs of (5.34) and solving for $\dot{\theta}_3(0)$ gives:

$$\begin{aligned} \dot{\theta}_3(0) = & \frac{Mg}{TA_3(0)} \int_0^T (T-t) X_G dt - \frac{h(0)}{A_3(0)} \\ & + \frac{1}{TA_3(0)} \int_0^T h dt + \frac{1}{TA_3(0)} \int_0^T A_3 \dot{\theta}_3 dt \quad (5.35) \end{aligned}$$

When trajectories for the leg links are imposed, then a certain rotation of the upper body $\Delta\theta_3 = \theta_3(T) - \theta_3(0)$ will be measured after the step. Varying the initial condition $\dot{\theta}_3(0)$ will influence the solution of the differential equation (5.28) and also the value of $\Delta\theta_3$. With expression (5.35) a suitable value for $\dot{\theta}_3(0)$ can be estimated. This can be done by introducing a desired trajectory $\theta_3^*(t)$ in the rhs of the equation.

Since $\theta_3(t)$ and $\theta_3^*(t)$ have to approximate each other, substituting θ_3^* into (5.35) yields a condition on $\dot{\theta}_3(0)$. The function θ_3^* is chosen such that $\theta_3^*(T) = \theta_3^*(0)$ or $\Delta\theta_3^* = 0$, leading to:

$$\begin{aligned} \dot{\theta}_3(0) = & \frac{Mg}{TA_3(0)} \int_0^T (T-t) X_G^* dt - \frac{h(0)}{A_3(0)} \\ & + \frac{1}{TA_3(0)} \int_0^T h^* dt + \frac{1}{TA_3(0)} \int_0^T A_3^* \dot{\theta}_3^* dt \quad \Leftrightarrow \quad \Delta\theta_3 \approx 0 \quad (5.36) \end{aligned}$$

All variables containing a * are calculated with the desired function $\theta_3^*(t)$. Condition (5.36) states that if $\theta_3^*(t)$ is a good approximation of $\theta_3(t)$, then when setting the initial condition on the upper body angular velocity to the computed value in the lhs, the real value of the upper body angle at the end of the single support phase will approximate its initial value. This would be accomplished without ankle actuation. Since a desired function has to be introduced in the rhs and since $\dot{\theta}_3(0)$ appears in the lhs, (5.36) has to be used iteratively.

Establishing body polynomial function

At this point, the desired function $\theta_3^*(t)$ is unknown, because the boundary values for θ_3^* and $\dot{\theta}_3^*$ are not known. These values will be estimated by using (5.36) by iteration. The first choice for $\theta_3^*(t)$ will be:

$$\theta_3^{*,1}(t) = \theta_3(0) \quad (5.37)$$

which is most likely a poor approximation of $\theta_3(t)$. It corresponds to a zero initial angular velocity $\dot{\theta}_3^*(0) = 0$. Implementing $\theta_3^{*,1}(t)$ in (5.36) yields a new value $\dot{\theta}_3^*(0)$

($= \dot{\theta}_3^*(T)$) for the angular velocity, which forms the basis for a new desired function $\theta_3^{*,2}(t)$. Indeed, when evaluating (5.28) at $t = 0$, one can solve this equation for the second derivative $\ddot{\theta}_3^*(0)$:

$$\ddot{\theta}_3^*(0) = -\frac{1}{A_3(0)} \left(MgX_G(0) + \dot{A}_3^*(0)\dot{\theta}_3^*(0) + \dot{h}^*(0) \right) = \ddot{\theta}_3^*(T) \quad (5.38)$$

allowing one to establish a fifth order polynomial for $\theta_3^{*,2}$. However, when designing the trajectory to be tracked by the ankle actuator, this trajectory should try to mimic the natural trajectory as good as possible. Large deviations from the natural trajectory will cause higher values for the ankle torque, whereas an exact copy of the natural trajectory would cause a zero torque. Simulations showed that trying to mimic the natural trajectory with a fifth order polynomial function $\theta_3^*(t)$ does not lead to good results. The value of the ankle torque depends mainly on the value of the angular acceleration of the upper body. With a fifth order polynomial function for the angle, the acceleration is only a third order polynomial function having to mimic the solution of the differential angular momentum equation. Due to the fact that the slopes in the end points of the trajectory for the acceleration do not correspond to the slopes of the natural trajectory, the two trajectories differ significantly in between the boundary points. Substituting the fifth order polynomial in equation (5.28) and differentiating with respect to time allows one to estimate the necessary third order derivative of $\theta_3^*(t)$:

$$\ddot{\theta}_3^* = -\frac{1}{A_3^*} \left(Mg\dot{X}_G^* + \ddot{h}^* + 2\dot{A}_3^*\ddot{\theta}_3^* + \ddot{A}_3^*\dot{\theta}_3^* \right) \quad (5.39)$$

Evaluating this expression at $t = 0$ and $t = T$ allows one to determine the third order derivative in the end points of the trajectory, which are used to design a seventh order polynomial function for the upper body angle θ_3 . A variety of simulations showed that a seventh order polynomial function sufficiently mimics the natural trajectory. Additionally altering the order of the polynomial is not considered, since this could lead to the so-called Runge phenomenon [Saidouni and Bessonnet, 2002]. If necessary, other techniques based on cubic spline interpolations [Tondu and Bazaz, 1999] can be used, as was already proven to produce good results [Shih, 1997a], [Huang et al., 2001], [Saidouni and Bessonnet, 2002].

The calculation of the polynomial function $\theta_3^*(t)$ has to be repeated until a certain convergence of $\dot{\theta}_3(0)$ is reached. Note that at this point it is not guaranteed that indeed $\theta_3^*(t)$ is a good approximation of $\theta_3(t)$. In the following sections it will be shown how the angular momentum equation can be manipulated to produce a natural trajectory that satisfies the boundary conditions (5.30) and (5.31), such that the polynomial and natural trajectories approximate each other.

5.6.2 Upper body angular velocity

It is assumed that the boundary conditions for the leg links, specified in section 5.5, are satisfied. If the initial condition on the angular velocity $\dot{\theta}_3(0)$ is chosen such that $\theta_3(T) = \theta_3(0)$, then the condition $\dot{\theta}_3(T) = \dot{\theta}_3(0)$ corresponds to the condition:

$$\bar{v}_G(T) = \bar{v}_G(0) \quad (5.40)$$

This condition has to be satisfied when attempting to reach an impact-less steady walking motion. Due to the fact that the system is underactuated in absence of an ankle torque, the controllers can not act directly on the velocity of the COG. The angular momentum equation can however be used to determine under which circumstances the following will hold:

$$\bar{\mu}_G(T) = \bar{\mu}_G(0) \quad (5.41)$$

When taking into account the boundary conditions of the angles of the leg links of section 5.5, and when $\theta_3(T) = \theta_3(0)$, satisfying condition (5.41) will indeed result in $\dot{\theta}_3(T) = \dot{\theta}_3(0)$. When applying the transport equation for the angular momentum between G and F on (5.41), one has:

$$\bar{\mu}_{F_S}(T) - \bar{\mu}_{F_S}(0) = \overline{F_S G}(T) \times M\bar{v}_G(T) - \overline{F_S G}(0) \times M\bar{v}_G(0) \quad (5.42)$$

The right hand side of this expression becomes (when imposing (5.40)):

$$\overline{F_S G}(T) \times M\bar{v}_G(T) - \overline{F_S G}(0) \times M\bar{v}_G(0) = M \left[\Delta X_G \dot{Y}_G(0) - \Delta Y_G \dot{X}_G(0) \right] \bar{1}_z \quad (5.43)$$

with

$$\Delta X_G = X_G(T) - X_G(0) \quad (5.44)$$

$$\Delta Y_G = Y_G(T) - Y_G(0) \quad (5.45)$$

Since the left hand side of (5.42) is determined by the angular momentum equation (5.32), the following is obtained:

$$\text{if } \begin{cases} \int_0^T (\overline{F_S G} \times M\bar{g}) dt = M \left[\Delta X_G \dot{Y}_G(0) - \Delta Y_G \dot{X}_G(0) \right] \bar{1}_z \\ \Delta\theta_3 = 0 \end{cases} \Rightarrow \Delta\dot{\theta}_3 = 0 \quad (5.46)$$

And when expanding the cross-product on the lhs:

$$\text{if } \begin{cases} -g \int_0^T X_G dt = \Delta X_G \dot{Y}_G(0) - \Delta Y_G \dot{X}_G(0) \\ \Delta\theta_3 = 0 \end{cases} \Rightarrow \Delta\dot{\theta}_3 = 0 \quad (5.47)$$

which is a condition on the initial velocity of the COG, and on the integral of the horizontal position of the COG. When (5.47) is fulfilled, and when the initial condition of the angular velocity is chosen such that $\theta_3(T) = \theta_3(0)$, then the natural trajectory will have an angular velocity of the upper body at the end of the step equal to the one at the beginning of the step. Condition (5.47) can e.g. be satisfied by tuning the initial horizontal position of the hip, which determines the value of the integral on the lhs.

The integral of the horizontal position of the COG contains the unknown trajectory $\theta_3(t)$. Again this function will be replaced by a desired function $\theta_3^*(t)$. Also, from figure 5.3 it can be seen that:

$$\text{if } \Delta\theta_3 = 0 \quad \Rightarrow \quad \begin{cases} \Delta X_G = \lambda \\ \Delta Y_G = \delta \end{cases} \quad (5.48)$$

Indeed, due tot the fact that the legs are assumed as identical, the robot appears to be translated. Finally the following condition is found:

$$\text{if } \begin{cases} -g \int_0^T X_G^* dt = \lambda \dot{Y}_G(0) - \delta \dot{X}_G(0) \\ \Delta\theta_3 = 0 \end{cases} \quad \Rightarrow \quad \Delta\dot{\theta}_3 \approx 0 \quad (5.49)$$

5.6.3 Upper body angular acceleration

When assuming that $\theta_3(T) = \theta_3(0)$ and $\dot{\theta}_3(T) = \dot{\theta}_3(0)$ and taking into account the boundary conditions on the trajectories for the leg links, the condition $\ddot{\theta}_3(T) = \ddot{\theta}_3(0)$ corresponds to:

$$\bar{a}_G(T) = \bar{a}_G(0) \quad (5.50)$$

which is a condition that has to be satisfied in case of cyclic impact-less walking. One can not act directly on the acceleration of the COG, but the angular momentum equation can be manipulated such that:

$$\dot{\bar{\mu}}_G(T) = \dot{\bar{\mu}}_G(0) \quad (5.51)$$

Indeed, satisfying (5.51) will lead to $\ddot{\theta}_3(T) = \ddot{\theta}_3(0)$. Writing the angular momentum equation with respect to G, in absence of an ankle actuator, gives

$$\dot{\bar{\mu}}_G(t) = \overline{GF_S}(t) \times \bar{R} = \overline{GF_S}(t) \times M(\bar{a}_G(t) - \bar{g}) \quad (5.52)$$

with \bar{R} the ground reaction force. Substituting (5.52) in (5.51) leads to:

$$\overline{GF_S}(T) \times [\bar{a}_G(T) - \bar{g}] = \overline{GF_S}(0) \times [\bar{a}_G(0) - \bar{g}] \quad (5.53)$$

After imposing (5.50) one has:

$$[\overline{GF_S}(T) - \overline{GF_S}(0)] \times [\bar{a}_G(0) - \bar{g}] = 0 \quad (5.54)$$

or:

$$\Delta X_G \left[\ddot{Y}_G(0) + g \right] - \Delta Y_G \ddot{X}_G(0) = 0 \quad (5.55)$$

or when referring to (5.48):

$$\lambda \left[\ddot{Y}_G(0) + g \right] - \delta \ddot{X}_G(0) = 0 \quad (5.56)$$

So the following can be concluded:

$$\text{if } \begin{cases} \lambda \left[\ddot{Y}_G(0) + g \right] - \delta \ddot{X}_G(0) = 0 \\ \Delta \theta_3 = 0 \\ \Delta \dot{\theta}_3 = 0 \end{cases} \Rightarrow \Delta \ddot{\theta}_3 = 0 \quad (5.57)$$

The value of $\ddot{\theta}_3(0)$ is determined (see (5.38)) by the angular momentum equation. Condition (5.57) can e.g. be satisfied by tuning the initial hip acceleration.

Remark: Walking on flat terrain

In case of $\delta = 0$, a necessary condition to obtain $\Delta \ddot{\theta}_3 = 0$ is that $\ddot{Y}_G(0) = -g$. This means that the robot is in fact not in contact with the ground in the end points of the step. These end points correspond to the instantaneous double support phases, which only appear for an infinitesimally short time interval. This phenomena clearly indicates that walking with instantaneous double support phase is in fact a limit case between a walking motion and a running motion. Indeed the instantaneous double support phase is virtually a flight phase with an infinitesimal short duration, during which the ZMP transfers from the rear ankle to the front ankle.

5.7 Developing a trajectory generation strategy

In section 5.6 it was shown that defining the hip motion of the robot in a proper way, leads to a natural upper body motion which satisfies given boundary conditions, such that its behaviour can be approximated by a polynomial function based on these boundary conditions. This covers the first task of the trajectory generation strategy.

The second task, which has to ensure that the values for the different objective locomotion parameters are attained, will be treated now. Based on the objective locomotion parameters and a number of chosen boundary conditions for the hip point trajectory and the swing foot trajectory, polynomial trajectories will be established for the leg links. These trajectories will determine whether the conditions for the first task of the strategy are satisfied or not. An iterative procedure will be developed in order to perform both tasks of the planning strategy in a successful way.

5.7.1 Objective locomotion parameters

To clearly describe the motion of the robot, a number of objective locomotion parameters are introduced. These parameters describe the global motion itself, instead of the behaviour of the different joints of the robot. The parameters chosen here are (see figure 5.3):

- Horizontal Step Length $X_{F_S} - X_{F_A} = \lambda$ (steady walking: $\Delta X_{F_A} = 2\lambda$)
- Vertical Step Height $Y_{F_S} - Y_{F_A} = \delta$ (steady walking: $\Delta Y_{F_A} = 2\delta$)
- Mean Horizontal Hip Velocity $\widetilde{\dot{X}_H} = \nu$
- Foot Lift $Y_{F_A}(\frac{T}{2}) = \sigma$

Referring to figure 5.3, the horizontal displacement of the foot in the air during one step is twice the horizontal displacement of the hip point H:

$$\Delta X_H = \frac{\Delta X_{F_A}}{2} = \lambda \quad (5.58)$$

And since exactly the same configuration (with leg exchanging) is to be reached at the end of the step as at the beginning of the step, the horizontal displacement of the global COG is also determined:

$$\Delta X_G = \Delta X_H = \lambda \quad (5.59)$$

When choosing ν and λ , the stance time T is known:

$$T = \frac{\Delta X_H}{\widetilde{\dot{X}_H}} = \frac{\lambda}{\nu} \quad (5.60)$$

5.7.2 Boundary conditions - configuration level

Initial configuration at $t = 0$

Assume that at the beginning of the step the foot on the ground F_S is located at the origin of the coordinate system:

$$X_{F_S}(0) = 0 \quad \text{and} \quad Y_{F_S}(0) = 0 \quad (5.61)$$

$$X_{F_A}(0) = -\lambda \quad \text{and} \quad Y_{F_A}(0) = -\delta \quad (5.62)$$

The orientation of the upper body $\theta_3(0)$ at the beginning of the step can in theory be given an arbitrary value. Values in the neighborhood of $\frac{\pi}{2}$ are however preferred

from the viewpoint of stability, since gravity causes a destabilizing moment around the hip point.

Since at the switching instant the robot has 3 DOF due to the closed chain, apart from the upper body angle there are 2 coordinates left to be chosen. A good choice for these coordinates proves to be $X_H(0)$ and $Y_H(0)$, being respectively the horizontal and vertical position of the hip joint. The value of $X_H(0)$ is of crucial importance since it will determine if (5.49) is respected or not. Besides, the horizontal trajectory of the hip is the main factor that affects the stability of a biped robot walking in the sagittal plane [Huang et al., 2001]. The value of $Y_H(0)$ is however less important. Hip motion in the vertical direction hardly affects the position of the ZMP. It will only determine whether the robot walks with less or more stretched legs. Suppose that the following values are chosen:

$$X_H(0)^{,0} \quad (5.63)$$

$$Y_H(0) \quad (5.64)$$

Note that the superscript ,0 in $X_H(0)^{,0}$ indicates that this is a starting value which will be adapted by an iterative procedure, and that this is not the case for $Y_H(0)$. The kinematic expressions of the legs are used to calculate the initial configuration. The position of the hip point H, when calculated starting from the supporting foot, is obtained as:

$$\begin{cases} X_H^S &= X_{F_S} + l_1 \cos \theta_{1S} + l_2 \cos \theta_{2S} \\ Y_H^S &= Y_{F_S} + l_1 \sin \theta_{1S} + l_2 \sin \theta_{2S} \end{cases} \quad (5.65)$$

Evaluating at $t = 0$ gives:

$$\Rightarrow \begin{cases} X_H(0)^{,0} &= l_1 \cos \theta_{1S}(0) + l_2 \cos \theta_{2S}(0) \\ Y_H(0) &= l_1 \sin \theta_{1S}(0) + l_2 \sin \theta_{2S}(0) \end{cases} \quad (5.66)$$

This set can be solved analytically by applying the following substitution:

$$\begin{cases} X_1 &= \cos \theta_{1S}(0) \\ X_2 &= \cos \theta_{2S}(0) \\ Y_1 &= \sin \theta_{1S}(0) \\ Y_2 &= \sin \theta_{2S}(0) \end{cases} \quad (5.67)$$

which leads to the following set:

$$\begin{cases} X_1^2 + Y_1^2 = 1 \\ X_2^2 + Y_2^2 = 1 \\ l_1 X_1 + l_2 X_2 = X_H(0)^{,0} \\ l_1 Y_1 + l_2 Y_2 = Y_H(0) \end{cases} \quad (5.68)$$

This set is easily transformed into a quadratic equation in one of the unknowns, allowing one to calculate both the angles $\theta_{1S}(0)$ and $\theta_{2S}(0)$. The quadratic equation has two solutions, being one desired solution and the other solution with an overstretched knee.

Analogously the position of the hip point H, when calculated starting from the foot in the air, is obtained as:

$$\begin{cases} X_H^A &= X_{FA} + l_1 \cos \theta_{1A} + l_2 \cos \theta_{2A} \\ Y_H^A &= Y_{FA} + l_1 \sin \theta_{1A} + l_2 \sin \theta_{2A} \end{cases} \quad (5.69)$$

Evaluating at $t = 0$ gives:

$$\Rightarrow \begin{cases} X_H(0)^0 &= -\lambda + l_1 \cos \theta_{1A}(0) + l_2 \cos \theta_{2A}(0) \\ Y_H(0) &= -\delta + l_1 \sin \theta_{1A}(0) + l_2 \sin \theta_{2A}(0) \end{cases} \quad (5.70)$$

This set is analytically solved for the angles $\theta_{1A}(0)$ and $\theta_{2A}(0)$.

Final configuration at $t = T$

At the end of the step one has:

$$X_{FS}(T) = 0 \quad \text{and} \quad Y_{FS}(T) = 0 \quad (5.71)$$

$$X_{FA}(T) = \lambda \quad \text{and} \quad Y_{FA}(T) = \delta \quad (5.72)$$

The final values of the absolute angles of the leg links are immediately known since steady walking is assumed (see section 5.5).

5.7.3 Boundary conditions - velocity level

Initial velocity at $t = 0$

Since the foot of the stance leg remains fixed on the ground, one has:

$$\dot{X}_{FS}(0) = 0 \quad (5.73)$$

$$\dot{Y}_{FS}(0) = 0 \quad (5.74)$$

The swing leg is actually the stance leg of the previous step, so the velocity of that foot at $t = 0$ is also zero:

$$\dot{X}_{FA}(0) = 0 \quad (5.75)$$

$$\dot{Y}_{FA}(0) = 0 \quad (5.76)$$

Walking with a constant horizontal velocity would create a smooth walking motion. Suppose that horizontal velocity of the hip in the end points of the steps is chosen equal to the mean horizontal hip velocity ν :

$$\dot{X}_H(0) = \nu \quad (5.77)$$

The vertical velocity of the hip in the end points of the step can be chosen a value $\dot{Y}_H(0)$ depending on the desired trajectory for the vertical hip motion.

Differentiating the kinematic expressions (5.65) and evaluating at $t = 0$ gives:

$$\begin{cases} \nu &= -l_1 \sin \theta_{1S}(0) \dot{\theta}_{1S}(0) - l_2 \sin \theta_{2S}(0) \dot{\theta}_{2S}(0) \\ \dot{Y}_H(0) &= l_1 \cos \theta_{1S}(0) \dot{\theta}_{1S}(0) + l_2 \cos \theta_{2S}(0) \dot{\theta}_{2S}(0) \end{cases} \quad (5.78)$$

This is a linear set of equations solved for the 2 unknowns $\dot{\theta}_{1S}(0)$ and $\dot{\theta}_{2S}(0)$. The calculation of $\dot{\theta}_{1A}(0)$ and $\dot{\theta}_{2A}(0)$ is completely analogous after differentiating (5.69).

Final velocity at $t = T$

Since the foot of the stance leg stays fixed on the ground, one has:

$$\dot{X}_{F_S}(T) = 0 \quad (5.79)$$

$$\dot{Y}_{F_S}(T) = 0 \quad (5.80)$$

When assuming a soft touch-down of the swing leg, which means that there is no impact, one has:

$$\dot{X}_{F_A}(T) = 0 \quad (5.81)$$

$$\dot{Y}_{F_A}(T) = 0 \quad (5.82)$$

When taking into account the boundary conditions of section 5.5, the final angular velocities of the leg links are immediately known.

5.7.4 Boundary conditions - acceleration level

Initial acceleration at $t = 0$

For analogous reasons as at the velocity level, one has:

$$\ddot{X}_{F_S}(0) = 0 \quad (5.83)$$

$$\ddot{Y}_{F_S}(0) = 0 \quad (5.84)$$

$$\ddot{X}_{F_A}(0) = 0 \quad (5.85)$$

$$\ddot{Y}_{FA}(0) = 0 \quad (5.86)$$

The horizontal acceleration of the hip is chosen equal to zero, since the horizontal velocity is desired to be a constant:

$$\ddot{X}_H(0) = 0 \quad (5.87)$$

This choice is in fact contrary to the behaviour of an inverted pendulum that is decelerated when the COG lies behind the supporting point, and re-accelerated when it is in front of the supporting point. Due to the fact that the steps have to be identical combined with the absence of a double support phase, the horizontal acceleration of the hip has to have equal values in both the end-points of each step. The inverted pendulum prescribes a negative acceleration for the first half of the step and a positive one for the second half. Such a condition can not be imposed here, which indicates that walking without double support phase and without impact will probably not be interesting from an energetics point of view.

The value of $\ddot{Y}_H(0)$ is crucial since it will determine if (5.57) is satisfied or not. Suppose that $\ddot{Y}_H(0)^0$ is chosen, where the superscript , 0 indicates that it is a starting value that will be adapted by iteration. Again, the kinematic expressions for the legs are used to determine the unknown angular accelerations. Differentiating twice (5.65) and evaluating at $t = 0$ gives:

$$\begin{cases} 0 & = -l_1 \sin \theta_{1S}(0) \ddot{\theta}_{1S}(0) - l_2 \sin \theta_{2S}(0) \ddot{\theta}_{2S}(0) \\ & \quad - l_1 \cos \theta_{1S}(0) \dot{\theta}_{1S}^2(0) - l_2 \cos \theta_{2S}(0) \dot{\theta}_{2S}^2(0) \\ \ddot{Y}_H(0)^0 & = l_1 \cos \theta_{1S}(0) \ddot{\theta}_{1S}(0) + l_2 \cos \theta_{2S}(0) \ddot{\theta}_{2S}(0) \\ & \quad - l_1 \sin \theta_{1S}(0) \dot{\theta}_{1S}^2(0) - l_2 \sin \theta_{2S}(0) \dot{\theta}_{2S}^2(0) \end{cases} \quad (5.88)$$

This is again a linear set of equations, which is solved for the 2 unknowns $\ddot{\theta}_{1S}(0)$ and $\ddot{\theta}_{2S}(0)$. The calculation of $\ddot{\theta}_{1A}(0)$ and $\ddot{\theta}_{2A}(0)$ is analogous.

Final acceleration at $t = T$

For symmetry reasons, one states:

$$\ddot{X}_{Fs}(T) = 0 \quad (5.89)$$

$$\ddot{Y}_{Fs}(T) = 0 \quad (5.90)$$

$$\ddot{X}_{FA}(T) = 0 \quad (5.91)$$

$$\ddot{Y}_{FA}(T) = 0 \quad (5.92)$$

When referring to section 5.5, the final values for the leg angular accelerations are known.

5.7.5 Intermediate condition

To avoid sudden contact of the foot of the swing leg with the ground, an extra condition will be added to the polynomial functions for that leg, by introducing the foot lift σ . This parameter imposes the desired height of the swing foot at $t = \frac{T}{2}$:

$$Y_{F_A} \left(\frac{T}{2} \right) = \sigma \quad (5.93)$$

Assuming that at $t = \frac{T}{2}$ the swing foot has moved half of its total swing displacement:

$$X_{F_A} \left(\frac{T}{2} \right) = X_{F_A} (0) + \lambda = 0 \quad (5.94)$$

Then evaluating the kinematic expressions for the swing leg (5.69) at $t = \frac{T}{2}$ gives:

$$\begin{cases} X_H \left(\frac{T}{2} \right) &= l_1 \cos \theta_{1A} \left(\frac{T}{2} \right) + l_2 \cos \theta_{2A} \left(\frac{T}{2} \right) \\ Y_H \left(\frac{T}{2} \right) &= \sigma + l_1 \sin \theta_{1A} \left(\frac{T}{2} \right) + l_2 \sin \theta_{2A} \left(\frac{T}{2} \right) \end{cases} \quad (5.95)$$

To be able to solve this set for $\theta_{1A} \left(\frac{T}{2} \right)$ and $\theta_{2A} \left(\frac{T}{2} \right)$, the values of $X_H \left(\frac{T}{2} \right)$ and $Y_H \left(\frac{T}{2} \right)$ have to be known. These can be determined with the kinematic expressions (5.65) of the supporting leg evaluated at $t = \frac{T}{2}$. To be able to do this, polynomial trajectories are established for θ_{1S} and θ_{2S} based on the boundary conditions as calculated in the preceding paragraphs. Since there are six boundary conditions imposed, these would be fifth order polynomials. A rather unnatural behaviour however occurs when using fifth order polynomials, which can be easily understood as follows. The resulting vertical hip motion is a trajectory with the following boundary values:

$$t = 0 : \begin{cases} Y_H (0) \\ \dot{Y}_H (0) \\ \ddot{Y}_H (0) \end{cases} \quad t = T : \begin{cases} Y_H (T) = Y_H (0) + \delta \\ \dot{Y}_H (T) = \dot{Y}_H (0) \\ \ddot{Y}_H (T) = \ddot{Y}_H (0) \end{cases}$$

Due to condition (5.57) which has to be satisfied if continuity of the upper body angular acceleration between successive steps is required, the angular acceleration $\ddot{Y}_H(0)$ is likely to have a negative value close to $-g$. By approximating the trajectory of the vertical position of the hip by a fifth order polynomial function based on these boundary conditions, then in the case where the vertical velocity in the end-points is small, which is certainly the case for normal walking, the hip point will move downward during the swing. This unnatural motion when compared to a human walking pattern, is in literature referred to as Groucho running [McMahon et al., 1987]. Indeed the vertical hip acceleration and consequently also the vertical acceleration of the COG become the classical one-lobed function which is found for human running [Rose and Gamble, 1993], while there is no actual aerial phase.

This confirms the remark made higher concerning the fact that soft or impact-less walking without double support phase can be seen as a limit case of running with zero flight time. Since this type of motion is not the desired one, especially since one has to lift the swing foot during the step, the hip point will be forced upwards during the swing. This can be done by altering the order of the polynomial function. As a result, the vertical hip acceleration will then be a two-lobed function as what is found for human walking [Rose and Gamble, 1993].

To counter the downward motion of the hip point, an intermediate condition will be added to the polynomial function, such that the order is increased to 6. This will be done by specifying a value $\ddot{Y}_H\left(\frac{T}{2}\right)$ in order to avoid a possible loss of contact of the foot with the ground possibly caused by imposing a value for the desired hip position that is too high. One can easily verify that for the resulting sixth order polynomial function for the hip height at $t = \frac{T}{2}$ becomes:

$$Y_H\left(\frac{T}{2}\right) = Y_H(0) + \epsilon = Y_H(0) + \frac{\delta}{2} + T^2 \left[\frac{1}{96} \ddot{Y}_H(0) - \frac{1}{24} \ddot{Y}_H\left(\frac{T}{2}\right) \right] \quad (5.96)$$

Any value for the intermediate acceleration between $\ddot{Y}_H(0)$ and 0 will force the hip point to move upwards. This value ϵ , which is referred to as the intermediate hip elevation, will be used to establish the polynomial functions for the leg link angles.

Since the horizontal velocity of the hip is wanted to be a constant, the value of $X_H\left(\frac{T}{2}\right)$ is assumed to be the initial position altered with half of the horizontal displacement of the hip:

$$X_H\left(\frac{T}{2}\right) = X_H(0) + \frac{\lambda}{2} \quad (5.97)$$

Now the kinematic expressions (5.65) of the supporting leg evaluated at $t = \frac{T}{2}$ become:

$$\begin{cases} l_1 \cos \theta_{1S}\left(\frac{T}{2}\right) + l_2 \cos \theta_{2S}\left(\frac{T}{2}\right) & = X_H(0) + \frac{\lambda}{2} \\ l_1 \sin \theta_{1S}\left(\frac{T}{2}\right) + l_2 \sin \theta_{2S}\left(\frac{T}{2}\right) & = Y_H(0) + \epsilon \end{cases} \quad (5.98)$$

This set can be solved for $\theta_{1S}\left(\frac{T}{2}\right)$ and $\theta_{2S}\left(\frac{T}{2}\right)$, using the method described in section 5.7.2. Analogously the set (5.95) becomes:

$$\begin{cases} l_1 \cos \theta_{1A}\left(\frac{T}{2}\right) + l_2 \cos \theta_{2A}\left(\frac{T}{2}\right) & = X_H(0) + \frac{\lambda}{2} \\ l_1 \sin \theta_{1A}\left(\frac{T}{2}\right) + l_2 \sin \theta_{2A}\left(\frac{T}{2}\right) & = Y_H(0) + \epsilon - \sigma \end{cases} \quad (5.99)$$

which can be solved for $\theta_{1A}\left(\frac{T}{2}\right)$ and $\theta_{2A}\left(\frac{T}{2}\right)$.

5.7.6 Establishing polynomial trajectories - iterative procedure

Based on the six boundary conditions and one intermediate condition for each leg link, four sixth order polynomial functions θ_{1S} , θ_{2S} , θ_{1A} and θ_{2A} are established.

Then with the method described in section 5.6.1 a polynomial function $\theta_3^*(t)$ is derived to approximate the natural trajectory $\theta_3(t)$.

With the approximated function $\theta_3^*(t)$, one can calculate the trajectory of the horizontal position of the COG X_G from the kinematic expression (5.9):

$$X_G = X_H + a(\cos \theta_{1S} + \cos \theta_{1A}) + b(\cos \theta_{2S} + \cos \theta_{2A}) + c \cos \theta_3^* \quad (5.100)$$

with:

$$X_H = l_1 \cos \theta_{1S} + l_2 \cos \theta_{2S} \quad (5.101)$$

which allows one to calculate the integral:

$$\int_0^T X_G^* dt = I \quad (5.102)$$

The values of $\dot{X}_G(0)$ and $\dot{Y}_G(0)$ can be determined with:

$$\begin{aligned} \dot{X}_G = \dot{X}_H - a(\sin \theta_{1S} \dot{\theta}_{1S} + \sin \theta_{1A} \dot{\theta}_{1A}) - b(\sin \theta_{2S} \dot{\theta}_{2S} + \sin \theta_{2A} \dot{\theta}_{2A}) \\ - c \sin \theta_3^* \dot{\theta}_3^* \end{aligned} \quad (5.103)$$

$$\begin{aligned} \dot{Y}_G = \dot{Y}_H + a(\cos \theta_{1S} \dot{\theta}_{1S} + \cos \theta_{1A} \dot{\theta}_{1A}) + b(\cos \theta_{2S} \dot{\theta}_{2S} + \cos \theta_{2A} \dot{\theta}_{2A}) \\ + c \cos \theta_3^* \dot{\theta}_3^* \end{aligned} \quad (5.104)$$

evaluated at $t = 0$. This allows one to verify if:

$$I \approx -\frac{1}{g} (\dot{Y}_G(0) \lambda - \dot{X}_G(0) \delta) \quad (5.105)$$

or in other words, if condition (5.49) is satisfied or not. If not, then the value of $X_H(0)^0$ will be adapted iteratively as follows. Assuming that the COG moves with a horizontal velocity equal to the velocity of the hip, which is assumed to be constant, yields:

$$\dot{X}_G \approx \dot{X}_H = \nu \quad (5.106)$$

The COG propagates then with a constant speed from $X_G(0)$ to $X_G(T)$:

$$X_G = X_G(0) + \nu t \quad (5.107)$$

such that the integral is equal to

$$\int_0^T X_G dt = X_G(0)T + \nu \frac{T^2}{2} \quad (5.108)$$

and since $T = \frac{\lambda}{\nu}$, the integral I can roughly be estimated with:

$$I \approx \frac{\lambda}{\nu} \left(\frac{\lambda}{2} + X_G(0) \right) \quad (5.109)$$

The variation of this expression gives:

$$\Delta X_G(0) = \Delta I \frac{\nu}{\lambda} \quad (5.110)$$

which means that if a variation ΔI of the integral is desired, then the initial position of the COG has to be shifted with $\Delta I \frac{\nu}{\lambda}$.

Assuming that $\Delta X_H(0) \approx \Delta X_G(0)$, one gets the following iteration formula:

$$X_H(0)^{n+1} = X_H(0)^n + \Delta I_n \frac{\nu}{\lambda} \quad \text{for } n \geq 0 \quad (5.111)$$

with

$$\Delta I_n = I_n^{des} - I_n^{real} = -\frac{1}{g} \left(\dot{Y}_G(0) \lambda - \dot{X}_G(0) \delta \right) - \int_0^T X_G^* dt \quad (5.112)$$

Applying this iterative formula allows one to determine the initial configuration, for which (5.49) will be approximately respected. Note that for every iteration step the trajectories for the leg links, as well as the desired trajectory θ_3^* have to be recalculated.

The next step is to calculate the values of $\ddot{X}_G(0)$ and $\ddot{Y}_G(0)$ by differentiating (5.103) and (5.104) and evaluating these expressions at $t = 0$, and to check if (5.57) is satisfied. If not, then the value of $\dot{Y}_G(0)$ will be adapted iteratively as follows. Supposing that values $\dot{X}_G^{real}(0)$ and $\dot{Y}_G^{real}(0)$ are reached, the desired value $\dot{Y}_G^{des}(0)$ is calculated with (5.55):

$$\Delta X_G \left(\dot{Y}_G^{des}(0) + g \right) = \Delta Y_G \ddot{X}_G^{real}(0) \Rightarrow \dot{Y}_G^{des}(0) = \frac{\delta}{\lambda} \ddot{X}_G^{real}(0) - g \quad (5.113)$$

So the desired variation of $\dot{Y}_G^{des}(0)$ is:

$$\Delta \dot{Y}_G^{des} = \dot{Y}_G^{des}(0) - \dot{Y}_G^{real}(0) = \frac{\delta}{\lambda} \ddot{X}_G^{real}(0) - g - \dot{Y}_G^{real}(0) \quad (5.114)$$

then assuming that

$$\Delta \ddot{Y}_H^{des} \approx \Delta \dot{Y}_G^{des} \quad (5.115)$$

leads to the following iteration formula:

$$\ddot{Y}_H(0)^{n+1} = \ddot{Y}_H(0)^n + \Delta \ddot{Y}_{H,n}^{des} \quad \text{for } n \geq 0 \quad (5.116)$$

with $\Delta \ddot{Y}_{H,n}^{des} = \ddot{Y}_{G,n}^{des} - \ddot{Y}_{G,n}^{real}$

The iteration is repeated until (5.57) is approximately respected.

In order to clearly summarize the different steps of the strategy generating the trajectories, a flow chart is given in figure 5.4.

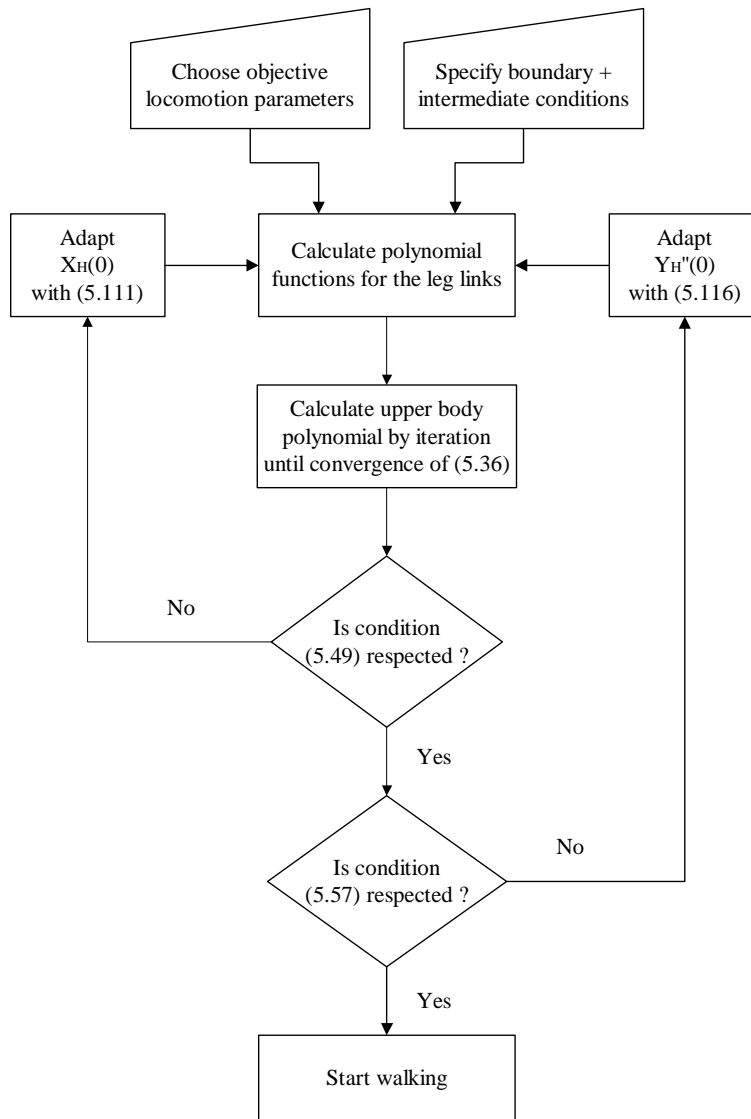


Figure 5.4: Flow chart describing different steps in strategy

Remark: Numerical integration

The trajectory generation strategy makes use of expressions resulting from integrating the angular momentum equation. These expressions contain certain integrals that have to be calculated numerically, namely in (5.36) for the calculation of $\theta_3(0)$ and in (5.102) for determining $X_H(0)$. For the simulations these integrals are calculated with Leo Tick's formula for integration [Hamming, 1989]. This is in fact a recursive digital filter and is defined as:

$$Y_n = Y_{n-2} + \kappa(0.3584U_n + 1.2832U_{n-1} + 0.3584U_{n-2}) \quad \text{for } n \geq 1 \quad (5.117)$$

where the U_n and Y_n respectively correspond to the values of the integrand and the integral at the different sample points. The time duration between two sample points is represented by κ .

5.8 Simulations

To test and evaluate the developed strategy, a variety of simulations was performed. The results of one specific simulation will be reported here. Since all steps are identical and the robot is assumed to be steered by ideal controllers, the graphs only show the results for one step.

The following values for the objective parameters characterize the walking pattern:

$$\nu = 0.7 \frac{m}{s} \approx 2.5 \frac{km}{h}$$

$$\lambda = 0.3m$$

$$\delta = 0$$

$$\sigma = 0.04m$$

With expression (5.60) the duration of one step becomes:

$$T_S = \frac{0.3}{0.7} \approx 0.43s$$

The following hip height in the end points was chosen:

$$Y_H(0) = Y_H(T) = 0.95m$$

with a leg length of $1m$ when it is fully stretched.

A negative value for the vertical hip velocity in the boundary points of the step is chosen:

$$\dot{Y}_H(0) = \dot{Y}_H(T) = -0.15 \frac{m}{s}$$

The upper body angle in the end points of the step is:

$$\theta_3(0) = \theta_3(T) = 87^\circ$$

corresponding to a slight forward inclination.

To get a clear view on how the robot moves, a stick diagram is given in figure 5.5. The successive robot positions are shown at equal time intervals ΔT , where in this case $\Delta T = 0.02s$ was chosen.

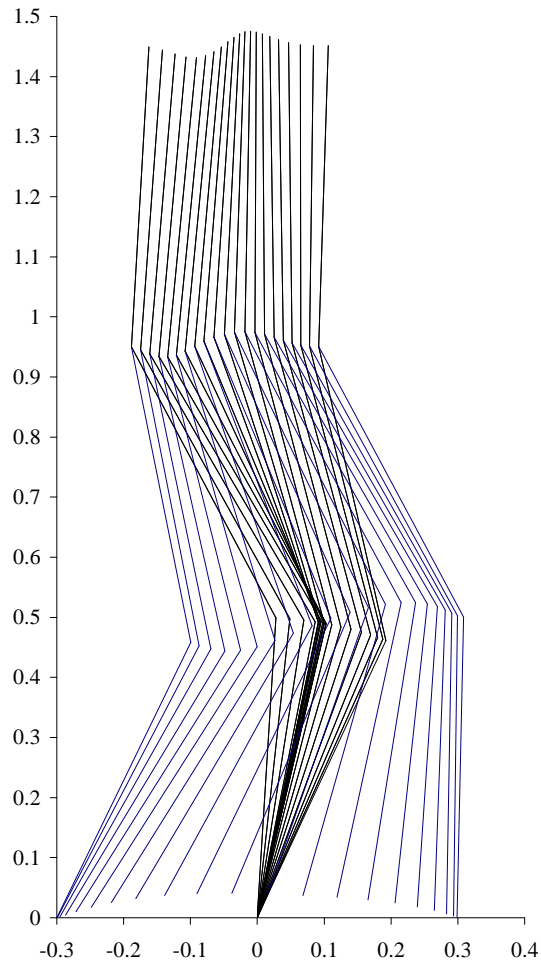


Figure 5.5: Stick diagram small steps

5.8.1 Hip and swing foot motion

The horizontal position of the hip point H is shown in graph 5.6. Due to the

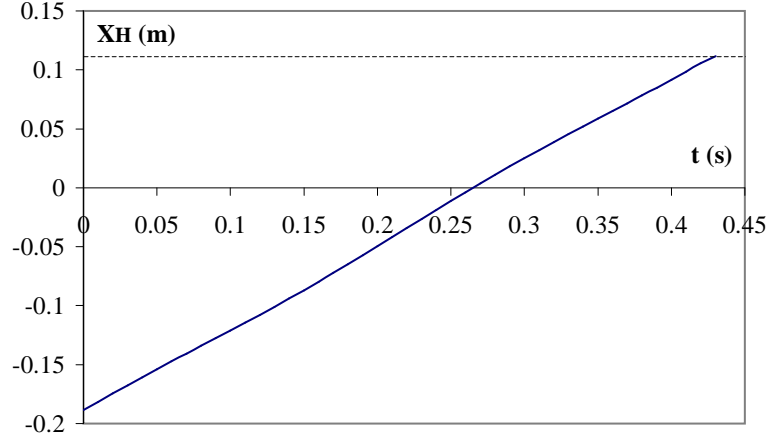


Figure 5.6: Horizontal hip position

choice of the step duration in combination with the boundary conditions for the horizontal hip position, a quasi linear trajectory is found. The iteration formula (5.111) prescribes the following value for the initial hip position (recall that the coordinate system is located in the ankle point of the supporting foot F_S):

$$X_H(0) = -0.19m$$

The end position becomes then:

$$X_H(T) = X_H(0) + \lambda = -0.19 + 0.3m = 0.11m$$

This value of $X_H(0)$ and consequently also the value of $X_H(T)$ result from applying the iterative formula (5.111). A starting value for the iteration formula (5.111) was found as follows. Initially one assumes:

$$\dot{X}_G(0) \approx \dot{X}_H(0)$$

$$\dot{Y}_G(0) \approx \dot{Y}_H(0)$$

allowing one to calculate a first value for the rhs of (5.105):

$$-\frac{1}{g} \left(\dot{Y}_G(0) \lambda - \dot{X}_G(0) \delta \right) \approx -\frac{1}{9.81} (-0.15 * 0.3 - 0.7 * 0) = 4.59 * 10^{-3} sm$$

Then the simplified expression (5.109) for the integral of the horizontal hip position is used by assuming that $X_G(0) \approx X_H(0)$, in order to become the lhs of (5.105):

$$I \approx \frac{\lambda}{\nu} \left(\frac{\lambda}{2} + X_G(0) \right) \approx \frac{0.3}{0.7} \left(\frac{0.3}{2} + X_H(0) \right) = 0.429 \left(0.15 + X_H(0) \right) sm$$

such that combining the last two expressions results in the following initial value for $X_H(0)$:

$$X_H(0)^0 = -0.14m$$

During the iteration steps the integral I_n^{real} is not estimated with (5.109), but numerically calculated with (5.117). The fast convergence of the iterative procedure (5.111) can be seen in table 5.2 where the consecutive values for $X_H(0)^n$ and the integrals I_n^{des} and I_n^{real} are given. Performing more iterations to find an optimal

n	$X_H(0)^n$ (m)	I_n^{real} ($\cdot 10^{-3} sm$)	I_n^{des} ($\cdot 10^{-3} sm$)
0	-0.140	21.2	4.21
1	-0.180	6.94	4.16
2	-0.186	4.77	4.14
3	-0.187	4.41	4.14
4	-0.188	4.05	4.14

Table 5.2: Iteration on initial horizontal hip position

value for $X_H(0)$ has no use, since on a real robot such a fine tuning of the position will not be possible. In this case, three iterations ($n = 2$) would be sufficient to conclude that a good initial value for the horizontal hip position is $X_H(0) = -0.19m$.

The vertical position of the hip during one step is depicted in graph 5.7. The

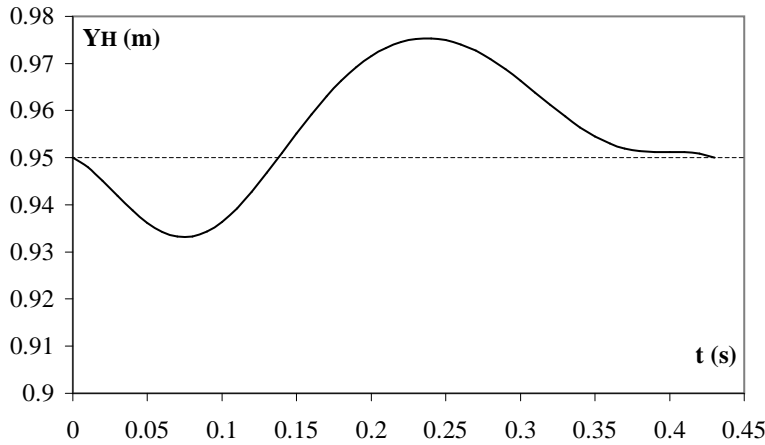


Figure 5.7: Vertical hip position

vertical hip trajectory shows a small downward oscillation at the beginning of the step. This is due to the fact that the vertical hip acceleration has a rather high

negative value, which is needed in order to satisfy condition (5.49). The iteration formula (5.116) procures the following value for the initial vertical hip acceleration:

$$\ddot{Y}_H(0) = -12.5 \frac{m}{s^2} = \ddot{Y}_H(T)$$

Such a negative value generates a negative radius of curvature for the trajectory that causes the hip point to move down at the beginning of the step. The following intermediate condition on the vertical hip acceleration was imposed:

$$\ddot{Y}_H\left(\frac{T}{2}\right) = \frac{\dot{Y}_H(0)}{2} = -6.25 \frac{m}{s^2}$$

which forces the hip point to move up. The corresponding hip position at $\frac{T}{2}$ calculated with (5.96) gives:

$$Y_H\left(\frac{T}{2}\right) = 0.974m$$

as can be seen in figure 5.7.

Note that the vertical hip velocity in the boundary points of the step was chosen a negative value, being $\dot{Y}_H(0) = -0.15 \frac{m}{s}$. This was done in order to avoid a second downwards oscillation of the hip point at the end of the step. The resulting trajectory looks rather similar to trajectories found for a walking motion with a non-instantaneous double support phase (see chapter 6). During the single support phase the hip of a walking robot generally reaches its highest position, whereas it reaches its lowest position during the double support phase. Since now the double support phase is missing, the trajectory of the hip shows the downward motion immediately after the impact, during the single support phase.

The fast convergence of the iterative procedure (5.116) can be seen in table 5.3 where the consecutive values for $\dot{Y}_H(0)^n$ and the values of $\ddot{Y}_{G,n}^{real}$ and $\Delta\dot{Y}_{H,n}^{des}$ are given. Note that the robot walks on a horizontal ground surface such that $\delta = 0$ and consequently from condition (5.57) $\dot{Y}_G^{des} = -g$ is found. The starting value for the iterative procedure is found by simply assuming

$$\dot{Y}_H(0) \approx \dot{Y}_G(0)$$

leading to

$$\ddot{Y}_H(0)^0 = -9.81 \frac{m}{s^2}$$

It would take four iterations to obtain the value $\ddot{Y}_H(0) = -12.5 \frac{m}{s^2}$. However, trying to make a real robot walk with a vertical acceleration for the COG being close to $-g$ in the endpoints of the steps is unrealistic, since this causes the vertical reaction force to be small, possibly causing the robot to slip or to tip over. It was already mentioned before that this kind of walking with instantaneous double

n	$\ddot{Y}_H(0)^n (m/s^2)$	$\ddot{Y}_{G,n}^{real} (m/s^2)$	$\Delta\ddot{Y}_{H,n}^{des} (m/s^2)$
0	-9.81	-7.74	-2.07
1	-11.88	-9.33	-0.480
2	-12.36	-9.70	-0.11
3	-12.47	-9.78	-0.03

Table 5.3: Iteration on initial vertical hip acceleration

support phase and without impact has to be seen as a purely theoretical study and will not be implemented in real.

The motion of the swing foot is represented by graphs 5.8 and 5.9 which show respectively the horizontal and vertical position of the foot F_A . Due to the calculation of the tracking trajectories based on the values of the objective parameters, the behaviour of the swing foot is as expected.

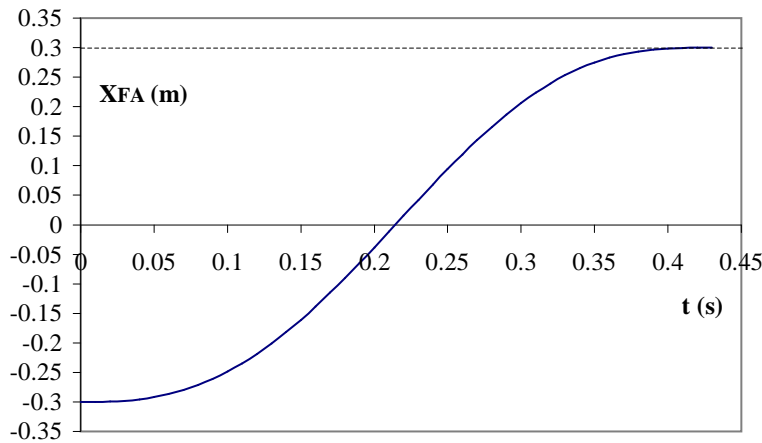


Figure 5.8: Horizontal air foot position

5.8.2 Upper body motion

Figure 5.10 shows the seventh order polynomial trajectory tracked by the ankle actuator, represented by θ_3^{pol} . The solution of the second order differential equation resulting from the angular momentum equation is also drawn, represented by θ_3^{nat} . It can be seen that the polynomial function mimics the natural trajectory quite well, which confirms the effectiveness of the applied strategy concerning upper body motion control. It was the scope of the trajectory generation strategy to define the motion of the leg links in such a way, that the natural upper body angle trajectory approximates the desired behaviour. Expressing the desired behaviour

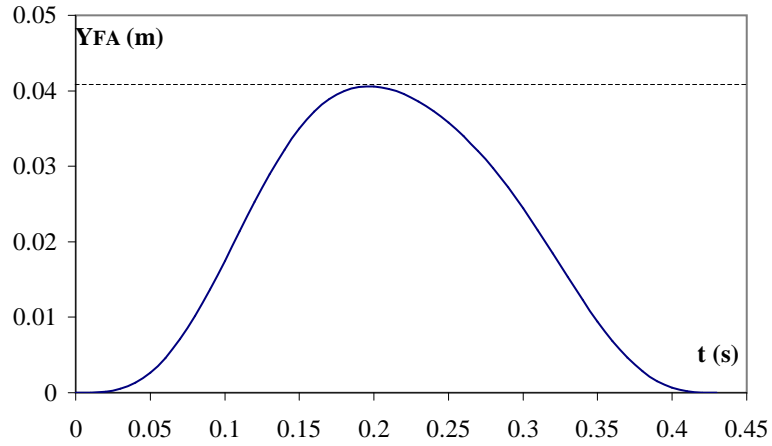


Figure 5.9: Vertical air foot position

by a polynomial function leads to the result that both functions are almost identical, meaning that the action of the ankle actuator is limited to covering the minor differences between the two trajectories. Furthermore one can remark that the overall upper body oscillation is small. The difference between the minimum and maximum value of the angle is approximately 0.1 rad, corresponding to 6° . The

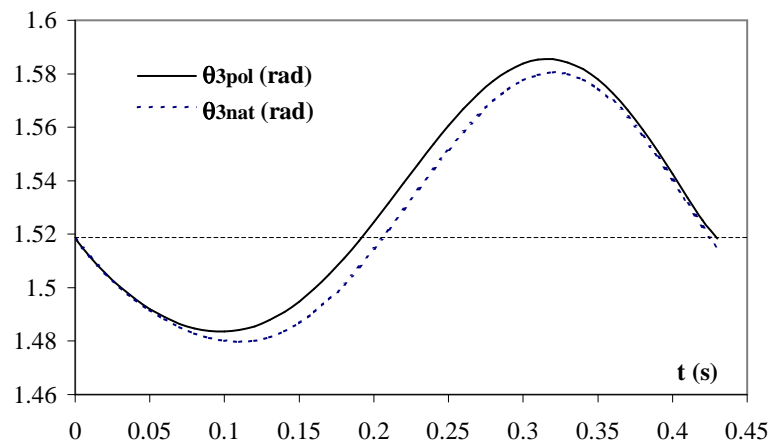


Figure 5.10: Upper body angle: polynomial and natural trajectory

upper body angle in the boundary points was chosen slightly inclined in the forward direction. If the upper body was chosen upright in the end points, then it would incline backwards during a long part of the step. This leads to a destabilizing moment caused by gravity with respect to the hip point. Combined with the

effect of the hip moving forwards, the overall rotation would become larger. Now, choosing a forward inclination reduces the overall rotation due to the compensating effect of the forward motion of the hip and the moment on the upper body with respect to the hip, caused by gravity.

The upper body angular velocity is depicted in figure 5.11. Again the polynomial trajectory $\dot{\theta}_3^{pol}$ is compared with the natural trajectory $\dot{\theta}_3^{nat}$. Both trajectories are almost identical, again confirming the effectiveness of the technique.

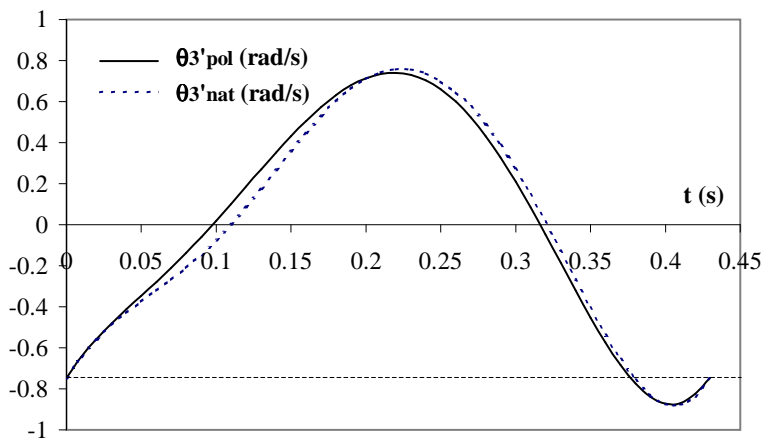


Figure 5.11: Upper body angular velocity: polynomial and natural trajectory

Figure 5.12 compares the polynomial angular acceleration trajectory $\ddot{\theta}_3^{pol}$ with the natural trajectory $\ddot{\theta}_3^{nat}$. The same conclusions can be drawn as for the position and the velocity.

5.8.3 Zero moment point and vertical ground reaction force

The position of the Zero Moment Point with respect to the ankle point is shown in figure 5.13. The largest deviation from the ankle point is found at $t = \frac{T}{2}$, with an amplitude of approximately 5 cm. On graph 5.14, representing the amplitude of the vertical reaction force, one can notice that this is caused by the low amplitude of the reaction force at that time. Taking into account that Lucy has feet of approximately 30 cm, with 20 cm in front and 10 cm behind the ankle joint, it is clear that the ZMP stays well within the stability region. One could consider a better approximation of the natural trajectory than the seventh order polynomial used here, such that the differences on the acceleration level become smaller. As was mentioned in section 5.6.1, this can be e.g. done by using spline interpolations for the upper body angle trajectory. Such an interpolation method significantly increases the number of computations, and was therefore not considered here.

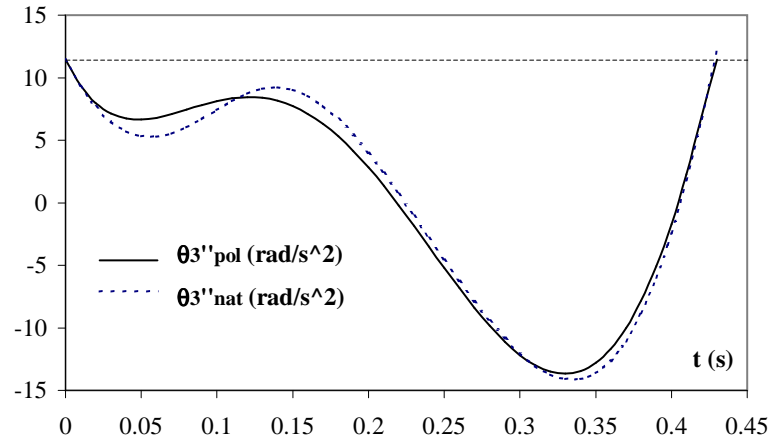


Figure 5.12: Upper body angular acceleration: polynomial and natural trajectory

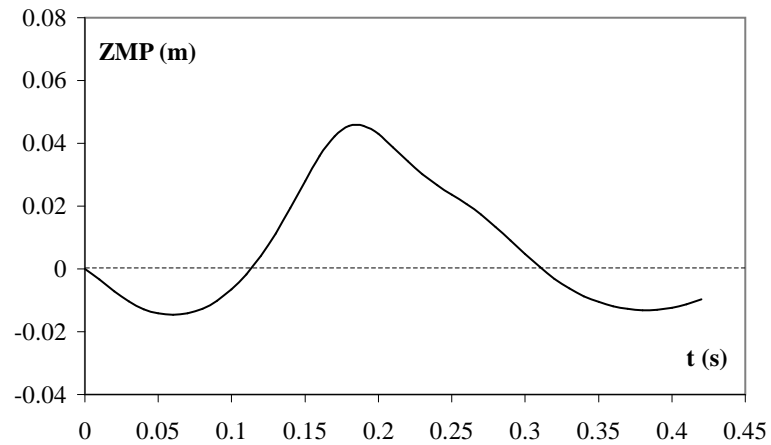


Figure 5.13: Zero moment point position

5.8.4 Torques applied by the different actuators

Figure 5.15 depicts the ankle torque on the supporting foot during the single support phase. The maximum amplitude of this torque is approximately $8Nm$, while position as well as velocity and acceleration of the upper body are controlled. The trajectory shows some minor oscillations, which are only due to the fact that the natural trajectory and the polynomial tracking function are not identical. On graph 5.12 two points of intersection between the two trajectories can be distinguished between the end points, leading to the fact that the ankle torque passes through zero at those time steps. Recall that the ankle torque is mainly determined by the differences between the natural and polynomial angular acceleration of the upper

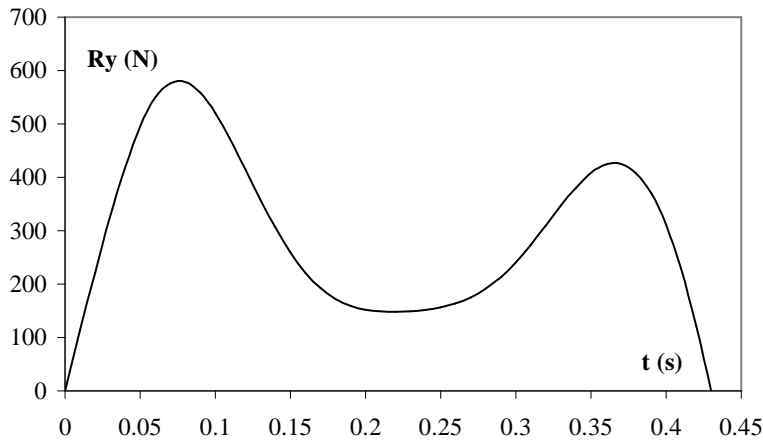


Figure 5.14: Vertical reaction force on supporting foot

body. The errors on the position and the velocity level also influence the torque, but these are considerably smaller as can be seen on graphs 5.10, 5.11 and 5.12 (note the different scales used on the axes).

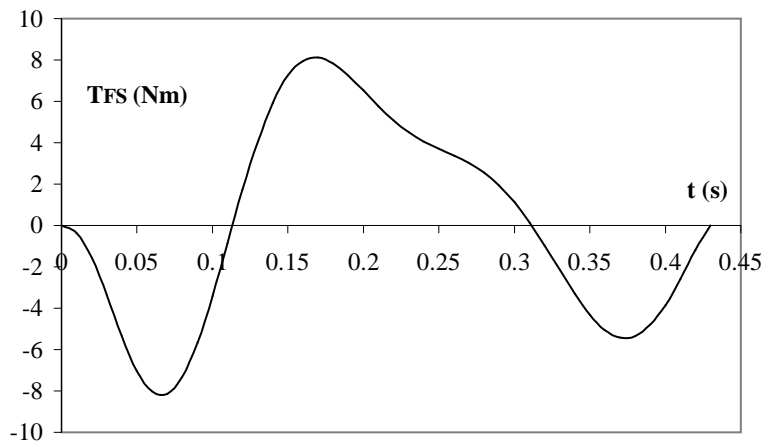


Figure 5.15: Ankle torque on supporting foot

The torques of the actuators used to steer the leg links during a step are respectively shown in figure 5.16 for the supporting leg, and in figure 5.17 for the swing leg. It is clearly visible that the values for the torques increase with the length of the kinematic chain to be carried by a specific actuator. Indeed the knee torque of the supporting leg is carrying the largest part of the load, leading to peak values of approximately 70 Nm. It should however be remarked that no passive elements are

included in the model, whereas Lucy is equipped with actuators having a significant passive behaviour. It is steered with pneumatic actuators who benefit from a stiffness being adaptable during the motion [Verrelst et al., 2002].

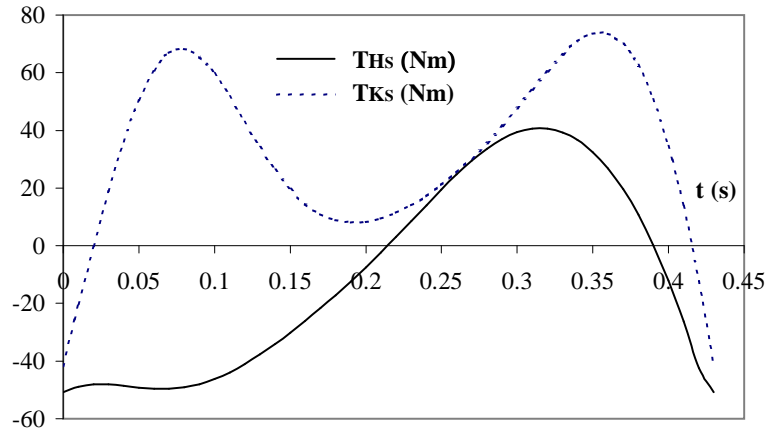


Figure 5.16: Knee and hip torques on supporting leg

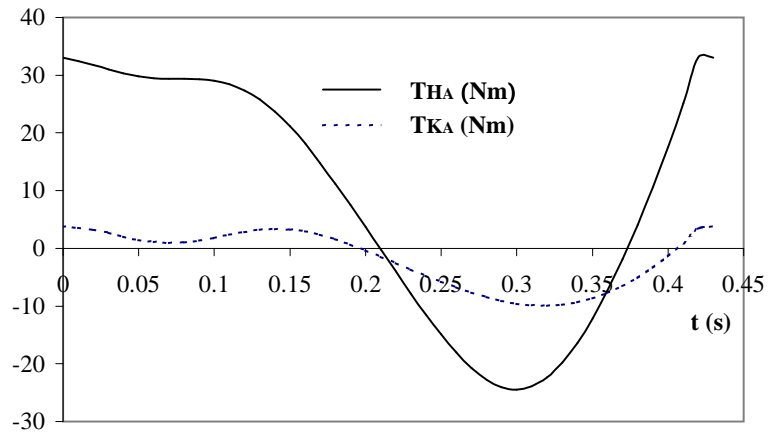


Figure 5.17: Knee and hip torques on swing leg

In figure 5.18, a stick diagram is shown for another simulation where Lucy takes longer steps and moves with a higher horizontal velocity. The following values for the objective parameters characterize the walking pattern:

$$\nu = 0.9 \frac{m}{s} \approx 3.2 \frac{km}{h}$$

$$\lambda = 0.4m$$

$$\delta = 0$$

$$\sigma = 0.04m$$

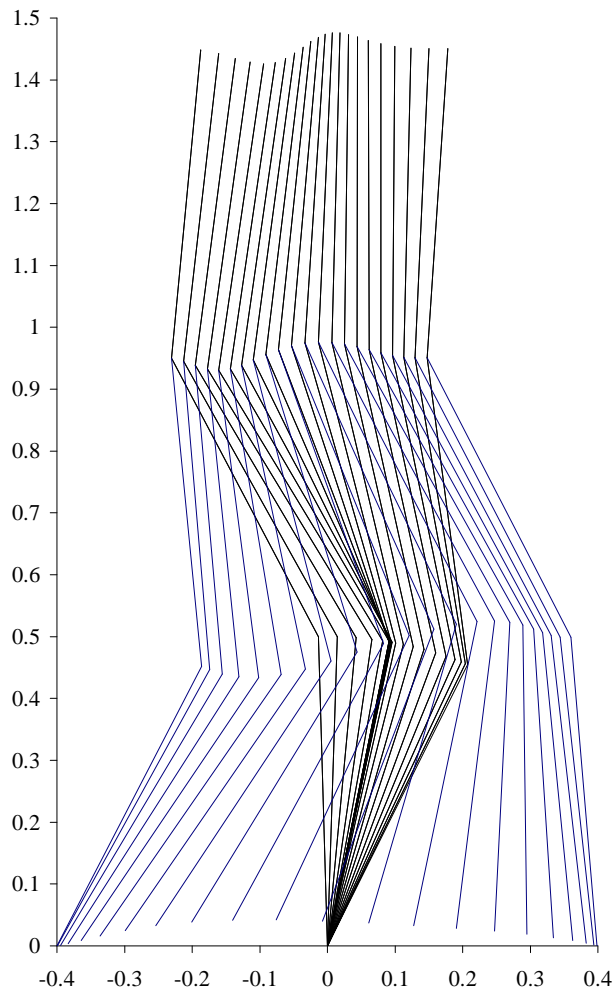


Figure 5.18: Stick diagram larger steps

5.9 Summary

A method for generating the joint trajectories for a walking biped has been developed. The robot considered has two feet that are assumed to have an ignorable mass and inertia. Each foot has an ankle actuator located at the ankle joint. Further, four other actuators are located at the hip and knee joint of each leg.

For simplification purposes, the walking motion is considered to be a steady walking pattern, consisting of successive single support phases separated by an instantaneous double support phase. These double support phases are used for the exchange of support between the two feet. Moreover, the impact phase generally accompanying the support exchange is avoided by choosing a zero touch-down velocity of the foot. A more general trajectory generation strategy for walking patterns with an impact and a non-instantaneous double support phase is developed in chapter 6.

The strategy described in this chapter fulfills two distinct requirements. Trajectories for all the links of the robot are established in such a way that all the desired values for the objective locomotion parameters are attained. These objective parameters are the horizontal hip velocity, the step length, the step height and the foot lift. The other task of the strategy is to generate trajectories for the leg links which cause the natural upper body motion to approximate a desired upper body motion. This is achieved by satisfying three specific conditions which have been established, starting from the angular momentum equation. One condition acts on the initial angular velocity of the upper body, whereas the two other conditions act on the hip motion. The strategy generates the leg link trajectories by using an iterative procedure in order to satisfy these three conditions. When the resulting natural trajectory for the upper body angle satisfies all desired boundary conditions, then it can be approximated by a polynomial function based on these boundary conditions. Using this polynomial function as a tracking function for the ankle actuator of the supporting foot, only small ankle torques are required, caused by the minor differences between the natural and the polynomial trajectory. The simulation results show the effectiveness of the technique. It is verified that all the objective parameters reach their desired values. The upper body motion is controlled on the position, the velocity and the acceleration level, with minimal ankle actuator action. The resulting upper body oscillations are limited to small back and forth motions, as can be seen on the stick diagrams.

The two iteration loops used by the strategy consist of a limited number of floating point operations. A variety of simulations showed that these iteration loops converge quickly. The calculation of all reference trajectories for one step was performed on an AMD Athlon 1.2 GHz processor, which took approximately 20 μs , proving that this strategy can be used for real-time application.

Chapter 6

A walking biped with impact and double support phase

6.1 Introduction

In chapter 5, the biped's walking motion was composed of consecutive single support phases separated by instantaneous double support phases, while impact was avoided by putting the swing foot down on the ground with a zero velocity. Basically walking with an instantaneous double support phase implies that the weight of the robot has to be shifted from the rear foot to the front foot in an infinitesimally short time interval, or in other words, the ZMP has to transfer infinitely fast from the rear ankle to the front ankle. Such a motion can therefore be considered as a limit case between running and walking, since it is in fact a running motion with a zero flight time. When referring to human locomotion, the walking motion is composed of two distinct phases, separated by a collision or impact. The first phase is called the *swing phase* which starts with a lift-off and ends with a foot impact. In human walking, this phase represents the major part of the duration of a walking cycle, being about 80 – 90% [Hardt et al., 1999]. The second phase is called the *double support phase*. During this phase both feet are in contact with the ground, which imposes geometrical holonomic constraints on the joint coordinates [Shih and Gruver, 1992; Mitobe et al., 1997]. The constrained system is modelled by mixed algebraic and differential equations [Hemami and Wyman, 1979]. As stated by Mitobe et al. [1997], the amount of time spent in the double support phase decreases with an increasing walking speed. At high walking speeds, it can even be ignored and considered as instantaneous. However, the double support phase is not only important for improving the smoothness of the biped locomotion system, but also to enable the robot to start and stop its motion [Shih and Gruver, 1992]. Indeed, starting and stopping of the motion logically occurs in a double support configuration, meaning that this phase has to be taken into consideration when steering a walking robot.

Regarding literature, it can be noticed that most of the work involving biped locomotion control has concentrated on the single support phase, which is probably due to the fact that this is the predominant part of the walking cycle. As correctly remarked by Shih and Gruver [1992], such systems can only start its motion from a preset position. Moreover, many of the authors which did focus on the double support phase, aimed at designing a controller in order to be able to follow a certain arbitrarily chosen motion, instead of focussing on the motion itself. In the late seventies, Hemami and Wyman [1979] derived an approach simultaneously applicable to the constrained system and the unconstrained system. They derived Lagrange multipliers as functions of the state and the input of the system. In their formulation, the dimension of the state of the constrained system is the same as that for the unconstrained dynamic system, but the motion of the system is limited to submanifolds of the state space. They simulated the motion of a simple biped model in the frontal plane. In [Narikiyo and Ito, 1985], the Lagrange's multipliers were eliminated from the constrained equations, in order to obtain reduced order equations. A control algorithm for the motion was designed in reduced space. Their method was applied to a biped performing a slow propagation from a given initial to a specific end position. An interesting approach was used by Sano and Furusho [1990], who reduced the dynamic model of their robot to that of an inverted pendulum. They used the angular momentum of the robot around the ankle of the supporting foot as a control input during the single support phase. During the double support phase they used the ankle actuators of both feet in order to attain a desired value of the angular momentum at the beginning of the next single support phase. Instead of choosing an arbitrary motion, they defined a reference function for the angular momentum, which is a technique that is also applied in this work. Shih and Gruver [1992] also studied the control of a biped in the double support phase. They partitioned the joint variables into independent and dependent variables that are related through a Jacobian matrix. A reduced dynamic model was formulated which only involves the selected independent variables. A control strategy based on feed-forward compensation and linear state feedback was introduced to track predefined trajectories and to stabilize perturbations of the joint variables. The technique involved however severe simplifications, and was therefore applicable to slow swaying motions only. Another contribution to the control problem during double support is made by Mitobe et al. [1997]. The control problem was defined as a pure trajectory planning problem, where the position and the velocity of the center of gravity of the trunk were controlled with respect to a frame fixed to the ground. Unfortunately the rotation of the trunk was neglected, or in other words, its orientation was assumed to be fixed. Later, several groups started taking the double support phase into account, aiming at the design of energy optimized trajectories, such as in [Hardt et al., 1999] and [Nikkhah et al., 2003]. Their goal is to obtain minimum energy trajectories during the double support phase, by using numerical optimization techniques. Clearly these methods are off-line techniques and are not suitable for real-time application. Recently, Ito et al. [2003], presented a control method for the center of pressure of ground reaction forces, based on its

feedback optimization. They applied this method to the weight shift in the double support phase of a biped system.

To properly model a real walking motion, the double support phase will be introduced in the walking pattern. At the same time, the impact phase will be considered, such that a discontinuity in the joint velocities will occur when transferring from the single support to the double support phase. A technique will be developed which allows the robot to transfer its weight from the rear foot to the front foot in a finite time interval, while controlling the upper body. The motion will be defined in such a way that the ZMP point does not leave the stability region, in order to avoid postural instability.

In section 6.2 the geometrical constraints corresponding to the closed kinematic chain are introduced in the kinematics of the biped. The impact phase, occurring after each single support phase, is assumed to be an inelastic impulsive impact on a closed chain, and is described in section 6.3. The natural upper body motion during the double support phase is examined in section 6.4. Instead of numerically integrating the angular momentum equation, this natural upper body motion will be approximated by an analytical solution. This approximated natural trajectory will be added with a well defined correction function, in order to steer the upper body to a desired value for the angle, the angular velocity and the angular acceleration, at the end of the double support phase. In section 6.5 it will be described how the natural upper body behaviour during a single support phase can be tuned such that a continuity of the upper body motion is achieved between the consecutive single support and double support phases. During both the single support phases and the double support phases, the upper body will be steered by tracking a reference trajectory that approximates a natural trajectory for that phase. As a result, only low torque values are required to actuate the upper body. In section 6.6 the stability region for the ZMP during a double support phase is determined, and it is explained how the reference trajectories for the leg links have to be defined such that postural stability is inherently guaranteed. The mathematical framework of the overall trajectory generation strategy is given in section 6.7. The effectiveness of the strategy is tested and verified by simulations of walking patterns, of which the results are reported in section 6.8. Finally, some concluding remarks are given in section 6.9.

6.2 Kinematical aspects during the double support phase

In figure 6.1 the biped is depicted during the double support phase. The R stands for Rear foot, whereas the F stands for Front foot.

Since both feet are in contact with the ground, a closed kinematic chain is formed by the two legs and the ground. It is desired that both feet stay in contact with

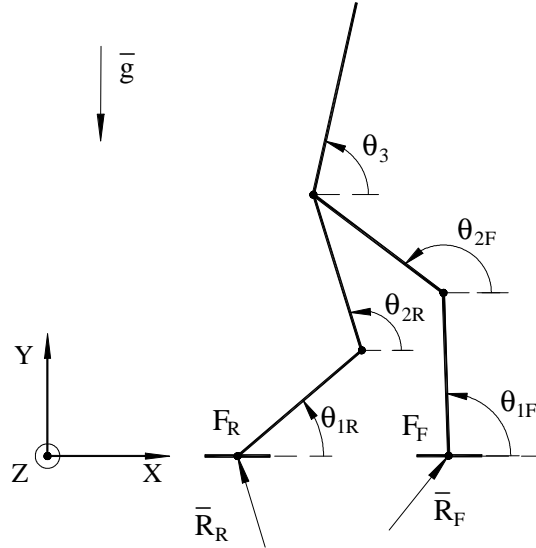


Figure 6.1: Biped during double support phase

the ground and that the feet do not slip during a double support phase. Due to these constraints, the robot's number of DOF is reduced to three. Indeed, during a single support phase the robot has five DOF, and during the double support phase two holonomic constraints are imposed, being:

$$\begin{cases} X_{F_R} + l_1 \cos \theta_{1R} + l_2 \cos \theta_{2R} &= X_{F_F} + l_1 \cos \theta_{1F} + l_2 \cos \theta_{2F} \\ Y_{F_R} + l_1 \sin \theta_{1R} + l_2 \sin \theta_{2R} &= Y_{F_F} + l_1 \sin \theta_{1F} + l_2 \sin \theta_{2F} \end{cases} \quad (6.1)$$

or since

$$X_{F_F} - X_{F_R} = \lambda \quad (\text{step length}) \quad (6.2)$$

$$Y_{F_F} - Y_{F_R} = \delta \quad (\text{step height}) \quad (6.3)$$

$$\Rightarrow \begin{cases} l_1 \cos \theta_{1R} + l_2 \cos \theta_{2R} - \lambda &= l_1 \cos \theta_{1F} + l_2 \cos \theta_{2F} \\ l_1 \sin \theta_{1R} + l_2 \sin \theta_{2R} - \delta &= l_1 \sin \theta_{1F} + l_2 \sin \theta_{2F} \end{cases} \quad (6.4)$$

Note that θ_3 does not appear in the holonomic constraints since the upper body is not a part of the closed kinematic chain. The coordinate θ_3 is a completely independent DOF. In the holonomic constraints, four coordinates appear, of which only two are independent. Assume that the angles on the rear leg are considered as the independent coordinates, and the angles on the front leg as the dependent ones. Trajectories will be established for the angles on the rear leg by the trajectory generation strategy. Then, the values of the dependent coordinates, as well as

their first and second derivatives, have to be determined at all times during the double support phase. The independent coordinates can be steered by developing trajectories once at the beginning of the double support phase, but the dependent ones have to be recalculated continuously.

6.2.1 The values of the dependent coordinates

If trajectories are defined for θ_{1R} and θ_{2R} , then the corresponding values of θ_{1F} and θ_{2F} at each time step can be found by solving the following set:

$$\begin{cases} l_1 \cos \theta_{1F} + l_2 \cos \theta_{2F} = A \\ l_1 \sin \theta_{1F} + l_2 \sin \theta_{2F} = B \end{cases} \quad (6.5)$$

with

$$A = l_1 \cos \theta_{1R} + l_2 \cos \theta_{2R} - \lambda \quad (6.6)$$

$$B = l_1 \sin \theta_{1R} + l_2 \sin \theta_{2R} - \delta \quad (6.7)$$

The set (6.5) can be transformed into a set of two decoupled quadratic equations, of which the solution is straightforward. The solution method was already described in section 5.7.2 of the previous chapter.

6.2.2 The first derivatives of the dependent coordinates

As suggested by Shih and Gruver [1992], the 4 leg link coordinates can be divided into a group of independent and dependent coordinates as follows:

$$Z = \begin{pmatrix} Z_R \\ Z_F \end{pmatrix} \quad (6.8)$$

with

$$Z_R = \begin{pmatrix} \theta_{1R} \\ \theta_{2R} \end{pmatrix} \quad \text{and} \quad Z_F = \begin{pmatrix} \theta_{1F} \\ \theta_{2F} \end{pmatrix} \quad (6.9)$$

where e.g. Z_R are the independent and Z_F the dependent coordinates.

The constraints (6.4) can then be rewritten as:

$$C(Z) = C_R(Z_R) + C_F(Z_F) = 0 \quad (6.10)$$

with

$$C_R(Z_R) = \begin{pmatrix} l_1 \cos \theta_{1R} + l_2 \cos \theta_{2R} - \lambda \\ l_1 \sin \theta_{1R} + l_2 \sin \theta_{2R} - \delta \end{pmatrix}$$

and

$$C_F(Z_F) = \begin{pmatrix} -l_1 \cos \theta_{1F} - l_2 \cos \theta_{2F} \\ -l_1 \sin \theta_{1F} - l_2 \sin \theta_{2F} \end{pmatrix}$$

The Jacobian matrix also consists of two different parts J_R and J_F :

$$J(Z) = \frac{\partial C}{\partial Z} = (J_R, J_F) \quad (6.11)$$

with

$$J_R = \frac{\partial C_R}{\partial Z_R} = \begin{pmatrix} -l_1 \sin \theta_{1R} & -l_2 \sin \theta_{2R} \\ l_1 \cos \theta_{1R} & l_2 \cos \theta_{2R} \end{pmatrix}$$

and

$$J_F = \frac{\partial C_F}{\partial Z_F} = \begin{pmatrix} l_1 \sin \theta_{1F} & l_2 \sin \theta_{2F} \\ -l_1 \cos \theta_{1F} & -l_2 \cos \theta_{2F} \end{pmatrix}$$

Differentiating the constraint equation gives

$$\dot{C}(Z) = 0 \quad \Leftrightarrow \quad J_R(Z_R)\dot{Z}_R + J_F(Z_F)\dot{Z}_F = 0 \quad (6.12)$$

The first derivatives of the dependent coordinates are then obtained with:

$$\dot{Z}_F = \frac{\partial Z_F}{\partial Z_R} \dot{Z}_R = -J_F^{-1} J_R \dot{Z}_R \quad (6.13)$$

The Jacobian J_F is invertible when $\det J_F \neq 0$, or:

$$\det J_F = l_1 l_2 \sin(\theta_{2F} - \theta_{1F}) \neq 0 \quad (6.14)$$

meaning that a fully stretched front leg corresponds to a singular configuration. This singularity near full leg extension is a well known issue for biped robots with articulated legs. In practice this situation is generally avoided by walking with sufficiently bent knees, in order not to complicate the controller design [Kajita et al., 2001]. This option will also be chosen here.

6.2.3 The second derivatives of the dependent coordinates

Differentiating twice the constraint equation gives

$$\ddot{C}(Z) = 0 \quad \Leftrightarrow \quad \dot{J}_R(Z_R)\dot{Z}_R + J_R(Z_R)\ddot{Z}_R + \dot{J}_F(Z_F)\dot{Z}_F + J_F(Z_F)\ddot{Z}_F = 0 \quad (6.15)$$

The second derivatives of the dependent coordinates are then computed with:

$$\ddot{Z}_F = J_F^{-1} \left[-J_R \ddot{Z}_R + \left(\dot{J}_F J_F^{-1} J_R - \dot{J}_R \right) \dot{Z}_R \right] \quad (6.16)$$

where

$$\dot{J}_R = \frac{\partial J_R}{\partial Z_R} \dot{Z}_R$$

$$\dot{J}_F = \frac{\partial J_F}{\partial Z_F} \dot{Z}_F$$

6.3 Impact of the swing leg on the ground

At the end of each single support phase the foot of the front leg hits the ground. The impact is assumed to be inelastic and without slip, meaning that the foot is assumed fixed to the ground immediately after the contact instance. The percussion on the front foot will cause repercussions in each joint of the robot, as well as between the rear foot and the ground. The rear foot is assumed to remain fixed to the ground as well.

The calculation of the percussions for the inelastic impulsive impact as well as the jump of the angular velocities of the links for an open kinematic chain was described by Zheng and Hemami [1985], and will be applied here to a closed kinematic chain.

Consider the equations of motion for the biped with five DOF in a single support phase:

$$D[q]\ddot{q} + C[q, \dot{q}]\dot{q} + G[q] = T \quad (6.17)$$

with $q = (\theta_{1R}, \theta_{2R}, \theta_3, \theta_{2F}, \theta_{1F})^T = (\theta_1, \theta_2, \theta_3, \theta_4, \theta_5)^T$, and $D[q]$ the inertia matrix, $C[q, \dot{q}]$ the centrifugal matrix, $G[q]$ the gravitational torque vector and T the external torque vector containing the actuator torques (see appendix D for the dynamic model).

Immediately after the impact of the swing leg, two geometrical constraints are enforced on the motion of the system. The equations of motion are then written as [Zheng and Hemami, 1985]:

$$D[q]\ddot{q} + C[q, \dot{q}]\dot{q} + G[q] = T + J^T \Lambda \quad (6.18)$$

where J is the Jacobian matrix and Λ is a column vector of Lagrange multipliers representing the generalized constraint forces. Assuming that the coordinate system is located at the rear ankle point, the following two constraints are imposed:

$$\begin{cases} S_1 &= l_1 \cos \theta_{1R} + l_2 \cos \theta_{2R} - l_1 \cos \theta_{1F} - l_2 \cos \theta_{2F} - \lambda = 0 \\ S_2 &= l_1 \sin \theta_{1R} + l_2 \sin \theta_{2R} - l_1 \sin \theta_{1F} - l_2 \sin \theta_{2F} - \delta = 0 \end{cases} \quad (6.19)$$

The elements of the Jacobian matrix are calculated with $J_{ij} = \frac{\partial S_i}{\partial q_j}$, such that

$$J = \begin{pmatrix} -l_1 \sin \theta_{1R} & -l_2 \sin \theta_{2R} & 0 & l_1 \sin \theta_{1F} & l_2 \sin \theta_{2F} \\ l_1 \cos \theta_{1R} & l_2 \cos \theta_{2R} & 0 & -l_1 \cos \theta_{1F} & -l_2 \cos \theta_{2F} \end{pmatrix} \quad (6.20)$$

The column vector of Lagrange multipliers has two elements since there are two extra constraints imposed:

$$\Lambda = \begin{pmatrix} \Lambda_1 \\ \Lambda_2 \end{pmatrix} \quad (6.21)$$

If q_F is now defined as

$$q_F = \begin{pmatrix} X_{F_F} \\ Y_{F_F} \end{pmatrix} \quad (6.22)$$

then one can write

$$\dot{q}_F = J\dot{q} \quad (6.23)$$

Since during the impact the configuration of the robot is assumed to remain unchanged, the variation of this condition becomes:

$$\Delta\dot{q}_F = J\Delta\dot{q} \quad (6.24)$$

Since an inelastic impact is considered for the front foot F_F , the velocity of the foot is assumed zero after the shock:

$$\Delta\dot{X}_{F_F} = \dot{X}_{F_F}^+ - \dot{X}_{F_F}^- = -\dot{X}_{F_F}^- \quad (6.25)$$

$$\Delta\dot{Y}_{F_F} = \dot{Y}_{F_F}^+ - \dot{Y}_{F_F}^- = -\dot{Y}_{F_F}^- \quad (6.26)$$

This leads to:

$$\Delta\dot{q}_F = \begin{pmatrix} -\dot{X}_{F_F}^- \\ -\dot{Y}_{F_F}^- \end{pmatrix} \quad (6.27)$$

In (6.24) the Jacobian is a non-square matrix, such that it can not be inverted. Zheng and Hemami [1985] derived however the following expression for the calculation of the velocity jumps during impact:

$$\Delta\dot{q} = D^{-1}J^T(JD^{-1}J^T)^{-1}\Delta\dot{q}_F \quad (6.28)$$

The percussions acting on the front foot can be calculated with [Zheng and Hemami, 1985]:

$$\Pi = \int_{t^-}^{t^+} \Lambda dt = (JD^{-1}J^T)^{-1}\Delta\dot{q}_F \quad (6.29)$$

and

$$\Pi = \begin{pmatrix} \Pi_{F_F}^x \\ \Pi_{F_F}^y \end{pmatrix} \quad (6.30)$$

Note that the repercussions on the rear foot are obtained by writing the linear momentum theorem during the infinitesimal short impact phase:

$$\Pi_{F_R}^x = M(\dot{X}_G^+ - \dot{X}_G^-) - \Pi_{F_F}^x \quad (6.31)$$

$$\Pi_{F_R}^y = M(\dot{Y}_G^+ - \dot{Y}_G^-) - \Pi_{F_F}^y \quad (6.32)$$

6.4 Upper body behaviour during the double support phase

The first scope of this section is to determine how an unactuated upper body will move during a double support phase, in case certain reference trajectories

are imposed to the leg links. This motion will be called the *natural* motion, a concept that was already introduced in the preceding chapters. When considering the free body diagram for the upper body, a second order non-linear differential equation for the body angle can be established by applying the angular momentum theorem. In order to avoid a numerical integration of the differential equation, the latter will be simplified such that an approximated natural motion is found. It will be shown that the error between the estimated natural motion and the solution of the differential equation can be limited by tuning the motion of the hip point. Eventually the estimated natural motion will form the basis for the construction of an actual tracking trajectory for an upper body actuator. The trajectory will try to mimic the shape of the natural motion, while a correction will be introduced to guarantee that the boundary values at the end point of the double support phase are equal to the desired ones for starting the next single support phase.

6.4.1 Approximating the natural upper body motion

In order to derive the natural motion of the upper body during the double support phase, it is assumed that no actuator torque is acting on it. In that case, the upper body behaves as an inverted pendulum with a moving supporting point, being the hip point H.

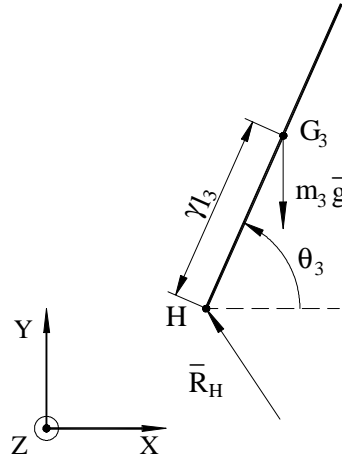


Figure 6.2: Free body diagram of the upper body

Considering the free body diagram of the upper body in figure 6.2, and applying the angular momentum theorem with respect to the hip point H, yields:

$$\dot{\bar{\mu}}_H = \overline{HG}_3 \times m_3 \bar{g} + m_3 (\bar{v}_{G_3} \times \bar{v}_H) \quad (6.33)$$

Writing the angular momentum theorem with respect to H has the advantage

that the unknown internal reaction force \bar{R}_H does not appear in the expression. Moreover, since only the upper body is considered instead of the whole robot, the ground reaction forces do not appear. If the angular momentum equation would have been written with respect to an ankle joint, analogously to what was done during the single support phase, then the unknown reaction force acting on the other foot would turn up in the equation, which unnecessarily complicates this equation.

Applying the transport equation for the angular momentum between H and G_3 , gives:

$$\bar{\mu}_H = \bar{\mu}_{G_3} + \overline{HG_3} \times m_3 \bar{v}_{G_3} \quad (6.34)$$

And when differentiating with respect to time:

$$\dot{\bar{\mu}}_H = \dot{\bar{\mu}}_{G_3} + \overline{HG_3} \times m_3 \bar{v}_{G_3} + \overline{HG_3} \times m_3 \bar{a}_{G_3} \quad (6.35)$$

Then further since

$$\dot{\overline{HG_3}} = \bar{v}_{G_3} - \bar{v}_H \quad (6.36)$$

and

$$\bar{\mu}_{G_3} = I_3 \dot{\theta}_3 \bar{1}_z \quad (6.37)$$

finally equation (6.33) can be rewritten as:

$$I_3 \ddot{\theta}_3 \bar{1}_z + \overline{HG_3} \times m_3 (\bar{a}_{G_3} - \bar{g}) = 0 \quad (6.38)$$

This equation can be used to compute the natural behaviour of the upper body during the double support phase. When taking into account the following kinematic expressions (see figure 6.2):

$$\overline{HG_3} = \gamma l_3 (\cos \theta_3, \sin \theta_3)$$

$$\dot{\overline{HG_3}} = \gamma l_3 \dot{\theta}_3 (-\sin \theta_3, \cos \theta_3)$$

$$\ddot{\overline{HG_3}} = \gamma l_3 \ddot{\theta}_3 (-\sin \theta_3, \cos \theta_3) - \gamma l_3 \dot{\theta}_3^2 (\cos \theta_3, \sin \theta_3)$$

$$\bar{a}_{G_3} = \bar{a}_H + \ddot{\overline{HG_3}}$$

$$\bar{a}_H = (\ddot{X}_H, \ddot{Y}_H)$$

the following second order non-linear differential equation is found for the upper body angle θ_3 :

$$\ddot{\theta}_3 = C \left[\ddot{X}_H \sin \theta_3 - (\ddot{Y}_H + g) \cos \theta_3 \right] \quad (6.39)$$

with

$$C = \frac{m_3 \gamma l_3}{I_3 + \gamma^2 l_3^2 m_3} \quad (6.40)$$

One can prescribe X_H and Y_H by e.g. polynomial functions and solve this equation numerically for θ_3 . Often such a problem is approached by linearizing the equation under the assumption that the rotation of the pendulum is small [Shih, 1997b]. Here this assumption leads to:

$$\begin{aligned}\sin \theta_3 &\approx 1 \\ \cos \theta_3 &\approx \frac{\pi}{2} - \theta_3\end{aligned}$$

Such that the differential equation becomes:

$$\ddot{\theta}_3 = C \left[\ddot{X}_H - \left(\ddot{Y}_H + g \right) \left(\frac{\pi}{2} - \theta_3 \right) \right] \quad (6.41)$$

With $X_H(t)$ and $Y_H(t)$ given functions of time, and with initial conditions $\dot{\theta}_3(0)$ and $\theta_3(0)$, this equation can be numerically integrated to obtain the upper body motion during the double support phase. The approximation will be reasonably good as long as the rotation of the upper body is small. However, the goal here is not to determine a natural motion exactly, but to develop a trajectory for the upper body angle which corresponds to a motion close to a natural motion.

A first, rough approximation of the upper body motion

In order to obtain a rough estimate of the rotation of the upper body during the double support phase, the second part of the rhs of (6.41) is neglected by assuming that $\theta_3 \approx \frac{\pi}{2}$. This leads to:

$$\ddot{\theta}_3 = C \ddot{X}_H \quad (6.42)$$

This equation describes the upper body behaviour resulting from the horizontal motion of the hip point only. Integrating (6.42) from 0 to t yields:

$$\dot{\theta}_3(t) = \dot{\theta}_3(0) + C \left[\dot{X}_H(t) - \dot{X}_H(0) \right] \quad (6.43)$$

and a second integration from 0 to t gives:

$$\theta_3(t) = \theta_3(0) + \dot{\theta}_3(0)t + C \left[X_H(t) - X_H(0) - t\dot{X}_H(0) \right] \quad (6.44)$$

which is a first approximation of a natural trajectory for the upper body angle θ_3 in the absence of an actuator acting on the body. By taking into account that a double support phase occurs after an impact phase, this trajectory can be written as:

$$\theta_3^{nat_1}(t) = \theta_3^+ + \dot{\theta}_3^+t + C \left[X_H(t) - X_H^+ - t\dot{X}_H^+ \right] \quad (6.45)$$

where the index $+$ is used to represent the state of the system immediately after the impact.

If the duration of the double support phase is chosen as $T_D = \frac{\Delta X_H}{\dot{X}_H^+}$, the following expression is found for the angle at the end of the double support phase:

$$X_H(T_D) - X_H^+ = T_D \dot{X}_H^+ \quad \Rightarrow \quad \theta_3^{nat_1}(T_D) = \theta_3^+ + \dot{\theta}_3^+ T_D \quad (6.46)$$

Since in general the duration of the double support phase is short, the rotation of the upper body during a double support phase is small. Expression (6.46) indicates that a desired value for the upper body angle can be reached by choosing an appropriate value for the angular velocity $\dot{\theta}_3$ at the end of the preceding single support phase.

Recalling (6.43), a rough estimate of the variation of the angular velocity during the double support phase is:

$$\dot{\theta}_3^{nat_1}(T_D) = \dot{\theta}_3^+ + C \left[\dot{X}_H(T_D) - \dot{X}_H^+ \right] \quad (6.47)$$

Evaluating expression (6.42) at $t = T_D$ and $t = t^+$ and subtracting the results leads to the variation of the acceleration:

$$\ddot{\theta}_3^{nat_1}(T_D) = \ddot{\theta}_3^+ + C \left[\ddot{X}_H(T_D) - \ddot{X}_H^+ \right] \quad (6.48)$$

Improving the approximation of the upper body motion

Referring to the differential equation (6.41), it is likely that the first term of the rhs will be the predominant one. This is especially the case when the upper body rotation is small, or in other words when the upper body is nearly vertically oriented. The approximation of the natural upper body motion can be improved by taking the vertical hip motion into account. This can be done by substituting the trajectory $\theta_3^{nat_1}(t)$ in the rhs of (6.41). The differential equation then becomes:

$$\ddot{\theta}_3^{nat_2} = C \left[\ddot{X}_H - \left(\ddot{Y}_H + g \right) \left(\frac{\pi}{2} - \theta_3^{nat_1} \right) \right] \quad (6.49)$$

Where the expression (6.45) for $\theta_3^{nat_1}(t)$ is introduced in the rhs. Equation (6.49) can then be solved for $\theta_3^{nat_2}(t)$, which will be a better estimate of the natural motion.

Once integrating over time yields an expression for the angular velocity:

$$\dot{\theta}_3^{nat_2}(t) = \dot{\theta}_3^{nat_1}(t) - C \int_0^t \left(\ddot{Y}_H(u) + g \right) \left(\frac{\pi}{2} - \theta_3^{nat_1}(u) \right) du \quad (6.50)$$

Twice integrating over time leads to the eventual natural trajectory:

$$\theta_3^{nat_2}(t) = \theta_3^{nat_1}(t) - C \int_0^t \int_0^w \left(\ddot{Y}_H(u) + g \right) \left(\frac{\pi}{2} - \theta_3^{nat_1}(u) \right) du dw \quad (6.51)$$

When the horizontal and vertical hip motion are known polynomial functions, the rhs of (6.51) is also a polynomial function, such that it can be integrated analytically. In this chapter (see section 6.7), the horizontal and vertical hip motion will be prescribed by fifth order polynomial functions. The trajectory $\theta_3^{nat_2}(t)$ will consequently be a seventh order polynomial function. Recall that this was also the case during the single support phase.

One should keep in mind that linearizing equation (6.39) also introduces errors. These errors are neglected here, which can be motivated by the fact that a correction function will be added to $\theta_3^{nat_2}(t)$.

6.4.2 Defining a reference trajectory for the upper body

From this point on, expression (6.51) is considered as a good approximation of a natural upper body motion during the double support phase. The double support phase occurs after an impact of the swing leg on the ground, which is preceded by a single support phase. After the impact phase, the values for \dot{X}_H^+ , \dot{Y}_H^+ , $\dot{\theta}_3^+$ and \ddot{X}_H^+ , \ddot{Y}_H^+ , $\ddot{\theta}_3^+$ are known, since they are calculated by an inelastic impulsive impact model. The differential equation (6.41) will only be a good model for the upper body motion during the double support phase, if the actual angular acceleration $\ddot{\theta}_3^+$ after impact approximately satisfies

$$\ddot{\theta}_3^+ \approx C \left[\ddot{X}_H^+ - \left(\dot{Y}_H^+ + g \right) \left(\frac{\pi}{2} - \theta_3^+ \right) \right] \quad (6.52)$$

In other words, a certain continuity on the acceleration level between the successive phases can be reached by choosing

$$\ddot{\theta}_3(T_S) = C \left[\ddot{X}_H(T_S) - \left(\dot{Y}_H(T_S) + g \right) \left(\frac{\pi}{2} - \theta_3(T_S) \right) \right] \quad (6.53)$$

at the end of the single support phase, where T_S represents the duration of the single support phase. Thus, the boundary values at the end of the single support phase, for the vertical and horizontal hip acceleration as well as the upper body angular acceleration, are chosen in such a way that they are a close to a solution of the differential equation (6.41), which describes the natural upper body motion during the double support phase. A similar continuity will be guaranteed for the transition from the double support phase to the single support phase.

Suppose now that the following boundary values for the upper body motion have to be attained at the end of the double support phase:

$$\theta_3(T_D) = \theta_3^* \quad (6.54)$$

$$\dot{\theta}_3(T_D) = \dot{\theta}_3^* \quad (6.55)$$

$$\ddot{\theta}_3(T_D) = \ddot{\theta}_3^* \quad (6.56)$$

where θ_3^* , $\dot{\theta}_3^*$ and $\ddot{\theta}_3^*$ are desired initial values for the next single support phase. The goal is then to define a suitable steering function $\theta_3^D(t)$ for the upper body angle. Two corrections are introduced in expression (6.51):

$$\theta_3^D(t) = \theta_3^{nat_2}(t) + j(t) + k \quad (6.57)$$

where

$$j(t) = at^3 + bt^4$$

with

$$a = \frac{(\ddot{\theta}_3^{nat_2} - \ddot{\theta}_3^*)}{3T_D} - \frac{(\dot{\theta}_3^{nat_2} - \dot{\theta}_3^*)}{T_D^2} \quad (6.58)$$

$$b = -\frac{(\ddot{\theta}_3^{nat_2} - \ddot{\theta}_3^*)}{4T_D^2} + \frac{(\dot{\theta}_3^{nat_2} - \dot{\theta}_3^*)}{2T_D^3} \quad (6.59)$$

and k being a constant defined as

$$k = \theta_3^* - \theta_3^{nat_2}(T_D) - aT_D^3 - bT_D^4$$

The quartic function $j(t)$ ensures that the desired values for the angular velocity and acceleration are attained at the end of the double support phase as defined in (6.55) and (6.56), whereas the constant k ensures that the desired value for the upper body angle is reached. Due to the fact that k is a constant, the trajectory does not exactly match θ_3^+ at the beginning of the double support phase. Indeed, when evaluating (6.57) at $t = 0$:

$$\begin{aligned} \theta_3^D(0) &= \theta_3^{nat_2}(0) + k \\ &= \theta_3^+ + k \\ &= \theta_3^+ + \theta_3^* - \theta_3^{nat_2}(T_D) - aT_D^3 - bT_D^4 \end{aligned} \quad (6.60)$$

Taking into account that

$$\theta_3^{nat_2}(T_D) \approx \theta_3^{nat_1}(T_D) = \theta_3^+ + \dot{\theta}_3^+ T_D \quad (6.61)$$

gives:

$$\theta_3^D(0) \approx \theta_3^* - \dot{\theta}_3^+ T_D - aT_D^3 - bT_D^4 \quad (6.62)$$

Since the duration of the double support phase is short:

$$-aT_D^3 - bT_D^4 \approx 0 \quad \Rightarrow \quad \theta_3^D(0) \approx \theta_3^* - \dot{\theta}_3^+ T_D \quad (6.63)$$

The strategy will be to choose the angular velocity $\dot{\theta}_3(T_S)$ ($\approx \dot{\theta}_3^+$) at the end of the preceding single support phase such that

$$\dot{\theta}_3^+ T_D \approx \theta_3^* - \theta_3^+ \quad \Rightarrow \quad \theta_3^D(0) \approx \theta_3^+ \quad (6.64)$$

In other words, the constant k is very small and will therefore not disturb the motion of the robot at the beginning of the double support phase.

6.5 Upper body behaviour during the single support phase

The strategy developed in section 5.6 of the previous chapter for a single support phase, will be adapted here to be used in combination with a double support phase.

6.5.1 Problem statement

Assume a steady walking pattern where the following is demanded for the upper body behaviour. Recall that index S stands for Single support phase, whereas D stands for Double support phase. Moreover T_S represents the duration of the single support phase and T_D the duration of the double support phase.

- **upper body angle**

$$\theta_3^S(0) \longrightarrow \theta_3^S(T_S) = \theta_3^+ = \theta_3^D(0) \longrightarrow \theta_3^D(T_D) = \theta_3^S(0) \quad (6.65)$$

which can also be formulated as

$$\Delta\theta_3^S + \Delta\theta_3^D = 0 \quad (6.66)$$

with

$$\Delta\theta_3^S = \theta_3^S(T_S) - \theta_3^S(0) \quad (6.67)$$

$$\Delta\theta_3^D = \theta_3^D(T_D) - \theta_3^D(0) \quad (6.68)$$

In order to limit the error on the estimated upper body motion during the double support phase, $\theta_3^D(T_D)$ ($= \theta_3^S(0)$) can be chosen a value in the neighborhood of $\frac{\pi}{2}$. In that case the second term on the rhs of the differential equation (6.39) is small at the end of the double support phase.

- **upper body angular velocity**

$$\dot{\theta}_3^S(0) \longrightarrow \dot{\theta}_3^S(T_S) \longrightarrow \dot{\theta}_3^+ = \dot{\theta}_3^D(0) \longrightarrow \dot{\theta}_3^D(T_D) = \dot{\theta}_3^S(0) \quad (6.69)$$

It will be assumed that the horizontal hip displacement during the double support phase behaves as a linear function. Such a behaviour can be provoked by choosing $T_D = \frac{\Delta X_H}{X_H^+}$ and by choosing an equal value for the horizontal hip velocity in the end points of the single support phase. Since at the end of every double support phase the upper body angle has to reach the same value, the body has to move back-and-forth during one full step. Under the assumption of a linear horizontal hip displacement during the double support

phase, the approximated natural trajectory $\theta_3^{nat_1}(t)$ suggests a monotonous, quasi linear behaviour of the upper body angle:

$$\theta_3^{nat_1}(t) \approx \theta_3^+ + \dot{\theta}_3^+ t \quad (6.70)$$

The approximated natural trajectory $\theta_3^{nat_2}(t)$ will deviate from this linear behaviour, but it is rather unlikely that the monotonicity of the trajectory will be violated. Indeed, since the rotation of the upper body during double support is small, its behaviour will mainly be determined by the first term on the rhs of the differential equation (6.41). Due to this expected monotonicity during double support, the angular velocity will not change its sign during that phase, such that the oscillation of the upper body has to occur during the single support phase. When taking into account that the global rotation during one full step has to be zero, such a behaviour can be provoked by choosing

$$\dot{\theta}_3^S(T_S) = \dot{\theta}_3^S(0) \quad (6.71)$$

during the single support phase. To clarify this reasoning, figure 6.3 illustrates a simplified upper body angle behaviour during a full step consisting of a single and a double support phase. For the sake of simplicity the impact

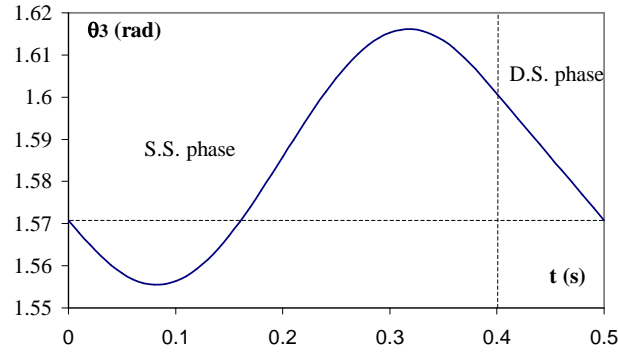


Figure 6.3: Simplified upper body angle behaviour during step

has been neglected, and the body angle behaviour during the double support phase is assumed to be linear.

- **upper body angular acceleration**

$$\ddot{\theta}_3^S(0) \longrightarrow \ddot{\theta}_3^S(T_S) = \longrightarrow \ddot{\theta}_3^+ = \ddot{\theta}_3^D(0) \longrightarrow \ddot{\theta}_3^D(T_D) = \ddot{\theta}_3^S(0) \quad (6.72)$$

In order to obtain a certain continuity with the double support phase, a good choice to respectively start and end a single support phase with, is:

$$\ddot{\theta}_3^S(0) = C \left[\ddot{X}_H^S(0) - \left(\ddot{Y}_H^S(0) + g \right) \left(\frac{\pi}{2} - \theta_3^S(0) \right) \right] \quad (6.73)$$

$$\ddot{\theta}_3^S(T_S) = C \left[\ddot{X}_H^S(T_S) - \left(\ddot{Y}_H^S(T_S) + g \right) \left(\frac{\pi}{2} - \theta_3^S(T_S) \right) \right] \quad (6.74)$$

since this corresponds to what the differential equation (6.41) for the natural upper body motion during the double support phase suggests.

6.5.2 Attaining the desired upper body angle at the end of the single support phase

In the previous section (see expression (6.46)) it was seen that the natural motion during the double support phase tends to a rotation of the upper body different from zero whenever the initial angular velocity $\dot{\theta}_3^D(0) \neq 0$. When neglecting the impact phase and when taking (6.71) into account, the rotation of the upper body during double support can be approximated by:

$$\Delta\theta_3^D \approx \dot{\theta}_3^+ T_D \approx \dot{\theta}_3^S(T_S) T_D = \dot{\theta}_3^S(0) T_D \quad (6.75)$$

Then according to (6.66) the desired upper body rotation during the single support phase is:

$$\Delta\theta_3^S = -\Delta\theta_3^D = -\dot{\theta}_3^S(0) T_D \quad (6.76)$$

In section 5.6.1 of the preceding chapter, equation (5.35) was found by integrating twice the angular momentum equation with respect to the supporting foot during the single support phase. For the sake of clarity it is repeated here:

$$\begin{aligned} \dot{\theta}_3^S(0) = & \frac{Mg}{T_S A_3(0)} \int_0^{T_S} (T_S - t) X_G dt - \frac{h(0)}{A_3(0)} \\ & + \frac{1}{T_S A_3(0)} \int_0^{T_S} h dt + \frac{1}{T_S A_3(0)} \int_0^{T_S} A_3 \dot{\theta}_3 dt \quad (6.77) \end{aligned}$$

When assuming small rotations of the upper body in the neighborhood of $\frac{\pi}{2}$, the function A_3 defined by (5.18), can be approximated by:

$$A_3(t) \approx I_3 + m_3 \gamma^2 l_3^2 + m_3 \gamma l_3 Y_H(t) \quad (6.78)$$

In practice, it is generally desired that the posture of the trunk is kept nearly stationary, in a straight-up position. This would allow the robot to carry objects in a stable manner, or to get scenery information with vision cameras [Park and Rhee, 1998]. Keeping the body fully stationary would cause too much power consumption of the actuator for the trunk, and would be difficult to realize from ZMP position point of view. It is however not desirable to make the trunk swing back and forth in a large range in order to stabilize the robot's motion. Moreover during a general

walking motion large variations of the vertical hip position are undesired and will certainly not be imposed by the applied trajectory generation strategy, meaning that

$$A_3(t) \approx A_3(0) \quad (6.79)$$

The last integral on the rhs of (6.77) can then be written as

$$\int_0^{T_S} A_3 \dot{\theta}_3 dt \approx A_3(0) \Delta \theta_3^S \quad (6.80)$$

One can isolate $\Delta \theta_3^S$ in (6.77):

$$\Delta \theta_3^S = \dot{\theta}_3^S(0) T_S + F \quad (6.81)$$

with

$$F = \frac{1}{A_3(0)} \left[-Mg \int_0^{T_S} (T_S - t) X_G dt + h(0) T_S - \int_0^{T_S} h dt \right] \quad (6.82)$$

Substituting expression (6.76) in (6.81) procures a necessary value for $\dot{\theta}_3^S(0)$:

$$\dot{\theta}_3^S(0) = \frac{-F}{T_D + T_S} \quad (6.83)$$

In section 5.6.1 of the preceding chapter it was explained that the value of $\dot{\theta}_3^S(0)$ has to be calculated by iteration. Indeed, the function F contains the trajectory of $\theta_3^S(t)$ which is unknown at this point. This function will be approximated by a polynomial function, as in section 5.6.1.

6.5.3 Attaining the desired upper body angular velocity at the end of the single support phase

Integrating the angular momentum equation with respect to the supporting foot (5.19) from $t = 0$ to $t = T_S$ during the single support phase, with a zero ankle torque, yields:

$$\mu_{F_S}(T_S) - \mu_{F_S}(0) = -Mg \int_0^{T_S} X_G dt \quad (6.84)$$

Recall the kinematic expression (5.15) for the angular momentum:

$$\mu_{F_S}(t) = A_3(t) \dot{\theta}_3^S(t) + h(t) \quad (6.85)$$

When introducing

$$\dot{\theta}_3^S(T_S) = \dot{\theta}_3^S(0) \quad (6.86)$$

then if trajectories for the leg links are defined, a required value for the angular momentum $\mu_{F_S}(T_S)$ can be calculated with:

$$\mu_{F_S}(T_S) = A_3(T_S)\dot{\theta}_3^S(0) + h(T_S) \quad (6.87)$$

One concludes that if the horizontal motion of the COG is defined such that its integral during the single support phase equals the following value, the angular velocity of the upper body at the end of the single support phase will have the same value as at the beginning of that phase:

$$\int_0^{T_S} X_G dt = \frac{-1}{Mg} \left[A_3(T_S)\dot{\theta}_3^S(0) + h(T_S) - \mu_{F_S}(0) \right] \Rightarrow \dot{\theta}_3^S(T_S) = \dot{\theta}_3^S(0) \quad (6.88)$$

In practice this condition can be satisfied by shifting iteratively the initial and final horizontal position of the hip point until the integral reaches the desired value.

6.5.4 Attaining the desired upper body angular acceleration at the end of the single support phase

When continuity of the upper body acceleration is desired between the single and double support phases, then in the boundary points of a single support phase the conditions (6.73) and (6.74) have to be satisfied. A possible strategy to achieve this is to write the derivative of the angular momentum with respect to the supporting foot as a function of the hip acceleration. Introducing the resulting kinematic expression in the angular momentum equation will lead to a dynamic relation between the upper body acceleration and the hip acceleration.

The position of the hip point H, when calculated starting from the supporting foot, is given by (5.65). Differentiating this set and rewriting it in matrix form leads to:

$$\dot{Z}_H = J_S \dot{Z}_S \quad (6.89)$$

with

$$Z_H = \begin{pmatrix} X_H \\ Y_H \end{pmatrix} \quad \text{and} \quad Z_S = \begin{pmatrix} \theta_{1S} \\ \theta_{2S} \end{pmatrix} \quad (6.90)$$

and the Jacobian:

$$J_S = \begin{pmatrix} -l_1 \sin \theta_{1S} & -l_2 \sin \theta_{2S} \\ l_1 \cos \theta_{1S} & l_2 \cos \theta_{2S} \end{pmatrix}$$

Differentiating (6.89) yields

$$\ddot{Z}_H = J_S \ddot{Z}_S + \dot{J}_S \dot{Z}_S \quad (6.91)$$

from which the generalized accelerations of the supporting leg can be calculated:

$$\ddot{Z}_S = J_S^{-1} \left(\ddot{Z}_H - \dot{J}_S \dot{Z}_S \right) \quad (6.92)$$

The position of the hip point H, when calculated starting from the swing foot, is given by (5.69). Differentiating the set and rewriting it in matrix form leads to:

$$\dot{Z}_H - \dot{Z}_{F_A} = J_A \dot{Z}_A \quad (6.93)$$

with

$$Z_A = \begin{pmatrix} \theta_{1A} \\ \theta_{2A} \end{pmatrix} \quad \text{and} \quad Z_{F_A} = \begin{pmatrix} X_{F_A} \\ Y_{F_A} \end{pmatrix} \quad (6.94)$$

and the Jacobian:

$$J_A = \begin{pmatrix} -l_1 \sin \theta_{1A} & -l_2 \sin \theta_{2A} \\ l_1 \cos \theta_{1A} & l_2 \cos \theta_{2A} \end{pmatrix}$$

Differentiating (6.93) yields

$$\ddot{Z}_H - \ddot{Z}_{F_A} = J_A \ddot{Z}_A + \dot{J}_A \dot{Z}_A \quad (6.95)$$

from which the generalized accelerations on the swing leg can be calculated:

$$\ddot{Z}_A = J_A^{-1} \left(\ddot{Z}_H - \ddot{Z}_{F_A} - \dot{J}_A \dot{Z}_A \right) \quad (6.96)$$

It can be shown that the angular momentum with respect to the supporting foot (5.15) can be written as (see appendix E):

$$\mu_{F_S} = A_3 \dot{\theta}_3 + A_S \dot{Z}_S + A_A \dot{Z}_A \quad (6.97)$$

Differentiating with respect to time yields

$$\dot{\mu}_{F_S} = A_3 \ddot{\theta}_3 + A_S \ddot{Z}_S + A_A \ddot{Z}_A + \dot{A}_3 \dot{\theta}_3 + \dot{A}_S \dot{Z}_S + \dot{A}_A \dot{Z}_A \quad (6.98)$$

After introducing (6.92) and (6.96) the following kinematic expression is found

$$\dot{\mu}_{F_S} = A_3 \ddot{\theta}_3 + (A_S J_S^{-1} + A_A J_A^{-1}) \ddot{Z}_H - A_A J_A^{-1} \ddot{Z}_{F_A} + R \quad (6.99)$$

The function R contains only centrifugal and coriolis terms and is defined as

$$R = \dot{A}_3 \dot{\theta}_3 + \dot{A}_S \dot{Z}_S + \dot{A}_A \dot{Z}_A - A_S J_S^{-1} \dot{J}_S \dot{Z}_S - A_A J_A^{-1} \dot{J}_A \dot{Z}_A \quad (6.100)$$

The angular momentum equation (5.19) in the absence of an ankle actuator was written as:

$$\dot{\mu}_{F_S} = -MgX_G \quad (6.101)$$

Introducing (6.99) in the angular momentum equation leads to a dynamic relation between the hip acceleration and the upper body acceleration:

$$-MgX_G = A_3 \ddot{\theta}_3 + (A_S J_S^{-1} + A_A J_A^{-1}) \ddot{Z}_H - A_A J_A^{-1} \ddot{Z}_{F_A} + R \quad (6.102)$$

Evaluating this relation at the beginning $t = 0$ of the single support phase and introducing condition (6.73) together with a chosen value for $\ddot{Y}_H(0)$, allows one to solve (6.102) for a required value of $\ddot{X}_H(0)$.

Evaluating (6.102) at $t = T_S$ and introducing condition (6.74) together with a chosen value for $\ddot{Y}_H(T_S)$ procures a value $\ddot{X}_H(T_S)$ in a similar way. Choosing these values for the hip acceleration as the boundary accelerations for the tracking functions, ensures a continuity between the consecutive single and double support phases (except for the effect of the impact phase) for the natural upper body acceleration.

6.6 Position of the ZMP during the double support phase

6.6.1 Motion on a horizontal ground

Figure 6.4 depicts the planar biped during a double support phase on a horizontal ground surface (note that the rear ankle point coincides with the origin of the coordinate system). The point P represents the ZMP point, located on the line connecting the two ankle points. As long as both $R_F^y > 0$ and $R_R^y > 0$ in the absence of external ankle torques, the ZMP point will be located between the two ankle points. The position of the ZMP point can easily be calculated by applying

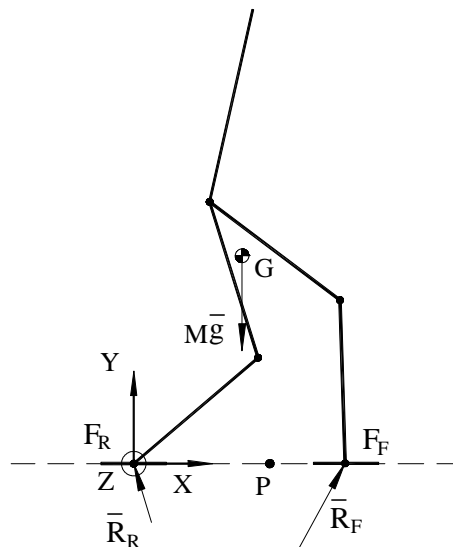


Figure 6.4: ZMP position during double support phase

the definition of Hemami and Golliday Jr. [1977]: *The ZMP point is the point where the total vertical reaction force intersects the ground.* Consequently, the moment around the ZMP caused by the vertical reaction forces in F_F and F_R has to be

zero:

$$R_F^y (\lambda - OP^x) = R_R^y OP^x \quad (6.103)$$

Note that the distance between the two ankle points is equal to the step length λ . The position of the ZMP is computed with:

$$OP^x = \frac{R_F^y \lambda}{R_R^y + R_F^y} \quad (6.104)$$

This expression states that

$$\begin{cases} R_F^y \geq 0 \\ R_R^y \geq 0 \\ R_R^y + R_F^y > 0 \end{cases} \Leftrightarrow 0 \leq OP^x \leq \lambda \quad (6.105)$$

The position of the ZMP point can also be expressed in terms of the motion of the robot instead of the ground reaction forces. Applying the angular momentum equation with respect to the rear ankle point gives:

$$\dot{\mu}_{FR} = \overline{FR} \overline{G} \times M \overline{g} + \overline{FR} \overline{F}_F \times \overline{R}_F \quad (6.106)$$

from which

$$\lambda R_F^y = \dot{\mu}_{FR} + MgX_G \quad (6.107)$$

Moreover, applying the linear momentum theorem in the vertical direction gives:

$$R_R^y + R_F^y = M(a_G^y + g) \quad (6.108)$$

Such that the position of the ZMP is determined with:

$$OP^x = \frac{\dot{\mu}_{FR} + MgX_G}{M(a_G^y + g)} \quad (6.109)$$

This means that in the absence of external foot torques, the trajectories for the leg links have to be defined in such a way that

$$\begin{cases} a_G^y > -g \\ \dot{\mu}_{FR} \geq -MgX_G \\ \dot{\mu}_{FR} \leq -MgX_G + \lambda M(a_G^y + g) \end{cases} \Leftrightarrow 0 \leq OP^x \leq \lambda \quad (6.110)$$

When assuming that at the beginning of the double support phase the zero moment point coincides with the rear ankle joint, this corresponds to a zero ground reaction force at the front ankle joint. The angular momentum equation with respect to the rear ankle evaluated at $t = 0$ then becomes:

$$\dot{\mu}_{FR}(0) = -MgX_G(0) \quad (6.111)$$

At the end of the double support phase the zero moment point has to be located at the front ankle joint. This corresponds to a zero ground reaction force at the rear ankle joint. The angular momentum equation with respect to the rear ankle evaluated at $t = T_D$ then becomes:

$$\dot{\mu}_{FR}(T_D) = -MgX_G(T_D) + \lambda M(a_G^y(T_D) + g) \quad (6.112)$$

When designing the trajectories for the leg links in such a way that always $a_G^y > -g$, then $\dot{\mu}_{FR}$ increases during the double support phase. Satisfying (6.110) can be achieved by limiting the oscillations on $\dot{\mu}_{FR}$ such that they never cross the functions $-MgX_G$ and $-MgX_G + \lambda M(a_G^y(T_D) + g)$ during the double support phase. An example is shown in figure 6.5, which is taken from a simulation (see section 6.8).

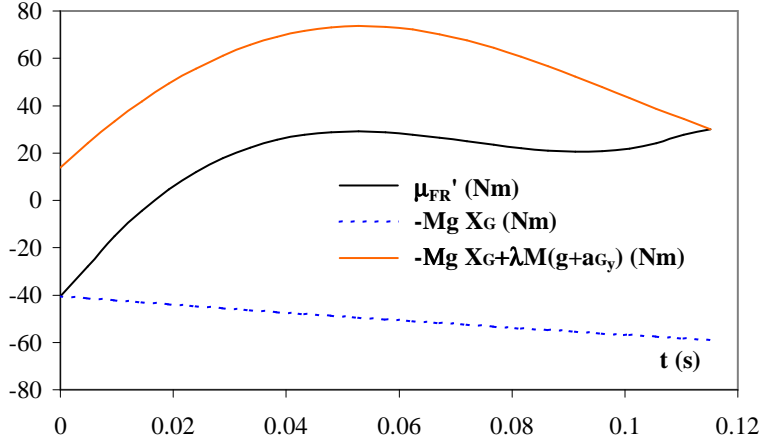


Figure 6.5: Possible behaviour of angular momentum derivative with respect to rear ankle joint during double support phase

These oscillations on the trajectory of $\dot{\mu}_{FR}$ are mainly caused by the horizontal and vertical hip accelerations. A kinematic expression for the derivative of the angular momentum with respect to the supporting foot during the single support phase (6.99) was established. During the double support phase this relation is still valid, when setting the velocity and acceleration of both feet equal to zero. The derivative of the angular momentum consists thus of coriolis and centrifugal terms expressed in \dot{X}_H , \dot{Y}_H and $\dot{\theta}_3$, and inertial terms expressed in \ddot{X}_H , \ddot{Y}_H and $\ddot{\theta}_3$. Recall that the natural acceleration $\ddot{\theta}_3$ is determined by the hip acceleration (see differential equation (6.41)). Due to the generally low walking speeds, the inertial terms are dominant. The shape of trajectories of the vertical and horizontal hip acceleration thus determine the ZMP position. When the robot is in a single support phase, a negative reaction force, which inevitably implies loss of contact with the ground, can be avoided by defining the reference trajectories for the DOF in

such a way that the vertical acceleration of the global COG never reaches gravity acceleration. During the double support phase, this condition will however only guarantee that the sum of the vertical reaction forces at the two different feet is positive and does not guarantee that both the vertical reaction forces remain positive. Using fifth order polynomial functions for describing the horizontal and vertical hip position during the double support phase, the trajectories for the horizontal and vertical hip acceleration are logically third order functions. If these trajectories show large oscillations during the duration T_D , then these oscillations are reflected on the acceleration of the global COG, as well as on $\dot{\mu}_{F_R}$. If $\dot{\mu}_{F_R}$ crosses one of the two borders given in (6.110), then one of the two reaction forces becomes negative, and the ZMP leaves the stability region. This can be avoided by choosing suitable hip acceleration values at the boundaries of the steps. In other words, the complex dynamical problem of postural stability during a double support phase is converted into a simpler kinematical task of limiting the oscillations on two polynomial trajectories.

6.6.2 Motion on a non-horizontal ground

In figure 6.6 the biped is shown during a double support phase on an inclined surface. The ZMP has to be located between the two ankle points in order to avoid tipping over. The physical length of the feet outside the area between the ankle points is neglected, such that the stability region indeed corresponds to the line connecting the two ankle points. The calculation of the position of the ZMP

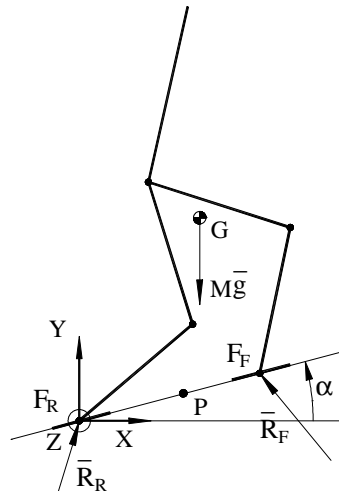


Figure 6.6: ZMP position non-horizontal ground

remains the same (see (6.109)):

$$OP^X = \frac{\dot{\mu}_{FR} + MgX_G}{M(a_G^y + g)} \quad (6.113)$$

while now the stability region becomes smaller due to the sloped surface. The ZMP has to lie between 0 and $\lambda \cos \alpha$, with α being the angle of the sloped surface with respect to the horizontal reference axis.

This means that in absence of external torques, the trajectories for the leg links have to be defined in such a way that

$$\begin{cases} a_G^y > -g \\ \dot{\mu}_{FR} \geq -MgX_G \\ \dot{\mu}_{FR} \leq -MgX_G + \lambda \cos \alpha M (a_G^y + g) \end{cases} \Rightarrow 0 \leq OP^X \leq \lambda \cos \alpha \quad (6.114)$$

which corresponds to demanding that both the vertical reaction forces in the two ankle points have to remain positive. Note that a similar situation is encountered when walking on the steps of a stair.

6.7 Trajectory generation strategy

6.7.1 General considerations

The duration of the double support phase will be chosen as 20 % of the total step duration, corresponding to its duration in human walking at low speeds [Hardt et al., 1999]. Consequently the single support phase will make up 80 % of the step. The definition of the 4 objective parameters introduced in the preceding chapter remains the same. During a steady walking pattern with specific values for these objective parameters the duration of the single support phase can be calculated as:

$$T_S = \frac{\Delta X_H^S}{\nu} \quad (6.115)$$

where ν is the mean horizontal hip velocity during the single support phase. It is well known that the behaviour of a biped during a single support phase can be compared with an inverted pendulum about the fixed ankle point [Shih, 1997b]. During the first half of the single support phase, when the COG lies behind the ankle point, the horizontal motion of the inverted pendulum is decelerated by gravity. When it lies in front of the ankle point, it is accelerated by gravity. Logically the mean horizontal hip velocity during a single support phase will then be smaller than the horizontal hip velocity in the end points of that phase:

$$\dot{X}_H^S(0) \geq \nu \quad (6.116)$$

$$\dot{X}_H^S(T_S) \geq \nu \quad (6.117)$$

During the double support phase, it is assumed here that the hip point moves forward with a constant horizontal speed equal to its initial value, which is an approximation. The duration of the double support phase is then:

$$T_D = \frac{\Delta X_H^D}{\dot{X}_H^D(0)} \quad (6.118)$$

Globally one has

$$T_S + T_D = T \quad (\text{with } T \text{ the total step duration}) \quad (6.119)$$

$$T_D = \frac{T}{5} = \frac{T_S}{4} \quad (6.120)$$

$$\Delta X_H^S + \Delta X_H^D = \lambda \quad (\text{with } \lambda \text{ the step length}) \quad (6.121)$$

It is then easily verified that

$$T_S = \frac{4\lambda}{4\nu + \dot{X}_H^D(0)} \quad (6.122)$$

$$T_D = \frac{\lambda}{4\nu + \dot{X}_H^D(0)} \quad (6.123)$$

In order to explain the trajectory generation strategy as clear and simple as possible, a steady or periodic walking pattern will be considered. After all, the extension to non-steady walking involves only changing the values of the objective parameters from one step to another. It will be assumed that the coordinate system is located at the ankle joint of the supporting foot during the single support phase. During the double support phase the coordinate system is then located at the ankle joint of the rear foot, which is physically the same joint.

6.7.2 Single support phase

Figure 6.7 shows the robot at the beginning and at the end of a single support phase (steady walking is assumed):

Boundary and intermediate conditions

- Moving foot F_A : determines 2 DOF of the robot

$\mathbf{t} = \mathbf{0}$:

$$\begin{aligned} X_{F_A}(0) &= -\lambda & Y_{F_A}(0) &= -\delta \\ \dot{X}_{F_A}(0) &= 0 & \dot{Y}_{F_A}(0) &= 0 \end{aligned}$$

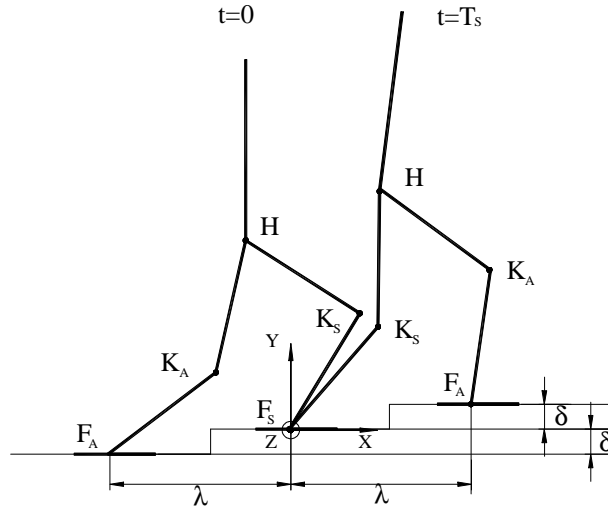


Figure 6.7: Biped during single support phase

$$\ddot{X}_{F_A}(0) = 0 \qquad \ddot{Y}_{F_A}(0) = 0$$

$t = T_S$:

$$\begin{aligned} X_{F_A}(T_S) &= \lambda & Y_{F_A}(T_S) &= \delta \\ \dot{X}_{F_A}(T_S) & & \dot{Y}_{F_A}(T_S) & \\ \ddot{X}_{F_A}(T_S) & & \ddot{Y}_{F_A}(T_S) & \end{aligned}$$

The values of $\dot{X}_{F_A}(T_S)$, $\dot{Y}_{F_A}(T_S)$, $\ddot{X}_{F_A}(T_S)$ and $\ddot{Y}_{F_A}(T_S)$ can be chosen here. The velocities $\dot{X}_{F_A}(T_S)$, $\dot{Y}_{F_A}(T_S)$ will determine the amount of kinetic energy lost during the collision on the one hand, and will on the other hand determine if the inelastic impulsive impact without slip is possible or not. The accelerations $\ddot{X}_{F_A}(T_S)$, $\ddot{Y}_{F_A}(T_S)$ will mainly influence the amplitude of the vertical and horizontal reaction forces acting on the front foot after impact, thus determining the position of the ZMP immediately after the impact.

$t = \frac{T_S}{2}$:

$$X_{F_A}\left(\frac{T_S}{2}\right) = 0 \qquad Y_{F_A}\left(\frac{T_S}{2}\right) = \gamma$$

The foot lift γ is particularly useful when the robot has to step over an obstacle. It is however known that a high foot clearance requires large peak

torques and velocities of all the joints. According to Huang et al. [2001], this is due to the fact that more energy is required to drive the joints when the foot has to be lifted higher in the gravity field. It is therefore desirable to keep the foot lift rather low when no obstacle has to be cleared.

The foot will cover a horizontal distance of 2λ during the swing. It is assumed for simplicity reasons that it clears equal distances during the first and the second half of the swing phase.

- Hip Point H: determines 2 DOF of the robot

$\mathbf{t} = \mathbf{0}$:

$$\begin{array}{ll} X_H(0) = X_H(0)^{,0} & Y_H(0) \\ \dot{X}_H(0) & \dot{Y}_H(0) \\ \ddot{X}_H(0) & \ddot{Y}_H(0) \end{array}$$

$\mathbf{t} = \mathbf{T}_S$:

$$\begin{array}{ll} X_H(T_S) = X_H(0)^{,0} + \nu T_S & Y_H(T_S) \\ \dot{X}_H(T_S) = \dot{X}_H(0) & \dot{Y}_H(T_S) \\ \ddot{X}_H(T_S) & \ddot{Y}_H(T_S) \end{array}$$

The superscript $,0$ for the initial horizontal hip position indicates that this is a starting value for an iterative procedure. It will be adapted by iteration until (6.88) is satisfied.

The vertical hip position in the end points $Y_H(0)$ and $Y_H(T_S)$ will influence the hip height during locomotion. Walking with low hip height and consequently more bent knee joints leads to larger knee actuator torques required to support the robot. From the viewpoint of reducing the load on the knee actuators, the hip height has to be chosen large. However, it has to be assured that the supporting leg does not reach a full extension (see section 6.2.2). In general it is desired that during a horizontal walking motion the vertical hip oscillation is limited. The vertical velocity in the endpoints of the single support phase, represented by $\dot{Y}_H(0)$ and $\dot{Y}_H(T_S)$, is related to the desired intermediate hip height behaviour. Taking into account that during walking the hip reaches its highest position during the single support phase and its lowest position during the double support phase [Huang et al., 2001], the following choice is logical:

$$\dot{Y}_H(0) \geq 0 \quad (6.124)$$

$$\dot{Y}_H(T_S) \leq 0 \quad (6.125)$$

which corresponds to what is found for an inverted pendulum.

The horizontal hip velocity is given equal values here in the endpoints of the swing phase since a steady walking pattern is considered. Choosing $\dot{X}_H(0)$ far from the mean velocity ν , increases the decelerating and re-accelerating behaviour of the robot, which can cause unnecessary energy consumption (see section 6.8.6).

Since the tracking trajectories are polynomial functions, the behaviour of the trajectories is fully determined by the boundary conditions. Boundary conditions on velocity and acceleration have to be chosen in such a way that undesired oscillations are avoided or at least limited. The vertical accelerations $\ddot{Y}_H(0)$ and $\ddot{Y}_H(T_S)$ will be chosen, in order to be able to design a trajectory for the vertical hip height. The horizontal accelerations $\ddot{X}_H(0)$ and $\ddot{X}_H(T_S)$ will be calculated by using the angular momentum equation as was explained in section 6.5.4. Since gravity decelerates the horizontal COG motion when it lies behind the ankle point and accelerates it when it lies in front of the ankle point, the following is logical:

$$\ddot{X}_H(0) \leq 0 \quad (6.126)$$

$$\ddot{X}_H(T_S) \geq 0 \quad (6.127)$$

- Upper body angle: determines 1 DOF of the robot

$$\theta_3(0)$$

$$\dot{\theta}_3(0)^{,0}$$

$$\ddot{\theta}_3(0)$$

$$\theta_3(T_S) = \theta_3(0) - \dot{\theta}_3(0)^{,0}T_D$$

$$\dot{\theta}_3(T_S) = \dot{\theta}_3(0)^{,0}$$

$$\ddot{\theta}_3(T_S)$$

For the rotation of the upper body during the single support phase, an opposite value of the rotation during the double support phase is chosen. The angular velocity of the upper body at the beginning of the single support phase will be calculated by integrating the angular momentum equation as was explained in section 6.5.2, such that it guarantees that the desired rotation is approximately attained without ankle torque. The values of the angular acceleration in the endpoints of the swing phase are determined by (6.73) and (6.74).

Iteratively calculating the reference trajectories

Assume that the starting value for the initial angular velocity of the upper body is chosen zero:

$$\dot{\theta}_3(0)^0 = 0 \quad (6.128)$$

Taking into account that $\dot{\theta}_3(T_S) = \dot{\theta}_3(0)$ was chosen, combined with the fact that during the double support phase an initial zero angular velocity corresponds to $\Delta\theta_3^D = 0$ (see (6.46)), consequently also during single support $\Delta\theta_3^S = 0$ is chosen for this first iteration.

The dynamic equation (6.102) combined with (6.41) evaluated at $t = 0$, can then be solved for a first value of $\ddot{X}_H(0)$. Analogously evaluating (6.102), combined with (6.41) evaluated at $t = T_S$, allows one to determine a first value of $\ddot{X}_H(T_S)$. Since all boundary conditions for the hip point and the moving foot point are known, the trajectories for both the supporting leg as well as the swing leg can be calculated. Two fifth order polynomial functions are thus established for respectively θ_{1S} and θ_{2S} of the supporting leg. Two sixth order polynomial functions are established for respectively θ_{1A} and θ_{2A} of the swing leg, since an intermediate condition was imposed for the swing foot.

A fifth order polynomial function for the upper body can be established based on the chosen boundary values. This polynomial function is a first approximation of the reference trajectory for the upper body. It will form the basis for the iterative procedure to approximate a natural trajectory during the single support phase, or in other words a trajectory that produces a low ankle torque.

The second iteration starts with the calculation of the required initial angular velocity of the upper body which ensures that the rotation of the upper body during single support will be equal and opposite to the one during the double support phase. This is done with (6.83):

$$\dot{\theta}_3(0)^1 = \frac{-F}{T_D + T_S} \quad (6.129)$$

with F defined by (6.82). The fifth order polynomial function for the upper body angle is used for the computation of F .

The rotation during the double support phase can be estimated with

$$\Delta\theta_3^D = \dot{\theta}_3(0)^1 T_D \quad (6.130)$$

such that the rotation during single support with this value for the initial angular velocity becomes:

$$\Delta\theta_3^S = -\dot{\theta}_3(0)^1 T_D \quad (6.131)$$

New values for $\ddot{X}_H(0)$ and $\ddot{X}_H(T_S)$ can be calculated with equation (6.102), in combination with (6.41). With these new boundary values the four polynomial functions for the leg links can also be recalculated. A new fifth order polynomial function for the upper body can be calculated as well.

Again a new value for the necessary initial angular velocity of the upper body can be determined with (6.83), allowing one to repeat the preceding calculations, until a convergence on the value of $\dot{\theta}_3(0)$ is reached.

The next step is to iterate on the initial condition of the horizontal hip position $X_H(0)$, in order to satisfy condition (6.88). Satisfying this condition leads to a natural motion of the upper body for which $\dot{\theta}_3(T_S) = \dot{\theta}_3(0)$. When setting

$$I^{real} = \int_0^{T_S} X_G dt \quad (6.132)$$

being the integral calculated with the actual trajectories, then condition (6.88) states that a desired value for this integral can be calculated with

$$I^{des} = \frac{1}{Mg} [\mu_{F_S}(0) - \mu_{F_S}(T_S)] \quad (6.133)$$

The value of $\mu_{F_S}(T_S)$ is calculated while setting $\dot{\theta}_3(T_S) = \dot{\theta}_3(0)$. An iterative procedure is defined which causes the integral I to vary with:

$$\Delta I = I^{des} - I^{real} = \frac{1}{Mg} [\mu_{F_S}(0) - \mu_{F_S}(T_S)] - \int_0^{T_S} X_G dt \quad (6.134)$$

The iterations will be performed by shifting the initial horizontal hip position. The integral I will be approximated as follows:

$$\int_0^{T_S} X_G dt \approx T_S \left(X_G(0) + \frac{vT_S}{2} \right) \quad (6.135)$$

which is the value of the integral when the COG propagates with a constant horizontal speed. The variation of this expression is

$$\Delta I \approx T_S \Delta X_G(0) \quad (6.136)$$

Assuming that shifting the hip will shift the COG with approximately the same distance gives

$$\Delta X_H(0) \approx \Delta X_G(0) \Rightarrow \Delta X_H(0) \approx \frac{\Delta I}{T_S} \quad (6.137)$$

where ΔI is calculated with (6.134). The following iteration formula is thus established:

$$X_H(0)^n = X_H(0)^{n-1} + \frac{\Delta I_n}{T_S} \quad \text{for } n > 0 \quad (6.138)$$

The calculation of the polynomial reference trajectories for the leg links and the upper body has to be performed during each iteration step.

Eventually, when a certain convergence is reached for (6.138), the tracking trajectory for the upper body which will steer the ankle actuator can be refined by adding a third derivative in the two end-points of the single support phase. As was explained in section 5.6.1 of the previous chapter, this leads to a seventh order polynomial reference trajectory for the upper body angle.

6.7.3 Double support phase

Impact of the closed kinematic chain

The initial time step of the double support phase will be the time step after the collision, denoted by $t = t^+$. Logically the end of the double support phase is denoted by $t = t^+ + T_D$.

The impact model was described in section 6.3. The configuration of the robot is supposed to remain unchanged during the collision, such that the values of the independent coordinates of the rear leg and the upper body are

$$\theta_{1R}(t^+) = \theta_{1S}(T_S) \quad (6.139)$$

$$\theta_{2R}(t^+) = \theta_{2S}(T_S) \quad (6.140)$$

$$\theta_3(t^+) = \theta_3(T_S) \quad (6.141)$$

With expression (6.28) the values of the angular velocities can be found:

$$\dot{\theta}_{1R}(t^+) = \dot{\theta}_{1S}(T_S) + \Delta\dot{\theta}_{1R} \quad (6.142)$$

$$\dot{\theta}_{2R}(t^+) = \dot{\theta}_{2S}(T_S) + \Delta\dot{\theta}_{2R} \quad (6.143)$$

$$\dot{\theta}_3(t^+) = \dot{\theta}_3(T_S) + \Delta\dot{\theta}_3 \quad (6.144)$$

Making the assumption that the actuator torques remain constant during the impact phase, the equations of motion can be used to estimate the value of the angular accelerations $\ddot{\theta}_{1R}(t^+)$ and $\ddot{\theta}_{2R}(t^+)$. Indeed, when the values of the actuator torques as well as the joint angles and angular velocities after impact are introduced, the dynamic equations can be solved for the angular accelerations.

Generating trajectories

The final values for the angles as well as their first and second derivatives of the rear leg during the double support phase of a steady walking motion, are the corresponding initial values of the previous single support phase of the swing leg:

$$\theta_{1R}(t^+ + T_D) = \theta_{1A}(0) \quad \theta_{2R}(t^+ + T_D) = \theta_{2A}(0) \quad (6.145)$$

$$\dot{\theta}_{1R}(t^+ + T_D) = \dot{\theta}_{1A}(0) \quad \dot{\theta}_{2R}(t^+ + T_D) = \dot{\theta}_{2A}(0) \quad (6.146)$$

$$\ddot{\theta}_{1R}(t^+ + T_D) = \ddot{\theta}_{1A}(0) \quad \ddot{\theta}_{2R}(t^+ + T_D) = \ddot{\theta}_{2A}(0) \quad (6.147)$$

The 5th order polynomial functions for θ_{1R} and θ_{2R} can then be established.

Further, with the kinematical relations established in section 6.2, the values of the dependent coordinates on the front leg θ_{1F} and θ_{2F} , as well as their first and second derivatives can be computed.

Finally, since the hip motion is fully determined by the kinematics as soon as the trajectories for the rear leg are established, also the steering function for the upper body (6.57) can be determined.

The different steps of the overall strategy are summarized in a flow-chart in figure 6.8. Note that the dotted branch on the left side of the chart represents an iteration loop, but in practice one can avoid iterations by using well-chosen values for the hip accelerations in the boundary points. Due to the strategy which exploits the natural dynamics of the upper body, problems with the ZMP can be avoided by choosing boundary values for the vertical and horizontal hip accelerations that do not cause large oscillations on the hip acceleration trajectories. For the simulations, a large range for these boundary accelerations which resulted in feasible trajectories was found. An example is shown in section 6.8 (see figure 6.15).

6.8 Simulation results

To test and evaluate the developed strategy, various simulations were performed. The results of a steady walking pattern on a horizontal ground at a walking speed corresponding to the state-of-the-art are extensively discussed here. In the near future, the prototype Lucy [Verrelst et al., 2002] will be used to validate the applied method experimentally.

The following values for the objective parameters characterize the walking pattern:

$$\nu = 0.5 \frac{m}{s} = 1.8 \frac{km}{h} \quad (6.148)$$

$$\lambda = 0.3m \quad (6.149)$$

$$\delta = 0 \quad (6.150)$$

$$\gamma = 0.02m \quad (6.151)$$

The horizontal hip velocity in the endpoints of the step is chosen

$$\dot{X}_H^S(0) = \dot{X}_H^S(T_S) = \dot{X}_H^D(T_D) = 0.55 \frac{m}{s}$$

With expression (6.122) the duration of the single support phase becomes:

$$T_S = \frac{4 * 0.3}{4 * 0.5 + 0.55} \approx 0.47s$$

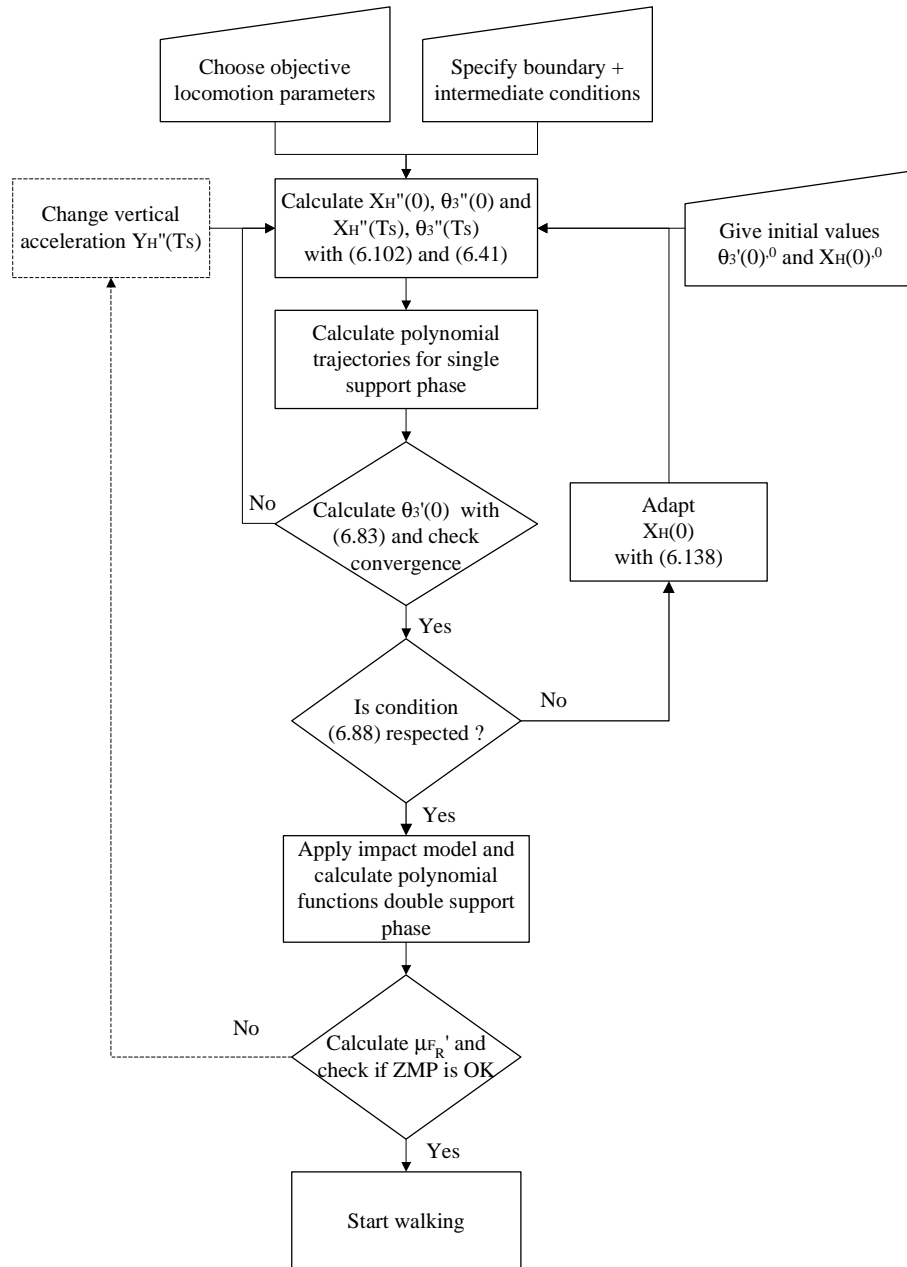


Figure 6.8: Flow chart describing different steps in strategy

and since the double support phase duration is 25 % of the single support phase duration:

$$T_D = \frac{T_S}{4} \approx 0.12s$$

Leading to a total step duration of $T = 0.59s$.

The upper body was chosen upright at the beginning of the single support phase:

$$\theta_3^S(0) = \theta_3^D(T_D) = \frac{\pi}{2}$$

The following values were chosen for the hip height in the boundary points:

$$Y_H^S(0) = Y_H^D(T_D) = 0.93m$$

$$Y_H^S(T_S) = Y_H^D(0) = 0.94m$$

with a fully stretched leg length of $1m$.

Figure 6.9 shows a stick diagram of one full step of the walking pattern.

6.8.1 Hip and foot motion

Graphs 6.10 and 6.11 show respectively the horizontal and vertical position of the hip point H versus time during one step, which is composed of one single support phase and one double support phase. Since a steady walking pattern is considered and all controllers are ideal, the hip trajectory will be identical for all consecutive steps. The initial horizontal hip position was determined by iteration with (6.138) and is equal to:

$$X_H^S(0) = -0.14m$$

Recall that the coordinate system is located at the supporting foot F_S . The final position of the hip is given by:

$$X_H^S(T_S) = X_H^S(0) + \nu T_S = -0.14 + 0.5 * 0.47 = 0.095m$$

These values can be distinguished on figure 6.10. The horizontal hip displacement is equal to

$$\Delta X_H^S = 0.235m$$

during the single support phase, and equal to

$$\Delta X_H^D = 0.065m$$

during the double support phase, such that the global displacement during the step is equal to the step length of $0.3m$. Moreover, the graph considered shows a smooth, quasi linear horizontal hip motion. During the single support phase the

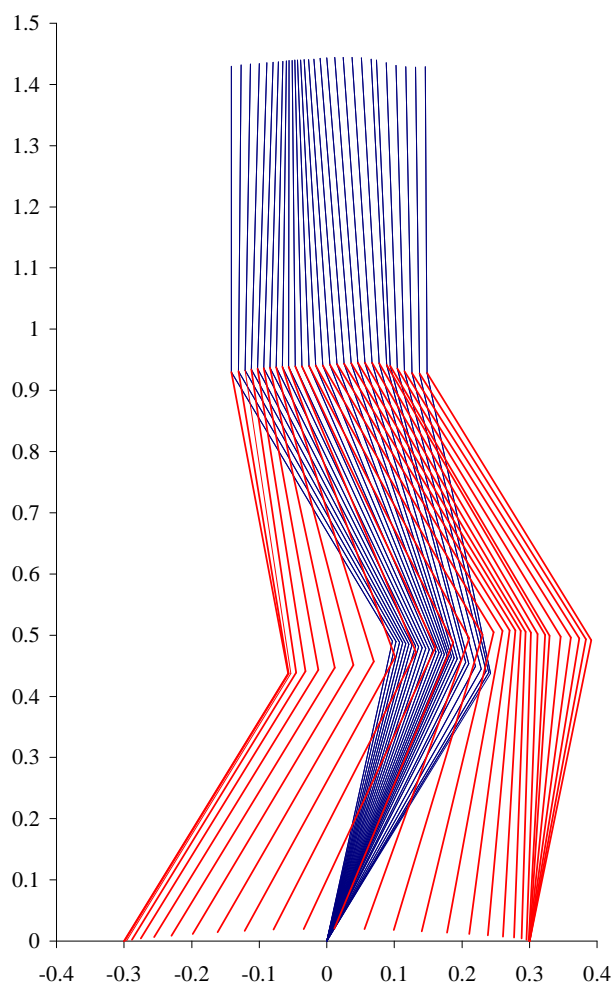


Figure 6.9: Stick Diagram

motion deviates more from a linear motion since the horizontal hip velocity was chosen larger than the mean velocity ν (see also graph 6.12).

On figure 6.11 one can verify that the vertical motion of the hip point is less than $2cm$. The hip point reaches its highest position during the single support phase, and in this specific case nearly at the end of this phase. It reaches its lowest point during the double support phase and returns to its initial height at the end of that phase as was desired.

The behaviour of horizontal hip velocity and the vertical hip velocity during the step considered, are respectively depicted in figures 6.12 and 6.13. The horizontal velocity decreases at the beginning of the single support phase due to gravity, which

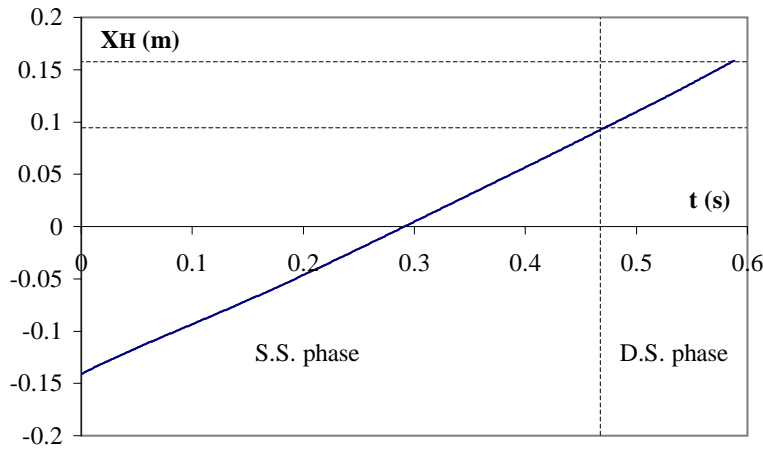


Figure 6.10: Horizontal hip position

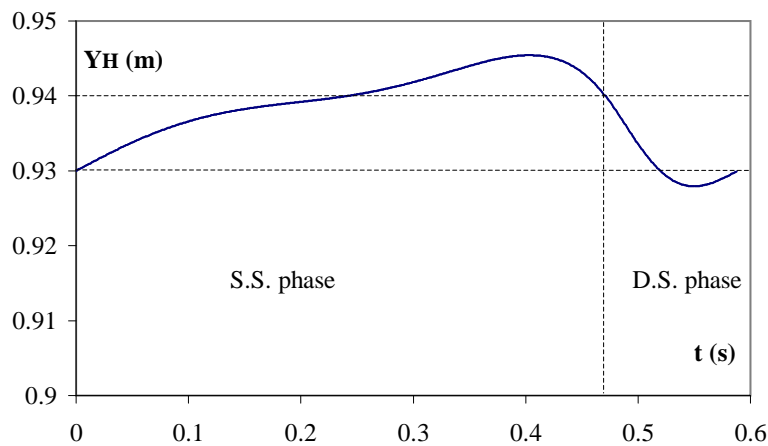


Figure 6.11: Vertical hip position

causes it to increase afterwards. The mean velocity is equal to the desired value of $\nu = 0.5m/s$. The effect of the shock is clearly visible at the instance where the transition occurs from single to double support. Globally one can conclude that the variation of the horizontal velocity with respect to the mean value ν is not excessive. The vertical hip velocity varies from $\dot{Y}_H^S(0) = 0.08m/s$ to $\dot{Y}_H^S(T_S) = -0.2m/s$ during the single support phase. The absolute value of the vertical velocity at the end of the single support phase is chosen larger than at the beginning of that phase, due to the values of the vertical acceleration of the hip point in the end points of the step (see graph 6.14). Giving the final vertical velocity a smaller absolute value would result in a downward motion of the hip point during the single support

phase. Such a motion is considered as unusual when compared to a motion of an inverted pendulum, and is undesired since the foot of the swing leg has to be lifted.

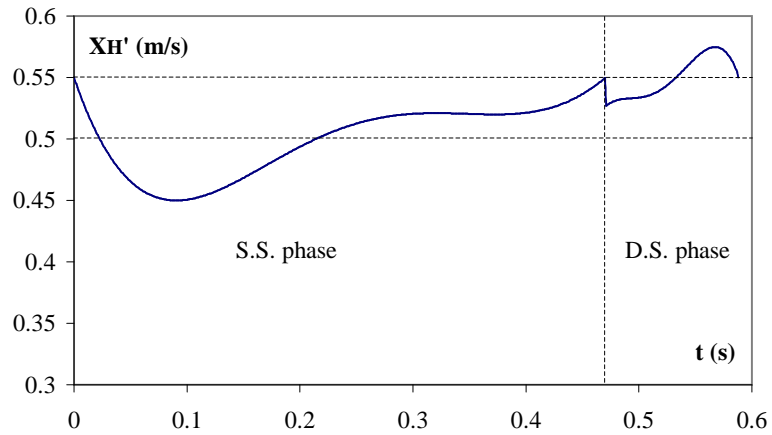


Figure 6.12: Horizontal velocity hip point

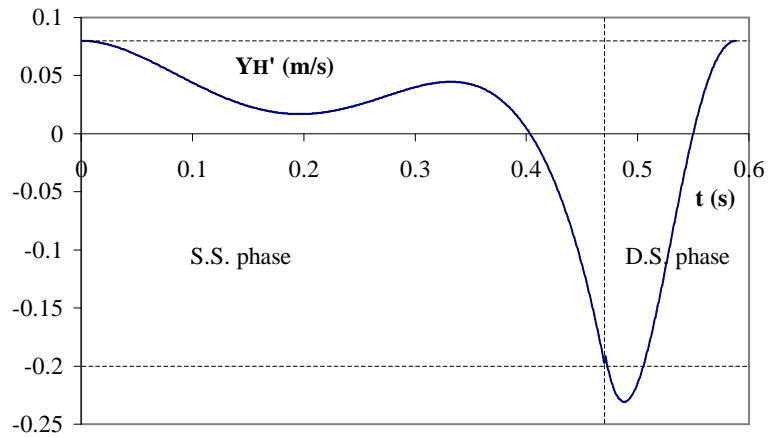


Figure 6.13: Vertical velocity hip point

Graph 6.14 depicts the horizontal as well as the vertical acceleration of the hip point. The vertical acceleration was chosen zero at the beginning of the single support phase. Solving expression (6.102) in combination with (6.73) leads to a negative horizontal acceleration at the beginning of that phase, which corresponds to the decelerating effect of gravity. Further, the vertical acceleration of the hip

point at the end of the single support phase was given a negative value of $-5m/s^2$ in order to obtain a desired vertical hip position trajectory, and also to have a positive value for the horizontal hip acceleration when solving (6.102) in combination with (6.73), in accordance with the accelerating effect of gravity on an inverted pendulum. The horizontal acceleration changes its sign during the single support phase, as well as during the double support phase. When using a fifth order polynomial function for the horizontal hip motion during the double support phase with equal values for the initial and final velocity, and with values for the horizontal acceleration with opposite signs at the boundary points, the third order polynomial for the horizontal acceleration always has two extremes in the time interval considered (recall that $T_D = \frac{\Delta X_H}{\dot{X}_H}$). This effect will be visual in the trajectory of the ZMP position as well, as can be seen in figure 6.27. In figure 6.15, different

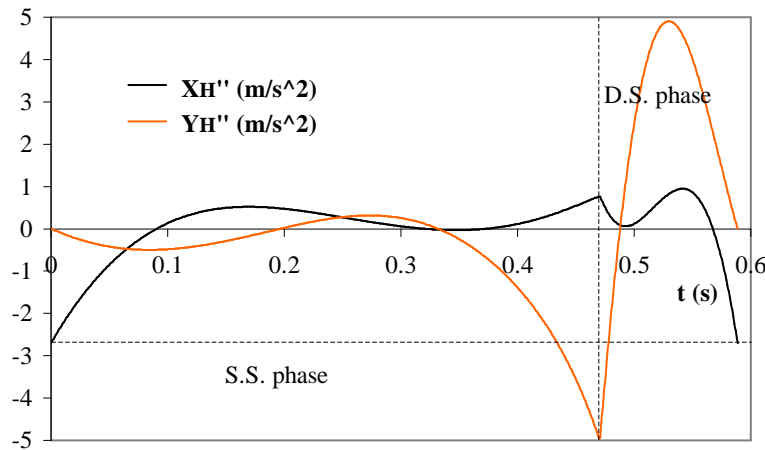


Figure 6.14: Horizontal and vertical acceleration hip point

possible boundary values for the vertical and horizontal hip accelerations are shown at the beginning and the end of the single support phase. For different values of \ddot{Y}_H the corresponding values of \ddot{X}_H are plotted. These values are solutions of the angular momentum equation (6.102) in combination with (6.41), or in other words solutions which guarantee the continuity on the acceleration level between the successive single support and double support phases. All possible combinations taken from the two drawn lines resulted in feasible ZMP trajectories, thus confirming the fact that the postural stability is not very sensitive to the choice of these boundary values.

The motion of the swing foot is represented by graphs 6.16 and 6.17 which show respectively the horizontal and vertical position of the foot F_A . Since the tracking trajectories are based on objective parameters, the behaviour of the swing foot is as expected. Note on figure 6.17 that the vertical position at $\frac{T_S}{2}$ is equal to the

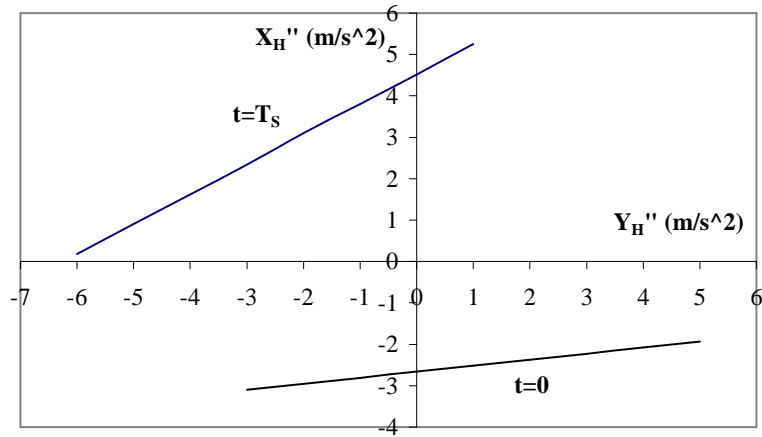


Figure 6.15: Possible boundary values for horizontal and vertical acceleration of hip point

prescribed value of $2cm$.

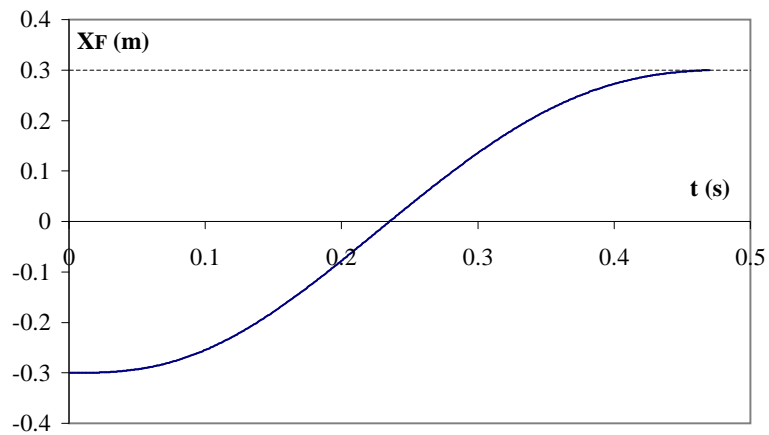


Figure 6.16: Horizontal swing foot position

6.8.2 Upper body motion

Figure 6.18 shows the upper body angle versus time during a step. It can be seen that the upper body angle behaves as was predicted (see figure 6.3 in section 6.5.1). The upper body slightly rotates forwards at the beginning of the single support phase, with an amplitude of approximately 1.5° . Subsequently it rotates

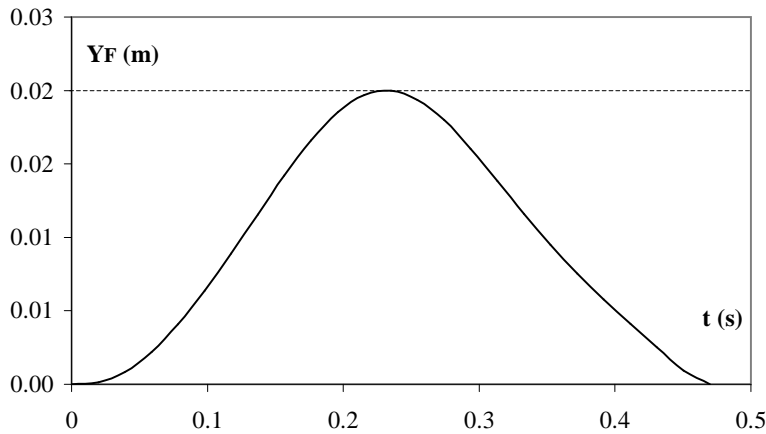


Figure 6.17: Vertical swing foot position

backwards with a maximum deviation from the vertical axis of approximately 4 degrees, followed by another forwards rotation which is continued during the double support phase. At the instance of the impact, the upper body angle is approximately 92.5° . The main conclusion here is that the upper body rotation is indeed very small. Note that the backwards rotation of the upper body can be avoided by choosing the upper body orientation slightly inclined forwards at the beginning of the single support phase.

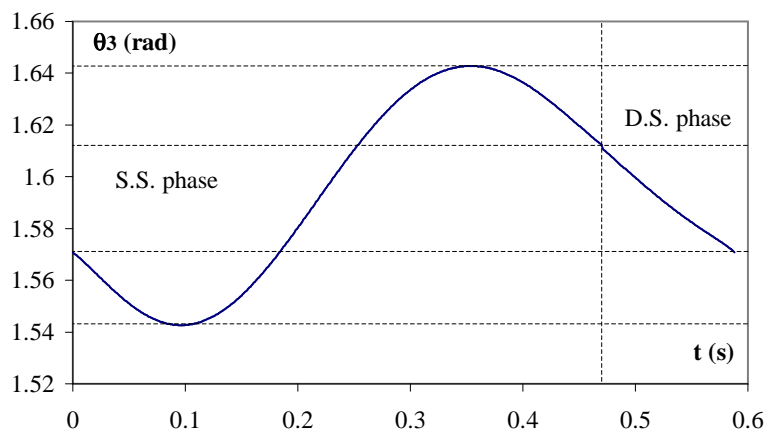


Figure 6.18: Upper body angle

The upper body angular velocity is depicted in figure 6.19. As was imposed by the trajectory generation strategy, the angular velocity reaches identical values in all transition points between single and double support phase. Its value is

approximately -0.35 rad/s there. One notes that during the double support phase the variation of the angular velocity is very small, contrary to its behaviour during the single support phase. Note that these variations during the single support phase occur naturally.

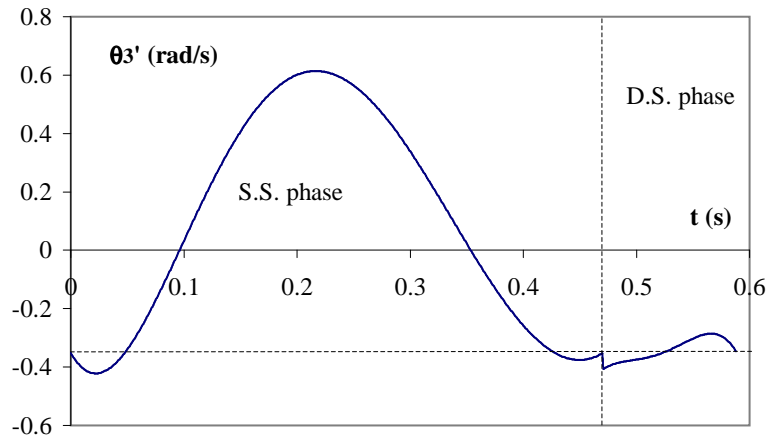


Figure 6.19: Upper body angular velocity

Graph 6.20 compares the trajectory of the natural angular acceleration $\ddot{\theta}_3^{nat}$ resulting from the angular momentum equation with respect to the foot during the single support phase, with the second derivative of the polynomial trajectory $\ddot{\theta}_3^{pol}$ calculated by the trajectory generation strategy. Due to the fact that these trajectories are almost identical, the torque applied at the ankle joint will be very small during the whole single support phase duration, as can be verified in figure 6.29. Consequently the ZMP will remain in the vicinity of the ankle joint, as can be seen in figure 6.27. The function f which is also plotted in figure 6.20, corresponds to the rhs of the differential equation (6.41). It shows that indeed in the end points conditions (6.73) and (6.74) are respectively satisfied, ensuring the continuity between the consecutive single and double support phases on the angular acceleration level.

The angular acceleration of the upper body $\ddot{\theta}_3^{pol}$ imposed by the trajectory generation strategy during the double support phase, is compared with the natural trajectory $\ddot{\theta}_3^{nat}$ resulting from the differential equation (6.41) on graph (6.21). The calculated trajectory mimics the natural trajectory quite well, resulting in a low hip torque required to track it, as can be verified in figure (6.30). Globally it can be concluded that the upper body during the whole step is controlled at the position, the velocity and the acceleration level, in such a way that the natural motion and the controlled motion are almost identical. The strategy for controlling the upper body behaviour works quite well, which results in the fact that the torque needed to actuate it is small (see 6.8.5).

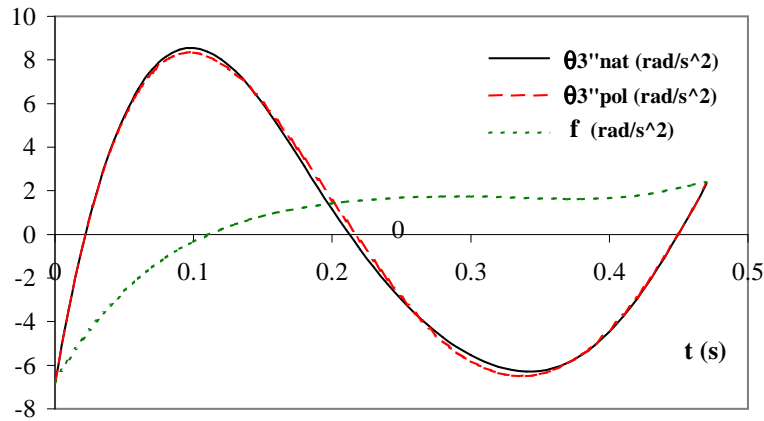


Figure 6.20: Upper body angular acceleration single support phase

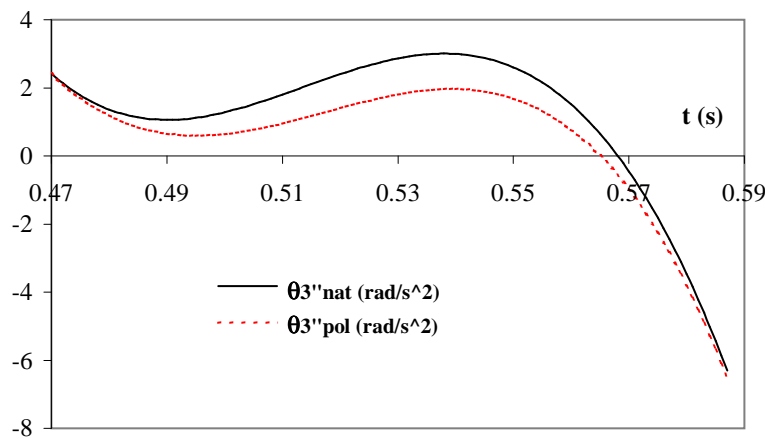


Figure 6.21: Upper body angular acceleration double support phase

6.8.3 Frequency components of the tracking trajectories

In order to make the robot move as desired, the actuators for the leg links as well as the upper body track trajectories generated by the proposed strategy. An important aspect of these trajectories is the frequency spectrum. Indeed, since the controller of a physical actuator will have a limited bandwidth, the frequency content of the tracking trajectories is preferred to be low. Figure 6.22 shows the trajectory for a lower leg link during two consecutive steps. The graph contains thus four different phases of the motion, being support leg during single support phase, rear leg during double support phase, swing (or air) leg during the next single support phase, and finally front leg during the second double support phase. Since a steady walking pattern is considered, the graph represents exactly one period of

the periodic lower leg angle function. A Fast Fourier Transform was applied to this trajectory, of which the results are shown in figure 6.23. Note that A_n represents the amplitude of the n-th frequency component.

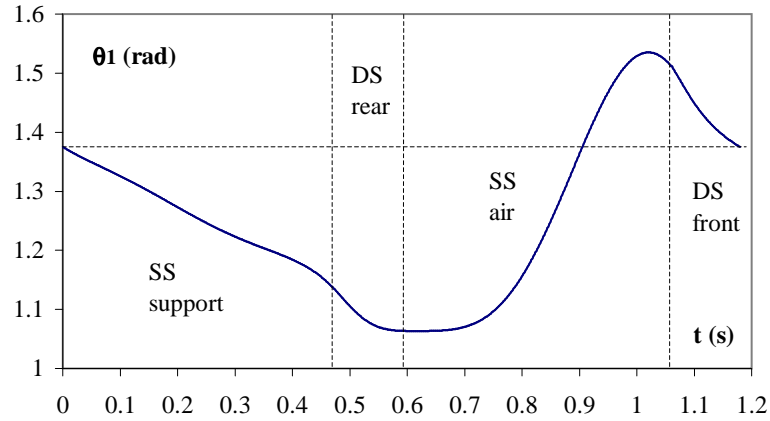


Figure 6.22: Lower leg trajectory during one period

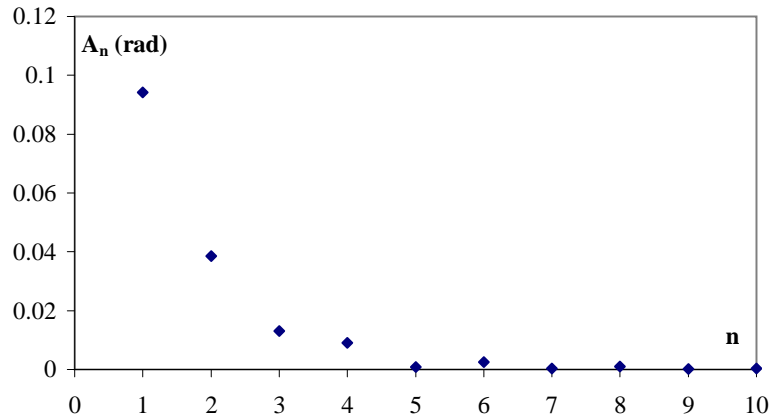


Figure 6.23: Spectrum of lower leg angle trajectory

The DC component is not shown but is equal to the mean value of the lower leg angle during the two steps. One can see that roughly speaking all frequency components starting from the fifth one are in fact unimportant. The maximum frequency would then be equal to:

$$f_{max} = \frac{4}{T} \quad \text{with} \quad T = 2(T_S + T_D) \quad (6.152)$$

Here $T = 2 * 0.59 = 1.18 \text{ s}$ such that $f_{max} = \frac{4}{1.18} \approx 3.4 \text{ Hz}$

Figure 6.24 shows the trajectory for an upper leg link during two consecutive steps, followed by the results of the Fast Fourier Transform on this function in figure 6.25.

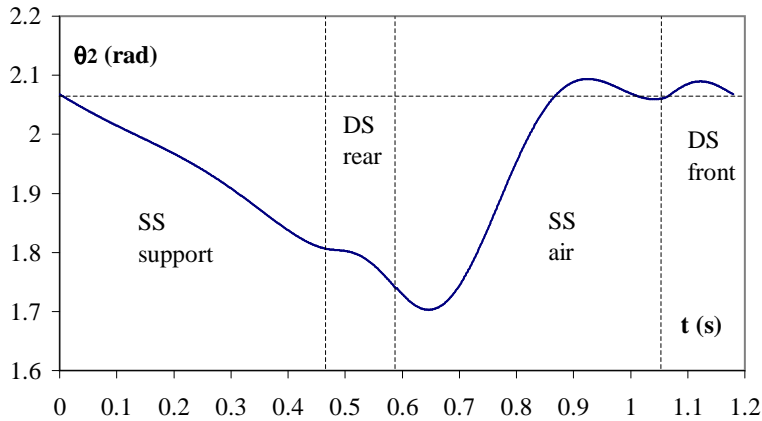


Figure 6.24: Upper leg trajectory during one period

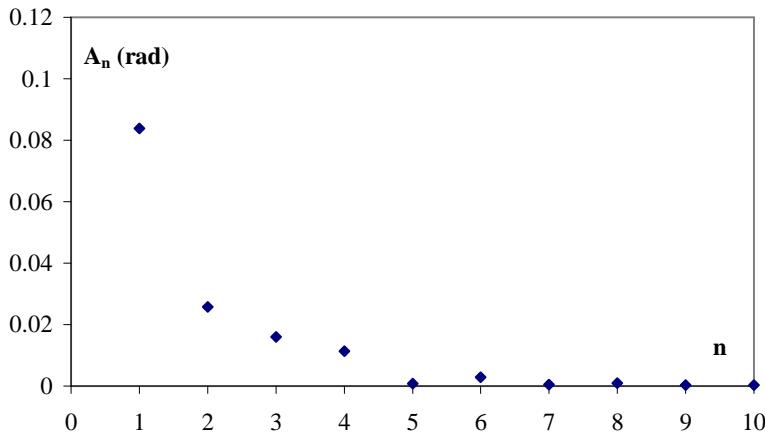


Figure 6.25: Spectrum of upper leg angle trajectory

Clearly the same conclusions can be drawn here. Taking the first five components ($n=4$) into account, approximately 3.4 Hz of bandwidth would be needed to track the trajectory.

The upper body angle trajectory is also a periodic function in case of a steady walking motion, but with a period equal to one step duration. The trajectory of

figure 6.18 was also submitted to a Fast Fourier Transform, of which the results are shown in figure 6.26. The maximum frequency component of importance here

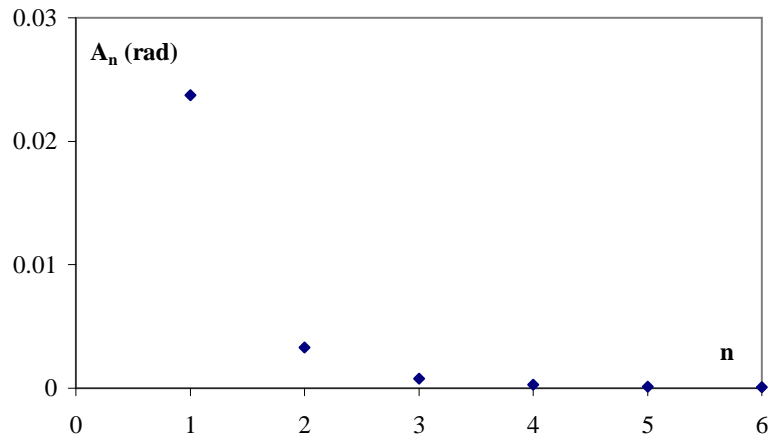


Figure 6.26: Spectrum of upper body angle trajectory

is $f_{max} = \frac{2}{0.59} \approx 3.4Hz$

6.8.4 Zero moment point and ground reaction forces

The position of the ZMP during one step, calculated with (6.109), is shown in figure 6.27. One can verify that during the single support phase the ZMP remains close to the ankle joint. Due to the minor differences between the natural trajectory and the polynomial function of the angular acceleration of the upper body, the ZMP moves only a few millimeters away from the ankle joint. During the double support phase the ZMP is transferred from the rear ankle joint to the front ankle joint. This can also be seen in figure 6.28 where clearly the weight shift from the rear foot to the front foot is visible. Note that in the motion of the ZMP during the double support phase a deceleration followed by an acceleration occurs. The same small oscillation is present in the behaviour of the vertical ground reaction forces in figure 6.28. As was explained before, this is due to the oscillation in the horizontal hip acceleration trajectory during the double support phase, which appears in the angular momentum equation and thus reflects on the upper body acceleration. Since the ZMP is not a physical point but is only used as an indication for postural stability [Goswami, 1999], this phenomenon does not disturb the motion of the robot during the double support phase.

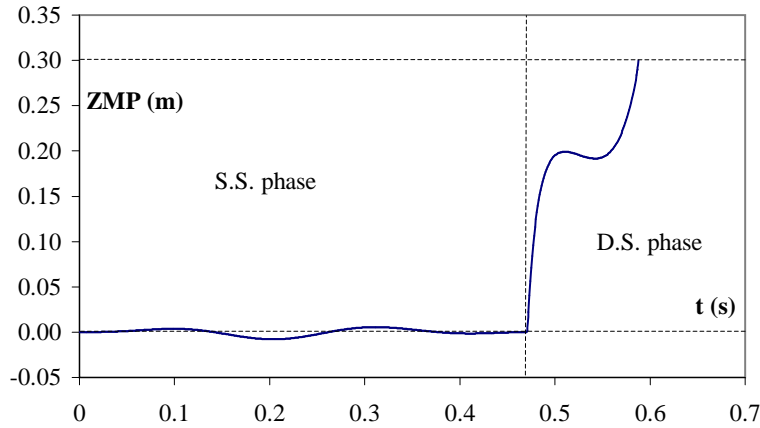


Figure 6.27: Zero moment point position

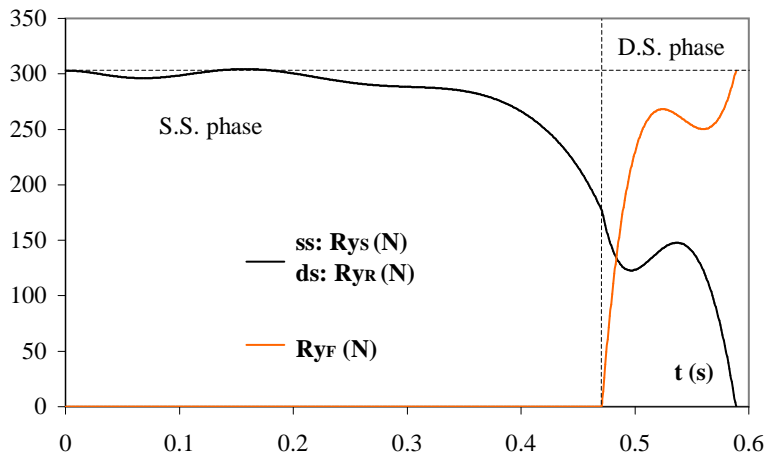


Figure 6.28: Vertical ground reaction forces

6.8.5 Applied torques and mechanical energy consumption

Since the tracking trajectories for the upper body during respectively single and double support phase successfully mimic the natural motion, the corresponding torques exerted by the actuators are indeed very small. Figure 6.29 shows the ankle torque on the supporting foot during the single support phase. The maximum amplitude of this torque is only $2.5Nm$, while the position as well as the velocity and the acceleration of the upper body is controlled. The trajectory shows some minor oscillations, which are only due to the fact that the natural trajectory and the polynomial tracking function are not identical. Indeed, figure 6.20 shows multiple points of intersection between the two acceleration trajectories. For each point

of intersection the ankle torque passes through zero. During the double support phase the upper body is considered to be actuated by the hip actuator on the front leg. Its behaviour is depicted in figure 6.30. A maximum amplitude of $1.5Nm$ is sufficient to steer the upper body to the desired motion. Since in figure 6.21 it can be seen that the natural and the polynomial trajectory of the upper body angular acceleration only intersect in the end points, the hip torque behaviour does not show oscillations.

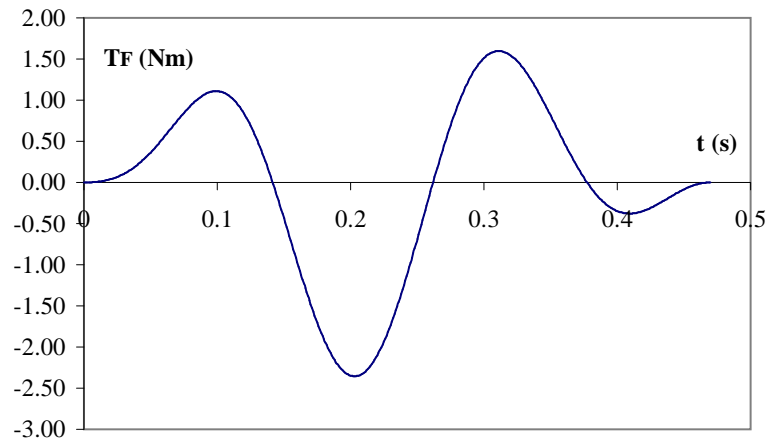


Figure 6.29: Ankle torque during single support phase

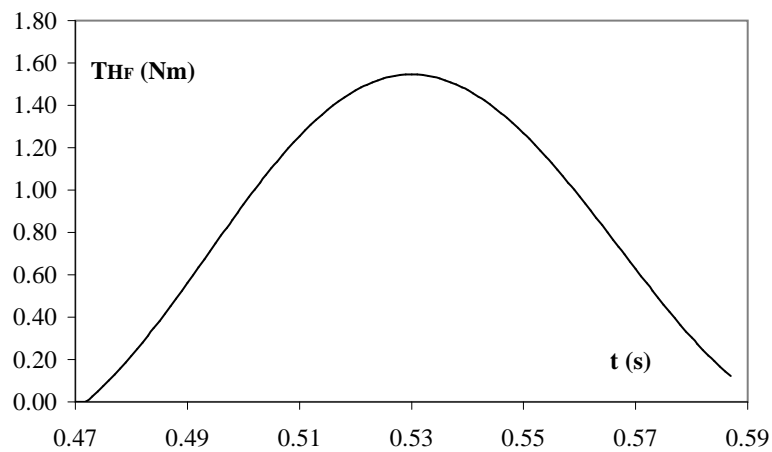


Figure 6.30: Hip torque front leg during double support phase

The torques of the actuators used to steer the other degrees of freedom during the

single support phase are respectively shown in figure 6.31 for the supporting leg, and in 6.32 for the swing leg. Peak torques of approximately $55Nm$ are found for both actuators on the supporting leg. On the swing leg the hip actuator reaches a maximum value of $40Nm$, whereas the knee torque is substantially smaller, showing a maximum value less than $10Nm$. Note that these torques can be reduced by e.g. decreasing the walking speed. The goal was however to develop a strategy for calculating reference trajectories for a walking robot which guarantee a controlled upper body motion with a ZMP point located at the ankle joint during the single support phase, and at the same time to generate a motion characterized by a given set of objective parameters. The graphs of the torque values show that the strategy for controlling the upper body motion does not imply excessively high torques for the other actuators.

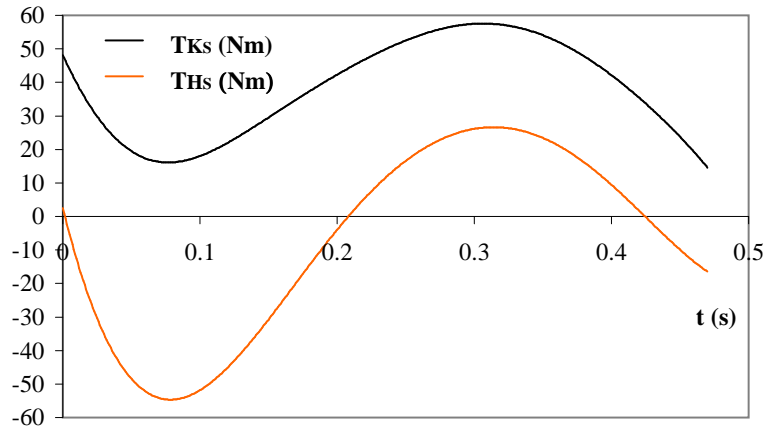


Figure 6.31: Knee and hip torque supporting leg during single support phase

Finally, the torques exerted by the knee actuators of the two legs during the double support phase are presented in figure 6.33. Apparently the knee actuator on the front leg has to exert higher torques than the one on the rear leg. This is obviously caused by the fact that the upper body actuator is located at the hip of the front leg. Its maximum value is approximately $45Nm$.

The power consumption P_i of each actuator can be calculated with:

$$P_i = T_i \omega_i \quad (6.153)$$

with T_i the torque and ω_i the corresponding relative joint angular velocity. The mechanical energy consumed by an actuator can be calculated as follows:

$$E_i = \int_0^T |T_i \omega_i| dt \quad (6.154)$$

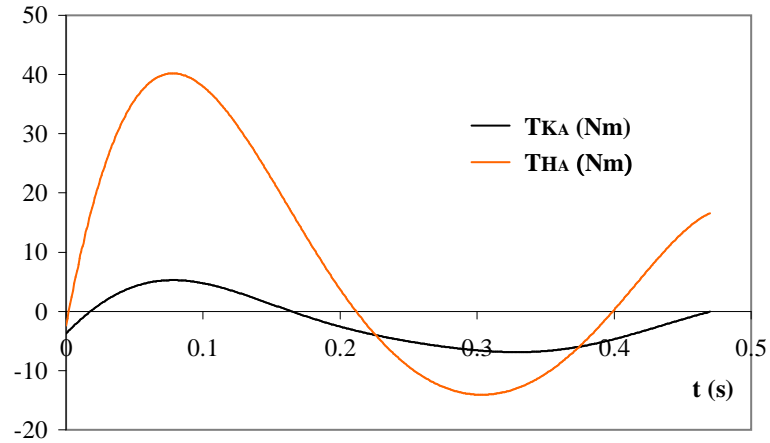


Figure 6.32: Knee and hip torque air leg during single support phase

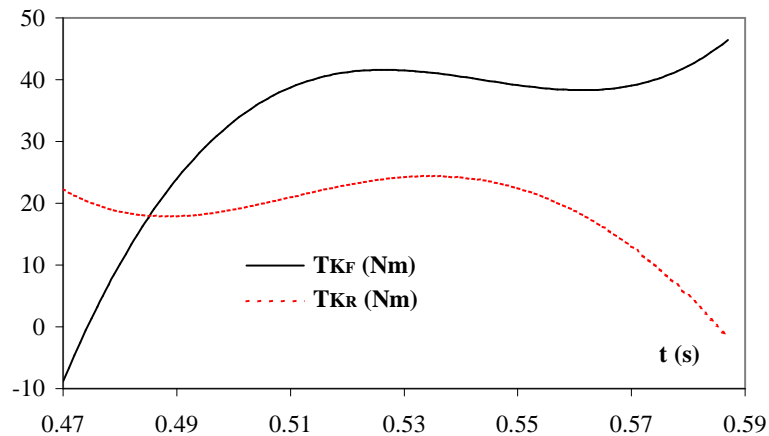


Figure 6.33: Knee torques during double support phase

Doing this for the five actuators during the single support phase of one step of the walking pattern and making the sum, results in an energy consumption of $18.3J$. Making a similar calculation for the three actuators during the double support phase leads to $5.4J$. Globally the actuators consume approximately $23.7J$ or $5.7cal$ during each step, for a robot weighing $30.5kg$ and walking at an average forward velocity of approximately $0.5m/s$ or $30m/min$. Since humans walk generally in an energy efficient manner, a comparison with a walking human might be interesting. In [Rose and Gamble, 1993] a very detailed study of human walking is presented, including a chapter on energetics of walking. A fairly accurate and easy expression was found, where the energy expended is a quadratic function of

the forward velocity:

$$E = 32 + 0.005\nu^2 \quad (6.155)$$

with ν the average forward velocity in m/min and E the energy requirement in $cal/kg/min$ for an average adult human subject. Suppose that an adult human would perform the walking pattern considered, then according to (6.155) the energy expenditure would be approximately $E = 36.5cal/kg/min$. Taking into account that the steps of the simulated model have a duration of $T = 0.59s$ and the robot weighs $30.5kg$, the $5.7cal$ energy expenditure per step corresponds to approximately $18.9cal/kg/min$. Although it is impossible to compare our very simplified walker with a human walker (since expression (6.155) is not valid for humans weighing only $30kg$), these results do indicate that the motion resulting from the applied method of generating trajectories is not excessively energy consuming.

6.8.6 Influence of certain parameter values on mechanical energy consumption

For the experiment considered, a number of parameters have been varied, in order to determine their influence on the mechanical energy consumption. In figure 6.34, the foot lift γ , has been varied over a range between 2 cm and 15 cm , while the other objective parameters remained unchanged. Since the foot lift has no influence on the energy consumption during double support, the graph only shows the consumption during the single support phase. A quasi linear relation between the energy consumption and the foot lift is found. Stepping over an obstacle increases the energy consumption significantly. Performing a step of the simulated walking pattern while stepping over an obstacle of 15 cm approximately doubles the energy consumption.

Figure 6.35 shows the influence of the initial horizontal hip velocity while keeping all the objective parameters equal to the values given by (6.148). The graph clearly indicates that the chosen value of 0.55 m/s was not ideal from the energy point of view. The minimum of the graph corresponds to:

$$\dot{X}_H(0) \approx 0.625 = 1.25\nu$$

or in other words, the mean velocity would approximately have to be 75% of the boundary velocity. It is however clear that the influence of the hip velocity is rather low since the variation of its value from 0.55 to 0.625 m/s only causes an energy expenditure reduction of less than 1 J .

For a given value of the step length λ , it is especially the value of ν that will determine the energy consumption, as can be seen in figure 6.36. Note that the foot lift is equal to 0.02 m for all experiments, and that $\dot{X}_H(0) = 1.25\nu$ is chosen. For an increasing value of the step length, the energy optimal value for the mean velocity also increases. Further it can be verified that the variation of energy consumption increases for an increasing value of the step length, or in other words, the distance

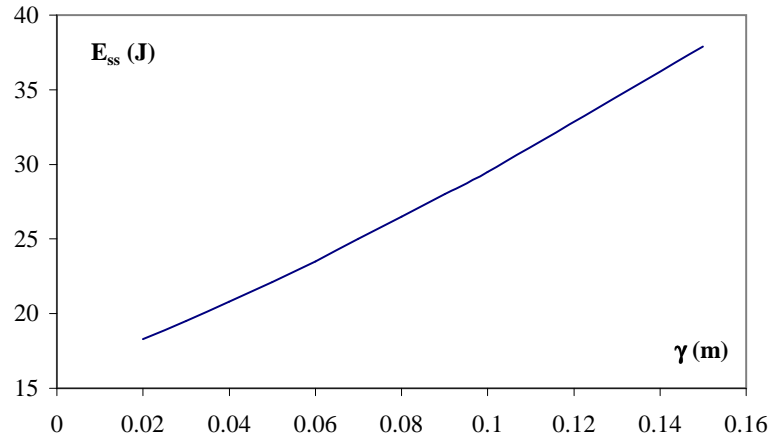


Figure 6.34: Mechanical energy consumption during single support phase versus foot lift

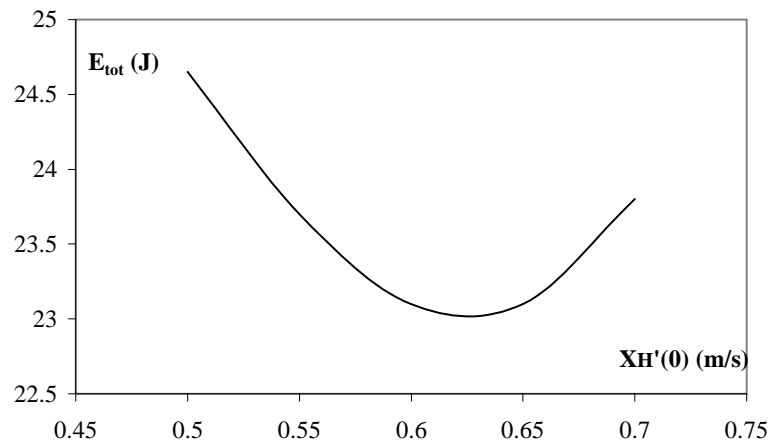


Figure 6.35: Mechanical energy consumption for a full step versus initial horizontal hip velocity

between the curves becomes larger. Below the energy optimal mean horizontal velocity for a certain step length, the energy consumption increases rapidly, due to the fact that the dynamics have to be slowed down. In other words, the robot walks then at a speed which is lower than its natural speed.

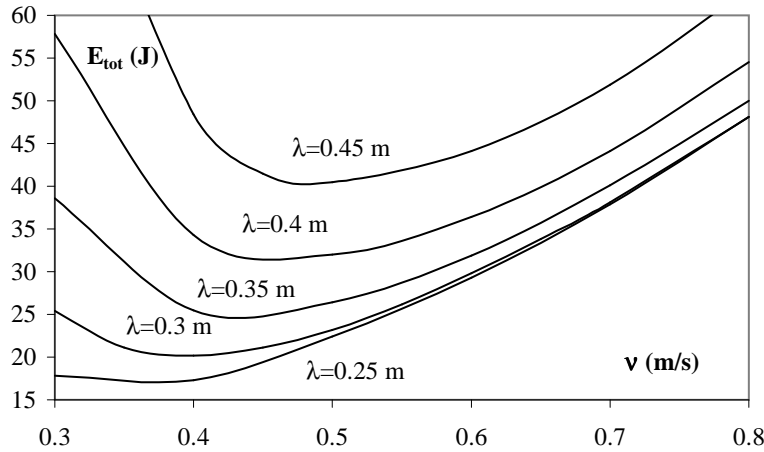


Figure 6.36: Mechanical energy consumption for a full step when varying mean velocity and step length

6.9 Summary

A trajectory generation strategy for a planar walking biped has been developed. The walking motion considered consists of alternating single and double support phases, where the transition from single to double support is accompanied by an impact of the swing leg on the ground. After the impact phase, two holonomic constraints are imposed on the system, which form the difference between the dynamic model in single support and double support.

The steps of the walking pattern are characterized by four objective locomotion parameters, being mean horizontal hip velocity, step length, step height and foot lift. The upper body motion is controlled during both the single and the double support phases, by using the concept of natural dynamics. The hip motion is defined in such a way that the natural upper body behaviour approximates the desired upper body behaviour. During the single support phase this is realized by using the angular momentum equation with respect to the supporting foot, resulting in a ZMP point position close to the ankle joint. During the double support phase the angular momentum equation for the upper body with respect to the hip joint is used, resulting in a ZMP motion from the rear ankle to the front ankle. The natural body motion during the single support phase and the double support phase, are respectively described by two different differential equations resulting from the angular momentum equation. Continuity between these differential equations is realized by choosing suitable values for the horizontal and vertical hip accelerations at the boundary points of the different phases.

The simulation results show the effectiveness of the technique. The objective parameters all reach their desired values, and the postural stability is ensured

during both the single and the double support phases. Due to using the concept of natural upper body dynamics, the motion planning is simplified to designing hip trajectories while satisfying specified conditions, or in other words, a dynamical problem is converted into a kinematical problem which automatically takes the dynamics into account.

The influence of a number of parameters on the mechanical energy consumption was considered. It was found that the mechanical energy consumption for a step increases quasi linear with the value of the foot lift. Moreover, it was observed that certain combinations of step length and horizontal velocity are preferred from an energy point of view. In other words, improper combinations of step length and velocity rapidly increases energy consumption. Finally, it was seen from the energy consumption point of view, that an ideal value exists for the horizontal hip velocity for a given value of the mean horizontal velocity.

Chapter 7

General conclusions and proposed future work

The presented thesis aimed to contribute to the study of the control of dynamically balanced legged robots, by addressing the subject of real-time gait or motion planning for monopods and bipeds. To exploit their potential for high mobility, legged robots have to coordinate the movements of their links in an adequate way, in order to be able to walk on flat as well as on irregular terrains, possibly including inclined surfaces, stairs or obstacles. A path planning algorithm of a real robot uses an input from a vision system or some kind of road-map, to gain information on the robot's environment, and prescribes objectives for the robot's motion. The gait planner or trajectory planner translates these objectives into reference trajectories for the different joint controllers. It is particularly this trajectory planning that forms the subject of this work.

A strategy has been developed for generating reference trajectories for a planar hopping monopod and a planar walking biped, of which the effectiveness has been verified by simulations. The underlying idea of the developed strategy was to convert a complex dynamical problem into a simpler, kinematical one, which inherently takes the dynamics into account. In other words, the dynamics of a robot is steered in a kinematical way. Two distinct concepts formed the basis for the trajectory planner, being the concept of objective locomotion parameters [Hurmuzlu, 1993] to characterize the overall robot motion, and the principle of natural (or unactuated) dynamics [Pratt, 2000] to steer the upper body motion.

To be able to study some conceptual features of robot locomotion, such as postural stability and upper body natural dynamics, the robots considered in this work were planar mechanisms, moving in the sagittal plane. This does not exclude the developed strategy for application on 3D models, since it has been shown for these systems that the dynamics in the sagittal plane are sufficiently decoupled from the dynamics in the frontal plane, such that their control can be treated separately [Bauby and Kuo, 2000; Fowble and Kuo, 1996]. Since especially the

postural stability was our subject of interest, monopods and bipeds were considered. These are the two types of legged robots most prone to such instabilities, with their COG generally located high above the supporting foot or feet.

The motivation for generating trajectories based on objective locomotion parameters, such as speed, step length, etc., was the fact that these parameters are easy to link to a given desired motion. When moving on irregular terrain for example, it makes more sense to express the locomotion pattern in terms of e.g. the coordinates of the feet than in terms of the internal joint angles. Moreover, objective parameters are easier to link to the information of a vision system.

Exploiting the concept of natural dynamics for steering the upper body motion, was motivated by the fact that such an approach assists to preventing the occurrence of postural instability. Generally the upper body of a legged robot has a large mass and inertia when compared to a leg and consequently large ankle torques are required for its actuation, especially when its motion is arbitrarily defined. Due to the limited physical length of a robot foot, large ankle torques can cause foot rotation, which has been identified as a cause for loss of balance and an eventual fall for monopods [Lee and Raibert, 1991] and bipeds [Goswami, 1999]. To avoid foot rotation and the resulting postural instability, the developed trajectory planner manipulates the angular momentum equation in such a way that the upper body naturally performs a prescribed motion. This is achieved without explicitly computing the natural trajectory, which in general is time-consuming.

The Zero Moment Point [Goswami, 1999] has been used continuously throughout this work, as an index for postural stability. Different from other existing approaches, no reference trajectory for the ZMP was established. The trajectory planner only generated trajectories for the joint angles, which inherently ensured postural stability. These trajectories were polynomial functions of which the boundary values depend on desired values of the objective locomotion parameters, and satisfied a number of conditions that guarantee postural stability by only requiring a limited action of the ankle actuator. These conditions were derived from the angular momentum equation, by considering the robot as an underactuated mechanism. Evaluating the angular momentum equation in the boundary points of a support phase, allowed us to introduce specific boundary values for the upper body motion, which led to conditions to be fulfilled by the motion of the leg links. This was done at the position as well as at the velocity and the acceleration level. By making the leg link trajectories satisfy the obtained conditions, the upper body moved to the prescribed end conditions during that phase. In order to use the ankle actuator, to compensate for external disturbances e.g., a reference trajectory for this actuator was obtained by establishing a polynomial function based on those boundary conditions. The advantage of this strategy is that this polynomial function automatically approximates the natural trajectory. Postural stability was thus obtained by defining trajectories for the leg links while satisfying some elementary conditions. More specifically, during the single support phases of the hopping monopod and the walking biped, the ZMP remained in the vicinity of

the ankle joint. During the double support phases of the walking biped, the ZMP travelled automatically from the rear ankle to the front ankle.

The first part of this thesis, consisting of chapters 2, 3 and 4, dealt with the generation of stable motion trajectories for hopping monopods, whereas the second part, formed by chapters 5 and 6, treated a dynamic walking motion of a biped.

In chapter 2, a monopod having an articulated leg and a horizontally oriented upper body, was considered. The upper body was connected to the leg in its COG, which resulted in a complete decoupling between the upper body motion and the leg motion. Due to the fact that the robot did not contain a foot and an ankle actuator, it was an underactuated mechanism in both the flight phases and the stance phases. The model was used to introduce the concept of trajectory generation based on a number of objective parameters, being horizontal velocity of the COG, step length and step height. Due to the decoupled motion of the upper body and the COG, the upper body behavior did not influence the values of the objective parameters, such that both requirements of the trajectory planning algorithm could be treated separately. The upper body control was realized without an ankle actuator, by using the concept of natural dynamics. The angular momentum with respect to the COG was tuned in order to become a zero upper body rotation during one full hop, whereas the duration of the stance phase was determined in order to obtain that specific value for the angular momentum at take-off. Simulations showed that the applied method succeeded in steering the underactuated mechanism such that all the objective parameters reached their desired values, and that the upper body motion was free of drift.

In chapter 3 a more general robot model was considered, with the upper body positioned upright and its COG not coinciding with the hip joint, which causes destabilizing torques due to gravity. Since the COG of the robot now depended on the upper body behavior, the two basic requirements for the trajectory planner were no longer decoupled, which led to the need for an iterative procedure. The robot now contained a foot, with an ankle actuator able to exert an external torque between the foot and the ground, which made the robot fully actuated during a stance phase. An extra objective parameter was introduced, being the foot lift or foot clearance, to avoid a sudden impact of the foot on the ground while swinging the leg during the flight phase. To clearly illustrate the use of exploiting the natural upper body dynamics, initially an arbitrary defined upper body polynomial function for the stance phase was established and used as a reference trajectory for the ankle actuator. Simulations indicated that depending on the values of the objective parameters and the chosen initial conditions, the ZMP point remained within the foot region, but that the use of a look-up table was inevitable to distinguish the stable motion patterns from the unstable ones.

The need for a look-up table was overcome in chapter 4, where the angular momentum equation during the stance phase, in absence of an ankle torque, was used to manipulate the natural dynamics of the upper body. By twice integrating the angular momentum equation, an iterative formula was obtained which allowed us

to compute a value for the stance time, guaranteeing a specific upper body rotation during the stance phase. Using a first integral of the angular momentum equation, it was shown that a specific value for the angular momentum with respect to the COG could be attained by adapting the integral over time of the horizontal position of the COG. This integral was adapted by iteratively varying the touch-down horizontal position of the COG. These two iterative procedures, which are based on elementary calculations and converge extremely fast, influenced the natural upper body motion such that it approximated a prescribed motion. In other words, the polynomial tracking function for the ankle actuator was based on the boundary conditions of the natural trajectory, which limited the work of the ankle actuator to covering the minor differences between the natural and the polynomial trajectory. It was found that a seventh order polynomial function for the upper body angle led to the best result. Using this technique, the monopod was able to perform steady hopping patterns, as well as non-steady patterns, which makes the strategy usable for motion on irregular terrain. Due to the limited number of elementary computations, it can be used for real-time applications.

In chapters 5 and 6, the dynamic walking motion of a planar biped was studied. The geometry of the robot model was based on the prototype Lucy [Verrelst et al., 2002], which has been constructed by the Multibody Mechanics Research Group of the Vrije Universiteit Brussel. In chapter 5, the walking motion was simplified by assuming that the double support phases were instantaneous. The impact accompanying the support switch was avoided by choosing a zero velocity of the foot at touch-down. Moreover, only cyclic walking patterns were considered. The objective parameters characterizing the steps of a walking pattern were the step length and step height, both measured between the two feet at the switching instant, the mean horizontal velocity of the hip, and the foot lift or foot clearance. By writing the angular momentum equation with respect to the supporting foot, it was found that the natural upper body motion could be manipulated by tuning the hip motion. It was observed that neglecting the double support phase did in fact not simplify the planning task. Since the motion was chosen to be cyclic, and due to the absence of a double support phase or flight phase, the upper body motion itself had to be cyclic during one single support phase. Although choosing a hip motion with boundary values satisfying some elementary conditions was sufficient to manipulate the natural upper body motion, especially the vertical acceleration of the hip had to be large in order to realize a cyclic behavior of the upper body angular acceleration. Nevertheless, the walking patterns were feasible and postural instability was successfully avoided. Walking patterns at relatively high walking speeds were simulated, while during all consecutive single support phases the ZMP remained closely to the ankle joint, thus far away from the limits of the stability region.

Finally, in chapter 6, a trajectory generation strategy for a walking motion with double support phase and an impact of the swing foot on the ground, has been developed. Due to the presence of the double support phase, the upper body

behavior did no longer have to be cyclic during the single support phase. The natural upper body motion during the double support phase was estimated by writing the angular momentum equation of the upper body only, with respect to the hip point. This approach avoids the appearance of ground reaction forces in the angular momentum equation. The natural upper body motion during the single support phase and the double support phase, are respectively described by two second order non-linear differential equations. It was shown that continuity of the natural angular upper body acceleration corresponding to these differential equations, can be obtained by choosing the hip accelerations in the boundary points of the different phases in an adequate way. Moreover, it was found that the weight shift during the double support phase could be achieved with polynomial reference trajectories for the robot links, by limiting the oscillations on the hip accelerations, or in other words, by giving the boundary values for the horizontal and vertical hip acceleration well-chosen values. The results of various simulations prove the good performance of the developed strategy. Based on elementary calculations and a number of fast converging iteration loops, ready-to-use joint trajectories for the robot Lucy were developed. These trajectories assure that all the values of the objective parameters are attained, and that the upper body of the robot is steered during both the single support phase and the double support phase by exploiting its natural dynamics. The resulting actuator torques associated with the upper body were extremely small, and postural stability was guaranteed. For the performed simulations at approximately 2 km/h, which is the maximum walking speed attained today by a real walking robot, the maximum frequency component of significance of the joint trajectories was no more than 3 or 4 Hz.

The effectiveness of the strategies developed for generating reference trajectories, has been verified by a variety of simulations, of which logically only a limited number of the results have been reported in this thesis. One of the first things to do in the near future is to validate the planning method with an experimental robot model. Unfortunately for the simulated hopping monopod no prototype is available, nor is its construction foreseen in the near future for budgetary reasons. The planning method for bipedal dynamic walking will however be used to steer the prototype of the biped Lucy [Verrelst et al., 2002]. Since Lucy is actuated by a novel type of pneumatic artificial muscles [Daerden, 1999], specific high- and low-level controllers had to be designed. A first design of these controllers is currently in a final stage. These controllers, as well as the characteristic dynamics of the actuators including specific time delays, have been modelled and are introduced in the dynamical model of Lucy. This dynamical model will allow us to validate the developed trajectory generation strategy, and to test its robustness. Due to the un-modelled dynamics, the real natural upper body motion will differ from the predicted natural motion by the planning algorithm. The ZMP will consequently move away from its predefined position. Since the planning algorithm locates the ZMP far away from the boundaries of the stability region, these ZMP motions are not expected to cause postural instability. Note that, except for the chapters

dealing with the hopping monopod, no controllers were included in the simulations in this work. Actuator torques were calculated with an inverse dynamical approach. This was done because at that time the actuator dynamics as well as a realistic controller model were not available. In chapters 2 and 3, simple PD-controllers were used to track the joint reference trajectories. Since this did not at all reflect a real situation, this was no longer considered in the following chapters.

Another interesting continuation of this work, will be to test if the developed method can be optimized from an energetics point of view. Although some basic computations concerning energy consumption of the actuators have been performed in chapter 6, a profound energy analysis will provide us a clear view on which specific combinations of objective parameters, as well as chosen boundary conditions for the state variables, are favorable. Since the upper body motion is quasi-naturally steered, its motion is consequently defined in an energy-efficient way. This is however not necessarily the case for the leg links. An important advantage of the pleated pneumatic artificial muscles is that they have an adaptable stiffness. In other words, their natural regimes can be adapted and possibly fitted in a certain way to the reference trajectories for the different joints, which can significantly reduce the energy consumption of the actuators.

Throughout this work, the action of the foot link has been limited to providing a support area for generating external ankle torques between the robot and the ground. Foot rotation during the support phases has been avoided based on ZMP considerations, while also during the flight or swing phases the swing foot was kept horizontally. Nature provides us however with numerous examples of systems that actively exploit foot rotation for many different reasons. For the hopping monopod considered, an extra toe-link combined with rotation of the foot at the end of the stance phase could be useful for injecting extra energy in the system at take-off. If equipped with a passive element, a foot could be used for reducing the shock and for storing energy resulting from the flight phase. For walking humans, exploitation of foot rotation is observed in two different ways, being the so-called *kick-action* at the end of the double support phase, and the *tiptoe rotation* at the end of the single support phase [Yamada et al., 1985; Sano and Furusho, 1990]. Although these types of foot rotation have been proven to be useful in different ways, the question remains if for the models considered in this work, the increasing complexity accompanying the introduction of an extra link possibly combined with an extra actuator will not be predominant over the possible advantages. Recall that exploiting foot rotation requires an accurate tracking of the ZMP and imposes high demands on the control system. The developed trajectory generation strategy would not necessarily have to be adapted, since foot rotation can be induced by generating an extra ankle torque. An interesting continuation of this work could be an extension of the technique, generating joint trajectories in such a way that the ZMP automatically transfers to the tiptoe joint, without the need for an extra actuator torque.

Finally, some more obvious extensions or continuations of this work can be formu-

lated. Development of a strategy specifically focussing on starting and stopping of the motion will be essential. Further, combining the techniques established for the hopping robots and the walking biped, will allow us to simulate a bipedal running motion in the near future. And eventually, if the strategy is fully optimized for locomotion in the sagittal plane, then the following logical step will be a planning and control strategy for locomotion in 3D.

Appendix A

Dynamic model of the hopping robot with foot

A.1 Flight phase

Recall figure 3.1 describing the model of the one-legged hopping robot. The dynamic model will be established in terms of the following set of absolute coordinates:

$$q = \{\theta_1, \theta_2, \theta_3, X_F, Y_F\}^T$$

The position of the centers of mass of the three links is given by:

$$\overline{OG}_1 = (X_F, Y_F)^T + \alpha l_1 (\cos \theta_1, \sin \theta_1)^T \quad (\text{A.1})$$

$$\overline{OG}_2 = (X_F, Y_F)^T + l_1 (\cos \theta_1, \sin \theta_1)^T + \beta l_2 (\cos \theta_2, \sin \theta_2)^T \quad (\text{A.2})$$

$$\overline{OG}_3 = (X_F, Y_F)^T + l_1 (\cos \theta_1, \sin \theta_1)^T + l_2 (\cos \theta_2, \sin \theta_2)^T + \gamma l_3 (\cos \theta_3, \sin \theta_3)^T \quad (\text{A.3})$$

The total kinetic energy can be found by making the following sum over the three links:

$$K = \sum_{i=1}^3 K_i = \frac{1}{2} \sum_{i=1}^3 \left(m_i v_{G_i}^2 + I_i \dot{\theta}_i^2 \right) \quad (\text{A.4})$$

with $\bar{v}_{G_i} = \left(\dot{X}_{G_i}, \dot{Y}_{G_i} \right)^T$.

The inertia matrix D^{fl} is related to the kinetic energy K:

$$K = \frac{1}{2} \dot{q}^T D^{fl} \dot{q} \quad (\text{A.5})$$

With (A.5) the elements of the inertia matrix can be found:

$$d_{11} = I_1 + l_1^2 (m_1 \alpha^2 + m_2 + m_3)$$

$$d_{12} = l_1 l_2 (\beta m_2 + m_3) \cos(\theta_1 - \theta_2) = d_{21}$$

$$d_{13} = l_1 l_3 \gamma m_3 \cos(\theta_1 - \theta_3) = d_{31}$$

$$d_{14} = -l_1 (\alpha m_1 + m_2 + m_3) \sin \theta_1 = d_{41}$$

$$d_{15} = l_1 (\alpha m_1 + m_2 + m_3) \cos \theta_1 = d_{51}$$

$$d_{22} = I_2 + l_2^2 (\beta^2 m_2 + m_3)$$

$$d_{23} = l_2 l_3 \gamma m_3 \cos(\theta_2 - \theta_3) = d_{32}$$

$$d_{24} = -l_2 (\beta m_2 + m_3) \sin \theta_2 = d_{42}$$

$$d_{25} = l_2 (\beta m_2 + m_3) \cos \theta_2 = d_{52}$$

$$d_{33} = I_3 + \gamma^2 l_3^2 m_3$$

$$d_{34} = -l_3 \gamma m_3 \sin \theta_3 = d_{43}$$

$$d_{35} = l_3 \gamma m_3 \cos \theta_3 = d_{53}$$

$$d_{44} = M$$

$$d_{45} = 0 = d_{54}$$

$$d_{55} = M$$

The centrifugal matrix C^{fl} contains the centrifugal terms and the coriolis terms, and can be found by calculating the Christoffel symbols c_{ijk} . The k,j -th element of the matrix C^{fl} is defined as:

$$c_{kj} = \sum_{i=1}^3 c_{ijk} \dot{\theta}_i = \sum_{i=1}^3 \frac{1}{2} \left\{ \frac{\partial d_{kj}}{\partial \theta_i} + \frac{\partial d_{ki}}{\partial \theta_j} - \frac{\partial d_{ij}}{\partial \theta_k} \right\} \dot{\theta}_i \quad (\text{A.6})$$

with the elements d_{ij} coming from the matrix D^{fl} . The elements of the centrifugal matrix become:

$$c_{11} = 0 = c_{22} = c_{33} = c_{44} = c_{55}$$

$$c_{12} = l_1 l_2 (\beta m_2 + m_3) \sin(\theta_1 - \theta_2) \dot{\theta}_2$$

$$c_{13} = l_1 l_3 \gamma m_3 \sin(\theta_1 - \theta_3) \dot{\theta}_3$$

$$c_{14} = 0 = c_{24} = c_{34} = c_{54}$$

$$c_{15} = 0 = c_{25} = c_{35} = c_{45}$$

$$c_{21} = -l_1 l_2 (\beta m_2 + m_3) \sin(\theta_1 - \theta_2) \dot{\theta}_1$$

$$\begin{aligned}
c_{23} &= l_2 l_3 \gamma m_3 \sin(\theta_2 - \theta_3) \dot{\theta}_3 \\
c_{31} &= -l_1 l_3 \gamma m_3 \sin(\theta_1 - \theta_3) \dot{\theta}_1 \\
c_{32} &= -l_2 l_3 \gamma m_3 \sin(\theta_2 - \theta_3) \dot{\theta}_2 \\
c_{41} &= -l_1 (\alpha m_1 + m_2 + m_3) \cos \theta_1 \dot{\theta}_1 \\
c_{42} &= -l_2 (\beta m_2 + m_3) \cos \theta_2 \dot{\theta}_2 \\
c_{43} &= -l_3 \gamma m_3 \cos \theta_3 \dot{\theta}_3 \\
c_{51} &= -l_1 (\alpha m_1 + m_2 + m_3) \sin \theta_1 \dot{\theta}_1 \\
c_{52} &= -l_2 (\beta m_2 + m_3) \sin \theta_2 \dot{\theta}_2 \\
c_{53} &= -l_3 \gamma m_3 \sin \theta_3 \dot{\theta}_3
\end{aligned}$$

The total potential energy of the robot can be calculated with:

$$U = \sum_{i=1}^3 m_i g Y_{G_i} \quad (\text{A.7})$$

which leads to the following gravitational torque vector:

$$G^{fl} = \begin{bmatrix} \frac{\partial U}{\partial \theta_1} \\ \frac{\partial U}{\partial \theta_2} \\ \frac{\partial U}{\partial \theta_3} \\ \frac{\partial U}{\partial X_F} \\ \frac{\partial U}{\partial Y_F} \end{bmatrix} = \begin{bmatrix} (\alpha m_1 + m_2 + m_3) g l_1 \cos \theta_1 \\ (\beta m_2 + m_3) g l_2 \cos \theta_2 \\ \gamma m_3 g l_3 \cos \theta_3 \\ 0 \\ Mg \end{bmatrix} \quad (\text{A.8})$$

The external torque vector can be found by giving the five DOF an infinitesimal variation and calculating the variation of work of the external forces δW :

$$\begin{aligned}
\delta W &= \tau_K (\delta \theta_1 - \delta \theta_2) + \tau_H (\delta \theta_2 - \delta \theta_3) \\
&= \tau_K \delta \theta_1 + (\tau_H - \tau_K) \delta \theta_2 - \tau_H \delta \theta_3
\end{aligned} \quad (\text{A.9})$$

Note that there are no forces acting on the foot point F, and only two torques can be exerted, namely the ones at the knee and the hip joint. The external torque vector becomes:

$$T^{fl} = \begin{bmatrix} Q_1 \\ Q_2 \\ Q_3 \\ Q_4 \\ Q_5 \end{bmatrix} = \begin{bmatrix} \tau_K \\ \tau_H - \tau_K \\ -\tau_H \\ 0 \\ 0 \end{bmatrix} \quad (\text{A.10})$$

The equations of motion become:

$$D^{fl} \ddot{q} + C^{fl} \dot{q} + G^{fl} = T^{fl} \quad (\text{A.11})$$

A.2 Stance phase

During the stance phase one gets analogously the dynamical model expressed in absolute angles:

$$q = \{\theta_1, \theta_2, \theta_3\}^T$$

Inertia matrix D^{st} :

$$\begin{aligned} d_{11} &= I_1 + l_1^2 (m_1 \alpha^2 + m_2 + m_3) \\ d_{12} &= l_1 l_2 (\beta m_2 + m_3) \cos(\theta_1 - \theta_2) = d_{21} \\ d_{13} &= l_1 l_3 \gamma m_3 \cos(\theta_1 - \theta_3) = d_{31} \\ d_{22} &= I_2 + l_2^2 (\beta^2 m_2 + m_3) \\ d_{23} &= l_2 l_3 \gamma m_3 \cos(\theta_2 - \theta_3) = d_{32} \\ d_{33} &= I_3 + \gamma^2 l_3^2 m_3 \end{aligned}$$

Centrifugal matrix C^{st} :

$$\begin{aligned} c_{11} &= 0 = c_{22} = c_{33} \\ c_{12} &= l_1 l_2 (\beta m_2 + m_3) \sin(\theta_1 - \theta_2) \dot{\theta}_2 \\ c_{13} &= l_1 l_3 \gamma m_3 \sin(\theta_1 - \theta_3) \dot{\theta}_3 \\ c_{21} &= -l_1 l_2 (\beta m_2 + m_3) \sin(\theta_1 - \theta_2) \dot{\theta}_1 \\ c_{23} &= l_2 l_3 \gamma m_3 \sin(\theta_2 - \theta_3) \dot{\theta}_3 \\ c_{31} &= -l_1 l_3 \gamma m_3 \sin(\theta_1 - \theta_3) \dot{\theta}_1 \\ c_{32} &= -l_2 l_3 \gamma m_3 \sin(\theta_2 - \theta_3) \dot{\theta}_2 \end{aligned}$$

Gravitational torque vector G^{st} :

$$G^{st} = \begin{bmatrix} (\alpha m_1 + m_2 + m_3) g l_1 \cos \theta_1 \\ (\beta m_2 + m_3) g l_2 \cos \theta_2 \\ \gamma m_3 g l_3 \cos \theta_3 \end{bmatrix} \quad (\text{A.12})$$

External torque vector T^{st} :

$$T^{st} = \begin{bmatrix} \tau_K - \tau_F \\ \tau_H - \tau_K \\ -\tau_H \end{bmatrix} \quad (\text{A.13})$$

The equations of motion become:

$$D^{st} \ddot{q} + C^{st} \dot{q} + G^{st} = T^{st} \quad (\text{A.14})$$

Appendix B

Kinetic energy loss during an impulsive impact

It will be shown that the loss of energy for a series of interconnected rigid bodies due to an impulsive impact is directly proportional to the velocity of the contact point before the impact. Note that in [Janssens, 1983] the prove has been made for a system of mass points.

Whenever having calculated the velocities of the joint after the shock with the impact model, one can calculate the amount of energy before and after the shock as follows:

$$K^- = \frac{1}{2}[\dot{q}^-]^T D[q][\dot{q}^-] \quad (\text{B.1})$$

$$K^+ = \frac{1}{2}[\dot{q}^+]^T D[q][\dot{q}^+] \quad (\text{B.2})$$

And then the amount of energy loss is found with

$$\Delta K = K^+ - K^- = \frac{1}{2}[\dot{q}^+]^T D[q][\dot{q}^+] - \frac{1}{2}[\dot{q}^-]^T D[q][\dot{q}^-] < 0 \quad (\text{B.3})$$

However, one can also express the amount of energy loss as a function of the percussions. To establish this relation a series of rigid bodies is considered, connected to each other by pin joints, as shown in figure B.1. Suppose that a percussion acts on the first link, in its end point F_1 , denoted by \bar{P}_1 . Suppose also that all links are connected in its end points, such that link i is connected to link $i - 1$ in end point F_i and connected to link $i + 1$ in end point F_{i+1} . Because of the percussion in F_1 , all links will have a percussion \bar{P}_i in its end point F_i , as well as as repercussion $-\bar{P}_{i+1}$ in its end point F_{i+1} . We will now determine the variation of translational energy and rotational energy of link i due to the shock.

- translational energy variation of link i

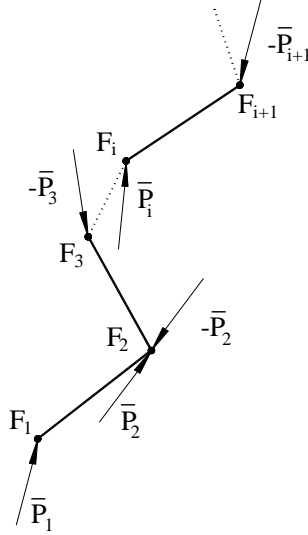


Figure B.1: Percussion on series of rigid bodies

Applying the linear momentum theorem to link i during the infinitesimal short collision gives:

$$\bar{P}_i - \bar{P}_{i+1} = m_i (\bar{v}_{G_i}^+ - \bar{v}_{G_i}^-) \quad (\text{B.4})$$

It is known that:

$$K_{i,tran}^- = \frac{1}{2} m_i (\bar{v}_{G_i}^-)^2 \quad (\text{B.5})$$

$$K_{i,tran}^+ = \frac{1}{2} m_i (\bar{v}_{G_i}^+)^2 \quad (\text{B.6})$$

From expression (B.4), one can write:

$$(\bar{P}_i - \bar{P}_{i+1}) \cdot \bar{v}_{G_i}^+ = m_i (\bar{v}_{G_i}^+ - \bar{v}_{G_i}^-) \cdot \bar{v}_{G_i}^+ \quad (\text{B.7})$$

$$(\bar{P}_i - \bar{P}_{i+1}) \cdot \bar{v}_{G_i}^- = m_i (\bar{v}_{G_i}^+ - \bar{v}_{G_i}^-) \cdot \bar{v}_{G_i}^- \quad (\text{B.8})$$

Expression (B.7) can be written as:

$$\begin{aligned} (\bar{P}_i - \bar{P}_{i+1}) \cdot \bar{v}_{G_i}^+ &= m_i (\bar{v}_{G_i}^+ \cdot \bar{v}_{G_i}^+ - \bar{v}_{G_i}^- \cdot \bar{v}_{G_i}^+) \\ &= \frac{1}{2} m_i (\bar{v}_{G_i}^+)^2 + \frac{1}{2} m_i (\bar{v}_{G_i}^-)^2 \\ &\quad - m_i \bar{v}_{G_i}^- \cdot \bar{v}_{G_i}^+ + \frac{1}{2} m_i (\bar{v}_{G_i}^+)^2 - \frac{1}{2} m_i (\bar{v}_{G_i}^-)^2 \\ &= K_{i,tran}^+ - K_{i,tran}^- + \frac{1}{2} (\bar{v}_{G_i}^+ - \bar{v}_{G_i}^-)^2 \end{aligned} \quad (\text{B.9})$$

and analogue calculations on expression (B.8) yield:

$$(\bar{P}_i - \bar{P}_{i+1}) \cdot \bar{v}_{G_i}^- = K_{i,tran}^+ - K_{i,tran}^- - \frac{1}{2} (\bar{v}_{G_i}^+ - \bar{v}_{G_i}^-)^2 \quad (\text{B.10})$$

So if the sum of equations (B.9) and (B.10) is made:

$$\begin{aligned} \Delta K_{i,tran} &= \frac{1}{2} (\bar{P}_i - \bar{P}_{i+1}) \cdot (\bar{v}_{G_i}^+ + \bar{v}_{G_i}^-) \\ &= \frac{1}{2} [\bar{P}_i \cdot (\bar{v}_{G_i}^+ + \bar{v}_{G_i}^-) - \bar{P}_{i+1} \cdot (\bar{v}_{G_i}^+ + \bar{v}_{G_i}^-)] \end{aligned} \quad (\text{B.11})$$

Since link i is a rigid body, one can write:

$$\begin{aligned} \bar{v}_{G_i} &= \bar{v}_{F_i} + \overline{G_i F_i} \times \bar{\omega}_i \\ &= \bar{v}_{F_{i+1}} + \overline{G_i F_{i+1}} \times \bar{\omega}_i \end{aligned} \quad (\text{B.12})$$

with $\bar{\omega}_i$ being the angular velocity of link i.

So now $\Delta K_{i,tran}$ for link i becomes:

$$\begin{aligned} \Delta K_{i,tran} &= \frac{1}{2} \bar{P}_i \cdot (\bar{v}_{F_i}^+ + \bar{v}_{F_i}^-) - \frac{1}{2} \bar{P}_{i+1} \cdot (\bar{v}_{F_{i+1}}^+ + \bar{v}_{F_{i+1}}^-) \\ &\quad + \frac{1}{2} \bar{P}_i \cdot [\overline{G_i F_i} \times (\bar{\omega}_i^+ + \bar{\omega}_i^-)] - \frac{1}{2} \bar{P}_{i+1} \cdot [\overline{G_i F_{i+1}} \times (\bar{\omega}_i^+ + \bar{\omega}_i^-)] \end{aligned} \quad (\text{B.13})$$

• rotational energy variation of link i

Applying the angular momentum theorem to link i during the collision gives:

$$\bar{\mu}_{G_i}^+ - \bar{\mu}_{G_i}^- = \overline{G_i F_i} \times \bar{P}_i - \overline{G_i F_{i+1}} \times \bar{P}_{i+1} \quad (\text{B.14})$$

which can also be written as:

$$I_i (\bar{\omega}_i^+ - \bar{\omega}_i^-) = \overline{G_i F_i} \times \bar{P}_i - \overline{G_i F_{i+1}} \times \bar{P}_{i+1} \quad (\text{B.15})$$

with I_i being the moment of Inertia with respect to an axis perpendicular to the working plane and placed in G_i .

It is known that:

$$K_{i,rot}^- = \frac{1}{2} I_i (\bar{\omega}_i^-)^2 \quad (\text{B.16})$$

$$K_{i,rot}^+ = \frac{1}{2} I_i (\bar{\omega}_i^+)^2 \quad (\text{B.17})$$

Now performing analogue calculations on (B.15) as in the preceding paragraph yields:

$$\begin{aligned}\Delta K_{i,rot} &= \frac{1}{2} (\overline{G_i F_i} \times \bar{P}_i - \overline{G_i F_{i+1}} \times \bar{P}_{i+1}) \cdot (\bar{\omega}_i^+ + \bar{\omega}_i^-) \\ &= \frac{1}{2} (\overline{G_i F_i} \times \bar{P}_i) \cdot (\bar{\omega}_i^+ + \bar{\omega}_i^-) - \frac{1}{2} (\overline{G_i F_{i+1}} \times \bar{P}_{i+1}) \cdot (\bar{\omega}_i^+ + \bar{\omega}_i^-)\end{aligned}\tag{B.18}$$

• **total energy variation**

When now calculating the total energy variation of link i :

$$\Delta K_i = \Delta K_{i,tran} + \Delta K_{i,rot} = \frac{1}{2} \bar{P}_i \cdot (\bar{v}_{F_i}^+ + \bar{v}_{F_i}^-) - \frac{1}{2} \bar{P}_{i+1} \cdot (\bar{v}_{F_{i+1}}^+ + \bar{v}_{F_{i+1}}^-)\tag{B.19}$$

since the other terms compensate each other.

Finally, when determining the total variation of energy of all the links, it is seen that all the percussions and reperussions compensate each other, except for the percussion on link 1:

$$\Delta K = \frac{1}{2} \bar{P}_1 \cdot (\bar{v}_{F_1}^+ + \bar{v}_{F_1}^-)\tag{B.20}$$

Appendix C

Applying the mean value theorem for integration

Consider the second integral on the rhs of equation (4.3), resulting from integrating the angular momentum equation with respect to G during the flight phase:

$$\int_0^{T^{fl}} A_3 \dot{\theta}_3 dt \quad (C.1)$$

In order to be able to apply the mean value theorem for integration, $\dot{\theta}_3$ has to be a positive function. When this is not the case, the integral can be rewritten as follows:

$$\int_0^{T^{fl}} A_3 \dot{\theta}_3 dt = \int_0^{T^{fl}} A_3 (\dot{\theta}_3 - \dot{\theta}_3^{min}) dt + \int_0^{T^{fl}} A_3 \dot{\theta}_3^{min} dt \quad (C.2)$$

such that $\dot{\theta}_3 - \dot{\theta}_3^{min}$ becomes a positive function and the mean value theorem for integration can be applied (note that $\dot{\theta}_3^{min} < 0$ whenever $\dot{\theta}_3$ is not a positive function):

$$\int_0^{T^{fl}} A_3 \dot{\theta}_3 dt = A_3(\kappa) \int_0^{T^{fl}} (\dot{\theta}_3 - \dot{\theta}_3^{min}) dt + \dot{\theta}_3^{min} \int_0^{T^{fl}} A_3 dt \quad (0 < \kappa < T^{fl}) \quad (C.3)$$

and further:

$$\int_0^{T^{fl}} A_3 \dot{\theta}_3 dt = A_3(\kappa) \Delta\theta_3^{fl} - A_3(\kappa) \dot{\theta}_3^{min} T^{fl} + \dot{\theta}_3^{min} \int_0^{T^{fl}} A_3 dt \quad (0 < \kappa < T^{fl}) \quad (C.4)$$

Finally applying the mean value theorem to the last integral leads to:

$$\int_0^{T^{fl}} A_3 \dot{\theta}_3 dt = A_3(\kappa) \Delta \theta_3^{fl} + (A_3(\eta) - A_3(\kappa)) \dot{\theta}_3^{min} T^{fl} \quad (0 < \kappa, \eta < T^{fl}) \quad (C.5)$$

In the special case where A_3 is not submitted to significant variations during the flight phase, one obtains:

$$\int_0^{T^{fl}} A_3 \dot{\theta}_3 dt \approx A_3(\kappa) \Delta \theta_3^{fl} \quad (0 < \kappa < T^{fl}) \quad (C.6)$$

Note that in the case where A_3 does vary significantly, one can use a polynomial function to approximate the upper body behaviour, such that the integral (C.1) can be calculated numerically.

Appendix D

Dynamic model of the walking biped

The dynamic model will be established for a single support phase. The equations of motion are:

$$D\ddot{q} + C\dot{q} + G = T \quad (\text{D.1})$$

with (see figure 5.1):

$$q = (\theta_{1S}, \theta_{2S}, \theta_3, \theta_{2A}, \theta_{1A})^T = (\theta_1, \theta_2, \theta_3, \theta_4, \theta_5)^T \quad (\text{D.2})$$

Inertia matrix D :

$$\begin{aligned} d_{11} &= I_1 + l_1^2 [(1 + \alpha^2) m_1 + 2m_2 + m_3] \\ d_{12} &= l_1 l_2 [m_1 + (1 + \beta) m_2 + m_3] \cos(\theta_1 - \theta_2) = d_{21} \\ d_{13} &= l_1 l_3 \gamma m_3 \cos(\theta_1 - \theta_3) = d_{31} \\ d_{14} &= l_1 l_2 [(\beta - 1) m_2 - m_1] \cos(\theta_1 - \theta_4) = d_{41} \\ d_{15} &= l_1^2 (\alpha - 1) m_1 \cos(\theta_1 - \theta_5) = d_{51} \\ d_{22} &= I_2 + l_2^2 [m_1 + (1 + \beta^2) m_2 + m_3] \\ d_{23} &= l_2 l_3 \gamma m_3 \cos(\theta_2 - \theta_3) = d_{32} \\ d_{24} &= l_2^2 [(\beta - 1) m_2 - m_1] \cos(\theta_2 - \theta_4) = d_{42} \\ d_{25} &= l_1 l_2 (\alpha - 1) m_1 \cos(\theta_2 - \theta_5) = d_{52} \\ d_{33} &= I_3 + \gamma^2 l_3^2 m_3 \\ d_{34} &= 0 = d_{43} \\ d_{35} &= 0 = d_{53} \end{aligned}$$

$$d_{44} = I_2 + l_2^2 [m_1 + (1 - \beta)^2 m_2]$$

$$d_{45} = l_1 l_2 (1 - \alpha) m_1 \cos(\theta_4 - \theta_5) = d_{54}$$

$$d_{55} = I_1 + l_1^2 m_1 (1 - \alpha)^2$$

Centrifugal matrix C :

$$c_{11} = 0 = c_{22} = c_{33} = c_{44} = c_{55}$$

$$c_{12} = l_1 l_2 [m_1 + (1 + \beta)m_2 + m_3] \sin(\theta_1 - \theta_2) \dot{\theta}_2$$

$$c_{13} = l_1 l_3 \gamma m_3 \sin(\theta_1 - \theta_3) \dot{\theta}_3$$

$$c_{14} = -l_1 l_2 [m_1 + (1 - \beta)m_2] \sin(\theta_1 - \theta_4) \dot{\theta}_4$$

$$c_{15} = -l_1^2 (1 - \alpha) m_1 \sin(\theta_1 - \theta_5) \dot{\theta}_5$$

$$c_{21} = -l_1 l_2 [m_1 + (1 + \beta)m_2 + m_3] \sin(\theta_1 - \theta_2) \dot{\theta}_1$$

$$c_{23} = l_2 l_3 \gamma m_3 \sin(\theta_2 - \theta_3) \dot{\theta}_3$$

$$c_{24} = -l_2^2 [m_1 + (1 - \beta)m_2] \sin(\theta_2 - \theta_4) \dot{\theta}_4$$

$$c_{25} = -l_1 l_2 (1 - \alpha) m_1 \sin(\theta_2 - \theta_5) \dot{\theta}_5$$

$$c_{31} = -l_1 l_3 \gamma m_3 \sin(\theta_1 - \theta_3) \dot{\theta}_1$$

$$c_{32} = -l_2 l_3 \gamma m_3 \sin(\theta_2 - \theta_3) \dot{\theta}_2$$

$$c_{34} = 0 = c_{35} = c_{43} = c_{53}$$

$$c_{41} = l_1 l_2 [m_1 + (1 - \beta)m_2] \sin(\theta_1 - \theta_4) \dot{\theta}_1$$

$$c_{42} = l_2^2 [m_1 + (1 - \beta)m_2] \sin(\theta_2 - \theta_4) \dot{\theta}_2$$

$$c_{45} = l_1 l_2 (1 - \alpha) m_1 \sin(\theta_4 - \theta_5) \dot{\theta}_5$$

$$c_{51} = l_1^2 (1 - \alpha) m_1 \sin(\theta_1 - \theta_5) \dot{\theta}_1$$

$$c_{52} = l_1 l_2 (1 - \alpha) m_1 \sin(\theta_2 - \theta_5) \dot{\theta}_2$$

$$c_{54} = -l_1 l_2 (1 - \alpha) m_1 \sin(\theta_4 - \theta_5) \dot{\theta}_4$$

Gravitational torque vector G :

$$G = \begin{bmatrix} [(\alpha + 1)m_1 + 2m_2 + m_3]gl_1 \cos \theta_1 \\ [m_1 + (\beta + 1)m_2 + m_3]gl_2 \cos \theta_2 \\ \gamma m_3 gl_3 \cos \theta_3 \\ [-m_1 + (\beta - 1)m_2]gl_2 \cos \theta_4 \\ (\alpha - 1)m_1 gl_1 \cos \theta_5 \end{bmatrix} \quad (\text{D.3})$$

External torque vector T (see figure 5.2):

$$T = \begin{bmatrix} T_{K_S} - T_{F_S} \\ T_{H_S} - T_{K_S} \\ -T_{H_S} - T_{H_A} \\ T_{H_A} - T_{K_A} \\ T_{K_A} \end{bmatrix} \quad (\text{D.4})$$

Appendix E

Angular momentum during a single support phase

Recall the equations of motion for the biped (see appendix D):

$$D\ddot{q} + C\dot{q} + G = T \quad (\text{E.1})$$

with (see figure 5.1):

$$q = (\theta_{1S}, \theta_{2S}, \theta_3, \theta_{2A}, \theta_{1A})^T = (\theta_1, \theta_2, \theta_3, \theta_4, \theta_5)^T \quad (\text{E.2})$$

With our choice of coordinates q_i , making the sum of all 5 equations results in the angular momentum equation with respect to the supporting foot. The resulting equation can be written as:

$$\sum_{i=1}^5 A_i \ddot{\theta}_i + \sum_{i=1}^5 \dot{A}_i \dot{\theta}_i + \sum_{i=1}^5 g_i = -T_F \quad (\text{E.3})$$

with:

$$A_i = \sum_{j=1}^5 d_{ji} \quad (\text{E.4})$$

where the d_{ij} are the elements from the inertia matrix D, and the g_i those from the gravity torque vector. Further one can write:

$$\frac{d}{dt} \left(\sum_{i=1}^5 A_i \dot{\theta}_i \right) + \sum_{i=1}^5 g_i = -T_F \quad (\text{E.5})$$

or:

$$\dot{\mu}_{FS} = -T_F - MgX_G \quad (\text{E.6})$$

with the following kinematic expression for μ_{F_S} :

$$\begin{aligned}\mu_{F_S} &= \sum_{i=1}^5 A_i \dot{\theta}_i \\ &= A_{1S} \dot{\theta}_{1S} + A_{2S} \dot{\theta}_{2S} + A_3 \dot{\theta}_3 + A_{2A} \dot{\theta}_{2A} + A_{1A} \dot{\theta}_{1A}\end{aligned}\tag{E.7}$$

with

$$(A_{1S}, A_{2S}, A_3, A_{2A}, A_{1A})^T = (A_1, A_2, A_3, A_4, A_5)^T\tag{E.8}$$

Eventually the kinematic expression for the angular momentum can be written as:

$$\begin{aligned}\mu_{F_S} &= A_3 \dot{\theta}_3 + (A_{1S}, A_{2S}) \dot{Z}_S + (A_{1A}, A_{2A}) \dot{Z}_A \\ &= A_3 \dot{\theta}_3 + A_S \dot{Z}_S + A_A \dot{Z}_A\end{aligned}\tag{E.9}$$

with

$$Z_S = \begin{pmatrix} \theta_{1S} \\ \theta_{2S} \end{pmatrix} \quad \text{and} \quad Z_A = \begin{pmatrix} \theta_{1A} \\ \theta_{2A} \end{pmatrix}\tag{E.10}$$

Bibliography

- Ahmadi, M. and Buehler, M. [1995]. A control strategy for stable passive running, *Proceedings International Conference on Intelligent Robots and Systems '95*, Pittsburgh, Pennsylvania, USA, pp. 152–157.
- Ahmadi, M. and Buehler, M. [1997]. Stable control of a simulated one-legged running robot with hip and leg compliance, *IEEE Transactions on Robotics and Automation* **13**(1): 96–103.
- Ahmadi, M. and Buehler, M. [1999]. The ARL monopod II running robot: Control and energetics, *Proceedings IEEE International Conference on Robotics and Automation*, Detroit, Michigan, USA, pp. 1689–1694.
- Bauby, C. and Kuo, A. [2000]. Active control of lateral balance in human walking, *Journal of Biomechanics* **33**: 1433–1440.
- Beletskii, V., Berbyuk, V. and Samsonov, V. [1982]. Parametric optimization of motions of a bipedal walking robot, *Mechanics of Solids* **17**(1): 24–35.
- Blajer, W. and Schiehlen, W. [1992]. Walking without impacts as a motion/force control problem, *Journal of Dynamic Systems, Measurement and Control* **114**: 660–665.
- Brown, B. and Zeglin, G. [1998]. The bow leg hopping robot, *Proceedings of the 1998 IEEE International Conference on Robotics and Automation*, Leuven, Belgium, pp. 781–786.
- Cabodevilla, G., Chaillet, N. and Abba, G. [1995]. Energy-minimized gait for a biped robot, *Proceedings Fachgespräch Autonome Mobile Systemer*, pp. 90–99.
- Capi, G., Nasu, Y., Barolli, L. and Mitobe, K. [2003]. Real time gait generation for autonomous humanoid robots: A case study for walking, *Robotics and Autonomous Systems* **42**: 107–116.
- Channon, P., Hopkins, S. and Pham, D. [1992]. Derivation of optimal walking motion for a bipedal walking robot, *Robotica* **10**: 165–172.
- Chevallereau, C. [2002]. Control for the running of a planar biped, *in* P. Bidaud

and F. Ben Amar (eds), *Proceedings of 5th International Conference on Climbing and Walking Robots and the Support Technologies for Mobile Machines (CLAWAR 2002)*, Professional Engineering Publishing, pp. 417–425.

Chevallereau, C. and Aoustin, Y. [1999]. Optimal running trajectories for a biped, in G. Virk, M. Randall and D. Howard (eds), *Proceedings 2nd International Conference on Climbing and Walking Robots and the Support Technologies for Mobile Machines (CLAWAR '99)*, Professional Engineering Publishing, pp. 559–570.

Chevallereau, C. and Aoustin, Y. [2001]. Optimal reference trajectories for walking and running of a biped robot, *Robotica* **19**: 557–569.

Crawford, L. and Sastry, S. [1995]. Biological motor control approaches for a planar diver, *Proceedings 34th Conference on Decision and Control*, New Orleans, USA, pp. 3881–3886.

Daberkow, A., Gao, J. and Schiehlen, W. [1990]. Walking without impacts, *Proceedings 8th Symposium on Theory and Practice of Robots and Manipulators*, Cracow, Poland, pp. 339–347.

Daerden, F. [1999]. *Conception and Realization of Pleated Pneumatic Artificial Muscles and Their Use as Compliant Actuation Elements*, PhD thesis, Vrije Universiteit Brussel.

De Luca, A. and Oriolo, G. [1995]. *Modeling and Control of Nonholonomic Mechanical Systems*, Springer Verlag, Wien, chapter 7, pp. 277–342.

De Man, H., Lefeber, D., Daerden, F. and Fagniet, E. [1996]. Simulation of a new control algorithm for a one-legged hopping robot (using the multibody code Mechanica Motion), *Proceedings International Workshop on Advanced Robotics and Intelligent Machines*, Manchester, UK, pp. 1–13 (paper nr8).

De Man, H., Lefeber, D. and Vermeulen, J. [1997]. Control on irregular terrain of a hopping robot with one articulated leg, *Proceedings 8th International Conference on Advanced Robotics: Workshop II: New Approaches on Dynamic Walking and Climbing Machines*, Monterey, California, USA, pp. 72–76.

De Man, H., Lefeber, D. and Vermeulen, J. [1998a]. Design and control of a one-legged robot hopping on irregular terrain, *Proceedings Euromech 375: Biology and Technology of Walking*, Munich, Germany, pp. 173–180.

De Man, H., Lefeber, D. and Vermeulen, J. [1998b]. Design and control of a robot with one articulated leg for locomotion on irregular terrain, in A. Morecki, G. Bianchi and M. Wojtyra (eds), *Proceedings 12th Symposium on Theory and Practice of Robots and Manipulators*, Springer Wien New York, Paris, France, pp. 417–424.

De Man, H., Lefeber, D. and Vermeulen, J. [1998c]. Hopping on irregular terrain with one articulated leg, *Proceedings 29th International Symposium on Robotics*, Birmingham, United Kingdom.

Dubowsky, S. and Papadopoulos, E. [1993]. The kinematics, dynamics, and control of free-flying and free-floating space robotic systems, *IEEE Transactions on*

Robotics and Automation **9**(5): 531–543.

Eberhart, H. [1976]. Physical principles of locomotion, in R. Herman, S. Grill, P. Stein and D. Stuart (eds), *Proceedings of International Conference on Neural Control of Locomotion*, Plenum Press, pp. 1–11.

Fowble, J. and Kuo, A. [1996]. Stability and control of passive locomotion in 3D, *Proceedings of the Conference on Biomechanics and Neural Control of Movement*.

François, C. and Samson, C. [1997]. Energy efficient control of the planar one-legged hopper, *Proceedings 5th IFAC Symposium on Robot Control*, Nantes, France, pp. 397–404.

François, C. and Samson, C. [1998]. A new approach to the control of the planar one-legged hopper, *The International Journal of Robotics Research* **17**(11): 1150 – 1166.

Furusho, J. and Sano, A. [1990]. Sensor-based control of a nine-link biped, *The International Journal of Robotics Research (Special Issue on Legged Locomotion)* **9**(2): 83–98.

Godhavn, J. M., Balluchi, A., Crawford, L. and Sastry, S. S. [1997]. Control of nonholonomic systems with drift terms, *Technical Report UCB/ERL M97/1*, Electronics Research Laboratory, College of Engineering, University of California, Berkeley, CA-94720, California, USA.

Gokan, M., Yamafuji, K. and Yoshinada, H. [1994]. Postural stabilization and motion control of the rope-hopping robot, *JSME International Journal Series C* **37**(4): 739–747.

Goldstein, H., Poole Jr., C. and Safko, J. [2000]. *Classical Mechanics*, 3rd edn, Addison Wesley.

Goswami, A. [1999]. Postural stability of biped robots and the foot-rotation indicator (FRI) point, *The International Journal of Robotics Research* **18**(6): 523–533.

Gregorio, P., Ahmadi, M. and Buehler, M. [1994]. Experiments with an electrically actuated planar hopping robot, *Experimental Robotics III* pp. 269–281.

Gregorio, P., Ahmadi, M. and Buehler, M. [1997]. Design, control, and energetics of an electrically actuated legged robot, *IEEE Transactions on Systems, Man and Cybernetics* **27B**(4): 626–634.

Hamming, R. [1989]. *Digital Filters*, Prentice-Hall International, Inc., London.

Hardarson, F. [1997]. Locomotion for difficult terrain, *Technical report*, Mechatronics Division, Department of Machine Design, Royal Institute of technology, Stockholm, Sweden.

Hardt, M., Kreutz-Delgado, K., Helton, J. and Stryk, O. V. [1999]. Obtaining minimum energy biped walking gaits with symbolic models and numerical optimal control, *Workshop - Biomechanics Meets Robotics, Modelling and Simulation of Motion*, Heidelberg, Germany, pp. 1–19.

- Helferty, J., Collins, J. and Kam, M. [1989]. A neural network learning strategy for the control of a one-legged hopping machine, *Proceedings IEEE International Conference on Robotics and Automation*, Scottsdale, USA, pp. 1604–1609.
- Hemami, H. and Golliday Jr., C. [1977]. The inverted pendulum and biped stability, *Mathematical Biosciences* **34**: 95–110.
- Hemami, H. and Wyman, B. [1979]. Modeling and control of constrained dynamic systems with application to biped locomotion in the frontal plane, *IEEE Transactions on Automatic Control* **24**(4): 526–535.
- Hirai, K., Hirose, M., Haikawa, Y. and Takenaka, T. [1998]. The development of honda humanoid robot, *Proceedings of the 1998 IEEE International Conference on Robotics and Automation*, pp. 1321–1326.
- Hodgins, J. [1989]. *Legged Robots on Rough Terrain: Experiments in Adjusting Step Length*, PhD thesis, Carnegie Mellon University.
- Hodgins, J., Koechling, J. and Raibert, M. [1986]. Running experiments with a planar biped, in Giralt and Ghallab (eds), *Proceedings 3rd International Symposium on Robotics Research*, MIT Press, pp. 349–355.
- Hodgins, J. and Raibert, M. [1990]. Biped gymnastics, *The International Journal of Robotics Research (Special Issue on Legged Locomotion)* **9**(2): 115–132.
- Huang, Q., Yokoi, K., Kajita, S., Kaneko, K., Arai, H., Koyachi, N. and Tanie, K. [2001]. Planning walking patterns for a biped robot, *IEEE Transactions on Robotics and Automation* **17**(3): 280–289.
- Hurmuzlu, Y. [1993]. Dynamics of bipedal gait part I: Objective functions and the contact event of a planar five-link biped, *Journal of Applied Mechanics* **60**: 331–336.
- Hyon, S., Emura, T. and Mita, T. [2003]. Dynamics-based control of a one-legged hopping robot, *Journal of Systems and Control Engineering* **217**(2): 83–98.
- Ito, S., Asano, H. and Kawasaki, H. [2003]. A balance control in biped double support phase based on center of pressure of ground reaction forces, *Preprints of the 7th IFAC Symposium on Robot Control*, Wroclaw, Poland, pp. 205–210.
- Janssens, P. [1983]. *Mécanique Rationnelle*, Vol. 2, 2nd edn, chapter 13 (Les Chocs Dans les Systèmes de Solides), pp. 298 – 321.
- Janssens, P. and Lefeber, D. [1984]. *Rationele Mechanica*, Vrije Universiteit Brussel.
- Jansson, P. and Grahn, R. [1995]. *Engineering Mechanics: Statics*, Vol. 1, Paramount Publishing International.
- Kagami, S., Kitagawa, T., Nishiwaki, K., Sugihara, T., Inaba, M. and Inoue, H. [2002]. A fast dynamically equilibrated walking trajectory generation method of humanoid robot, *Autonomous Robots* **12**: 71–82.
- Kajita, S., Kanehiro, F., Kaneko, K., Fujiwara, K., Yokoi, K. and Hirukawa, H. [2002]. A realtime pattern generator for biped walking, *Proceedings of the 2002 IEEE International Conference on Robotics and Automation*, Washington, DC,

pp. 31–37.

Kajita, S., Matsumoto, O. and Saigo, M. [2001]. Real-time 3D walking pattern generation for a biped robot with telescopic legs, *Proceedings of the 2001 IEEE International Conference on Robotics and Automation*, Seoul, Korea, pp. 2299–2306.

Kajita, S., Nagasaki, T., Yokoi, K., Kaneko, K. and Tanie, K. [2002]. Running pattern generation for a humanoid robot, *Proceedings of the 2002 IEEE International Conference on Robotics and Automation*, pp. 2755–2761.

Kajita, S. and Tani, K. [1991]. Study of dynamic biped locomotion on rugged terrain - derivation and application of the linear inverted pendulum mode, *Proceedings 1991 IEEE International Conference on Robotics and Automation*, Sacramento, California, USA, pp. 1405–1411.

Koditschek, D. and Bühler, M. [1991]. Analysis of a simplified hopping robot, *The International Journal of Robotics Research* **10**(6): 587–605.

Lapshin, V. [1983]. Dynamics and control of motion of a hopping robot, *Mechanics of Solids* **18**(5): 40–49.

Lapshin, V. [1991a]. Control of vertical and horizontal motion of a jumping machine, *Mechanics of Solids* **26**(3): 35–42.

Lapshin, V. [1991b]. Motion control of a legged machine in the supportless phase of hopping, *The International Journal of Robotics Research* **10**(4): 327–337.

Lapshin, V. [1992]. Vertical and horizontal motion control of a one-legged hopping machine, *The International Journal of Robotics Research* **11**(5): 491–498.

Larin, V. [1979]. Control of a jumping robot I: Choice of programmed trajectory, *Mechanics of Solids* **14**(6): 22–26.

Larin, V. [1980]. Control of a jumping robot II: Stabilization of programmed motion, *Mechanics of Solids* **15**(1): 32–40.

Lebaudy, A., Prosser, J. and Kam, M. [1993]. Control algorithms for a vertically-constrained one-legged hopping machine, *Proceedings 32nd Conference on Decision and Control*, San Antonio, Texas, USA, pp. 2688–2693.

Lee, W. and Raibert, M. [1991]. Control of hoof rolling in an articulated leg, *Proceedings 1991 IEEE International Conference on Robotics and Automation*, Sacramento, California, USA, pp. 1386–1391.

Lefeber, D., De Man, H., Daerden, F. and Fagniet, E. [1996]. A new control strategy for dynamically balanced machines, *Proceedings 6th International Symposium on Measurement and Control in Robotics*, Brussels, Belgium, pp. 382–387.

Li, Z. and He, J. [1990]. An energy perturbation approach to limit cycle analysis in legged locomotion systems, *Proceedings 29th Conference on Decision and Control*, Honolulu, Hawaii, USA, pp. 1989–1994.

Li, Z. and Montgomery, R. [1990]. Dynamics and optimal control of a legged robot in flight phase, *Proceedings IEEE International Conference on Robotics and*

Automation, Cincinnati, USA, pp. 1816–1820.

Ma, B. and Wu, Q. [2002]. Parametric study of repeatable gait for a planar five-link biped, *Robotica* **20**: 493–498.

Matsuoka, K. [1979]. A model of repetitive hopping movements in man, *Proceedings 5th World Congress on Theory of Machines and Mechanisms*, pp. 1168–1171.

Matsuoka, K. [1980]. A mechanical model of repetitive hopping movements, *Biomechanisms* **5**: 251–258.

M'Closkey, R. and Burdick, J. [1991]. An analytical study of simple hopping robots with vertical and forward motion, *Proceedings 1991 IEEE International Conference on Robotics and Automation*, Sacramento, California, USA, pp. 1392–1397.

M'Closkey, R. and Burdick, J. [1993]. Periodic motions of a hopping robot with vertical and forward motion, *International Journal of Robotics Research* **12**(3): 197–218.

McMahon, T., Valiant, G. and Frederick, E. [1987]. Groucho running, *Journal of Applied Physiology* **62**: 2326–2337.

Mehrandezh, M., Surgenor, B. and Dean, S. [1995]. Jumping height control of an electrically actuated, one-legged hopping robot: Modelling and simulation, *Proceedings 34th IEEE Conference on Decision and Control*, New Orleans, LA, USA, pp. 1016–1020.

Mita, T., Yamaguchi, T., Kashiwase, T. and Kawase, T. [1984]. Realization of a high speed biped using modern control theory, *International Journal of Control* **40**(1): 107–119.

Mitobe, K., Capi, G. and Nasu, Y. [2004]. A new control method for walking robots based on angular momentum, *Mechatronics* **14**: 163–174.

Mitobe, K., Mori, N., Nasu, Y. and Adachi, N. [1997]. Control of biped walking robot during the double support phase, *Autonomous Robots* **4**: 287–296.

Nakamura, Y. [1991]. *Advanced Robotics: Redundancy and Optimization*, Addison-Wesley Publishing Company.

Narikiyo, T. and Ito, M. [1985]. Control of a biped locomotion system in a double support phase, *Robotica* **3**: 73–77.

Nikkhah, M., Rostami, M. and Towhidkhah, F. [2003]. Sagittal optimal gait of biped robot during double support phase (DSP), *Proceedings 2nd International Conference on Mechatronics and Information Technology (ICMIT 2003)*, Jecheon, Korea, pp. 225–230.

Ono, K. and Liu, R. [2002]. Optimal biped walking locomotion solved by trajectory planning method, *Transactions of the ASME Journal of Dynamic Systems, Measurement and Control* **124**: 554–565.

Ostrowski, J. and Burdick, J. [1993]. Designing feedback algorithms for controlling the periodic motions of legged robots, *Proceedings 1993 IEEE International*

Conference on Robotics and Automation., pp. 260–266.

Papantoniou, K. [1991a]. Control architecture for an electrical, actively balanced multi-leg robot, based on experiments with a planar one-leg machine, *Proceedings IFAC Robot Control*, Vienna, Austria, pp. 283–290.

Papantoniou, K. [1991b]. Experiments concerning the power efficiency during locomotion of an electrical, actively balanced one-leg planar robot, *Proceedings 4th World Conference on Robotics Research*, Pittsburgh, PA, USA, pp. 5/1–5/16.

Park, J. and Cho, H. [2000]. An on-line trajectory modifier for the base link of biped robots to enhance locomotion stability, *Proceedings of the 2000 IEEE International Conference on Robotics and Automation*, San Francisco, California, USA, pp. 3353–3358.

Park, J. and Chung, H. [1999]. ZMP compensation by on-line trajectory generation for biped robots, *Proceedings of IEEE Conference on Systems, Man and Cybernetics (SMC'99)*, Tokyo, Japan, pp. 960–965 (IV).

Park, J. and Kim, K. [1998]. Biped robot walking using gravity-compensated inverted pendulum mode and computed torque control, *Proceedings of the 1998 IEEE International Conference on Robotics and Automation*, pp. 3528–3533.

Park, J. and Rhee, Y. [1998]. ZMP trajectory generation for reduced trunk motions of biped robots, *Proceedings of IEEE/RSJ International Conference on Intelligent Robots and Systems (IROS'98)*, Victoria, Canada, pp. 90–95.

Pfeiffer, F., Löffler, K. and Gienger, M. [2003]. Humaoid robots, in G. Muscato and D. Longo (eds), *Proceedings of the 6th International Conference on Climbing and Walking Robots and the Support Technologies for Mobile Machines (CLAWAR 2003)*, Professional Engineering Publishing, Catania, Italy, pp. 505–516.

Playter, R. and Raibert, M. [1992]. Control of a biped somersault in 3D, *Proceedings 1992 IEEE/RSJ International Conference on Intelligent Robots and Systems*, Raleigh, NC, USA, pp. 582–589.

Pratt, J. [2000]. *Exploiting Inherent Robustness and Natural Dynamics in the Control of Bipedal Walking Robots*, PhD thesis, Massachusetts Institute of Technology.

Prosser, J. and Kam, M. [1992a]. Height control of a one-legged hopping machine using a near-inverse model, *Proceedings 1992 Conference on Information, Science and Systems*, Princeton, NJ, USA, pp. 995–1002.

Prosser, J. and Kam, M. [1992b]. Vertical control for a mechanical model of the one-legged hopping machine, *Proceedings 1st IEEE Conference on Control Applications*, Princeton, USA, pp. 136–141.

Rad, H., Gregorio, P. and Buehler, M. [1993]. Design, modeling and control of a hopping robot, *Proceedings 1993 IEEE/RSJ International Conference on Intelligent Robots and Systems*, Yokohama, Japan, pp. 1778–1785.

Raibert, M. [1986]. *Legged Robots That Balance*, MIT Press, Cambridge, Mas-

sachusetts.

Raibert, M. [1990]. Trotting, pacing and bounding by a quadruped robot, *Journal of Biomechanics* **23**(1): 79–98.

Raibert, M. and Brown Jr., H. [1984]. Experiments in balance with a 2D one-legged hopping machine, *Journal of Dynamic Systems, Measurement and Control* **106**: 75–81.

Raibert, M., Brown Jr., H. and Chepponis, M. [1984]. Experiments in balance with a 3D one-legged hopping machine, *The International Journal of Robotics Research* **3**(2): 75–92.

Raibert, M., Chepponis, M. and Brown Jr., H. [1986]. Running on four legs as though they were one, *IEEE Transactions on Robotics and Automation* **2**(2): 70–82.

Ramey, M. [1973]. Significance of angular momentum in long jumping, *The Research Quarterly* **44**(4): 488–497.

Regele, R., Bott, W. and Levi, P. [2003]. Pro-robot: Predictions for the future development of humanoid robots, *Robocup 2003 Symposium*, Padova, Italy.

Ridderström, C. [1999]. Legged locomotion control - a literature study, *Technical report*, Mechatronics Lab, Department of Machine Design, Royal Institute of technology, Stockholm, Sweden.

Rose, J. and Gamble, J. [1993]. *Human Walking*, 2nd edn, Williams & Wilkins, Baltimore, Maryland.

Rostami, M. and Bessonnet, G. [2001]. Sagittal gait of a biped robot during the single support phase. part II: Optimal motion, *Robotica* **19**: 241–253.

Roussel, L., de Wit, C. C. and Goswami, A. [1998]. Generation of energy optimal complete gait cycles for biped robots, *Proceedings IEEE International Conf. Robotics and Automation*, pp. 2036–2041.

Saidouni, T. and Bessonnet, G. [2002]. Gait trajectory optimization using approximation functions, in P. Bidaud and F. Ben Amar (eds), *Proceedings of 5th International Conference on Climbing and Walking Robots and the Support Technologies for Mobile Machines (CLAWAR 2002)*, Professional Engineering Publishing, pp. 709–716.

Saidouni, T. and Bessonnet, G. [2003]. Generating globally optimized sagittal gait cycles of a biped robot, *Robotica* **21**: 199–210.

Sano, A. and Furusho, J. [1990]. Realization of natural dynamic walking using the angular momentum information, *Proceedings IEEE International Conference on Robotics and Automation*, pp. 1476–1481.

Schwind, W. and Koditschek, D. [1995]. Control of forward velocity for a simplified planar hopping robot, *Proceedings IEEE International Conference on Robotics and Automation*, pp. 691–696.

Shih, C.-L. [1997a]. Gait synthesis for a biped robot, *Robotica* **15**: 599–607.

Shih, C.-L. [1997b]. Inverted pendulum-like walking pattern of a 5-link biped

robot, *Proceedings 8th International Conference on Advanced Robotics*, Monterey, California, USA, pp. 83–88.

Shih, C.-L. and Gruver, W. [1992]. Control of a biped robot in the double-support phase, *IEEE Transactions on Systems, Man and Cybernetics* **22**(4): 729–735.

Shih, C.-L., Li, Y., Lee, T.-T. and Gruver, W. [1990]. Trajectory synthesis and physical admissibility for a biped robot during the single-support phase, *Proceedings IEEE International Conference on Robotics and Automation*, Cincinnati, USA, pp. 1646–1652.

Spong, M. and Vidyasagar, M. [1989]. *Robot Dynamics and Control*, JohnWiley and Sons, Inc.

Sugihara, T., Nakamura, Y. and Inoue, H. [2002]. Realtime humanoid motion generation through ZMP manipulation based on inverted pendulum control, *Proceedings of the 2002 IEEE International Conference on Robotics and Automation*, Washington, DC, pp. 1404–1409.

Sznaier, M. and Damborg, M. [1989]. An adaptive controller for a one-legged mobile robot, *IEEE Transactions on Robotics and Automation* **5**(2): 253–259.

Takanishi, A., Ishida, M., Yamazaki, Y. and Kato, I. [1985]. The realization of dynamic walking by the biped walking robot WL-10RD, *Proceedings International Conference on Advanced Robotics '85*, pp. 459–466.

Todd, D. [1985]. *Walking Machines: An Introduction to Legged Robots*, Kogan Page Ltd, London.

Tondu, B. and Bazaz, S. [1999]. The three-cubic method: An optimal online robot joint trajectory generator under velocity, acceleration and wandering constraints, *The International Journal of Robotics Research* **18**(9): 893–901.

Vakakis, A., Burdick, J. and Caughey, T. [1991]. An 'interesting' strange attractor in the dynamics of a hopping robot, *International Journal of Robotics Research* **10**(6): 606–618.

Vermeulen, J., Lefeber, D. and De Man, H. [2000]. A control strategy for a robot with one articulated leg hopping on irregular terrain, in M. Armada and P. G. de Santos (eds), *Proceedings 3rd International Conference on Climbing and Walking Robots and the Support Technologies for Mobile Machines (CLAWAR 2000)*, Professional Engineering Publishing, pp. 399–406.

Vermeulen, J., Verrelst, B. and Lefeber, D. [2003]. Control of foot placement, forward velocity and body orientation of a one-legged hopping robot, *Robotica* **21**(1): 45–57.

Verrelst, B., Van Ham, R., Daerden, F. and Lefeber, D. [2002]. Design of a biped actuated by pleated artificial muscles, *Proceedings of the 5th International Conference on Climbing and Walking Robots (CLAWAR 2002)*, pp. 211–218.

Vukobratovic, M., Borovac, B., Surla, D. and Stokic, D. [1990]. *Scientific Fundamentals of Robotics 7: Biped Locomotion (Dynamics, Stability, Control and Ap-*

plication), Springer-Verlag, Berlin, Heidelberg.

Yamada, M., Furusho, J. and Sano, A. [1985]. Dynamic control of walking robot with kick-action, *Proceedings International Conference on Advanced Robotics '85*, pp. 405–412.

Zeglin, G. [1991]. Uniroo: A one legged dynamic hopping robot. B.S. thesis, MIT Dept. of Mechanical Engineering.

Zeglin, G. and Brown, B. [1998]. Control of a bow leg hopping robot, *Proceedings IEEE International Conference on Robotics and Automation*, Leuven, Belgium, pp. 793–798.

Zeglin, G. and Brown Jr, H. [2002]. First hops of the three-dimensional bow leg, in P. Bidaud and F. Ben Amar (eds), *Proceedings of 5th International Conference on Climbing and Walking Robots and the Support Technologies for Mobile Machines (CLAWAR 2002)*, Professional Engineering Publishing, pp. 357–364.

Zheng, Y.-F. and Hemami, H. [1985]. Mathematical modeling of a robot collision with its environment, *Journal of Robotic Systems* **2**(3): 289–307.